

**Tribological and Tribochemical Behaviour of Machine
Elements Having DLC/Cast Iron Interfaces and Lubricated
with MoDTC-Type Friction Modifier**

YASIR AKRAM ABDALREDA AL-JEBOORI

Submitted in accordance with the requirements for the degree of
Doctor of Philosophy

The University of Leeds
Institute of Functional Surfaces (IFS)
School of Mechanical Engineering

September, 2018

The candidate confirms that the work submitted is his own and that appropriate credit has been given where reference has been made to the work of others.

In the papers contributing to this thesis, the candidate (first author) carried out all the experiments, analysis and preparation of the manuscripts. All other authors contributed by proof reading and providing insight on the discussions.

This copy has been supplied on the understanding that it is copyright material and that no quotation from the thesis may be published without proper acknowledgement.

The right of Yasir Akram Al-Jeboori to be identified as Author of this work has been asserted by him in accordance with the Copyright, Designs and Patents Act 1988.

© 2018 The University of Leeds and Yasir Akram Al-Jeboori.

Papers Contributing to this Thesis

- **Al-Jeboori Y**, Kosarieh S, Ofune M, Morina A, Neville A. Measuring tappet rotation in a valvetrain rig when lubricated in a fully formulated oil containing MoDTC-type friction modifier. Tribology International. 2018; 121C: 442-9. Featured in Chapter 4, 7 and 9.
- **Al-Jeboori Y**, Kosarieh S, Morina A, Neville A. Investigation of pure sliding and sliding/rolling contacts in a DLC/Cast iron system using MoDTC-Type friction modifier. Tribology International. 2018; 122: 23-37. Featured in Chapter 4, 5 and 9.
- **Al-Jeboori Y**, Kosarieh S, Ofune M, Neville A, Morina A. The effect of clearance between tappet insert and camlobe on the tribological and tribochemical performance of cam/follower surfaces. Tribology International; <https://doi.org/10.1016/j.triboint.2018.09.021>. Featured in Chapter 4, 6, 8 and 9.
- **Al-Jeboori Y**, Kosarieh S, Morina A, and Neville A. Mapping the tribochemical films across the cam profile when lubricated with oils containing MoDTC-type friction modifier. Tribology International (In preparation). Featured in Chapter 4, 8 and 9.

Conferences – Oral presentation

- **Al-Jeboori Y**, Kosarieh S, Morina A, Neville A. Tribochemical analysis of a DLC/cast iron system when lubricated with MoDTC-type friction modifier under sliding and rolling contacts, 6th World Tribology Congress (WTC), Beijing-China 2017.
- **Al-Jeboori Y**, Kosarieh S, Morina A, Neville A. Tappet rotation measurement in the presence of MoDTC-type friction modifier, STLE 73rd Annual Meeting, Minnesota Minneapolis, USA 2018.
- **Al-Jeboori Y**, Kosarieh S, Morina A, and Neville A. Analysis of cam/follower surfaces in the presence of MoDTC-type friction modifier, 45st Leeds-Lyon Symposium on Tribology, Leeds, UK 2018.
- **Al-Jeboori Y**, Kosarieh S, Morina A, and Neville A. Mapping the tribochemical films across the cam profile when lubricated with oils containing MoDTC-type friction modifier. STLE Tribology Frontiers Conference, Chicago, Illinois, USA 2018.

Acknowledgments

I would like to express my deepest and sincere gratitude towards my supervisors, Professor Anne Neville, Professor Ardian Morina and Doctor Shahriar Kosarieh for being such supportive and encouraging supervisors who are invaluable on both an academic and a personal level. I would also like to thank them for their discussions into the direction of my work and understanding the novelty of my research. Their diligence to reviewing papers, presentations and this thesis is truly appreciated. I am deeply grateful to my primary supervisor Professor Anne Neville with whom it has been a privilege to work. Her patient guidance and enthusiastic encouragement, throughout all the highs and lows, not only made this work possible, but also made it enjoyable.

I would like to thank the Higher Committee for Education Development in Iraq (HCED) for funding this project and Mr. Sandeep Jhand of Oerlikon Balzers Coating UK Ltd. for supplying the DLC coatings. Also, I wish to thank TOTAL for supplying the lubricant as well as Dr. James Chandler and Dr. Earle Jamieson of Resolve Research Engineering (UK) for their assistance with the development of the tappet rotation technique.

My thanks to the staff of Leeds University Mechanical Engineering department for the great help and support they offered to complete the present work. Thanks also to my workmates, Doris, Cayetano, Chun, Sean, Abdul, Farnaz, Ali, Mohammed and Sikiru who have been a great support team. I couldn't have asked for a better group of friends to work with. Also, I would like to especially thank MacDonald who has contributed hours of discussion, insight and support in to the delivery and completion of this work.

Lastly not the less, I would like to dedicate this work in loving memory of my father Akram Abdalreda Al-Jeboori who left us and rest in heaven twelve years ago. I also dedicate it to my mother Maysoon Jabar Al-Abassi who is waiting for me to finish, and my beloved wife Rusul, my daughter Jumana and my son Jood, for being with me in all circumstances, giving me support and love to continuously spur me on through this period. I here extend my dedication to my brother Laith as well as my sisters Maha and Rusha.

Abstract

Due to the importance of reducing CO₂ emissions and improving fuel economy, many researchers have focused on studying the cam/follower contact and the ways to reduce friction (improve engine efficiency) and avoid wear (enhance engine durability). This thesis addresses aspects of tribology and tribochemistry of a cam/follower interface with consideration of how the surface/lubricant interaction affect the system performance.

A Mini Traction Machine (MTM) was used to evaluate different lubricant formulations as well as to examine the tribofilm formation under pure sliding and sliding/rolling contacts. A Single Cam Rig (SCR), taken from 1.25L FORD Zetec (SE) engine, was also used in this work in order to investigate the friction, wear and tribochemical performance of the camlobes/tappets as a function of tappet clearance and type of coating. In addition, a new technique of measuring tappet rotation using a giant magnetoresistance (GMR) sensor coupled with a split pole ferrite disk magnet has also been developed in this study.

Raman Spectroscopy, Scanning Electron Microscope (SEM), Energy-Dispersive X-Ray (EDX), X-ray Photoelectron Spectroscopy (XPS), Focused Ion Beam (FIB) and Transmission Electron Microscopy (TEM) were performed on the surfaces to understand the tribochemical interactions between oil additives and the cam/follower interface.

Results obtained from MTM tribometer showed that the sliding/rolling ratio affects friction, wear and tribochemistry in CI/DLC systems; pure sliding enhances MoDTC activation. MoDTC decomposes to form MoS₂, FeMoO₄ and not MoO₃. In addition, it was observed that the MoS₂/FeMoO₄ ratio depends on test conditions and affects the friction performance.

The results obtained from SCR tribometer closely support those in the MTM tribometer and that link between tribometer and component testing is discussed. In addition, the chemistry of the tribofilm derived on camlobes and tappets varies as a function of tappet clearance and cam profile. In terms of tappet rotation, results showed that Molybdenum Dialkyl Dithiocarbamate (MoDTC) and Diamond-Like Carbon (DLC) coating promoted the rotation of the tappet. Furthermore, the tappet rotation is strongly dependent on oil formulation, clearance, speed/temperature, and surface roughness of the coating.

Table of Contents

Acknowledgements	iv
Abstract	v
List of Tables	xii
List of Figures	xiv
Nomenclature	xxi
Chapter 1. Introduction	1
1.1. Motivation.....	1
1.2. Objectives and Scope of Research	5
1.3. Thesis Outline	5
Chapter 2. Fundamentals of Tribology	7
2.1. Introduction	7
2.2. Friction	7
2.3. Wear	8
2.3.1 Adhesive Wear	8
2.3.2 Abrasive Wear.....	9
2.3.3 Fatigue Wear.....	10
2.3.4 Corrosive Wear.....	11
2.3.5 Erosive Wear.....	11
2.4. Lubrication.....	11
2.4.1 Lubrication Regimes.....	12
2.4.2 Lubricants.....	17
2.4.3 Additives.....	18
2.5. Hertzian Elastic Contact Analysis.....	23
2.6. Cam/Follower Tribology Kinematics.....	25
2.7. Cyclic Film Thickness and Entrainment Velocity Variations	28
2.8. Torque Cycle.....	29
2.9. Fuel Economy	29
Chapter 3. Literature Review	31
3.1. Introduction	31
3.2. Overview of Valvetrain Systems.....	31
3.3. Cams and Followers	34

3.3.1	Materials.....	34
3.3.2	Surface Coatings.....	35
3.3.3	Friction.....	36
3.3.4	Wear.....	39
3.3.5	Lubrication.....	43
3.4.	Diamond-Like Carbon (DLC) Coatings.....	43
3.4.1	Structure of DLC Coatings.....	44
3.4.2	Deposition of DLC Coatings.....	46
3.4.3	The Graphitization of Hydrogenated DLC.....	48
3.5.	Zinc Dialkyldithiophosphate (ZDDP).....	49
3.5.1	Tribological Performance of ZDDP.....	50
3.5.2	Tribochemical Performance of ZDDP.....	51
3.6.	Molybdenum Dialkyl Dithiocarbamate (MoDTC).....	52
3.6.1	Tribological Performance of MoDTC.....	54
3.6.2	Tribochemical Performance of MoDTC.....	56
3.7.	Additive/Additive Interactions.....	59
3.7.1	MoDTC Interaction with ZDDP.....	59
3.7.2	ZDDP Interaction with Detergents and Dispersants.....	60
3.8.	DLC/Additive Interactions.....	61
3.9.	Gaps in the Literature.....	64
3.9.1	Tappet Rotation.....	64
3.9.2	Tappet Clearance.....	66
3.9.3	Tribochemistry and Wear of Camlobe.....	68
3.9.4	Sliding and Rolling Contacts.....	68
3.10.	Summary of Gaps in the Literature.....	69
Chapter 4. Experimental Methodology and Surface Analysis		
Techniques.....		71
4.1.	Introduction.....	71
4.2.	Mini Traction Machine (MTM) Tribometer.....	71
4.2.1	Test Materials and Coatings.....	72
4.2.2	Test Lubricants.....	73
4.2.3	Test Conditions.....	76

4.2.4	Experimental Methodology / MTM	77
4.3.	Single Cam Rig (SCR) Tribometer	79
4.3.1	Test Materials and Coatings	80
4.3.2	Test Lubricants	81
4.3.3	Test Conditions	81
4.3.4	Tappet Rotation Measurement	82
4.3.5	Experimental Methodology / SCR	85
4.4.	Surface Analysis Techniques	86
4.4.1	Optical Microscope	86
4.4.2	NPFLEX White Light Interferometer (WLI)	86
4.4.3	Scanning Electron Microscope (SEM) / Energy Dispersive X-Ray (EDX)	87
4.4.4	Focused Ion Beam (FIB) / Transmission Electron Microscopy (TEM)	88
4.4.5	X-ray Photoelectron Spectroscopy (XPS)	89
4.4.6	Raman Spectroscopy	90
4.4.7	Contact Profilometry	91
Chapter 5. Mini Traction Machine (MTM): Investigation of Friction, Wear and Tribochemistry of Different Lubricant Formulations under Pure Sliding and Sliding/Rolling Contacts		95
5.1.	Introduction	95
5.2.	Friction Results	95
5.2.1	The Correlation between SRR and Friction	95
5.2.2	The Correlation between SRR and Stribeck Curve Evaluation	97
5.2.3	Range of Friction Values in the Boundary Lubrication Regime	102
5.3.	Wear Results	104
5.4.	Chemical Analysis of Tribofilm	106
5.4.1	SEM-EDX Results	106
5.4.2	Raman Spectroscopy Results	109
5.4.3	X-ray Photoelectron Spectroscopy Results	112
5.5.	Effect of Oil Formulation and Contact Type on Stribeck Curve Evaluation	116
5.6.	Effect of MoDTC on Wear	117

5.7. Effect of Contact Type on Tribofilm Evolution	118
5.8. Summary of Findings	120
Chapter 6. Single Cam Rig (SCR): Investigation of Friction and Wear of Cam/Follower Surfaces When Lubricated in a Fully Formulated Oil With and Without MoDTC-Type Friction Modifier	122
6.1. Introduction	122
6.2. Torque Profile Data	122
6.3. Repeatability of Friction Torque Data	123
6.4. First Stage and Second Stage Results	124
6.4.1 Friction Torque	124
6.4.2 Wear Evaluations	129
6.5. Third Stage and Fourth Stage Results	134
6.5.1 Friction Torque	134
6.5.2 Wear Evaluations	135
6.6. The Comparison of Tribological Performance for All Stages	138
6.7. Summary of Findings	139
Chapter 7. Single Cam Rig (SCR): Investigation of Tappet Rotation When Lubricated in a Fully Formulated Oil With and Without MoDTC-Type Friction Modifier	140
7.1. Introduction	140
7.2. Repeatability of Tappet Rotation Data	140
7.3. First Stage and Second Stage Results	142
7.3.1 Effect of Tappet Clearance and Camshaft Speed on Tappet Rotation	142
7.3.2 Effect of Coating on Tappet Rotation	144
7.4. Third Stage and Fourth Stage Results	146
7.4.1 Effect of Tappet Clearance and Camshaft Speed on Tappet Rotation	146
7.4.2 Effect of Coating on Tappet Rotation	147
7.5. The Comparison of Tappet Rotation for All Stages	148
7.6. Summary of Findings	149
Chapter 8. Tribochemistry Evaluation of Tribofilms Formed from Single Cam Rig (SCR) Tribometer When Lubricated in a Fully Formulated Oil With and Without MoDTC-Type Friction Modifier	150

8.1. Introduction	150
8.2. First Stage and Second Stage	150
8.2.1 SEM-EDX Results	150
8.2.2 Raman Spectroscopy Results	156
8.2.3 X-ray Photoelectron Spectroscopy Results	160
8.2.4 FIB-SEM Results	168
8.2.5 TEM Results	169
8.3. Third Stage and Fourth Stage	171
8.3.1 SEM-EDX Results	171
8.3.2 Raman Spectroscopy Results	175
8.3.3 X-ray Photoelectron Spectroscopy Results	178
8.3.4 FIB-SEM Results	182
8.3.5 TEM Results	183
8.4. Summary of Findings	186
Chapter 9. Discussion	189
9.1. Introduction	189
9.2. Characteristics of MoDTC Tribofilm	189
9.3. Effect of Sliding/Rolling Ratio (SSR) on MoDTC Tribofilm	190
9.4. Effect of Sliding/Rolling Ratio (SSR) on Friction.....	191
9.5. Effect of MoDTC on Friction and Wear	191
9.6. Coating Performance on SCR.....	193
9.7. Chemistry and Thickness of Tribofilm on SCR.....	195
9.8. Effect of Tribofilm Formation on Tappet Rotation.....	197
9.9. The Link between MTM and SCR Tribometers	198
9.9.1 Tribological Comparison	199
9.9.2 Tribochemical Comparison	203
9.10. Optimising Friction and Wear.....	204
Chapter 10. Conclusions and Future Work	207
10.1. Introduction	207
10.2. Overall Conclusions.....	207
10.2.1 Mini Traction Machine (MTM).....	207
10.2.2 Single Cam Rig (SCR).....	208

10.3. Suggestions for Future Work	211
List of References	213

List of Tables

Table 2-1 The definitions of lubrication regimes [28].....	12
Table 2-2 Base oil categories [37, 38].....	17
Table 2-3 Typical ranges of composition of engine crankcase lubricants [43].....	19
Table 3-1 Tribo-materials for valvetrain assembly	35
Table 3-2 Causes of cam/follower wear [74]	39
Table 3-3 Properties of various forms of carbon [146]	46
Table 3-4 Performance parameters of ZDDP types [35].....	50
Table 3-5 Binding energies of various molybdenum compounds [198].....	57
Table 4-1 Physical properties of balls, discs and DLC coating.....	73
Table 4-2 Test lubricants	74
Table 4-3 General, physical and chemical characteristics	75
Table 4-4 Test parameters ranges of MTM tribometer	76
Table 4-5 Mechanical properties of samples	77
Table 4-6 MTM test steps.....	78
Table 4-7 Typical tribological and performance parameters for IC engines.....	81
Table 4-8 Contact pressure across camlobe	92
Table 5-1 Range of surface roughness for balls and discs at the end of each test.....	101
Table 5-2 Average of steady state friction in boundary lubrication at the last hour of each test.....	103
Table 5-3 Effect of SRR on the tribofilms detected on the DLC coated balls using XPS.....	119
Table 5-4 XPS quantification of tribofilms on the CI discs and DLC balls lubricated in O5.....	120
Table 8-1 EDX semi-quantification of CI camlobes and coated inserts (2.75mm).....	153
Table 8-2 EDX semi-quantification of CI camlobes and coated inserts (2.575mm and 2.275 mm)	154
Table 8-3 Wear depth, BO/NBO area ratio, $\Delta(\text{Zn } 3s - \text{P } 2p)$ (eV), and P 2p/Zn 3s area ratio for the seven specified positions on CI camlobe rubbing against MnPO_4 insert with thickness of 2.75 mm at 100 °C.....	164
Table 8-4 Binding energies of XPS spectra of Zn 3s, P 2p, S 2p, MoS_2 and MoO_3 , and spectra at two temperatures (100 °C and 130 °C) and the corresponding species formed on top surface	

of camlobes rubbed against tappets with different thicknesses.....	164
Table 8-5 BO/NBO area ratio, Δ (Zn 3s– P 2p) (eV), and P 2p/Zn 3s area ratio for MnPO ₄ and DLC inserts inside and outside the wear track at 100 °C	167
Table 8-6 Binding energies of XPS spectra of Zn 3s, P 2p, S 2p, MoS ₂ and MoO ₃ , and the corresponding species formed on top surface of MnPO ₄ and DLC inserts inside the wear track at 100 °C	167
Table 8-7 EDX semi-quantification of Cl camlobes and coated inserts (2.75mm).....	174
Table 8-8 EDX semi-quantification of Cl camlobes and coated inserts (2.575mm and 2.275 mm) at 100 °C	175
Table 8-9 Binding energies of XPS spectra of Mo, Zn 3s, P 2p and S 2p formed on top surface of camlobes rubbed against tappets with different thicknesses and coatings at 100 °C	181
Table 8-10 BO/NBO area ratio, Δ (ZN 3s– P 2p) (eV), and P 2p/ZN 3s area ratio for MnPO ₄ and DLC inserts inside and outside the wear track at 100 °C	181
Table 8-11 Binding energies of XPS spectra of Mo, Zn 3s, P 2p and S 2p formed on top surface of tappets with different thicknesses and coatings at 100 °C	182
Table 9-1 Effect of surface roughness and hardness on coating performance	194
Table 9-2 Similarities and differences between MTM and SCR.....	199
Table 9-3 Showing the comparison of the tribofilm from mini traction machine and single cam rig tribometers when lubricated in a lubricant containing MoDTC and ZDDP (i.e. O5)	203

List of Figures

Figure 1-1 Breakdown of passenger car energy consumption [4].....	2
Figure 1-2 Mechanical losses in an internal combustion engine.....	2
Figure 2-1 Steps leading to adhesive wear [26].....	9
Figure 2-2 Abrasive wear, scratching [22]	10
Figure 2-3 Fatigue wear in a roller bearing [26].....	10
Figure 2-4 Corrosive wear, coupling [26]	11
Figure 2-5 The modified Stribeck diagram [30]	13
Figure 2-6 Boundary lubrication [16].....	14
Figure 2-7 Mixed lubrication [16]	15
Figure 2-8 Elastohydrodynamic lubrication [16]	16
Figure 2-9 Hydrodynamic lubrication [16].....	16
Figure 2-10 Chronology of development of main classes of lubricant additive [44]	19
Figure 2-11 Equivalent elastic solid on a rigid plane [16].....	24
Figure 2-12 Geometry of a direct acting cam and follower [6]	26
Figure 2-13 Typical variation of film thickness between direct acting cam and follower: (a) as a function of cam angle (b) around the cam circumference [6].....	28
Figure 2-14 Effect of camlobe profile on entrainment velocity [54]	29
Figure 2-15 Input torque curve for a cam/follower mechanism [55]	29
Figure 2-16 Minimising total engine power loss and wear [46].....	30
Figure 3-1 Schematic diagram of a valvetrain system [61].....	32
Figure 3-2 Classification of valvetrain architectures [13]	33
Figure 3-3 Typical failures of camlobe and follower [15].....	33
Figure 3-4 Pitting and scuffing resistance of convention materials [6].....	40
Figure 3-5 sp^3 , sp^2 and sp^1 hybridised bonding [142].....	44
Figure 3-6 Ternary phase diagram of bonding in amorphous carbon-hydrogen alloys [142]	45
Figure 3-7 Schematic of various deposition systems for DLC [142]	48
Figure 3-8 Structure of Zinc dialkyl dithiophosphate [35]	49
Figure 3-9 ZDDP film structure [178]	51
Figure 3-10 MoS_2 solid state structure [193].....	53
Figure 3-11 The structures of MoDTC and MoDTP [192]	53

Figure 3-12 Typical friction curve obtained during tests with MoDTC additive [189].....	54
Figure 3-13 Influence of MoDTC concentration on friction [191]	55
Figure 3-14 MoDTC decomposition: chemical model [112].....	56
Figure 3-15 New reaction pathway of MoDTC additives [201].....	58
Figure 3-16 Schematic structure for films generated by: (a) ZDDP and (b) ZDDP/ Detergents/Dispersant	61
Figure 3-17 Wear steps of DLC coating in oil containing MoDTC [229].....	62
Figure 3-18 Multi-step of DLC coating in oil containing MoDTC [232].....	63
Figure 3-19 2D-schematic diagram of direct acting mechanical type valvetrain [115].....	64
Figure 3-20 2D-schematic diagram of camlobe and follower	67
Figure 4-1 MTM tribometer (a) photograph of MTM (b) inside the test chamber (c) 2D schematic of MTM [250].....	71
Figure 4-2 Photograph showing six representative oil samples.....	74
Figure 4-3 MTM experimental outline	77
Figure 4-4 Single cam rig tribometer (SCR)	80
Figure 4-5 Tappet rotation test rig	83
Figure 4-6 Sensor and magnet information: (a) sensor position on the single cam rig, (b) different sizes of magnets were initially tested, (c) a magnet force fitted onto the underside of a shim (d) magnet dimensions and position.....	84
Figure 4-7 SCR experimental outline.....	85
Figure 4-8 Single cam rig test cycle	86
Figure 4-9 Typical NPFLEX wear measurements of the CI disc.....	87
Figure 4-10 Schematic of Scanning Electron Microscope [256]	88
Figure 4-11 Typical FIB preparation section for TEM.....	89
Figure 4-12 Typical survey scan (a) and long scan (b) obtained from XPS	90
Figure 4-13 2D schematic representation of Raman spectroscopy [259].....	91
Figure 4-14 The seven positions of surface profilometer traces on the camlobes [134].....	92
Figure 4-15 Calculations for: (a) lubricant entrainment velocity, (b) load per unit length, (c) cam lift profile, (d) velocity profile and (e) acceleration profile [115]	93
Figure 4-16 Cam nose profile (a) pre-test and (b) post-test.....	94

Figure 5-1 Friction coefficients for a CI/DLC system as a function of time: (a) at 50%SRR and (b) 200%SRR	96
Figure 5-2 Average friction coefficient values for the last hour for all oils at 50% SRR and 200% SRR	97
Figure 5-3 Stribeck curves for (a) BO, (b) O1, (c) O2, (d) O3, (e) O4 and (f) O5 as a function of time at 50% SRR.....	98
Figure 5-4 Stribeck curves for (a) BO, (b) O1, (c) O2, (d) O3, (e) O4 and (f) O5 as a function of time at 200% SRR.....	99
Figure 5-5 Friction coefficients for (a) BO, (b) O1, (c) O2, (d) O3, (e) O4 and (f) O5 at mean speed = 10 mm/s under 50% SRR and 200% SRR	100
Figure 5-6 Range of friction values $\Delta\mu$ at $\lambda < 1$ for all oils: (a) at 50% SRR and (b) at 200% SRR.....	103
Figure 5-7 Representative optical images of the wear scar formed on uncoated cast iron discs (a) at 50%SRR (b) at 200%SRR	104
Figure 5-8 Representative optical images of the wear scar formed on DLC coated balls (a) at 50%SRR (b) at 200%SRR, the arrows on the left side of the images show sliding directions ...	104
Figure 5-9 Representative interferometer images of the wear track that formed on: (a) uncoated cast iron disc and (b) DLC coated ball	105
Figure 5-10 Average of wear depths that formed on: (a) uncoated cast iron discs and (b) DLC coated balls (note different wear depth scales)	105
Figure 5-11 SEM micrographs of CI disks at end of test	107
Figure 5-12 Data from regions inside the wear track under both contacts on: (a) uncoated cast iron discs and (b) DLC balls (note different wt% scales).....	108
Figure 5-13 Raman spectroscopy for the CI discs under: (a) sliding/rolling contact, (b) pure sliding contact	110
Figure 5-14 the intensity of MoS ₂ and FeMoO ₄ for the CI discs under both contacts.....	111
Figure 5-15 Raman spectroscopy for the DLC coated balls under: (a) sliding/rolling contact, (d) pure sliding contact	111
Figure 5-16 XPS spectra of the discs lubricated with MoDTC under: (a) sliding/rolling contact, (b) pure sliding contact.....	113
Figure 5-17 XPS spectra of the discs lubricated with ZDDP: (a) Zn 2p under sliding/rolling contact, (b) Zn 2p under pure sliding contact, (c) P 2p under sliding/rolling contact, (d) P 2p under pure sliding contact	114

Figure 5-18 XPS spectra of the DLC coated balls lubricated with MoDTC under: (a) sliding/rolling contact, (b) pure sliding contact	114
Figure 5-19 XPS spectra of the balls lubricated with ZDDP: (a) Zn 2p under sliding/rolling contact, (b) Zn 2p under pure sliding contact, (c) P 2p under sliding/rolling contact, (d) P 2p under pure sliding contact	115
Figure 5-20 Depth profiles of the discs and balls lubricated in O5: (a) Fe, (b) Zn, (c) P, (d) Mo (note different at. % scales).....	115
Figure 6-1 Torque profile of different tappet thicknesses at 300 rpm: (a) MnPO₄ inserts and (b) DLC inserts	123
Figure 6-2 Repeatability of friction torque data for MnPO₄ insert (2.75mm tappet thickness) over 80 hrs test duration at 100 °C ..	124
Figure 6-3 Average friction torque versus camshaft speed for MnPO₄ inserts at different thicknesses (a) at 100 °C, (b) at 130 °C	125
Figure 6-4 the start point of contact on the camlobe under different tappet thicknesses.....	126
Figure 6-5 Effect of tappet thickness on valve spring	127
Figure 6-6 Average friction torque versus camshaft speed for DLC inserts at 100 °C	128
Figure 6-7 Average wear depth versus tappet thickness for MnPO₄ inserts at 100 °C and 130 °C.....	130
Figure 6-8 Typical wear scar of MnPO₄ tappet insert.....	130
Figure 6-9 Average wear depth versus tappet thickness for DLC inserts at 100 °C	131
Figure 6-10 Average wear depth across the camlobe when interacting with MnPO₄ insert: (a) at 100 °C, (b) at 130 °C.....	132
Figure 6-11 Average wear depth across the camlobe when interacting with DLC insert at 100 °C	133
Figure 6-12 Average friction torque versus camshaft speed at 100 °C: (a) third stage (MnPO₄ inserts), (b) fourth stage (DLC inserts)	135
Figure 6-13 Average wear depth versus tappet thickness at 100 °C: (a) third stage (MnPO₄ inserts), (b) fourth stage (DLC inserts)	136
Figure 6-14 Average wear depth across the camlobe: (a) third stage (when interacting with MnPO₄ inserts), (b) fourth stage (when interacting with DLC inserts)	137
Figure 7-1 Number of counts for MnPO₄ insert with thickness of 2.75mm during an 80 hour test	141

Figure 7-2 Repeatability of tappet rotation for MnPO₄ insert with thickness of 2.75mm at 1200 rpm	141
Figure 7-3 Average tappet rotation versus camshaft speed for MnPO₄ inserts at different thicknesses: (a) at 100 °C, (b) at 130 °C	142
Figure 7-4 Average tappet rotation versus camshaft speed for DLC inserts at 100 °C	144
Figure 7-5 Effect of coatings on the rotation of 2.75mm tappet thickness at 100 °C	145
Figure 7-6 Average tappet rotation versus camshaft speed at 100 °C: (a) third stage (MnPO₄ inserts), (b) fourth stage (DLC inserts)	146
Figure 8-1 Scanning Electron micrograph (SEM) at 100 °C: (a) CI camlobe rubbed against (2.75 mm) MnPO₄ shim, (b) MnPO₄ shim with thickness 2.75 mm, (c) CI camlobe rubbed against (2.75 mm) DLC shim, (d) DLC shim with thickness 2.75 mm, (e) CI camlobe rubbed against (2.575 mm) MnPO₄ shim, (f) MnPO₄ shim with thickness 2.575 mm (g) CI camlobe rubbed against (2.575 mm) DLC shim, (h) DLC shim with thickness 2.575 mm (i) CI camlobe rubbed against (2.275 mm) MnPO₄ shim, (j) MnPO₄ shim with thickness 2.275 mm, (k) CI camlobe rubbed against (2.275 mm) DLC shim, (l) DLC shim with thickness 2.275 mm	151
Figure 8-2 Typical wear process on tappet inserts (a) polishing process (b) abrasive process.....	156
Figure 8-3 Raman spectroscopy for the CI camlobes (rubbed against MnPO₄ inserts) at 100 °C: (a) before test, (b) at cam nose, (c) +14° from cam nose, (d) -14° from cam nose	157
Figure 8-4 Raman spectroscopy for the MnPO₄ inserts at 100 °C: (a) before test, (b) inside wear track, (c) outside wear track	158
Figure 8-5 Raman spectroscopy for the CI camlobes (rubbed against DLC inserts) at 100 °C: (a) before test, (b) at cam nose, (c) +14° from cam nose, (d) -14° from cam nose	159
Figure 8-6 Raman spectroscopy for the DLC inserts at 100 °C: (a) before test, (b) inside wear track, (c) outside wear track.....	160
Figure 8-7 XPS analysis of cast iron camlobes rubbed against tappets coated with MnPO₄ and DLC coatings at 100 °C: (a) S 2p peaks, (b) P 2p peaks, (c) Zn 2p peaks, (d) Mo 3d peaks, (e) Ca 2p peaks and (f) O1 s peaks	163
Figure 8-8 XPS analysis of steel tappets coated with MnPO₄ and DLC coatings at 100 °C: (a) S 2p peaks, (b) P 2p peaks, (c) Zn 2p peaks, (d) Mo 3d peaks, (e) Ca 2p peaks and (f) O1 s peaks..	165

Figure 8-9 XPS survey scan for the tribofilms formed on the: (a) CI camlobe rubbed against (b) MnPO ₄ insert with thickness of 2.75 mm.....	168
Figure 8-10 FIB-SEM showing tribofilm thickness for: (a) camlobe rubbed against MnPO ₄ insert, (b) MnPO ₄ insert, (c) camlobe rubbed against DLC insert and (d) DLC insert	169
Figure 8-11 TEM images showing tribofilm at cam nose rubbed at: (a) MnPO ₄ insert and (b) DLC insert	170
Figure 8-12 TEM images showing tribofilm at: (a) MnPO ₄ insert and (b) DLC insert	171
Figure 8-13 Scanning Electron micrograph (SEM) at 100 °C: (a) CI camlobe rubbed against (2.75 mm) MnPO ₄ shim, (b) MnPO ₄ shim with thickness 2.75 mm, (c) CI camlobe rubbed against (2.75 mm) DLC shim, (d) DLC shim with thickness 2.75 mm, (e) CI camlobe rubbed against (2.575 mm) MnPO ₄ shim, (f) MnPO ₄ shim with thickness 2.575 mm (g) CI camlobe rubbed against (2.575 mm) DLC shim, (h) DLC shim with thickness 2.575 mm (i) CI camlobe rubbed against (2.275 mm) MnPO ₄ shim, (j) MnPO ₄ shim with thickness 2.275 mm, (k) CI camlobe rubbed against (2.275 mm) DLC shim, (l) DLC shim with thickness 2.275 mm	173
Figure 8-14 Raman spectroscopy for the CI camlobes (rubbed against MnPO ₄ inserts) at 100 °C: (a) before test, (b) at cam nose, (c) +14° from cam nose, (d) -14° from cam nose	176
Figure 8-15 Raman spectroscopy for the MnPO ₄ inserts at 100 °C: (a) before test, (b) inside wear track, (c) outside wear track	177
Figure 8-16 Raman spectroscopy for the CI camlobes (rubbed against DLC inserts) at 100 °C: (a) before test, (b) at cam nose, (c) +14° from cam nose, (d) -14° from cam nose	177
Figure 8-17 Raman spectroscopy for the DLC inserts at 100 °C: (a) before test, (b) inside wear track, (c) outside wear track.....	178
Figure 8-18 XPS analysis of cast iron camlobes rubbed against tappets coated with MnPO ₄ and DLC coatings at 100 °C: (a) S 2p peaks, (b) P 2p peaks, (c) Zn 2p peaks, (d) O1 s peaks	179
Figure 8-19 XPS analysis of steel tappets coated with MnPO ₄ and DLC coatings at 100 °C: (a) S 2p peaks, (b) P 2p peaks, (c) Zn 2p peaks, (d) O1 s peaks	180
Figure 8-20 FIB-SEM showing tribofilm thickness for: (a) camlobe rubbed against MnPO ₄ insert, (b) MnPO ₄ insert, (c) camlobe rubbed against DLC insert and (d) DLC insert	183
Figure 8-21 TEM images showing tribofilm at camlobe rubbed at: (a) MnPO ₄ insert and (b) DLC insert	184
Figure 8-22 TEM mapping showing tribofilm at MnPO ₄ insert	185
Figure 8-23 TEM mapping showing tribofilm at DLC insert.....	186

Figure 9-1 2D Schematic diagram showing adsorbed MoDTC in (a) unidirectional linear sliding contact and (b) sliding/rolling contact [198]	191
Figure 9-2 2D schematic diagram showing the tribofilm distribution on cam/follower tribopair.....	196
Figure 9-3 Schematic diagram of cam/follower tribopair (a) when the insert is lubricated with MoDTC (b) without MoDTC.....	197
Figure 9-4 Friction analysis as a function of MoDTC for (a) SCR tribometer (b) MTM tribometer	200
Figure 9-5 Wear analysis as a function of MoDTC for (a) SCR tribometer (b) MTM tribometer (note different scales).....	202
Figure 9-6 2D schematic diagram showing the optimum performance for (a) MTM and (b) SCR.....	206

Nomenclature

OHC	Over-Head Camshaft
DAMB	Direct Acting Mechanical Bucket
MoDTC	Molybdenum Dithiocarbamate
MoDTP	Molybdenum Dithiophosphate
MFM	Metal-containing Friction Modifiers
ZDDP	Zinc Dialkyldithiophosphate
DLC	Diamond-Like Carbon
MnPO ₄	Mn-Phosphate
SCR	Single Cam Rig
MTM	Mini Traction Machine
PoP	Pin on Plate
CI	Cast Iron
μ	Friction coefficient
F	Friction force (N)
W	Normal load (N)
V	Wear volume (m ³)
K	Dimensionless wear coefficient (mm ³ N ⁻¹ mm ⁻¹)
x	Sliding distance (m)
λ	Lambda ratio
h_{min}	Minimum film thickness (m)
RMS	Root Mean Square
R_q	RMS roughness of the two surfaces
R_a	Roughness average
U	Entrainment speed (ms ⁻¹)
η_0	Dynamic viscosity at atmospheric pressure of the lubricant (Pas)
α	Viscosity-pressure coefficient (m ² N ⁻¹)

R	Reduced radius of curvature (m)
E'	Reduced Young's modulus (Pa)
E	Young's modulus (Pa)
η	Dynamic viscosity (Pas)
R_e	Equivalent radius (m)
FF	Fully Formulated
BO	Base Oil
PAO	Polyalphaolefins
BL	Boundary Lubrication
ML	Mixed Lubrication
EHL	Elastohydrodynamic Lubrication
HL	Hydrodynamic Lubrication
API	American Petroleum Institute
ASTM	American Society for Testing and Measuring
VI	Viscosity Index
EP	Extreme Pressure
a	Radius of the contact area (m)
ν	Poisson's ratio
P_{max}	Maximum contact pressure
$P_{average}$	Average contact pressure
δ	Maximum deflection
τ_{max}	Maximum shear stress
Ω	Angular velocity
SRR	Sliding/Rolling Ratio
V_c	Cam velocity
V_f	Follower velocity
u_d	Disc velocity
u_b	Ball velocity
G	Dimensionless material parameter

U	Dimensionless speed parameter
W	Dimensionless load parameter
u_1	Cam velocity along x-axis
w_1	Cam velocity along y-axis
u_2	Follower velocity along x-axis
w_2	Follower velocity along y-axis
HRC	Hardness Rockwell scale
SLA	Surface Layer Activation
TLA	Thin Layer Activation
CMP	Chemo Mechanical Polishing
a-C: 15H	15 at. % hydrogenated DLC
a-C	Amorphous carbon
ta-C: H	Hydrogenated tetrahedral amorphous carbon
ta-C	Tetrahedral amorphous carbon
PVD	Physical Vapour Deposition
CVD	Chemical Vapour Deposition
PECVD	Plasma Enhanced Chemical Vapour Deposition
RF	Radio Frequency
WLI	White Light Interferometer
SEM	Scanning Electron Microscopy
EDX	Energy Dispersive X-ray
XPS	X-ray Photoelectron Spectroscopy
FIB	Focused Ion Beam
TEM	Transmission Electron Microscopy

Chapter 1. Introduction

1.1. Motivation

The target set by the UK government in the 2008 climate change act was to reduce the CO₂ emissions of 1990 by at least 80% by 2050 [1]. The transport sector is accountable for almost 24% of the UK national CO₂ emissions [2]. Fuel efficiency in vehicles is considered as an indicator of the emitted levels of CO₂ (i.e. emissions reduce by improving fuel economy) [3]. Thus, engine developers and lubricant formulators are continuously challenged to reduce fuel consumption and emissions of automotive engines.

It is generally accepted that in order to solve emission issues in the transport sector, alternative technologies had to be explored such as reducing vehicle weight, reducing rolling resistance, engine downsizing with both ferrous and non-ferrous materials, using advanced petrol and diesel, use of hybrid powertrains and electric motors. However, most of these alternative technologies are expensive and still limited (i.e. do not provide sufficient emission reductions) [2].

In addition, as emissions would be reduced by improving fuel economy, several new techniques are currently being considered. These techniques include variable compression ratio, variable cam timing, variable valve lift, direct injection of gasoline and advanced transmission technologies.

It is however important to note that the tribology and tribochemistry fundamentals can also play a vital role in improving the fuel economy through the use of new surface coating techniques, new materials and lubricant additive chemistry.

In the transport sector, fuel energy in a typical passenger car is consumed in three main parts (i) the mechanical power, (ii) the exhaust system and (iii) the cooling system. The mechanical power consists of the engine, transmission system, rolling resistance, brakes and drag. Fig. 1-1 shows that only about 21.5% of the fuel energy is used to move a passenger car [4].

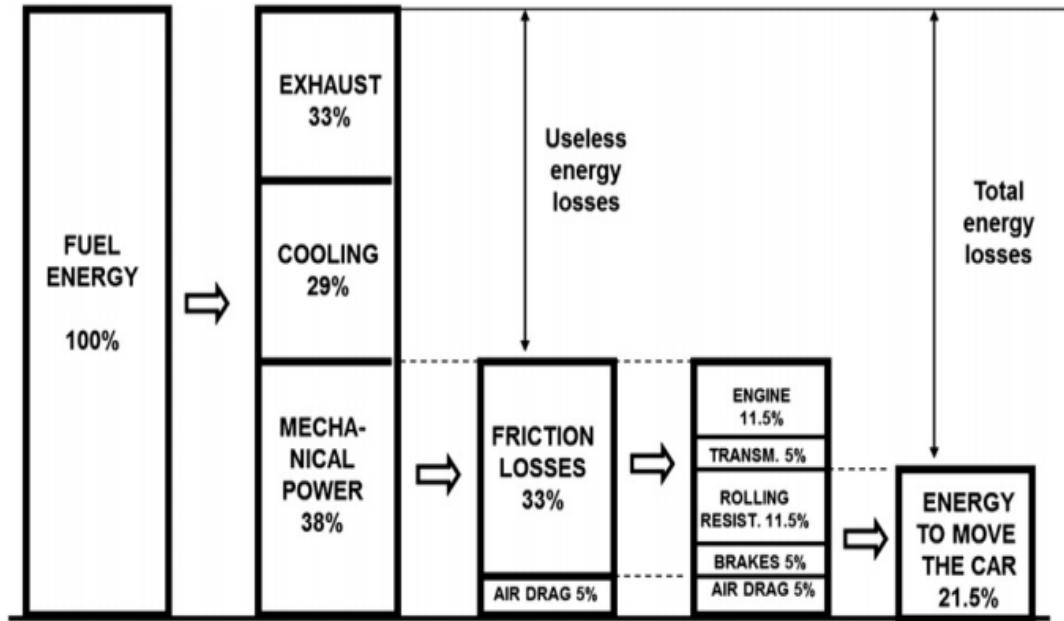


Figure 1-1 Breakdown of passenger car energy consumption [4]

In an internal combustion engine with a crankshaft rotating at 6000 rpm, the frictional losses mostly come from three main components, namely piston assembly, bearings and valvetrain [5, 6]. The mechanical energy consumption from these components has been reported previously [4, 7] (see Fig. 1-2).

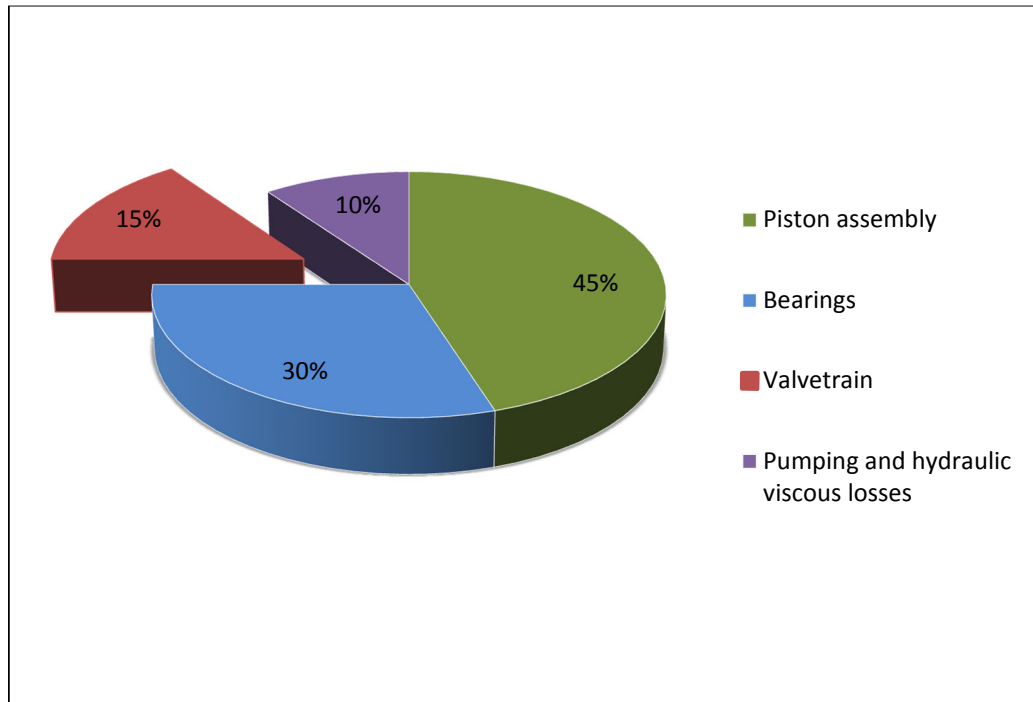


Figure 1-2 Mechanical losses in an internal combustion engine

The valvetrain tribological performance has practically become more important with ever increasing trend of using lower viscosity engine oils and novel engine technologies such as start/stop technology. The valvetrain has the third largest energy loss and it experiences the greatest contact pressure among these four components. Moreover, frictional loss from the valvetrain is generally found to be lower than piston assembly and engine bearings, but at low engine speeds (mainly under boundary lubrication regime), its relative importance is much greater. The valvetrain is believed to be responsible for 6-10% of the total frictional loss in an engine, depending on the design [8, 9]. Thus, the valvetrain assembly has also been the focus of efforts to improve fuel efficiency by minimising friction losses. For example, the move to overhead camshaft (OHC) configurations was successful but resulted in high friction and wear [6, 10].

In addition, the components of valvetrain are considered complicated in terms of design and effective lubrication [6, 10, 11]. In terms of wear, valvetrain components are considered the most critical factors limiting the life and performance of automotive engines [12]. A potential reason for this is that the valvetrain is subjected to sliding/rolling motion, different lubrication regimes, and high acceleration speeds causing increased inertia forces and applying high stress on the structure. Therefore, many researchers have focused on studying the valvetrain system in order to improve engine efficiency and durability which in return leads to improved fuel economy and reduced emissions.

Cams and followers are considered the most important and interesting tribological components of the automobile valvetrain [13]. They are reported to possibly be responsible for 85-90% of the total friction losses in engine valvetrains [14]. In addition, the camlobe is considered a critical area that suffers from high wear which increases rapidly with time [15].

Thus, in order to support the UK to achieve their target in 2050, optimizing this tribopair (cam and follower) is crucial and it is important to determine how changes in design, additives, oil formulations, materials and coatings affect wear, friction and lubrication.

Based on the literature, many gaps were identified. This research addresses the following gaps:

- Poor understanding of the effect of tribochemistry on real cam/follower contacts.
- Significant attention has been focused on the tribochemistry and wear of the follower/tappet with little consideration of the camlobe.
- No reports have been published which address the impact of clearance on friction, wear and tribochemical responses in a valvetrain system.
- No work has been reported on the performance of tappet rotation under the effect of different coatings, thicknesses of tappets and formulations with Molybdenum Dialkyl Dithiocarbamate (MoDTC) which has been found to be problematic to Diamond-Like Carbon (DLC) wear.
- Pure sliding contacts of DLC/cast iron systems have traditionally been the focus of research; consequently less is understood about sliding/rolling contact systems.
- No studies have investigated how sliding/rolling ratios affect tribofilm build-up and oil chemistry in a DLC/cast iron system lubricated with MoDTC-type friction modifier.
- Tribochemistry of DLC is essentially an area which needs more systematic attention to accurately define how the characteristics of DLC affect the interactions with the lubricant additives (especially MoDTC) under the effect of type of contact and tappet clearance.

With the assistance of tribological and tribochemical principles, focusing on the behaviour of cam/follower tribopair as a function of various factors (e.g. tappet rotation, tappet clearance, type of contact, oil formulations and additives, surface coating, camlobe wear and tribofilm across the camlobe) is essential to provide a better understanding of engine valvetrains, which could potentially lead to reduced emissions and fuel consumption (i.e. support the UK to meet the target for 2050 [1]).

1.2. Objectives and Scope of Research

The key objectives of this project are:

- To examine the friction and wear modes of the camlobes/tappets under the effect of tappet clearance and type of coating.
- To map the tribochemical films across the camlobes as well as the tappets, with the tappet coating and clearance being the parameters of focus.
- To develop a novel technique to measure tappet rotation.
- To link the rotation of different thicknesses/coatings of tappets to the tribological and tribochemical characteristics of cam/follower interface when lubricated in a fully formulated oil with and without MoDTC.
- To investigate the tribofilm formation towards changes in the tribological system, such as changing the type of contact (i.e. pure sliding contact and sliding/rolling contact).
- To link a bench top tribometer Mini Traction Machine (MTM) to a component level Single Cam Rig (SCR).

1.3. Thesis Outline

The thesis is divided into ten chapters including this introduction. **Chapter 2** presents the fundamentals of tribology. The literature review in the field of cam/follower tribology and tribochemistry is presented in **Chapter 3**. This chapter also addresses the nature of the tribofilm formed from known friction modifier and anti-wear additives. Further, additive/additive and additive/DLC interactions are also discussed in this Chapter. The development of tappet rotation technique, materials, equipment and experimental methodology are presented in **Chapter 4**. Mini traction machine (MTM) results are reported in **Chapter 5**. This Chapter evaluates friction, wear and tribochemistry of different lubricant formulations under pure sliding and sliding/rolling contacts. **Chapter 6** presents the tribological results (i.e. friction and wear results as a function of temperature, oil formulation, tappet clearance and type of coating)

obtained from single cam rig (SCR) tribometer. **Chapter 7** presents tappet rotation results when lubricated in a fully formulated oil with and without MoDTC-type friction modifier. **Chapter 8** evaluates the tribochemistry of tribofilms formed from single cam rig tribometer using different surface analysis techniques. Discussions on results obtained from Chapter 5 to Chapter 8 are presented in **Chapter 9**. Main conclusions from this study are detailed in **Chapter 10**. In addition, recommendations for future work are also outlined in this Chapter.

Chapter 2. Fundamentals of Tribology

2.1. Introduction

Tribology is defined as “the science and technology of two interacting surfaces in relative motion and of related subjects and practices” [16, 17]. Tribology comes from the Greek word *tribos*, which relates to rubbing or sliding. Important aspects of tribology have been friction, wear and lubrication since the introduction of this science. The term tribology was first used in a landmark report by Peter Jost in 1966 as a result of a government report in England which highlighted the importance of tribology to the UK economy by reporting the economic impact of poor tribological principles and practices. The Jost report provided potential savings of over £500 million annually for British industry through better understanding of tribological application, which in return led to improved design of lubrication procedures [17-21].

Tribology is relatively a new word but definitely is not a new field. Early practical applications of tribology have been recognized before the initiation of any historical records. Ignition of fire by the Palaeolithic people and development of the wheel. The first recorded tribologist was 2400 B.C., when Egyptians used a lubricant to transport the statue of Ti – from a tomb at Saqqara [22]. However, tribology science started with friction observations issued by Leonardo Da Vinci (1452 to 1519), lubrication studies reported by Sir Isaac Newton (1642 to 1727) and wear studies featured in the middle of the twentieth century [16, 23].

2.2. Friction

Friction is resistance to motion encountered when one body moves tangentially over another [16]. Different regimes of friction can be found between interacting surfaces, such as dry friction, boundary friction, fluid film friction and mixed friction [21]. The coefficient of friction (μ) is defined by $\mu = \frac{F}{W}$ where (F) is the tangential force and (W) is the normal applied load. The typical ranges of the coefficient of friction are from 0.03 for a lubricated surface to 0.5 - 0.7 for a dry sliding [24].

Friction is undesirable phenomena to many applications because the continuous friction causes energy loss, unnecessary wear, noise and heat. It should be mentioned, however, that not all friction is undesirable. High friction plays a vital role in particular applications (e.g. brakes, clutches. etc.).

2.3. Wear

Wear is defined as “a progressive damage, involving material loss, which occurs on the surface of a body as a result of its motion over another” [16]. It is considered as the major cause of loss in mechanical performance [25]. Wear occurrence is undesirable in most applications, except few cases, wear becomes necessary either in running-in procedures [21] or in metal machining (e.g. grinding, polishing and lapping) [16]. Volume of wear is commonly measured by using the volume loss method (Archard wear equation) as follows:

$$V = KWx \qquad 2 - 1$$

Based on Archard equation, the total wear volume is proportional to the real contact area multiplied by the sliding distance, where V represents the worn volume (m^3), K is the dimensional wear factor with units generally expressed as ($mm^3N^{-1}mm^{-1}$), W represents the normal load and x represents the sliding distance. The dimensional wear factor, K , is a function of the interacting materials, the lubricant and the operating conditions.

It should be mentioned that there are more than 35 mechanisms of wear [26]. Generally, there are five basic wear mechanisms; adhesive wear, abrasive wear, fatigue wear, corrosive wear and erosive wear.

2.3.1 Adhesive Wear

This mechanism causes plastic deformation, adhesion and sometimes welding of the contacting asperities. The cold welding at asperity injections leads to material transfer from one surface to another. Adhesive wear is considered the most common and least preventable form of wear. There are

three general steps leading to adhesive wear (see Fig. 2-1). It should be noted that any severe adhesive wear can lead to produce two phenomena, galling and scuffing. In lubricated components, it is called scuffing and in systems without lubrication, it is called galling [16, 22]. These phenomena result in a catastrophic damage and roughened surface.

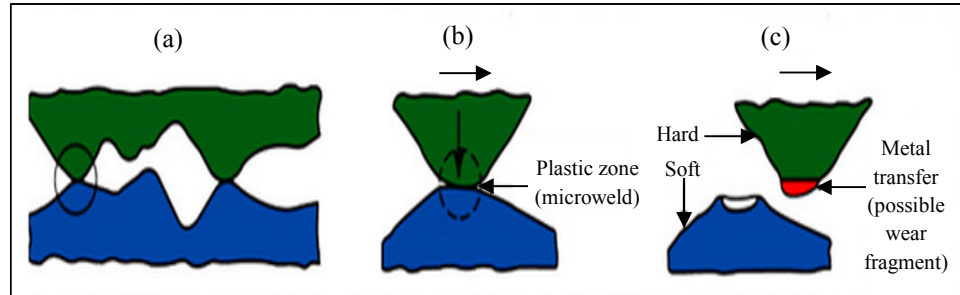


Figure 2-1 Steps leading to adhesive wear [26]

2.3.2 Abrasive Wear

This form of wear is called also cutting wear and can be defined as wear due to hard particles or hard protuberances forced against and moving along a solid surface. Abrasive wear is typically caused by non-metallic materials. The most common reason to produce the mechanisms of abrasive wear is the Micro-cutting (i.e. sharp particle or hard asperity cuts the softer surface). Other reasons are micro-fracture, micro-fatigue and removal of material grains [24, 26].

There are two main mechanisms of abrasive wear; two-body abrasion and three-body abrasion. Two-body abrasion is the mechanism that happens between two interacting surfaces, one of these surfaces is harder than the other. Three-body abrasion is the mechanism that happens between three bodies, two interacting surfaces with a piece removed from softer surface by hard particles.

Scoring or sometimes called scratching is a phenomenon which occurs due to abrasive wear. From Fig. 2-2, it can be seen that the harder surface scratches the softer surface. As a result, this produces a pattern of scratches on the surface which can lead to severe failure in some cases. Polishing is another phenomenon which caused by mild abrasive wear. It is worth

mentioning that the polished surface is unable to keep enough lubricant and will be starved of sufficient lubricant; this in turn could lead to a catastrophic failure in lubricated components [16].

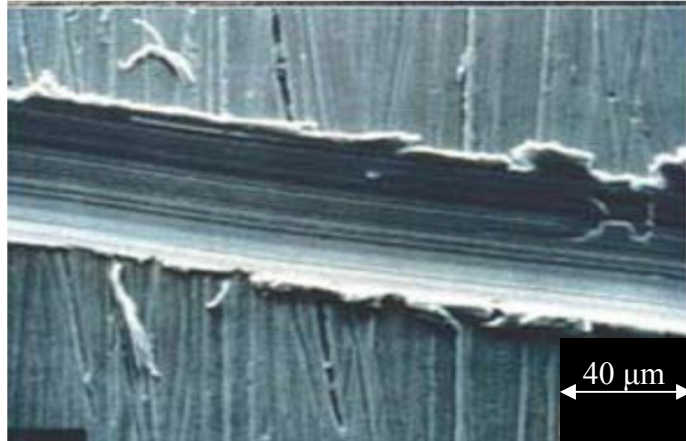


Figure 2-2 Abrasive wear, scratching [22]

2.3.3 Fatigue Wear

This mechanism causes the removal of material from the contacting surfaces by fatigue due to cyclic stress changes over a long period of time [16]. Fatigue wear occurs in many applications (e.g. cam/follower system, rolling bearings and gears) due to cyclic loading [26]. Pitting is a phenomenon which results from a consequence of fatigue wear; this can lead to produce pits on the surface. It is considered a common phenomenon in rolling bearings that run under high vibration and noise [16] (see Fig. 2-3).



Figure 2-3 Fatigue wear in a roller bearing [26]

2.3.4 Corrosive Wear

Corrosive wear is caused by a combination of chemical reaction and mechanical action (rubbing) [16]. The chemical reaction occurs between the material and a corroding medium (e.g. a chemical reagent, reactive lubricant or air) [26]. Corrosive wear is a common damage in couplings used for connecting shaft and motor (see Fig. 2-4). Fretting is a phenomenon that results from a synergy between corrosive, adhesive and abrasive wear [16]. In addition, fretting typically occurs in metal surfaces where the degree of relative motion is small (e.g. splined flanges).

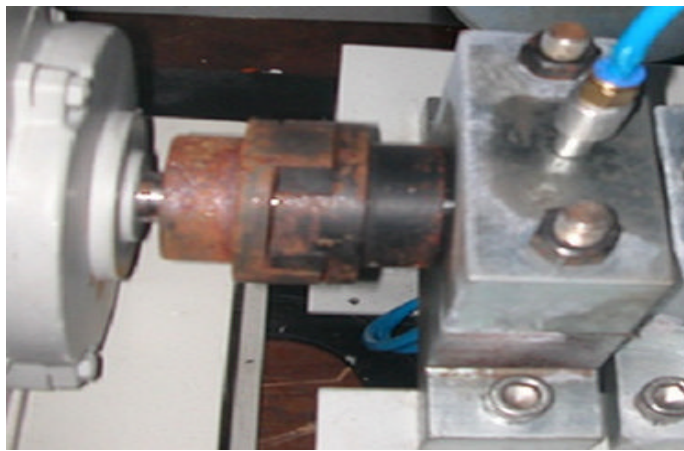


Figure 2-4 Corrosive wear, coupling [26]

2.3.5 Erosive Wear

This mechanism is caused by the impact of hard solid particles carried by a fluid and can lead to a damage to the surface. This type of wear has three basic mechanisms, (i) fluid erosion caused when small droplets of fluid hit the surface under high speeds, (ii) cavitation erosion caused from the collapse of vapour bubbles in the fluid and (iii) spark erosion caused from an electrical spark between two surfaces and can lead to the removal of material [16, 26].

2.4. Lubrication

Lubrication can be defined as effective interposition of a material between two bodies with the purpose of reducing/preventing both wear and the lost energy

due to friction. The material is called a lubricant which contains a wide range of materials including mineral oil, synthetic oil, vegetable oil, grease, process fluid, water, air, solid, etc. Likewise, the lubricant is any substance used to reduce friction and wear. Accordingly, this would lead to smooth running and longer life of tribological components [27].

The form of lubrication is dependent on materials of the surfaces, lubricant properties, operating conditions (e.g. speed, load, temperature, environment and etc.), surface conformity and texture. Four lubrication regimes can be identified depending on the thickness of the tribofilm and the geometric conformity of the surfaces. These four regimes allow the performance analysis of a tribological system usually in terms of friction and wear.

2.4.1 Lubrication Regimes

The lubrication regimes are hydrodynamic lubrication, boundary lubrication, mixed lubrication and elastohydrodynamic lubrication. Table 2-1 represents the definitions of these regimes.

Table 2-1 The definitions of lubrication regimes [28]

Regime of Lubrication	Characteristics
Hydrodynamic	Full fluid film lubrication in which the surfaces are completely separated. The dynamic viscosity of the lubricant is its most important property
Elastohydrodynamic	Nominally also full fluid film lubrication with surface separation, but a more concentrated mechanism where elastic deformation of the surfaces and the effect of pressure on viscosity are important
Mixed	There is surface asperity interaction to some degree and the characteristics of both Elastohydrodynamic and Boundary Lubrication are influential
Boundary	The surfaces are in normal contact with behaviour characterized by the chemical (and physical) actions of thin films of molecular proportions

Early in the 20th century, an original research presented by Stribeck explained the relationship between the coefficient of friction and lubrication regime for engine components. Figure 2-5 shows a modified Stribeck diagram where the lambda ratio (λ) is defined as the ratio between minimum film thickness and the composite surface roughness (see Equation 2-2).

$$\lambda = \frac{h_{min}}{\sigma_{rms}} = \frac{h_{min}}{\sum R_q} = \frac{h_{min}}{\sqrt{R_{q1}^2 + R_{q2}^2}} \quad 2 - 2$$

Where h_{min} is the minimum film thickness, R_q is the Root Mean Square (RMS) roughness of the two surfaces in contact. The minimum film thickness (h_{min}) for a point contact is numerically defined as [29]:

$$\frac{h_{min}}{R} = 3.63 \left(\frac{U\eta_0}{E'R} \right)^{0.68} (\alpha E')^{0.49} \left(\frac{W}{E'R^2} \right)^{-0.073} (1 - e^{-0.68k}) \quad 2 - 3$$

Where R is the reduced radius of curvature, U is the entraining surface velocity, η_0 is the dynamic viscosity of the lubricant at atmospheric pressure, α is the viscosity-pressure coefficient, W is the normal load, E' is the reduced Young's modulus, K is the ellipticity parameter defined as: $K = a/b$, where 'a' is the semiaxis of the contact ellipse in the transverse direction (m) and 'b' is the semiaxis in the direction of motion (m), for point contact $K=1$.

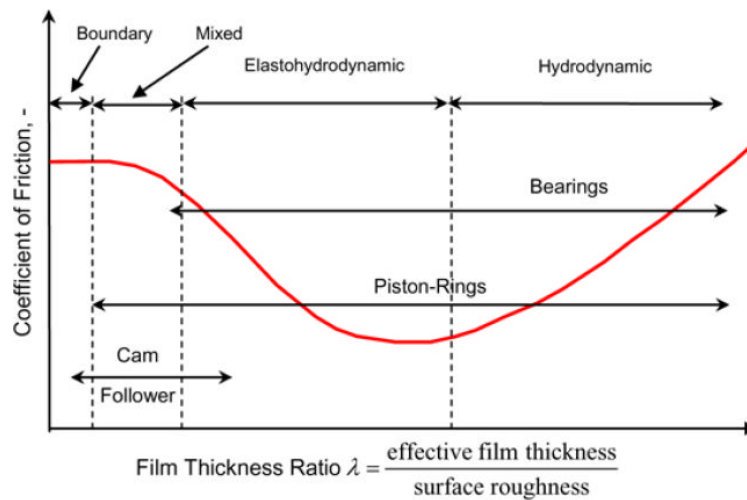


Figure 2-5 The modified Stribeck diagram [30]

For a line contact, the minimum film thickness can be calculated from the Dowson and Higginson equation [31].

Minimum film thickness formula $\frac{h_{min}}{R_e} = \frac{2.65G^{0.54}U^{0.7}}{W^{0.13}}$ 2 – 4

Dimensionless material parameter $G = \alpha E'$ 2 – 5

Dimensionless speed parameter $U = \frac{\eta_0 \times u}{E' \times R_e}$ 2 – 6

Dimensionless load parameter $W = \frac{w}{E' \times R_e}$ 2 – 7

Where η is the dynamic viscosity, w is the load per unit length (N/m), E' is the equivalent elastic modulus (N/m²), u is the entrainment velocity (m/s) and R_e is the equivalent radius (m).

2.4.1.1 Boundary Lubrication

Under boundary lubrication (BL) ($\lambda < 1$) (see Fig. 2-6), extensive interactions occur in this region and these interactions become more severe with low speed and high load. Density and viscosity and all other physical properties of the bulk lubricant are not as important as the chemical properties of the lubricant and the properties of the surfaces in contact [16, 30, 32].

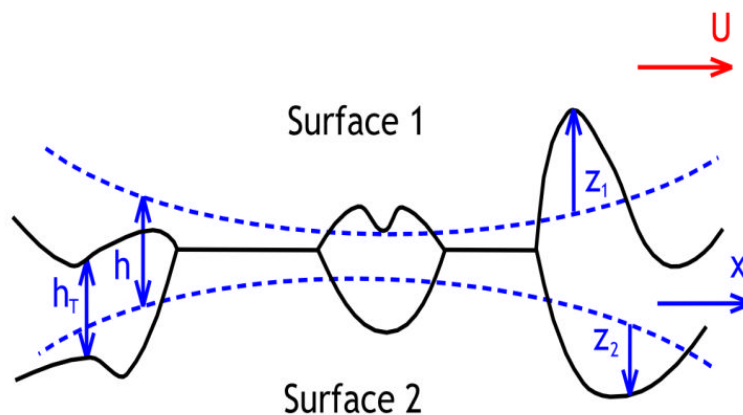


Figure 2-6 Boundary lubrication [16]

In Fig. 2-6, the dashed lines are the centre lines of the two surface profiles and

x : is the horizontal coordinate

Z_1 : is the vertical displacement of surface 1 from the centre line at any x

Z_2 : is the vertical displacement of surface 2 from the centre line at any x

h : is the vertical separation of the centre lines of surface 1 and 2 at any x

h_T : is the vertical separation of surface 1 and 2 at any x

U : is the relative sliding velocity between surface 1 and surface 2

2.4.1.2 Mixed Lubrication

In mixed lubrication (ML) ($1 < \lambda < 5$) (see Fig. 2-7), the full film lubrication becomes relatively difficult to maintain if the speed is further decreasing and if the load is high. In this regime, the lubricant film provides partial separation whereas the contact load is shared between the contacting asperities and the film resulted in some mechanical interactions [16, 30].

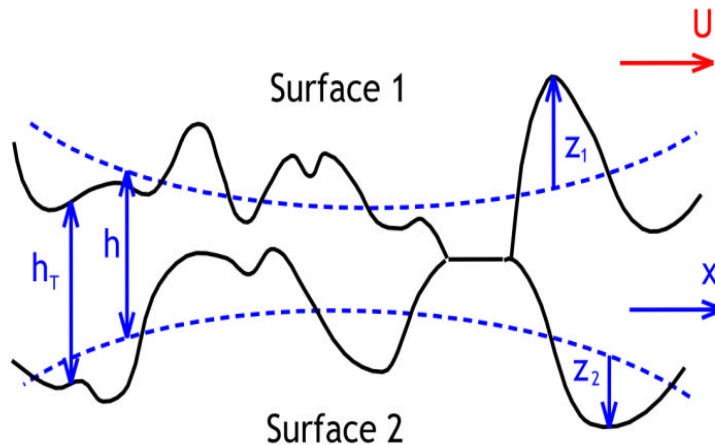


Figure 2-7 Mixed lubrication [16]

2.4.1.3 Elastohydrodynamic Lubrication

Elastohydrodynamic lubrication (EHL) ($4/5 < \lambda < 10$) (see Fig. 2-8), is an extension of hydrodynamic lubrication. In other words, in EHL, the two

surfaces are also separated with a lubricant film, although the film is thinner (typically $0.5\text{-}5\ \mu\text{m}$) than that in the hydrodynamic lubrication regime, but with high local pressure causes increase in viscosity and elastic deformation of the contacting bodies [16, 32-34].

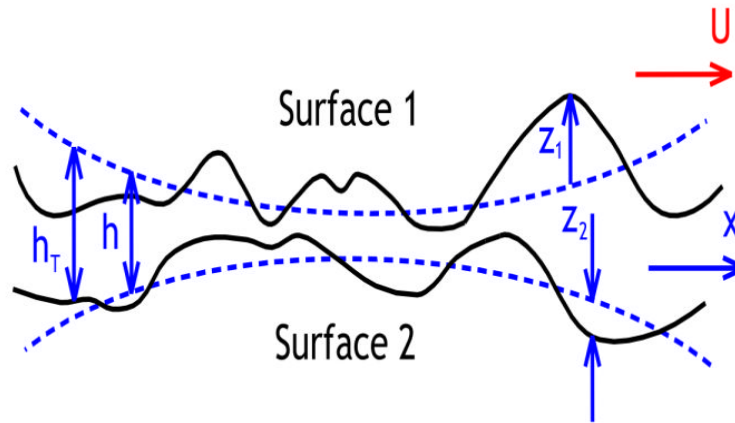


Figure 2-8 Elastohydrodynamic lubrication [16]

2.4.1.4 Hydrodynamic Lubrication

Hydrodynamic lubrication regime (HL) ($\lambda > 6$) (see Fig. 2-9), is the most desirable form of lubrication because the contacting surfaces are completely separated by the lubricant fluid film (i.e. the film is sufficiently thick, typically $5\text{-}500\ \mu\text{m}$) and there is no wear should occur. Therefore, friction is the main concern in this regime. To reduce friction, oils with low viscosities are usually preferred.

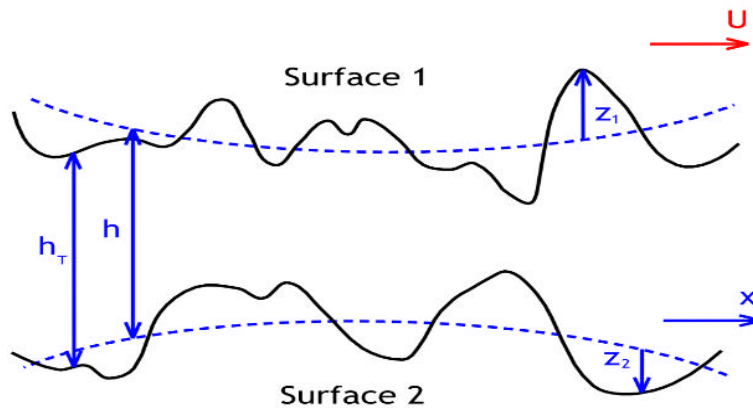


Figure 2-9 Hydrodynamic lubrication [16]

2.4.2 Lubricants

Lubricants are used between interacting surfaces in order to control friction and wear. The appropriate selection of lubricants leads to better lubrication (i.e. provides an assistance to improve lubricity, reduce friction and prevent wear).

Generally speaking, until the 1930s, the engine crankcase lubricants were mainly base oils with no additives [35]. Nowadays, a lubricant typically consists of more than 20 additives blended with the base oil [36].

There are different types of base oils such as mineral oils, synthetic oils and vegetable oils. According to the American Petroleum Institute (API 1509), base oils are grouped into five main categories (see Table 2-2) based on certain properties of base oils, including viscosity index and the proportion of saturates and sulphur content.

Table 2-2 Base oil categories [37, 38]

		API BASE OIL CATEGORIES				
		Base Oil Category	Sulfur (%)	Saturates (%)	Viscosity Index	
Mineral		Group I (solvent refined)	>0.03	and/or	<90	80 to 120
		Group II (hydrotreated)	>0.03	and	>90	80 to 120
		Group III (hydrocracked)	<0.03	and	>90	>120
Synthetic		Group IV	PAO Synthetic Lubricants			
		Group V	All other base oils not included in Groups I, II, III or IV			

In automotive lubricants which contain base oils and additives, the proper selection of base oils is also essential because their physical and chemical properties would influence the effectiveness of the additives [38]. Base oils can be mineral or synthetic oils. Mineral oils are produced in very large

quantities from natural crude oil. They typically consist of hydrocarbons together with nitrogen, oxygen and sulphur. However, at temperatures above 80 °C, mineral oils start to degrade and thus their oxidation stability is not as good as synthetic oils.

Synthetic oils are hydrocarbons with a fully controlled chemical structure. They are more expensive than mineral oils but they can offer high performance based on their interacting properties (i.e. synthetic oils provide a better thermal stability, oxidative stability, viscosity and flow characteristics). There are different types of synthetic oils; Polyalphaolefins (PAO) is considered the most common type and are derived from ethylene and esters [38, 39].

In general, base oils do not have sufficient properties such as engine cleanliness, sufficient cooling, oxidation stability, soot handling, friction and wear-resistant. Thus, several additives have been used to increase the performance of the lubricants. For example, antioxidants, detergents, dispersant, anti-wear, metal deactivators, corrosion inhibitors, rust inhibitors, friction modifiers, extreme pressure, viscosity index improvers and others.

2.4.3 Additives

Increasing demands for improved fuel economy and reduced emissions have led to the development of different additives. Initially, the additives are chemicals blended with the base oil. These additives enhance the quality of base oils through forming a complete package (fully formulated oils) which is capable to achieve performance objectives. Fully formulated (FF) oils typically contain friction modifiers, an antiwear agent, one or perhaps two dispersants, one or two detergents, corrosion inhibitors, oxidation inhibitors, foam inhibitors, pour point depressants and viscosity modifiers [39, 40].

The typical concentration range of additives used in the formulation of automotive crankcase engine oils has been summarized in Table 2-3. Also, Fig. 2-10 illustrates the steps of developments of the most common additives. In 1918, oiliness additives were first discovered and used to reduce friction in marine engine lubricants [41]. In addition, between 1930 and 1940, a wide range of additive glasses were discovered (e.g. extreme pressure (EP), pour

point depressants, antioxidants, viscosity modifiers, corrosion inhibitors and detergents). Furthermore, to solve issues in aviation applications, antiwear additives were also developed in the 1940s [42]. However, antiwear additives shortly became an essential component of engine motor oils. In addition, although most additive classes were identified in the 1940s, much remains to be done in developing new chemistries.

Table 2-3 Typical ranges of composition of engine crankcase lubricants [43]

Function	Component	Concentration, wt%
Base oil (mineral and/or synthetic)		75 – 95
Friction and wear	Viscosity index improver	0 – 6
	Anti-wear additive	0.5 – 2
	Friction reducer	0 – 2
	Rust/corrosion inhibitors	0 – 1
Contamination and cleanliness	Antioxidant	0 – 1
	Dispersant	1 – 10
	Detergent	2 – 8
Maintain fluid properties	Pour point depressant	0 – 0.5
	Anti-foam additive	0 – 0.001

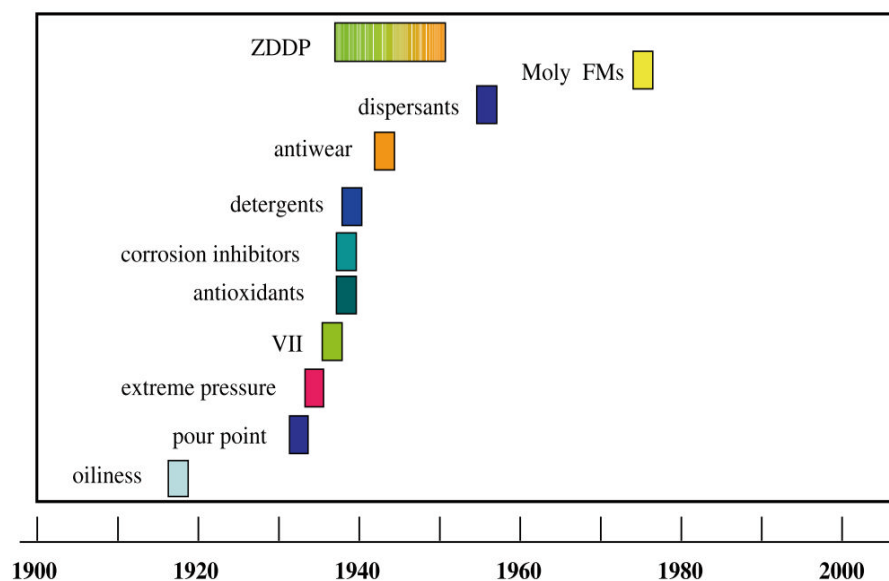


Figure 2-10 Chronology of development of main classes of lubricant additive

Each additive has a specific function, the main functions typically are friction reduction, corrosion protection, heat transfer, operating at extremes of temperature, engine seals protection, suspension of crankcase oil contaminants, ensure continued efficient performance [35]. In general, lubricant additives can be classified into two categories. Firstly, additives that protect metal surfaces in the engines, such as anti-wear, anti-corrosion and anti-rust additives. Secondly, additives that reinforce base oil performance, such as antioxidants, dispersants and viscosity modifiers. The typical additive package range in the lubricant is about 5–25% [43]. The main additive component families used in lubricants are summarized below:

2.4.3.1 Detergents

These additives are chemical compounds that form under high temperature conditions or due to combustion processes in an engine. They can be neutral or overbased and they are well-known as stabilizers or deposit control agents. The main function is to reduce or remove deposits from forming on metal surfaces which commonly due to oil oxidation and contamination. Thus, detergents keep the engine clean and maintain emissions performance long-term. In addition, they are used as organic soaps and salts. It should be mentioned that calcium, sodium and magnesium are the most common metals used in detergents [35, 39, 40, 45].

2.4.3.2 Dispersants

Dispersants are also chemical compounds that do not contain metal to form ash on combustion. Thus, they are usually referred to as ashless dispersants. Three main types of ashless dispersant are typically in use, succinimides, succinic esters of polyols, and mannich bases. Dispersants disperse and control insoluble contaminants and sludge deposit at relatively low temperatures (100 °C or below). Therefore, they are generally used in engine oil to control soot effects and to minimize harmful engine exhaust emissions, and extend engine life. Dispersants are more effective than detergents in

terms of some functions, such as suspending and cleaning, due to their high molecular weight [35, 39, 40, 45].

2.4.3.3 Oxidation Inhibitors

The main purpose of oxidation inhibitors is to prevent, minimize or reduce oil oxidation, which initially leads to the oil darkening and thickening (increase of oil viscosity). Further oxidation contributes to build polymeric materials which in turn cause varnish deposits in some engine components.

The important and common antioxidants classes are hindered phenols, amines, sulfur and phosphorus compounds. It is largely important to maximize oxidation stability in lubricants because it will assist in preventing oil degradation [35, 39, 45].

2.4.3.4 Pour Point Depressants

These additives keep the oil flowing at low temperatures, by lowering the pour point. In cold climates, the formation of wax crystal structure will not permit an oil flow.

The most common chemical types are the polyacrylates and the polymethacrylates, their function is to inhibit the formation of interlocking crystal networks. Accordingly, this would prevent the lubricant from solidifying at low temperatures [35, 39, 40].

2.4.3.5 Viscosity Index Improvers

Also known as viscosity modifiers, function by providing increased viscosity contribution at higher temperatures and minimizing viscosity at lower temperatures. They are high molecular weight polymers. The main chemical families are olefin copolymers, hydrogenated styrene-diene copolymers and polyalkylmethacrylates [35, 45].

2.4.3.6 Friction Modifiers

Friction modifiers or lubricity additives form films to reduce the frictional losses between the moving surfaces. In an engine, it is generally proven that these additives are essential for components that mostly operate under boundary and mixed lubrication regimes such as the valvetrain. Friction modifiers are closely related to anti-wear additives and extreme-pressure (EP) additives in mode of action.

There are two types of friction modifiers, (i) metal-containing friction modifiers (MFMs) such as molybdenum dithiocarbamate (MoDTC) or molybdenum dithiophosphates (MoDTP) and (ii) organic friction modifiers (carbon, hydrogen and oxygen only).

The common friction modifier types are molybdenum compounds (e.g. MoDTC or MoDTP), Polyol esters of fatty acids (e.g. glyceryl monooleate), and amides of fatty acids. It should be mentioned that MoDTC and MoDTP are considered as excellent friction modifiers and antiwear agents [35, 40, 45-47].

2.4.3.7 Anti-Wear Additives

Their mode of action is by reacting with metal surfaces and forming films that can reduce wear under elastohydrodynamic and boundary lubrication conditions. The most widely used in practice are organometallic (ZDDP, MoDTP, MoDTC) organosulphur, organochlorine, organophosphorus and organic borate compounds.

Zinc dithiophosphates (ZDDP) has been the most regularly used in engines lubrication [39, 40, 45-47]. This additive forms sulphides and phosphates to offer the antiwear property to the interacting surfaces [48]. ZDDP has also been reported to be corrosion inhibitor and antioxidant [35, 44].

2.4.3.8 Other Additives

There are many other important additive groups (e.g. antifoaming agents, corrosion inhibitors, rust inhibitors, emulsifiers, tackiness, etc.) which play an essential role on the lubricant performance in the tribological system. The use of hybrid nanomaterials as nano-lubricant additives have also been reported to reduce frictional power losses in automotive engines and can lead to an improvement in the efficiency of engines and fuel economy [49]. Results of a wide spectrum of nanoscale additives have been reported in the tribology literature and a review is beyond the scope of this work. It is important to note that the optimisation of the frictional and durability of a tribological contact relies upon the understanding of the surface/lubricant interactions and with replacements to conventional steel now being common place, a major priority is to understand how some of the conventional friction modifiers (like Molybdenum Dialkyl Dithiocarbamate (MoDTC)) interact with conventional (steel) and less conventional (DLC) surfaces. The heavy elements can be harmful to catalytic convertors but if some of the friction reduction can be offered by the inherent surface properties then there is potential to optimise formulations.

2.5. Hertzian Elastic Contact Analysis

According to Hertzian theory of elastic deformation in 1881, the contact between two elastic solids is assumed to be non-conformal [16, 50-52]. Therefore, it will be a point contact at a small area with high pressure. Hertz analysed the stresses at the contact of an elastic solid on a rigid plane (see Fig. 2-11), where this case represents many tribological applications (such as gears, ball and roller bearings, seals, cams and tappets, and wheels on rails). There are different types of contacts depending on the shape of the rubbing surfaces.

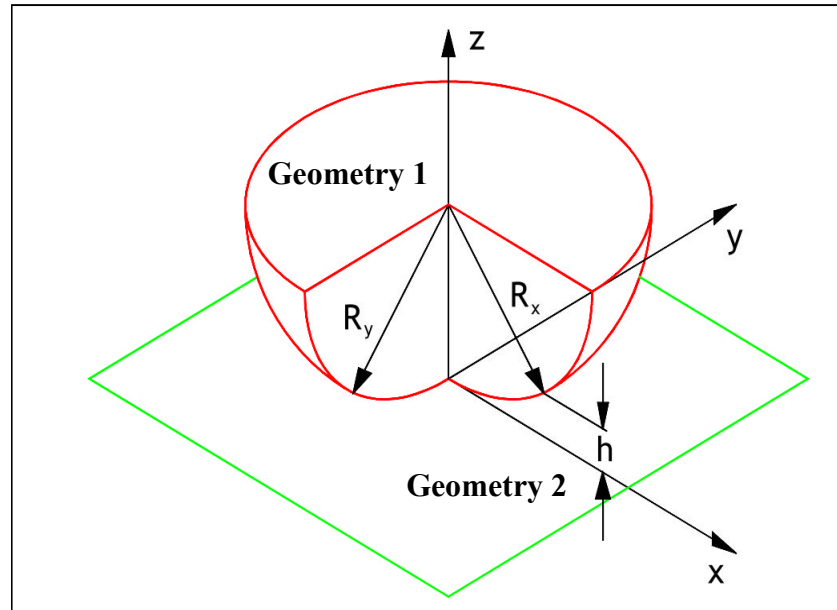


Figure 2-11 Equivalent elastic solid on a rigid plane [16]

The radius of the contact area (a) is given by:

$$a = \left(\frac{3WR}{2E'} \right)^{\frac{1}{3}} \quad 2 - 8$$

Where (W) is the normal load and (R) is the reduced radius of curvature and is defined as:

$$\frac{1}{R} = \frac{1}{R_x} + \frac{1}{R_y} \quad 2 - 9$$

Also, (E') is the reduced Young's modulus and is defined as:

$$\frac{1}{E'} = \frac{1}{2} \left(\frac{1 - \nu_1^2}{E_1} + \frac{1 - \nu_2^2}{E_2} \right) \quad 2 - 10$$

Where E_1, E_2 are the elastic moduli and ν_1, ν_2 the Poisson's ratios associated with each body.

Maximum contact pressure is defined as:

$$P_{max} = \frac{3W}{2\pi a^2} \quad 2 - 11$$

Average contact pressure is defined as:

$$P_{average} = \frac{2}{3} P_{max} = \frac{W}{\pi a^2} \quad 2 - 12$$

Maximum deflection is defined as:

$$\delta = 1.0397 \left(\frac{W^2}{E'^2 R} \right)^{\frac{1}{3}} \quad 2 - 13$$

However, the material of contact in some systems such as gears, cam/followers and rolling element bearings is subjected to high cyclic stresses and this can lead to the initiation of fatigue cracks [53].

In addition, maximum shear stress is defined as:

$$\tau_{max} = \frac{1}{3} P_{max} \quad 2 - 14$$

2.6. Cam/Follower Tribology Kinematics

Generally, kinematic analysis represents the calculations of displacement, velocity and acceleration. The analysis of cam motion that involves a direct

acting cam with a flat faced follower is crucial for the knowledge of cam/follower tribology.

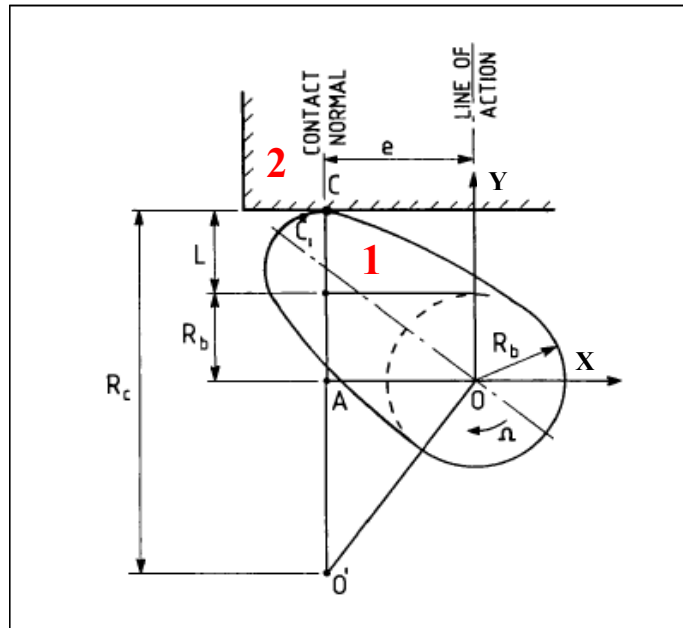


Figure 2-12 Geometry of a direct acting cam and follower [6]

Based on Fig. 2-12, the cam is designated as component number one while the follower (which is taken not to rotate about Y axis) is designated as component number two. There are two velocities for both cam and follower along the [x, y] direction. The velocity of cam along the x axis is u_1 and along the y axis is w_1 while the velocity of follower is $[u_2, w_2]$ along the [x, y] direction respectively. The cam rotates about its centre at O whilst O' is the centre of curvature of the cam surface at the instantaneous contact point (C). The follower linear velocity along the x axis is zero [6].

$$u_2 = 0 \quad 2 - 15$$

$$w_2 = e\Omega \quad 2 - 16$$

Where e is the lift and Ω is the angular velocity. From the derivative of Equation 2-16, the acceleration of the follower can be calculated as;

$$a = \frac{dw_2}{dt} = \dot{e}\Omega \quad 2 - 17$$

The x-velocity of the point on the cam in contact with the follower is derived as;

$$u_1 = (R_b + L)\Omega \quad 2 - 18$$

The velocity along the contact point on the cam surface can be calculated due consideration to sign as;

$$\dot{s} = u_1 + \dot{e} = [(R_b + L)\Omega] + \dot{e} \quad 2 - 19$$

The instantaneous radius of curvature of a point moving along a curve with velocity \dot{s} such that the angular velocity of the tangent to the point of contact at $\dot{\gamma}$ is given by;

$$R_c = \frac{\dot{s}}{\dot{\gamma}} = \frac{ds}{dt} \times \frac{dt}{d\gamma} \quad 2 - 20$$

For a flat faced follower, however, the mathematical expression is given by;

$$\frac{dt}{d\gamma} = \frac{1}{\Omega} \quad 2 - 21$$

$$R_c = \frac{\dot{s}}{\Omega} \quad 2 - 22$$

$$R_c = (R_b + L) + \frac{\dot{e}}{\Omega} = (R_b + L) + \frac{a}{\Omega^2} \quad 2 - 23$$

A sufficient accuracy can be obtained from the velocity of the cam contact point on the follower and the velocity at the corresponding points on the instantaneous radius of curvature.

$$u_{c1} = u_1 = (R_b + L)\Omega = \left(R_c - \frac{a}{\Omega^2}\right)\Omega \quad 2 - 24$$

2.7. Cyclic Film Thickness and Entrainment Velocity Variations

The cam profile plays an important role on the behaviour of the breathing and exhaust process in an engine. The typical variation of film thickness of direct-acting mechanical type is shown in Fig. 2-13. The area of interest is from the beginning of the opening flank through the cam nose to the end of the closing flank (-60° , 0° , 60°). The modest film over the nose and the two critical areas of 'zero' lubricant film-thickness is evident in Figure 2-13 (a). In addition, Figure 2-13 (b) illustrates an alternative presentation of variation of cyclic film thickness. It can be seen that there is a sufficient film on both flanks due to the high entraining velocity into the contact, but the film is thin over the cam nose due to the low entraining velocity [6]. Fig. 2-14 shows the effect of the camlobe profile on entrainment velocity. For most cams, the lubrication regime is expected to go through boundary at the nose, mixed and elastohydrodynamic lubrications at the flank.

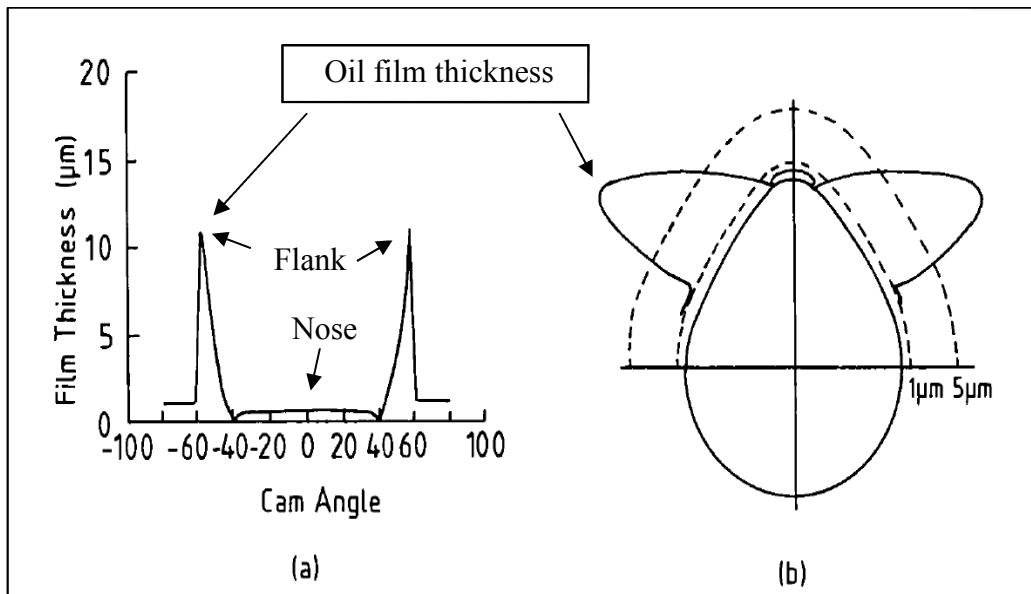


Figure 2-13 Typical variation of film thickness between direct acting cam and follower: (a) as a function of cam angle (b) around the cam circumference [6]

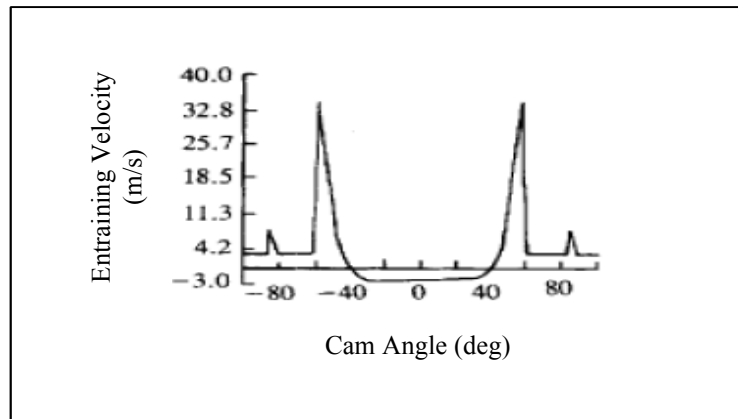


Figure 2-14 Effect of camlobe profile on entrainment velocity [54]

2.8. Torque Cycle

Figure 2-15 shows a typical variation in the input torque for a cam/follower contact which is based on one full revolution of the camshaft. The torque varies with each cycle and normally has both positive and negative pulses. Generally, positive pulses of torque represent energy delivered by the driver (the motor) and stored from moving of the follower as kinetic energy. The negative pulses as kinetic energy trying to return from the follower to the camshaft.

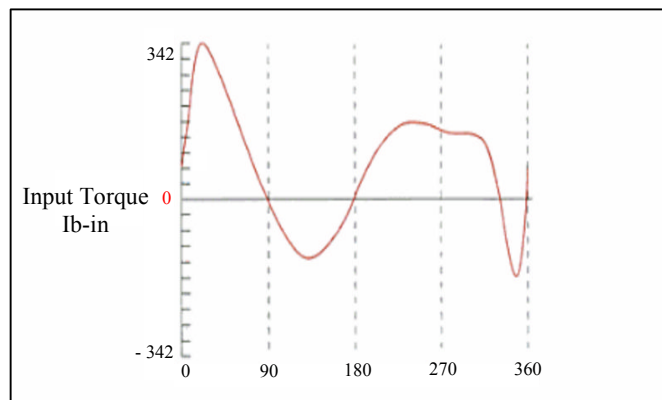


Figure 2-15 Input torque curve for a cam/follower mechanism [55]

2.9. Fuel Economy

To meet the emissions legislations, concerns in vehicle fuel economy have increased dramatically in the last few years. It is largely accepted that there is a direct correlation between fuel economy and friction losses (i.e., reducing

friction losses lead to increasing automotive engine fuel efficiency). As engine components (mainly piston assembly, bearings and valvetrain) experience different lubrication regimes, the simplest way to create a fuel-efficient lubricant is to reduce the viscosity (to give benefits in pistons and bearings) while at the same time adding an effective friction modifier (which gives benefits in the valvetrain) [56]. Fig. 2-16 illustrates the correlation between power loss and speed/load at different location regimes. Fig. 2-16 clearly shows that if the lubricant viscosity is reduced, the total engine power loss will reduce immediately. Additionally, MoDTC is necessary in the components that operate in the boundary lubrication regime; it makes an attractive reduction of power loss [57].

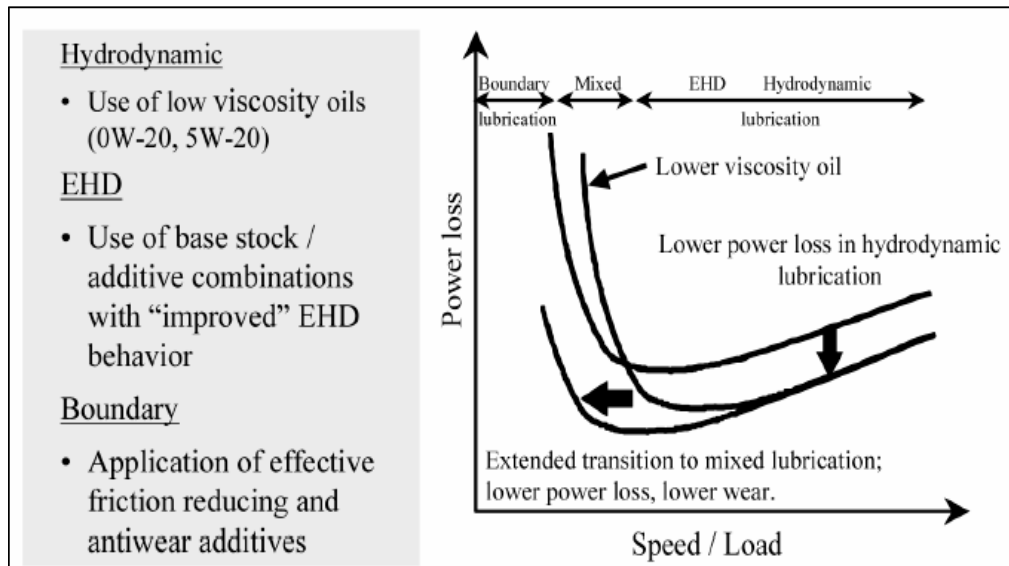


Figure 2-16 Minimising total engine power loss and wear [46]

Chapter 3. Literature Review

3.1. Introduction

In this chapter, a comprehensive literature review will be conducted on valvetrain systems, mainly on the cam/follower tribopair. Furthermore, Diamond-Like Carbon (DLC) coatings and their properties will be described. In addition, the nature of the tribofilm formed from MoDTC and ZDDP additives will be presented. This review will also aim to cover the interactions between MoDTC/ZDDP additives and lubricant/DLC coating. The gaps in the literature in terms of tappet rotation, tappet clearance, tribochemistry and wear of camlobe as well as sliding/rolling contacts will be presented and discussed. Finally, a summary of the gaps will be reported in the last section of this chapter.

3.2. Overview of Valvetrain Systems

Over the years, many studies and developments have been made in valvetrain systems for the reason of reducing emissions and increasing fuel economy. These studies and developments are followed several procedures such as using new or modified designs, materials, surfaces coating and additives.

The valvetrain assembly is the group of components that controls the operation of the valves. In other words, it controls the induction and exhaust processes of an internal combustion engine. The components of valvetrain would vary based on the engine design. Typically, the valvetrain consists of valves, cams, valvetrain lash compensators, seat inserts, valve guides, rocker arms, valve springs, retainers, and other components [58].

Fig. 3-1 shows the main components of a direct acting mechanical bucket (DAMB) type valvetrain [59]. The major function of the valvetrain system is to transfer rotary camshaft motion into linear valve motion. The camshaft is considered as the heart of the engine and responsible for opening the valves, through pushing the camlobes against the valvetrain parts resulting in opening the valves at specific times [60].

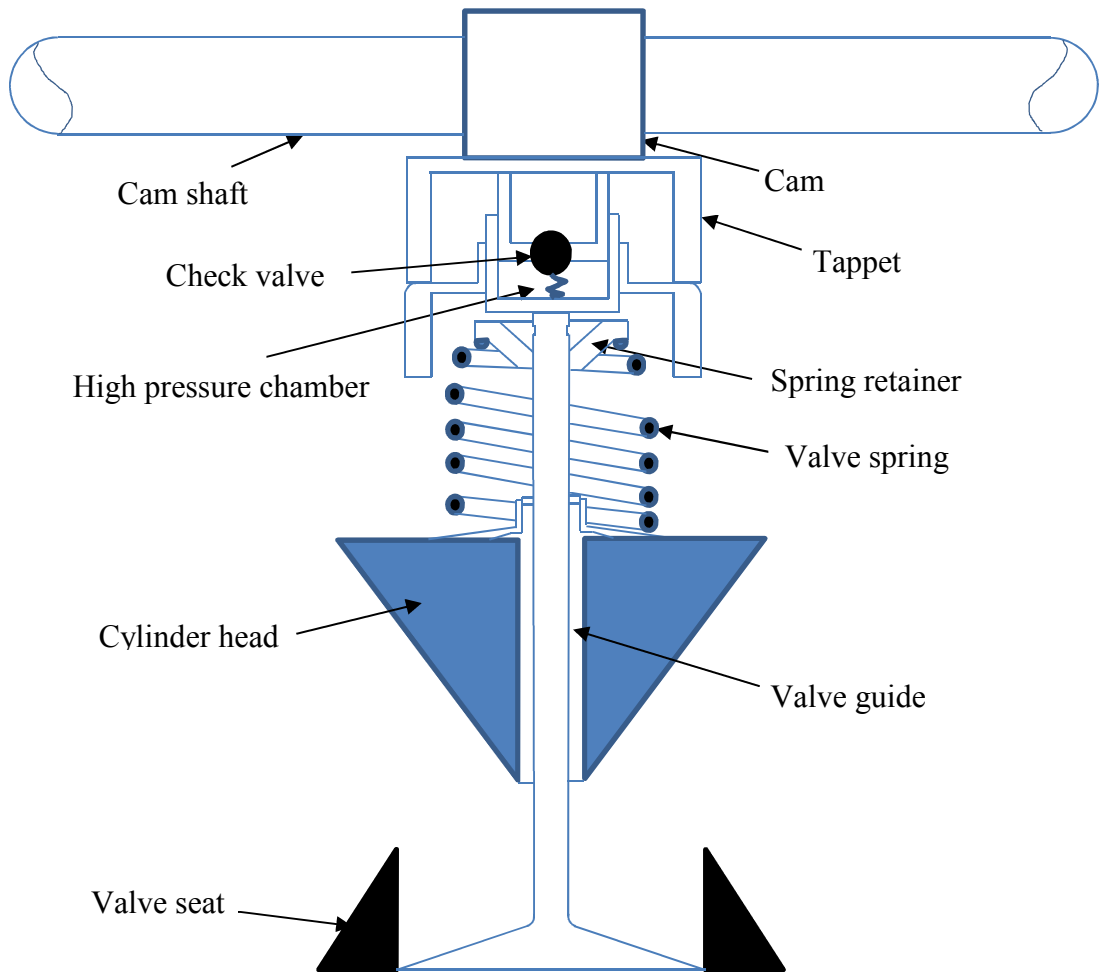


Figure 3-1 Schematic diagram of a valvetrain system [61]

Due to the complexity of valvetrain systems, many mechanisms of valvetrains were developed with many unique features in terms of design, friction, wear and lubrication (see Fig. 3-2). Each has its own features, advantages and disadvantages. Essentially, valvetrains can be classified into either sliding contact (direct acting mechanical/hydraulic bucket tappet) or rolling contact (roller follower) [62]. In the direct acting mechanical tappet architecture, the cam/tappet contact contributes about 85-90% of the frictional loss [14] due to the sliding action between the cam and tappet/follower contact. Nevertheless, this design is preferred and desirable in many modern engines due to offering a lower cost and a lower height of cylinder cover [9, 62] and due to its simplicity [63, 64]. The roller follower offers lower friction than the sliding contact but it is more expensive and complicated [55]. However, both types require a similar level of wear protection for durability [65].

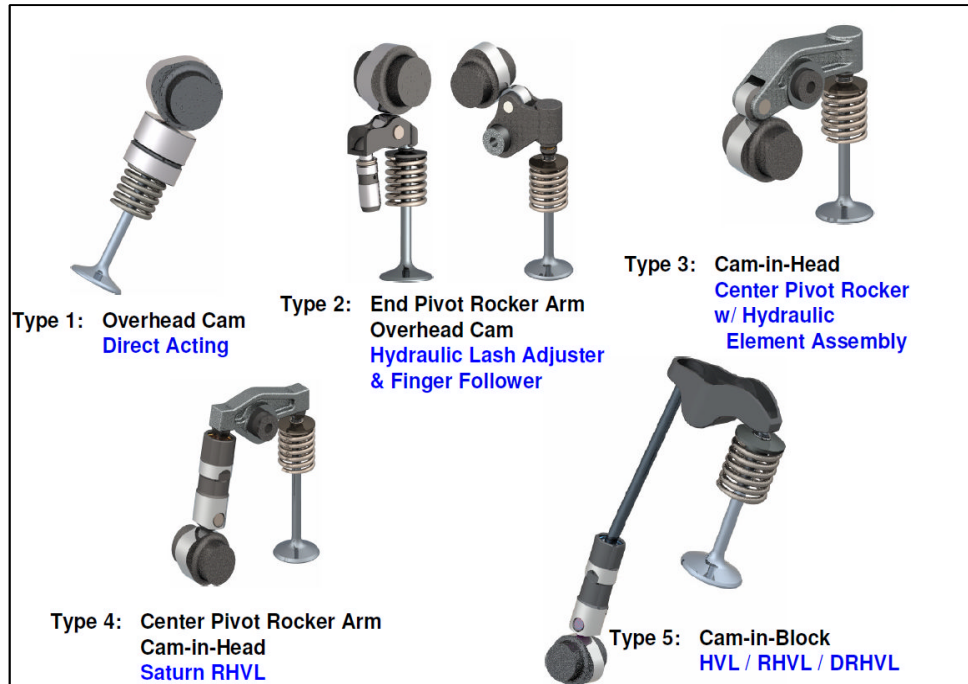


Figure 3-2 Classification of valvetrain architectures [13]

Cam/follower contacts are typically reported to operate in mixed and elastohydrodynamic (EHD) lubrication regimes [66]. However, cam/follower contact is also witnessed to operate under boundary lubrication regime (where extensive interactions occur and behaviour is characterised by the formation and removal of thin films of molecular proportions called tribofilms) [28]. From boundary lubrication regime, the severe operating conditions (e.g. low speed, high load, high temperature, and high pressure) indicate that cam and follower experience high wear, and this in turn would lead to the failure of cam/follower system. Typically, the failure of cams and followers (see Fig. 3-3) is resulted from three main factors, severe contact pressure, poor quality of material and poor lubricant formulations [67].

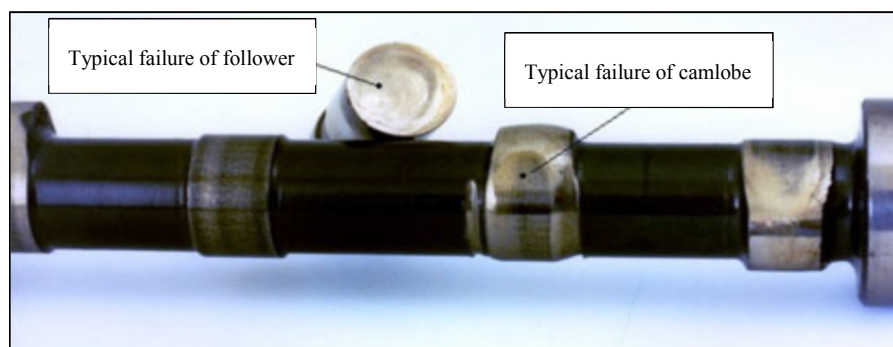


Figure 3-3 Typical failures of camlobe and follower [15]

3.3. Cams and Followers

3.3.1 Materials

A wide range of cam materials have been used such as plastics, bronze, cast iron and steels. The material choice is basically depending on the application [68] and factors such as weight reduction, cost, material availability and wear-resistant [69]. Cast iron is commonly used for cams because it is readily available, good wear-resistant, low cost, good sliding and good machinability [68, 70, 71].

The most popular used cast irons are grey cast iron [72] and chilled hardened alloy cast iron [69, 73]. Tappets are usually made of ferro-based powder sintered metal with high chromium, high chromium cast iron, silicon nitride ceramics [69, 74], 16MnCr5 steel or typically harder than the camshaft [75, 76].

The increasing demands for fuel economy and wear durability have led to use newly developed materials for cams and followers (see Table 3-1), such as forced steel, ceramic, titanium, high wear-resistant and composite materials [74, 77-80]. Steel materials have been used for low volume of production because it is causing a huge material loss in order to machine a camshaft [77]. Ceramic materials have not been widely used for valvetrain components because of some reasons; they are less ductile and do not have enough strength as compared to steel materials [80]. Furthermore, they cannot be used in applications that have high stress because of their low fracture toughness [81]. In particular, tappets made of ceramic materials have not proven to be economically viable [72]. Nevertheless, the use of ceramic materials probably could be one of the promising candidates in the future. Recently, lightweight aluminium has been used as tappet materials and showed good results in terms of reduction in friction [82]. However, it showed poor tribological properties and several difficulties in manufacturing [72]. Titanium has great properties in terms of corrosion and wear but it is fairly expensive. Overall, each material has certain advantages and disadvantages, mostly depending on cost, weight, availability and performance.

Table 3-1 Tribo-materials for valvetrain assembly

	Cam	Follower
Conventional Materials	Grey CI	Nodular iron, high Cr- Containing ferro-based powdered sintered metal
	Nodular CI	High chromium cast iron
	Chilled hardened CI	Silicon nitride ceramic
Recently used Materials	Forced steel	Low chromium steel
	Titanium	Carburized steel
	Ceramic and Composite Material	Powder sintered alloy (Fe–Cr–Mo–C)

Adapted from [77]

3.3.2 Surface Coatings

It is generally believed that coatings have a huge role to play in reducing wear and friction in a large range of applications [83]. A wide variety of coatings have been used in cam/follower systems. Among which, Mn-Phosphate ($MnPO_4$) and Diamond-Like Carbon (DLC) coatings are considered to be the most commonly and widely used [84]. $MnPO_4$ coating has a crystalline, porous, soft and rougher surface finish which provides good oil wettability, absorbance and oil retention characteristics [85, 86]. In addition, DLC coatings have attracted attention for solving surface engineering problems as they offer outstanding friction properties, high wear resistance, high electrical resistance, high corrosion resistance, high optical gap, high hardness and excellent running-in properties [87-92]. As a result, DLC coatings are considered as good candidates for reducing friction and improving durability of automotive engine components [93]. In terms of surface treatments, different coatings (e.g. phosphate coatings, carbon bearing epsilon FeN layers, oxide coatings and others) were deposited on the cam surface to improve the wettability of the surface; this in return would offer improved running-in performance and prevent early stage failure [52, 94]. In addition,

different surface modification techniques (such as the chemical conversion method that includes phosphating, oxidizing, sulfidizing and nitriding) were conducted to enhance the running-in properties of metallic tappets [69, 95]. Moreover, depending on the type of materials used, other methods of surface modifications (e.g. carburizing of low carbon steel, induction hardening or flame hardening of cast iron, induction hardening of medium carbon steel, electroplating and depositing hard coatings) were also employed in cam and follower surfaces [96].

3.3.3 Friction

In many applications, friction is undesirable because it causes energy losses that lead to reductions in machine efficiency [97]. In a typical automotive engine, the frictional loss accounts for 41% of the total energy [98] and the valvetrain is responsible for 6-10% of the total frictional loss [8, 9]. However, Sandoval and Heywood [99] have reported that valvetrain contributes about 25% of the total frictional loss.

In the literature, different techniques and methods have been used in order to study friction, such as mini-traction machine (MTM) apparatus, pin-on-plate (PoP) apparatus and a combination of valvetrain rigs. Historically, Dyson and Naylor [100] were probably the first to investigate friction at the cam/follower contact through using a push rod assembly. It should also be mentioned that numerous authors have used and developed valvetrain rigs [9, 62, 63, 65, 75, 76, 85, 100-103], because rigs typically offer low cost, short test durations and high accuracy.

It is largely accepted that the friction between two lubricated surfaces basically depends on four main parameters: load, material, lubrication regime, and lubricant formulations. Friction at the cam/follower contact is relatively complicated due to film thickness variation, high contact stress/pressure, different sliding/rolling ratios and the combination of lubrication regimes. Therefore, efforts have been made to reduce frictional loss at this contact through using and/or modifying surface coatings, surface engineering, design, lubricant formulations and material selection.

Accordingly, friction loss has been reduced by lowering the weight of valvetrain components, such as reducing the spring load and the reciprocating mass and/or using lightweight materials. Kotoh and Yasuda [104] reduced valvetrain friction by 40 %, through reducing the spring load and improving the cam/follower surface finish. Also, Fukuoka *et al.* [82] observed a 40% reduction in friction, by reducing the reciprocating mass (i.e. replacing steel tappets with thinner aluminium tappets).

Surface finishing techniques such as diamond finish, CMP finish, and ford finish have also been reported as an attractive option [62]. In addition, surface texturing is another essential approach for reducing friction and numerous authors have reported a friction reduction with texturing [9, 105-107]. Gangopadhyay and Mcwatt [9] observed a 35% reduction in friction when using parallel V-grooves on a tappet surface. Parallel V-grooves allow free flow of lubricants among all other surface patterns, including parallel square grooves, circular V-grooves, spiral V-grooves and shot peening. However, shot peening may increase the surface roughness and does not offer any reduction in friction [9]. It is worth mentioning that most authors have focused to modify tappet surface rather than camshaft surface due to its small size and simple geometry.

Some work has reported a significant reduction in friction loss through reducing the surface roughness of cam/follower surfaces [101, 104, 108]. A 20-25% reduction in friction through using silicon nitride inserts with mirror-finished surfaces has been reported with 2-3% saving in the fuel economy [109].

Diamond-Like Carbon (DLC) coatings have also been used and developed in order to reduce engine cam/follower friction due to their low friction and wear resistant characteristics. In particular, Kano [110] found that DLC coatings have super low friction properties, 45% reduction in friction was observed when using DLC coatings as compared to common phosphate coatings. Also, steel tappet inserts coated with DLC have been reported with encouraging results [111]. Moreover, deposition of thin-low friction coatings has also been considered as an active factor for friction reduction [85]. On the other hand,

fully formulated (FF) engine oils or oils with specific additives (such as Molybdenum Dialkyl Dithiocarbamate (MoDTC)) have been commonly employed in order to reduce friction and wear. MoDTC is well-known as a friction modifier and it offers low friction at the tribological contacts due to forming MoS₂ low friction sheets [112, 113].

As cam/follower tribopair experience different sliding and rolling motions, the effects of sliding/rolling ratio (SRR) (Equation 3-3) have also been reported using a plane surface of a glass disc with steel ball in contact [114]. It was found that the sliding/rolling ratio had an effect on the EHL friction coefficient (i.e. higher SRR causes a rapid decline of film thickness). One method of reducing valvetrain friction is to employ rolling element bearings at specific location in the cam/follower interface [115].

$$\text{Sliding speed} = V_c - V_f \quad 3 - 1$$

$$\text{Mean entraining speed} = \left(\frac{V_c + V_f}{2} \right) \quad 3 - 2$$

$$\text{Slide roll ratio} = \left(\frac{\text{Sliding speed}}{\text{Mean entraining speed}} \right) = \left(\frac{2(V_c - V_f)}{V_c + V_f} \right) \quad 3 - 3$$

Where V_c is the velocity of the cam and V_f is the velocity of the follower.

In the literature, the link between the sliding/rolling ratio (SRR) and the tribological/tribochemical performance was reported previously [116-123]. For the friction performance, it has been generally shown that the increase of the sliding/rolling ratio (SRR) causes an increase of friction. For example, increasing SRR from 100% to 200% increases boundary friction [119]. In addition, it was reported that elastohydrodynamic friction was increased when increasing sliding/rolling ratio from 10% to 50% [118]. Vengudusamy *et al.* [124] studied the friction behaviour of five gear oils at three different sliding/rolling ratios, 30%, 50% and 200%. They reported that the increase of the boundary friction was significant when SRR was 200% (i.e. pure sliding) while it was marginal between 30% and 50%.

3.3.4 Wear

Cam/follower wear is not a problem of the past. It is still a concern that has to be taken into consideration during the research and the design especially with the trends of using lower viscosity engine oils (to reduce the internal drag) and new engine technologies (e.g. start/stop technology). Cam/follower wear is mainly due to high contact pressure, film thickness variation, lower allowable wear limits, lubrication difficulties, temperature effect, high soot contamination, and other factors. Various types of wear experience in cam/follower region and the causes of these types have been summarized in Table 3-2 [74].

Table 3-2 Causes of cam/follower wear [74]

Roller, tappet	Type of follower	Swing arm Rocker arm
Rolling wear Pitting	← Pattern of wear →	Sliding wear Scuffing
Fatigue Excessive numbers of contacts (over 1×10^8) Excessive load Edge load Lower material fatigue strength Mismatched material combination Defects in material (blow-hole) Corrosive blow-by gas (SO_x , NO_x) Water mixing into Lubrication oil	Probable causes of wear ← Interaction → ↓ (Design factors) Lubrication oil film thickness $= 0 \mu m$ at $ V_{cam} = V_{follower} $ (opposite direction) Excessive sliding ratio	Adhesion Breakage of lubricated oil film (poor lubrication condition) Oil degradation (depleted ZnDTP) Excessive load Rough surface Contaminants at sliding interface (casing sand, cutting chips) Mismatched material combination Excessive carbon soot in oil (increased viscosity) Corrosive blow-by gas (SO_x , NO_x)

In general, scuffing, polishing and pitting are the most essential and serious types of wear occurring in cam/follower contact. These wear mechanisms have been considered as the main forms of cam/follower failure [6, 67]. Bell and Willems [125] observed that scuffing can occur after an extended period of steady wear. Kano and Tanimoto [74] suggested that adhesion is the main reason to cause scuffing while pitting is believed to be caused by fatigue resulting from repeated stressing under high contact loads. In addition, boundary lubrication regime (at low speed and low oil temperature) can assist to produce scuffing wear. On the other hand, a historically report by Dyson and Naylor [100] suggests that scuffing and polishing wear occur at high

engine speeds and controlled by the temperature in the contact zone. It is important to note that the camlobe is normally designed to be more scuff resistant while the tappet is more resistant to pitting [6].

The most critical factors affecting the wear of cam/follower are the materials between cam/follower, speed, temperature, oil viscosity and operational conditions [78, 126]. The link between materials and wear has been illustrated by Taylor [6] (see Figure 3-4). This explains the trend of scuffing and pitting for several common materials.

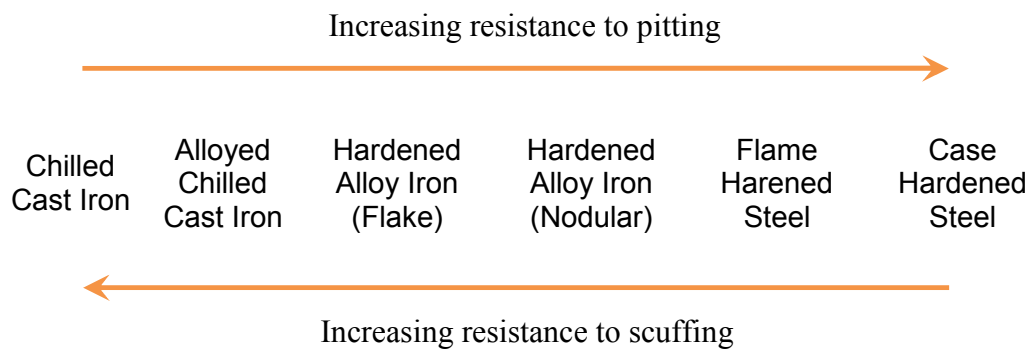


Figure 3-4 Pitting and scuffing resistance of convention materials [6]

Several condition monitoring techniques have been used to study, measure and/or reduce the wear of cam/follower contact. Classically, methods of wear measurements based on a level sensor have been employed. Typically, Surface Layer Activation technique (SLA) has been adapted to measure the wear effectively in a real time. This method uses beam irradiations of charged particles, like protons, accelerated on a small volume at the surface of the metal part to create a thin active layer. The wear of this activated layer is measured using radiation detectors as a loss of surface material. Many authors have analysed cam wear using SLA technique [65, 127-129]. Ipek and Selcuk [130] measured the wear as thickness loss by using a level meter (LM) under sliding conditions. Others used electrostatic sensors focused on the cams [10] or used a radionuclide technique (Thin Layer Activation (TLA)) [9, 131]. Ofune *et al.* [76] used talysurf contact with the assistance of monitoring the tribochemistry of cam/follower surfaces based on different techniques, such as SEM/EDX-FIB, XPS, and Raman Spectroscopy. Purmer and Vandenberg [126] developed a technique to measure the camlobe wear.

This technique included two electronic transducers, one to measure the cam lift and the other to measure the angle. It was observed that the wear changes in each location on the camlobe (i.e. there is a direct correlation between the wear rate and the geometry of the camlobe). In addition, Roper and Bell [132] modified a twin-disc test machine in order to evaluate the wear performance in valvetrain components.

Engine performance is directly affected by camshaft wear. Therefore, many efforts have been made either to study the wear mechanism or to measure the wear amount affected by material selection [130]. It was reported that the main mechanism on the camlobe surfaces is normally caused by fatigue and surface deformation [71]. Akemi *et al.* [133] observed a cam wear mechanism at the cam/tappet contact. A modern configuration was developed to measure the wear mechanism and friction, by using two strain gauges mounted on a push-rod and shaft. It was reported that there is a good correlation between friction and wear (i.e. friction could predict the presence of wear in engine components). However, wear results showed that the oil deterioration and high oil supply temperature are essential factors for the cam abnormal wear. Others tried to monitor the wear of a camlobe in different locations. Eric and Sylvain [134] studied the relationship between camlobe wear and tribofilm chemical composition using fully formulated oils. Seven angular locations on the camlobe were selected ($\pm 14^\circ$, $\pm 10^\circ$, and cam nose 0° degree) to trace the profile in order to investigate the tribofilm at each location and their effect on camlobe wear. This was achieved by using a surface profile meter to measure wear depths during 50 h for each camlobe test. It was shown that tribofilms were different at each location. Various chain lengths of polyphosphate glass were found on all camlobe tribofilms. Long chain polyphosphates tribofilms had good antiwear characteristics than the short one. However, Camlobe wear was reported to be the highest near the camlobe nose [3].

Material selection of cam/follower interface has an attractive impact on wear. Therefore, several types of materials have been adopted (especially the wear-resistant materials) [79, 135]. Kano and Tanimoto [74] developed high wear-resistant materials, ferro-based powder metals, alloyed cast iron and silicon nitride ceramics. Some researchers focused on the properties of different

materials, Michalski *et al.* [78] recommended after using certain concentrations, that a cam shaft made of chilled grey cast iron mating with a follower made of toughened, surface hardened, and steel ensure small frictional resistance and less wear. In addition, surface finishing of cam/follower surfaces has found to be essential for preventing camshaft wear [80]. Furthermore, Alamsyah *et al.* [136] investigated effects of initial surface finish on cam wear under controlled conditions of contacts.

Zinc DialkylDithioPhosphate (ZDDP) is one of the most common anti-wear additives. Many modern engine oils have been formulated with this additive in order to extend the life of a component by avoiding the wear. In particular, it was reported that ZDDP additive is essential to improve the anti-wear properties but the friction will increase in the presence of ZDDP [137]. Gangopadhyay *et al.* [65] observed that ZDDP offer low wear under low load and high wear under high load. As a result, this additive (i.e. ZDDP) is basically affected by test conditions. It should be mentioned that authors usually prefer to use fully formulated (FF) oils because they contain detergents, dispersants, friction modifiers and ZDDP.

In addition, fresh and aged oils have also been investigated in order to understand their relationship with friction and wear. It was found that the film composition of both fresh and used oils is very different; this could explain why wear rate improved significantly and friction reduced when tested with used oils (drained from vehicles after 12,000 miles) compared to fresh oils [65]. Similar findings were reported by Dairene *et al.* [138]. Alain and Thierry [131] reported a serious wear problem in the engine components caused by soot that contaminates the lubricants.

DLC coatings have good wear resistance and low friction; they play an essential role at the cam/follower interface. Kosarieh *et al.* [113] observed the friction and wear properties of a DLC coating (a-C: 15H) with using base oils and four fully formulated oils with different concentrations. It was reported that the durability of the coating is controlled by the right selection of oil additives. Also, fully formulated oils had good wear prevention with DLC coatings but the friction reduction was not significant.

3.3.5 Lubrication

The lubrication mechanism of the cam/follower interaction is relatively complex. The lubrication regime varies around the cam cycle due to various reasons such as change in load and velocity. Although hydrodynamic lubrication is observed on the cam flanks [66] and boundary lubrication is witnessed around the cam nose [95], it is generally accepted that cam/follower contacts are considered to operate in regimes of mixed and elastohydrodynamic (EHD) lubrication [66] (especially on the cam base circle, flank and nose) [10, 139]. However, some authors considered the mixed lubrication is the best described of the cam/follower lubrication [6, 9]. In general, cam/follower performance depends upon the modes of lubrication and it may enjoy more than one form of lubrication during a single cycle.

In conclusion, to understand cam/follower friction, wear and lubrication, it is important to appreciate the interaction among oil formulations, surface coatings, material choice and surface topography. All these parameters are an attractive approach to understand how is possible to ensure optimum friction reduction with adequate wear protection.

3.4. Diamond-Like Carbon (DLC) Coatings

The first synthetic diamond was made in 1950s. This was achieved using high pressure and high temperature techniques. Lately, in 1980s, CVD deposition technique (under low pressure) was conducted to make diamond in the form of polycrystalline coating [140, 141]. Diamond-Like Carbon (DLC) is a carbon coating which displays properties similar to diamond, including mechanical, optical, electrical and chemical properties but it is a metastable form of amorphous carbon (do not have a crystalline lattice structure) with significant fraction of sp^2 (graphite-like), sp^3 (diamond-like) and hydrogen bonds [113, 137].

Typically, the properties of DLC coatings (e.g. low coefficient of friction, high wear resistance, chemical inertness, high hardness, high electrical resistance and high optical gap) are dependent on the ratio of sp^2/sp^3 bonds.

3.4.1 Structure of DLC Coatings

Carbon is able to exist in three types of hybridizations, sp^3 , sp^2 , and sp^1 (see Fig. 3-5). In the sp^3 configuration, as in diamond, the 2s orbital and three 2p orbitals of carbon are hybridized to form four equivalent sp^3 hybrid orbitals of equivalent energies. As a result, these four orbitals can form strong C-C bonds with adjacent atoms (i.e. when the sp^3 orbitals of adjacent carbon atoms overlap), arranged in a tetrahedral structure. In the three-fold coordinated sp^2 configuration as in graphite, three trigonally sp^2 hybrid orbitals lie in a plane, where each carbon is bonded to three other carbon atoms with strong covalent bonds. These carbon atoms are bonded to each other by weak Van der Waals forces; this in return responsible for the low friction behaviour of graphite [52]. The structure of DLC coatings contain both sp^3 and sp^2 and the proportions of them (i.e. sp^3/sp^2) are dependent on the technique and parameters used in deposition.

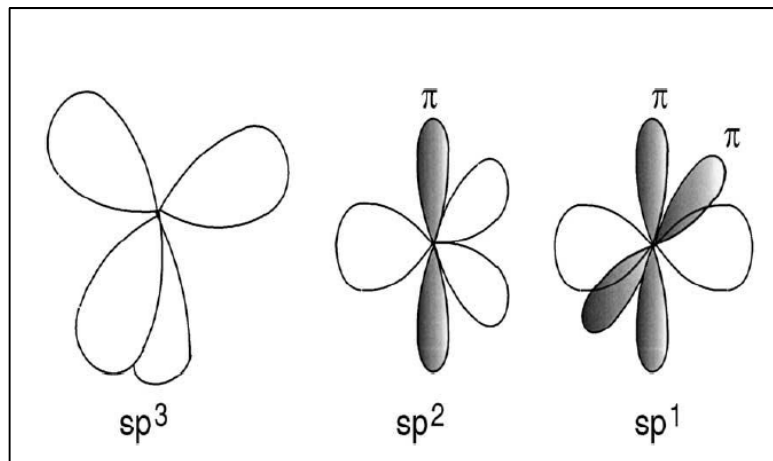


Figure 3-5 sp^3 , sp^2 and sp^1 hybridised bonding [142]

DLC coatings have been generally classified into four categories, amorphous carbon a-C, hydrogenated amorphous carbon a-C: H with a domination of sp^2 bonds, tetrahedral amorphous carbon ta-C and hydrogenated tetrahedral amorphous carbon ta-C: H with a domination of sp^3 bonds [91]. Each type offers specific coatings properties like hardness, friction coefficient, wear durability and toughness [84]. These properties, including type and structure, depend significantly on hydrogen content and sp^2/sp^3 ratio, accordingly, depend on deposition process and applied parameters [143, 144]. For a

hydrogenated DLC film (a-C: H and ta-C: H), the hydrogen in these coatings helps to stabilize the diamond structure by maintaining the sp^3 hybridization configuration [89]. Also, the hydrogen in a-C: H and ta-C: H coatings plays a key role to gain a wide optical gap and high electrical resistivity.

The DLC forms are shown by the phase ternary diagram as in Fig. 3-6. This diagram proposed by Ferrari and Robertson [145], has provided a concept that helps to understand the chemical and structural properties of DLC films using different spectroscopic techniques. The a-C coatings lie in the left side of the diagram and the mechanical properties of a-C coatings depend on the ratio of sp^3/sp^2 . In addition, a-C: H coatings typically sit in the middle of the diagram which display a varying ratio of sp^3/sp^2 bonding and hydrogen content. The ta-C coatings are placed at the left side of the diagram depending on the ratio of sp^3/sp^2 . Moreover, the sp^2 bonded graphitic carbon lies in the lower left-hand corner. Lastly, the content of hydrogen lies at the lower right-hand corner of the diagram. It is however important to note that the high content of hydrogen is unable to form an interconnected molecular structure, rather form gas or liquid molecules [146]. Furthermore, the higher the hydrogen content the lower friction but the hardness of the coating is usually lost.

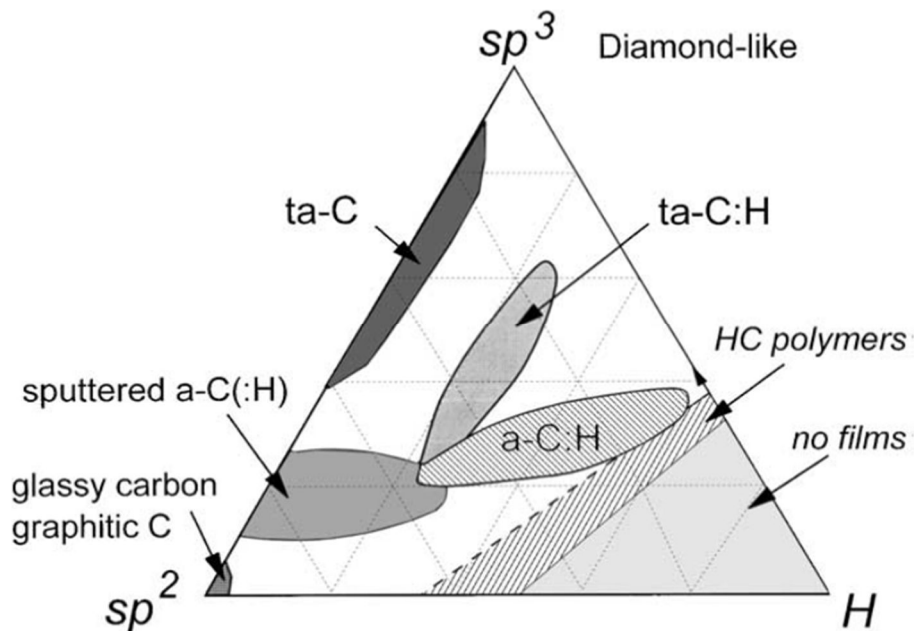


Figure 3-6 Ternary phase diagram of bonding in amorphous carbon-hydrogen alloys [142]

In terms of density, hardness, sp^3 and H content, various forms of carbon are shown in Table 3-3. As can be seen, DLC coatings may contain as high as 65% hydrogen (a-C: H) and as low as 1-8% hydrogen (a-C). In addition, from Table 3-3, DLC coatings can provide high hardness. Recently, however, it was reported that nanocomposite coatings are capable of providing super hardness but lack lubricity or low friction was witnessed [147].

Table 3-3 Properties of various forms of carbon [146]

	Density (gm cm ⁻³)	Hardness (GPa)	sp^3 (%)	H (at %)	Gap (eV)
Diamond	3.515	100	100		5.5
Graphite	2.267		0		-0.04
Glassy C	1.3-1.55	2-3	~0		0.01
a-C (evaporated)	1.9-2.0	2-5	1		0.4-0.7
a-C (MSIB)	3.0	30-130	90±5	<9	0.5-1.5
a-C:H (hard)	1.6-2.2	10-20	30-60	10-40	0.8-1.7
a-C:H (soft)	0.9-1.6	<5	50-80	40-65	1.6-4
Polyethylene	0.92	0.01	100	67	6

3.4.2 Deposition of DLC Coatings

A wide range of deposition systems were developed to produce DLCs. Historically, Aisenberg and Chabot [148] were the first to prepare thin films of DLCs using ion beam deposition. Typically, DLC coatings are formed when ionized and decomposed hydrocarbon or carbon species hit the surface with energies up to 200 eV [149, 150]. DLC coatings can be deposited at temperatures between 200 °C to 325 °C [89, 151]. Likewise, this property makes deposition of DLC coatings applicable on most engineering materials including polymers [149]. In contrast to metallic and ceramic substrates, carbide- and silicide-forming substrates (e.g. Si, Ti, W and Cr) can promote a strong interfacial bonding to the substrate. However, prior to DLC deposition, the deposition of an initial bond layer on these substrate could enhance the adhesion of the DLC film to the substrate. These interlayers (which typically made in the same chamber prior to the actual DLC deposition) make a chemical reaction with the substrate and offer a strong bonding [147].

Deposition methods of DLC coatings can be classified into two major categories, chemical vapour deposition (CVD) techniques and physical vapour deposition (PVD) techniques. CVD techniques include radio frequency (RF) plasma and DC plasma methods. PVD techniques include sputter deposition, ion-plating techniques and ion beam techniques, which can be conducted to make DLCs containing hydrogen content [52]. However, PVD techniques (including magnetron sputtering, mass selected ion beam (MSIB), cathodic arc and laser plasma deposition) can also be employed to form hydrogen-free a-C and ta-C coatings.

The Plasma Enhanced Chemical Vapour Deposition (PECVD) technique is a combination of PVD and CVD systems, where the glow discharge of PVD facilitates plasma creation of the reacting gases. In this technique, good deposition rates and high quality product can be maintained even with a lower deposition temperature compared to that of thermally driven CVD [52]. Each method has its own advantages and disadvantages whereas the selection of the appropriate method is depending on the coating type and coating purpose (i.e. whether the coating is most suitable for laboratory studies or industrial production) [142].

A schematic of various deposition systems for DLC is shown in Fig. 3-7. In a typical ion beam deposition method, plasma sputtering of a graphite cathode produces the carbon ions through the use of an ion source [142]. Sputtering can be defined as “the removal of material from a solid target by the bombardment of high energy ion particles.” [52]. The ejected atoms will then form/deposit the desired thin film of the target material onto the substrate surface.

DC magnetron sputtering is one of different types of sputtering which sputtering occurs in a vacuum chamber. In other words, target material and substrate is placed in a vacuum chamber. A voltage is applied between target (cathode) and substrate (anode). Accordingly, a plasma is created by ionizing a sputtering gas (heavy gas like Argon). The generated high energy plasma hits the target and results in ejection of atoms from the target material to the substrate.

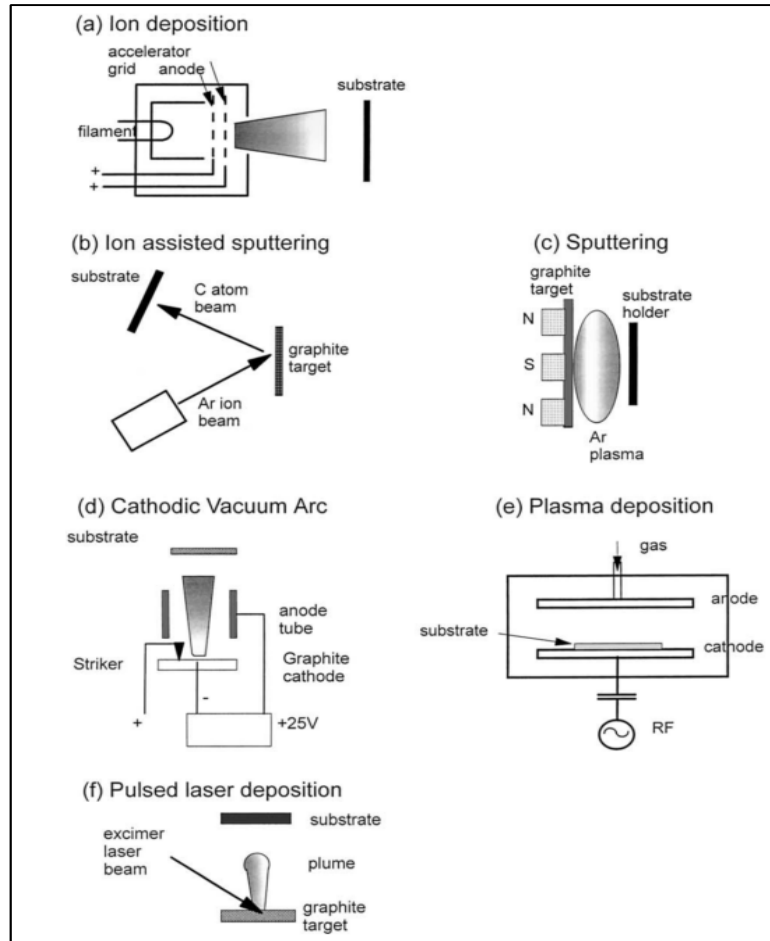


Figure 3-7 Schematic of various deposition systems for DLC [142]

3.4.3 The Graphitization of Hydrogenated DLC

At high temperatures, hydrogen in the hydrogenated DLC (a-C: 15H) coating starts to diffuse out of the coating matrix. As a result, this would give rise to collapse of the tetrahedral sp^3 structure to a graphite-like sp^2 structure. This process (often called graphitization) typically starts at temperature between 200 °C to 300 °C but is however be more pronounced at temperature above 300 °C or 400 °C [152, 153]. The graphitization of DLC is mostly dependent on the thermal and/or straining effects [154, 155]. The transformation process needs high temperature (700 °C or more) to be completed [153].

For the hydrogenated DLC coating, however, a lower transition temperature is needed. This is attributed to the high strain of hydrogenated DLC coating [147, 152, 156].

3.5. Zinc Dialkyldithiophosphate (ZDDP)

Zinc dialkyldithiophosphate ZDDP (sometimes referred to as ZDTP) has been the most frequently used in engine lubricants since its discovery in 1940s. More specifically, ZDDP was first introduced by Lubrizol in 1941 as an antioxidant additive but its ability as anti-wear additive was noticed in 1955. ZDDP has mostly been used to prevent excessive wear in engines (mainly in cam and follower contact) [39, 40, 45-47, 134]. ZDDP was also known to have other positive characteristics such as antioxidation and extreme pressure (EP) action. The general structure of a ZDDP additive is shown in Fig. 3-8, but it should be noted that more complex structures are detected in solution.

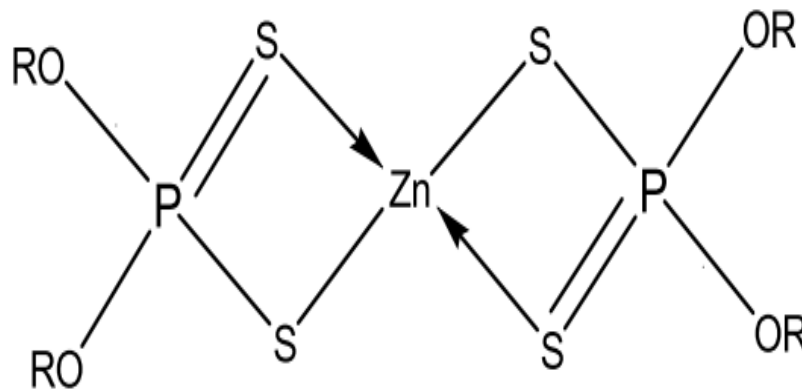


Figure 3-8 Structure of Zinc dialkyl dithiophosphate [35]

ZDDP can be subdivided into three different types, aryl ZDDP, primary ZDDP ($\text{CH}_3\text{CH}_2\text{CH}_2\text{CH}_2\text{O}-$) and secondary ZDDP ($\text{CH}_3\text{CH}_2\text{CH}(\text{CH}_3)\text{O}-$). Aryl ZDDPs are used in diesel engine whereas primary and secondary ZDDPs are extensively used in gasoline engines. It is worth mentioning that both primary and secondary ZDDPs have more anti-wear effectiveness as compared to aryl ZDDP. Comparing secondary ZDDP to primary ZDDP (see Table 3-4), the secondary ZDDP experiences lower wear than the secondary ZDDP which might be due to the difference in thermal stability of both types and also their molecular weight [157]. However, it was reported that all types of ZDDP react differently but the films typically consisted of Zn, P, S and O [158].

Table 3-4 Performance parameters of ZDDP types [35]

	Primary	Secondary
	Alkyl	Alkyl
Thermal Stability	Medium	Low
Antiwear Protection	Medium	High
Hydrolytic Stability	Medium	High

3.5.1 Tribological Performance of ZDDP

Test conditions, such as temperature and contact pressure, play a key role to determine the effectiveness of ZDDP in wear reduction [134]. In terms of contact load, ZDDP was observed to reduce wear under low loads but the wear was increased under high loads. This is due to the formation of a film at high loads that contains the lower sulphide content [159]. Likewise, as sulphides are harder than polyphosphates, reduction in sulphite content would lead to lower mechanical strength and higher wear [160]. At 50 °C, ZDDP could form a physisorbed film while ZDDP starts to form a chemisorbed film at temperatures above 80 °C [161]. The film formation from ZDDP was also reported to influence by sliding speed [162]. It was reported that higher sliding speed would promote the chemisorbed film formation from ZDDP [163]. The thickness of the tribofilm formed from ZDDP varies as a function of temperature and the ZDDP concentration in the lubricant [164, 165]. Inside wear track, the thickness of the tribofilm formed from ZDDP was reported in the range of 5-50 nm [166]. Typically, more ZDDP would be detected on the tribofilm when increasing the concentration of ZDDP in the lubricant.

In some literature, the effect of ZDDP on friction was observed to be either neutral [158] or a decrease on friction [167]. However, in most literature, lubricants containing ZDDP have been reported to increase friction [52, 160, 168-171], suggesting that this increase was attributed to the formation of ZDDP film [169]. The film formation would increase the roughness in boundary lubrication; this in turn would lead to an increase in friction [171]. It is worth mentioning that friction change was not detected in EHL lubrication [172] while

the increase in friction was mostly observed in mixed lubrication regime and to some extent in boundary lubrication.

3.5.2 Tribochemical Performance of ZDDP

ZDDP tribofilm typically contains inorganic polymer materials (e.g. zinc, phosphorus, oxygen and sulphur) [173-175]. Pereira *et al.* [176] showed that the thick pads from ZDDP additives consisted mainly of medium chain polyphosphates with sulphur present primarily as ZnS. Yin *et al.* [177] revealed that increasing the test duration would enhance the long chain polyphosphate formation on the surface. Also, ZDDP tribofilms were suggested to be composed of iron oxide interwoven with short polyphosphate covered by thin long chain metal phosphate [177]. Bell *et al.* [178] suggested that the ZDDP tribofilm (top layer in particular) was composed of glassy phosphate films whereas the layer near the surface was rich in iron sulphide and iron oxides, as shown in Fig. 3-9.

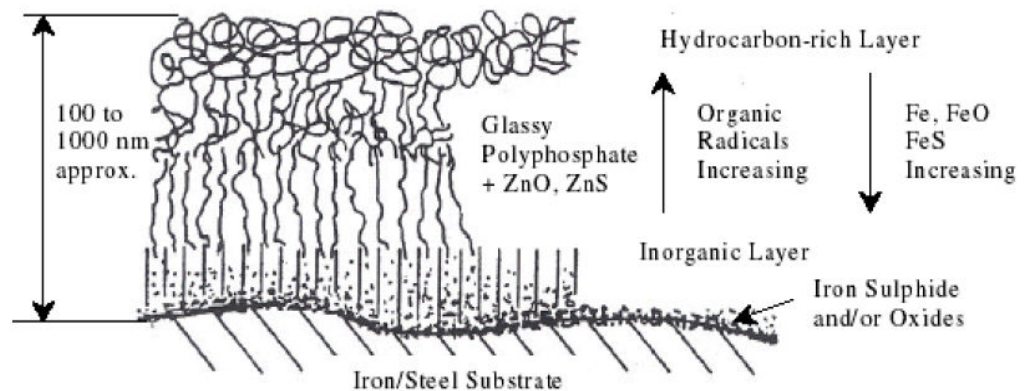


Figure 3-9 ZDDP film structure [178]

The ZDDP decomposition was reported to have many mechanisms such as surface adsorption, thermal degradation, thermal oxidation and hydrolysis [173, 174, 179-182]. Coy and Jones [181] concluded that the decomposition of ZDDP has a thermal nature (i.e. the higher temperature increases the decomposition rate of ZDDP). Hydrolytic mechanism of ZDDP was proposed by Spedding and Watkins [173, 174]. This mechanism revealed that the

elimination of water from the reaction was found to suppress the decomposition of ZDDP. Martin *et al.* [183] proposed a model for ZDDP tribofilm, where the top layer was found to be rich in long chain zinc poly(thio)phosphate polymer-like material. Further, in the bulk containing metal sulphide precipitates, a mixed iron and zinc short chain polyphosphate was observed. It is also important to note that no oxide/sulphide layer was seen at the interface between the phosphate and the steel surface [183].

The mechanisms by which ZDDP could facilitate low wear have been widely investigated. Typically, the wear protection by ZDDP was suggested to be attributed to two simultaneous processes, (i) the catalytic decomposition of hydroperoxides, and (ii) the surface layer formation. The first process prevents the direct oxidation of the metal surface and the second process provides additional wear protection [184]. In addition, Martin [185] suggested that the effectiveness of ZDDP in reducing wear was related to the action of ZDDP phosphate film as a viscous lubricant in boundary lubrication. Furthermore, if a tribofilm which containing ZDDP elements is softer than the substrate, the formation of this tribofilm could reduce the asperities in contact [186].

3.6. Molybdenum Dialkyl Dithiocarbamate (MoDTC)

Molybdenum dialkyl dithiocarbamate (MoDTC) is the most common friction modifier used in crankcase lubricant formulations. This additive has also other positive characteristics, including antiwear, antioxidant and extreme pressure (EP) properties [45, 187]. MoDTC additive contains Mo-S compounds; these compounds provide low friction under boundary lubrication by forming MoS₂ low friction sheets on the tribological contact [112, 188-191], low wear and high load carrying capacity [192]. The layer-lattice structure of the molybdenum disulphide with low shear strength makes it possible to achieve low friction between the interacting surfaces [193]. In MoS₂ molecules, the bonding between atom species are strong covalent. However, weak Van der Waals forces were observed between the layers. These weak Van der Waals forces maintain easy shear within the molecule, which in return would lead to low friction [52]. The MoS₂ solid state structure is shown in Fig. 3-10.

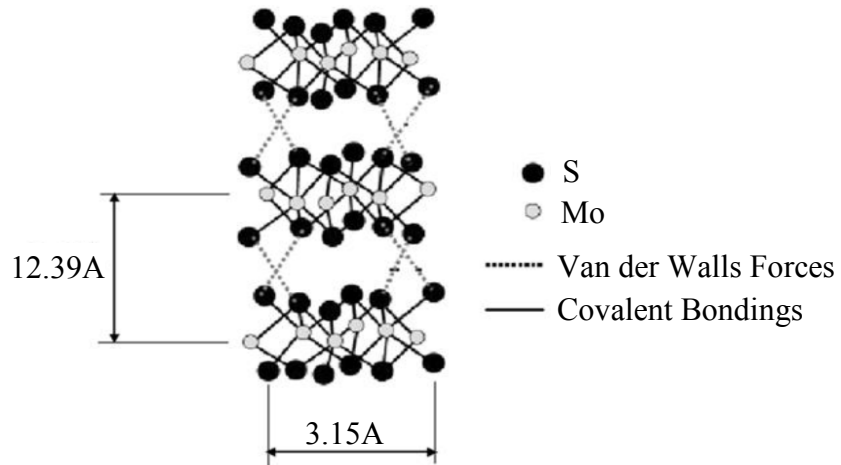


Figure 3-10 MoS₂ solid state structure [193]

MoDTC compounds have been reported to possess better thermal stability than many other organic molybdenum compounds [108]. Comparing molybdenum dialkyl dithiocarbamate (MoDTC) to molybdenum dithiocarbamates (MoDTP), MoDTC forms a surface film composing of MoS₂ while MoDTP forms a surface film composing mainly of MoS₂ and FePO₄ at 120 °C temperature and MoS₂, MoO₃ and FePO₄ at 200 °C. Thus, MoDTC was more able to form MoS₂ than MoDTP [111, 117]. Accordingly, MoDTC has been reported to provide more reduction in friction than MoDTP. Nevertheless, Unnikrishnan *et al.* [194] reported that both MoDTC and MoDTP additives provide the same friction reduction but MoDTP was found to offer better wear prevention characteristics than MoDTC. Their structures are illustrated in Fig. 3-11.

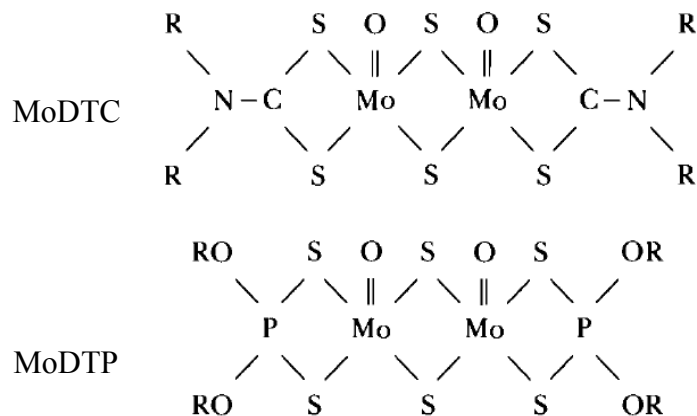


Figure 3-11 The structures of MoDTC and MoDTP [192]

3.6.1 Tribological Performance of MoDTC

Factors, such as Mo concentration, nature of the tribological contact, load, surface roughness, temperature and environment, play an essential role to control the tribological performance of MoDTC. In boundary lubrication conditions, MoDTC is able to reduce friction coefficients typically 0.06 to 0.75 [189]. Spikes [195] reported a very low friction coefficient of about 0.05 when using MoDTC in the mixed-to-boundary lubrication regime. A typical friction curve with MoDTC additive (obtained during test) is shown in Fig. 3-12. It can be seen that MoDTC shows high friction at the start of the test followed by a friction drop to low steady values after rubbing for a short period. The time from the start of the test to the time low steady values is known as the induction time.

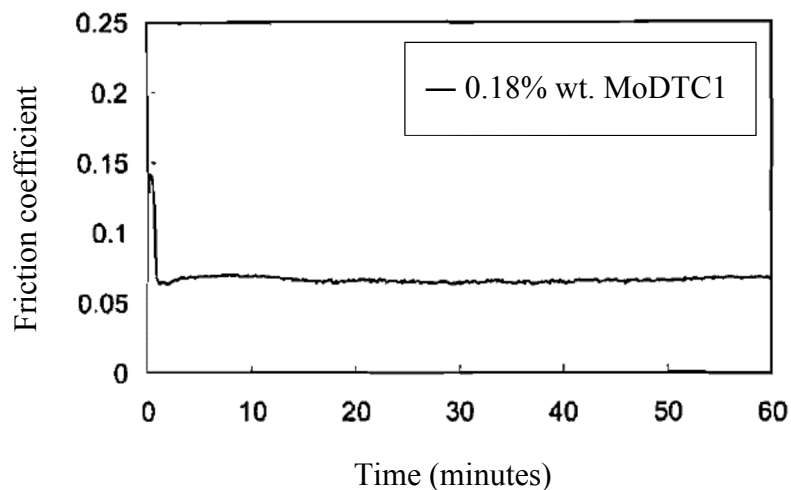


Figure 3-12 Typical friction curve obtained during tests with MoDTC additive [189]

In order to understand and explore more about the nature of MoDTC film, a range of friction tests have been achieved where taking into consideration the influence of factors such as concentration, temperature, load, type of contact and speed. Mo-FM additives are more effective in reducing friction at high concentration (>400 ppm) and temperature (>200 °C) as these parameters facilitate the formation of MoS₂ sheets [190]. Graham *et al.* [190] reported that the minimum concentration of MoDTC for friction reduction was around 180 ppm while Sorab *et al.* [196] noticed that a MoDTC concentration more than 500 ppm was essential for most effective friction reduction. Yamamoto and

Gondo [192] observed that the time required to reduce friction reduced with increasing MoDTC concentration. Miklozic *et al.* [191] showed high friction when lubricants contained 0.05 wt% MoDTC while low friction was observed when 0.125 wt% MoDTC was used (see Fig. 3-13).

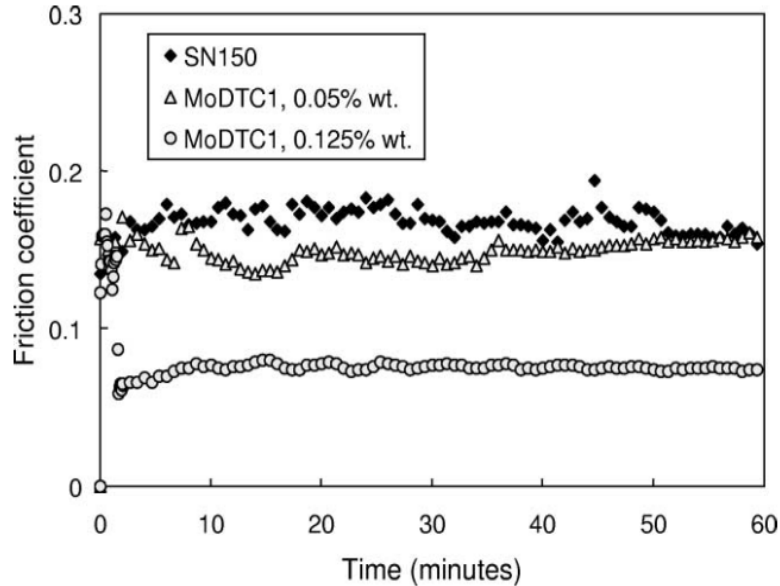


Figure 3-13 Influence of MoDTC concentration on friction [191]

MoDTC additives were found to be most effective in reducing friction at a combination of high additive concentrations and high temperatures (up to 0.4% wt. and 200°C) [189]. In addition, many workers have observed the durability of MoDTCs in engine tests and all have reported friction reduction during engine running [190]. Muraki *et al.* [197] suggested that a significant friction reduction can be achieved when MoDTC additives are used in combination with other additives, such as ZDDP. The type of contact was also considered as an essential factor in effectiveness of MoDTC in friction reduction. Graham *et al.* [189] concluded that MoS₂ formation in the sliding/rolling contact is hindered by the micro-elastohydrodynamic lubrication whereas MoDTC was only effective in direct solid-solid contacts (i.e. in boundary lubrication regime). As mentioned earlier, the effectiveness of MoDTC would depend on several parameters. Therefore, it is crucial to control these parameters which in return would provide low friction and low wear.

3.6.2 Tribochemical Performance of MoDTC

Many analytical techniques, such as Energy-Dispersive X-ray (EDX), X-ray Photoelectron Spectroscopy (XPS), Auger Electron Spectroscopy (AES), Raman spectroscopy and Transmission Electron Micrograph (TEM), have been used to investigate the chemical analysis of a tribofilm formed from MoDTC. By using dual of the above analytical techniques, the tribofilm of MoDTC is found to be a carbon-based composite material containing a few per cent of individual MoS₂ sheets (less than 10 nm length), these sheets have the same crystal structure and electron binding energy as pure MoS₂ [188]. In addition, numerous tiny domains with diameter 10-25 nm and height 1-2 nm have been observed in MoDTC films [188, 191]. They are believed to represent the tiny, flake-like nanocrystals of MoS₂.

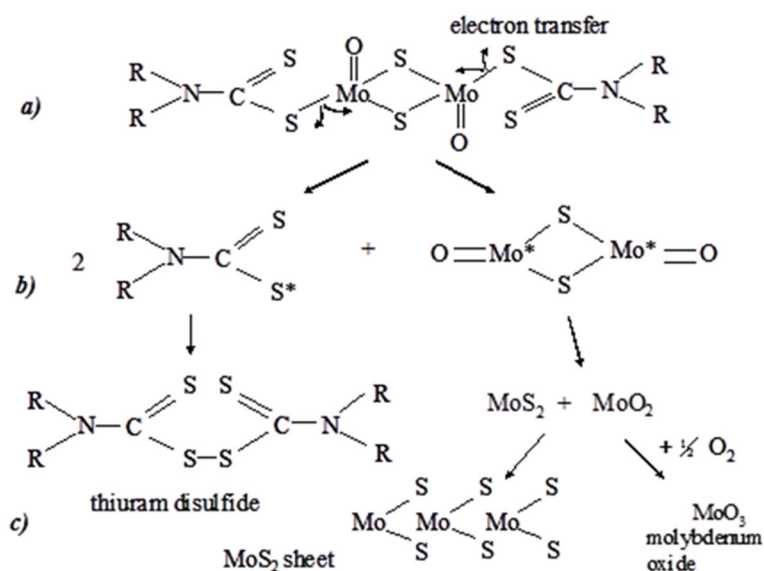


Figure 3-14 MoDTC decomposition: chemical model [112]

As shown in Fig 3-14, Grossiord *et al.* [188] reported a two-step process towards MoS₂ formation in terms of the chemical point of view. The first step involves electron transfer on Mo-S chemical bondings, leading to three free radicals, one corresponding to the core of MoDTC and the other two corresponding to the chain ends. The second step represents the recombination of chain end radicals with the formation of thiuram disulphide, whereas the other radical decomposes into MoS₂ and MoO₂.

The presence of MoS₂ and MoO_x has been reported by using different analytical techniques such as Raman spectroscopy, X-ray Photoelectron spectroscopy (XPS), energy-dispersive x-ray (EDX) and others. Morina *et al.* [112], Bouchet *et al.* [90] and Haque *et al.* [96] have used the XPS surface analytical technique and they reported that MoDTC additive formed MoS₂ and MoO₃ compounds in the tribofilm and the Increasing of MoS₂/MoO₃ ratio reduces the coefficient of friction. Moreover, Sun *et al.* [117] reported two chemical reactions from MoDTC. The first one forms MoS₂ while the second reaction is oxidative decomposition that forms MoO₃. These reactions have a direct correlation to frictional properties (i.e. the lubricant had low reduction friction properties in the presence of MoO₃).

It should be mentioned that XPS analysis of MoDTC tribofilms is conducted by obtaining spectra at different binding energies. The binding energies of the different molybdenum compounds are presented in Table 3-5.

Table 3-5 Binding energies of various molybdenum compounds [198]

Compound	Binding energy (eV)			
	Mo 3d _{5/2}	O (1s)	S (2p _{3/2})	Fe 2p _{3/2}
Mo (0)	227.8			
MoO₂ (+4)	229.2	529.9		
MoS₂ (+4)	229.0		161.9	
MoS₃ (+4)	229.1		161.6	
MoS₄ (+4)	229		163.1	
MoDTC (+5)			163.5	
MoS_xO_y (+5)	231.1		161.7	
MoO₃ (+6)	232.3	530.6		
FeMoO₄ (+6)	232.3	531.9		710.5

From previous XPS analyses, tribofilms of lubricants containing MoDTC indicated Mo 3d peaks at 229, 232.3 and 235 eV [188, 194]. These XPS studies showed that the tribofilms of lubricants containing MoDTC were

3.7. Additive/Additive Interactions

3.7.1 MoDTC Interaction with ZDDP

Different studies have been focused to evaluate interactions between lubricant additives namely between MoDTC and ZDDP. As MoDTC contains MoS₂ low friction sheets, it was found that the presence of ZDDP might promote MoS₂ formation from MoDTC. Consequently, ZDDP was reported to enhance the performance of MoS₂ sheets [77, 112, 137]. Likewise, MoDTC is more effective when used together with the ZDDP [112, 197, 204, 205] and the combination of both was reported to provide an interesting friction/wear reduction [197]. A two-step reaction occurs in the presence of MoDTC/ZDDP. Firstly, a reaction between phosphate and iron oxide. Secondly, a reaction between the nascent iron surface and a sulphide species. Each additive has a particular role, MoDTC creating MoS₂ and MoO₃ while ZDDP creating the zinc phosphate glass. Also, it was suggested that the elimination of MoO₃ was the reason for wear reduction [206, 207].

The effect of MoDTC on ZDDP additive is still not completely understood. Thus, different researchers have focused on that effect. For example, Kasrai *et al.* [204] reported more evidence about the chemical interactions of the tribofilms formed from MoDTC alone and from ZDDP/MoDTC together. It was found that the friction was higher during the use of MoDTC alone and the reason for that was thought to be due to the presence of sulphate. Also, it was reported that the uppermost layer of the tribofilm consists of ZnS while a dense matrix of metal phosphate and MoS₂ sheets was seen in the bulk. Martin *et al.* [206] investigated the formation of sulphates when used only MoDTC. They reported a significant reduction in both friction and wear when MoDTC was blended with ZDDP compared to using ZDDP or MoDTC separately. This suggests that the reaction of MoO₃ (and possible iron oxides with zinc polyphosphate) was responsible for wear reduction. Consequently, in terms of friction, MoS₂ will be reserved from oxidation and this could enhance the friction performance. Sogawa *et al.* [208] observed the source of sulphur in the MoS₂ tribofilm that formed from a ZDDP/MoDTC combination. The percentage of sulphur derived from ZDDP in MoS₂ is about 40%. This

percentage is a proof that an interaction happened between Mo from the MoDTC with S from ZDDP but this interaction is still unclear.

MoDTC additive has been reported to have a detrimental effect on the structure of ZDDP film. In other words, a thick patchy pad-like tribofilm, formed by ZDDP alone, became much thinner and the patchy structure was vanished [209]. In addition, the tribofilm of ZDDP alone was seen to be softer than MoDTC/ZDDP together, which could explain any relation between lower friction observed and the transformation to elastohydrodynamic lubrication [210].

3.7.2 ZDDP Interaction with Detergents and Dispersants

Detergents are generally accepted to offer anti-wear properties through the forming of carbonates in the wear scar [211-213]. However, an antagonistic effect from detergents were observed on the film formation properties (i.e. wear performance) of ZDDP [212, 214, 215]. This effect was attributed to the reduction in the amount of ZDDP available for film formation by forming a complex [52], where the strength of these complexes (formed with various dispersants and with amines) will however determine the degree of their impact on wear. Under the presence of ZDDP, the film typically consists of short Ca phosphate films with increased wear than ZDDP alone [214, 215]. Succinimide dispersants were reported to increase wear when added to ZDDP solutions in valvetrain tests [216] and 4-ball wear tests [211]. In addition, the decomposition temperature was reported to increase when using succinimide dispersant and detergents together with ZDDP. This in turn would lead to scuffing wear on valvetrain systems [217]. The film thickness typically increases when both detergent and dispersant are blended with ZDDP additive.

A schematic structure for tribofilms generated by ZDDP additive and ZDDP/detergents/dispersant additives is shown in Fig. 3-16. The dispersants are not contributed in the film structure and they typically form a thin layer of nitrogen-containing material on the outer surface [218]. In addition, by

blending different dispersants with a lubricant containing ZDDP, chemical and association reactions were observed [219, 220]. ZDDP and the amino group or Nitrogen from the dispersant form complexes (N=P, C=N) and affect the P=S bonds which in turn hinder the formation of ZDDP film during rubbing on metal surfaces [219, 220].

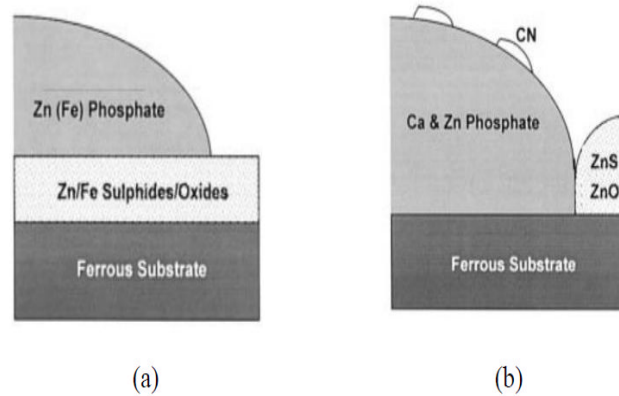


Figure 3-16 Schematic structure for films generated by: (a) ZDDP and (b) ZDDP/ Detergents/Dispersant

3.8. DLC/Additive Interactions

Extensive research has been carried out to focus on the interactions between DLC coatings and lubricant additives, namely MoDTC and ZDDP. It was generally proven that DLC coatings offer a friction reduction due to forming MoS₂ sheets (from MoDTC additive) on DLC surfaces [221-224]. ZDDP typically supplies more sulphur and that could facilitate the formation of low friction MoS₂. Thus, ZDDP/MoDTC solution provided lower friction (on the DLC coating) than ZDDP alone [225]. The hydrogenated DLC films are considered to provide the counterbody with a carbon layer. These layers are responsible for reducing friction on DLC surfaces [96].

Wear performance between DLC coatings and MoDTC is still not fully understood. Recently, it has been reported [221, 226-230] that DLC coatings wear faster in the presence of MoDTC when rubbed against a ferrous counterpart. Shinyoshi *et al.* [229] concluded that MoO₃ (which is formed from MoDTC) reacted with DLC and promoted the wear of DLC coating. The

mechanism by which MoDTC (MoO_3 in particular) is promoting high wear on DLC coating is shown in Fig. 3-17.

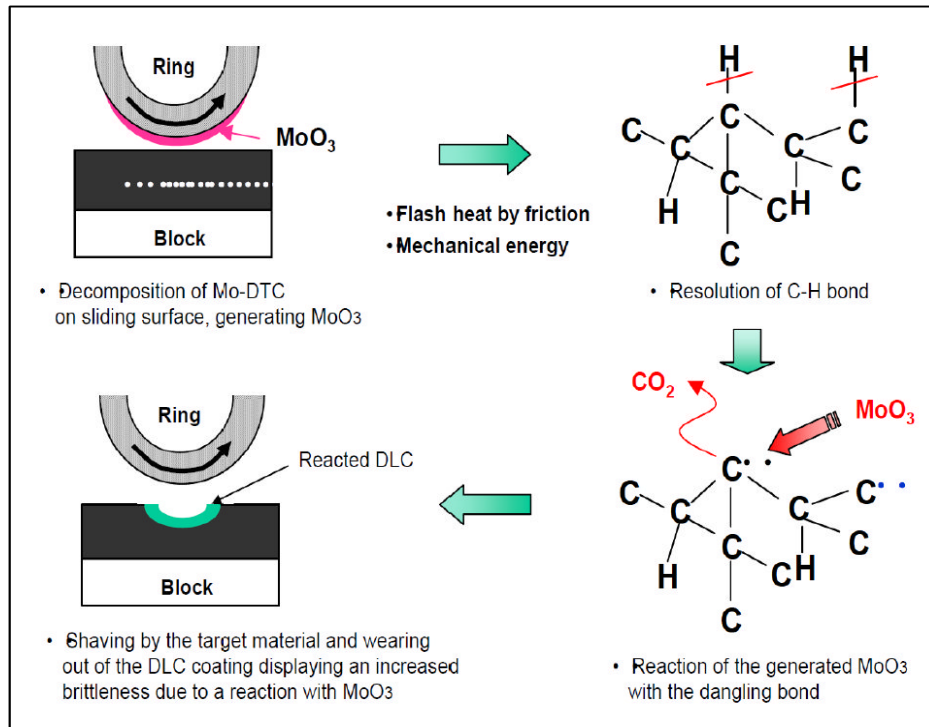


Figure 3-17 Wear steps of DLC coating in oil containing MoDTC [229]

Kosarieh *et al.* [230] showed that high concentration of MoDTC helped to increase wear of the DLC coating in oils without ZDDP but this wear was reduced by the addition of ZDDP. Likewise, ZDDP stopped the MoDTC from giving high wear to DLC in the DLC/ferrous combinations [231]. MoDTC-induced wear of the DLC coatings was only observed when the DLC was rubbed against a ferrous counterpart [221, 231]. That was attributed to the formation of molybdenum-containing compounds in the presence of ferrous counterparts leading to oxidation and accelerated wear of the DLC coating [231]. However, the reason for this performance is not yet clear whether it is chemical or only mechanical due to the reaction of MoO_3 [221]. Haque *et al.* [226] also reported that the presence of MoDTC in a DLC/steel contact gives high wear but the addition of ZDDP would limit this phenomenon. In contrast, Tung *et al.* [59] found that DLC coatings are able to reduce wear in the presence of MoDTC additive.

More recently, a new DLC mechanism has been proposed and validated by Feo *et al.* [232, 233], which suggests that the abrasion wear mechanism of DLC is not predominant. The multi-step proposed model for DLC-coated plate when lubricated by MoDTC-containing base oil is schematized in Fig. 3.18. It has been proposed that $\text{MoS}_{2-x}\text{O}_x$ compounds firstly form on the steel counterface (Molybdenum-based tribofilm). At the same time, during the friction experiment, Si–C bonds of the Si-doped DLC break due to temperature and mechanical stresses. As a result, the molybdenum formed on the steel ball reacts with C dangling bond generated on the DLC surface. This in turn generates the molybdenum carbide as a matrix of Mo-O-Fe-S compounds. In other words, the reaction between the molybdenum formed on the steel ball and the carbon of the DLC coating leads to the formation of molybdenum carbide (Mo_xC) species. As a result, an increase in the friction and wear rate of DLC surface can be observed.

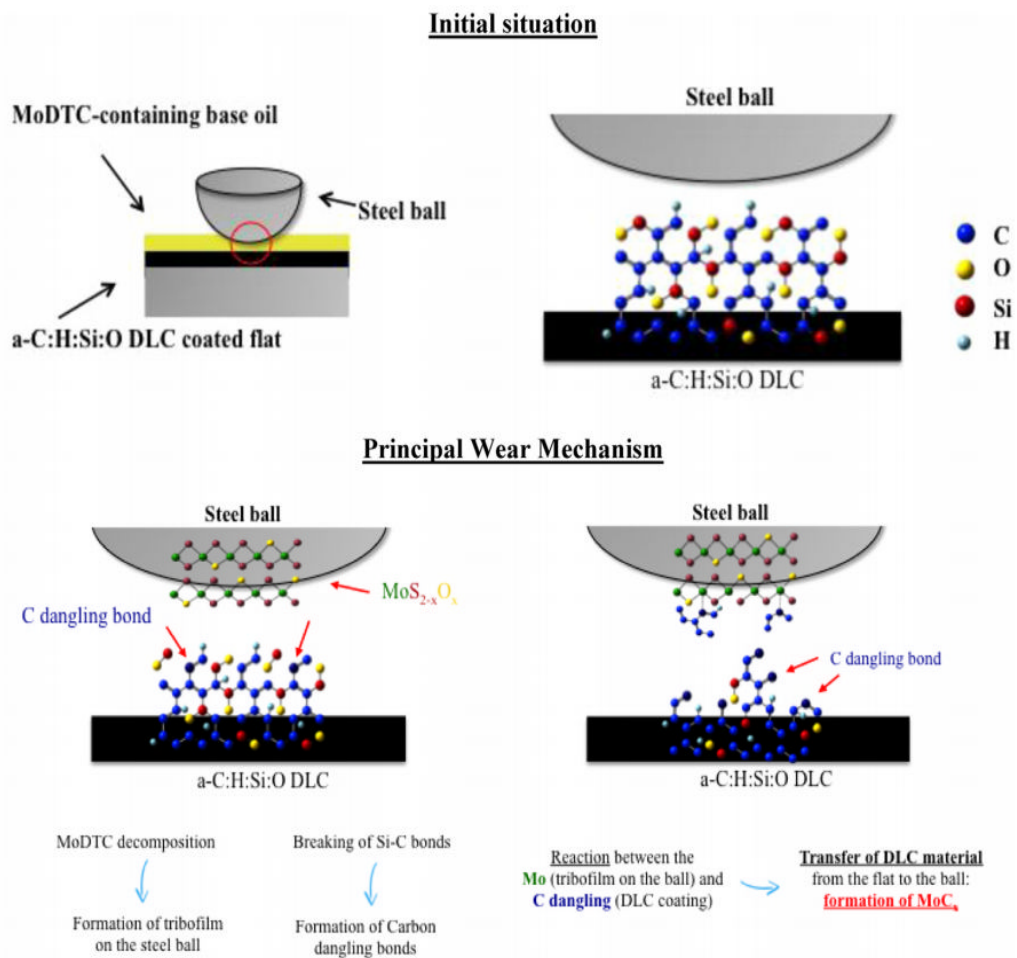


Figure 3-18 Multi-step of DLC coating in oil containing MoDTC [232]

Overall, the interactions of MoDTC/ZDDP additives with DLC coatings are not completely clear and their results of interactions in terms of friction and wear would depend on several parameters such as the chemistry of additives and coatings, lubrication regimes, lubrication formulations and other parameters.

3.9. Gaps in the Literature

3.9.1 Tappet Rotation

The direct acting valvetrain configuration (see Fig. 3-19) is one of the most commonly used in internal combustion engines. In this configuration, the camlobe is moved to provide an offset to tappet bore so as to facilitate tappet rotation for friction reduction. Tappet rotation is considered to have a unique effect on the durability of components (i.e. the rotation reduces wear caused by the contact with the camlobe, improves lubrication and then increases the lifecycle of the components) [234-237].

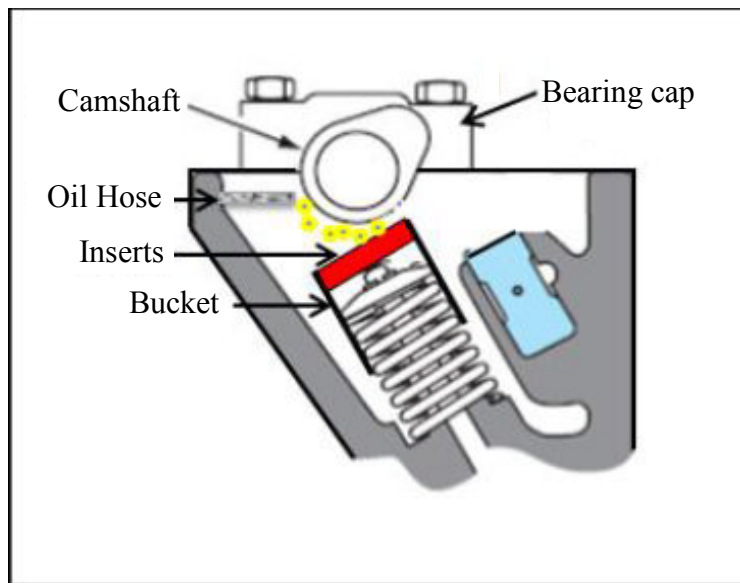


Figure 3-19 2D-schematic diagram of direct acting mechanical type valvetrain [115]

In the literature [238-240], limited models have been developed to investigate the influence of tappet rotation. However, the validation of such models (i.e. mathematical modelling and simulation) is still a challenge due to lack of experimental techniques and the complex mechanism of cam/follower

tribopair. The mechanism of this particular tribopair is complicated due to sliding/rolling motion, large contact pressure variations, changing film thickness, different lubrication regimes, and high acceleration speeds.

Various experimental techniques have been used to evaluate the effect of tappet rotation [235, 241-247]. Monteil *et al.* [241] used radioactive markers in the tappet surface while other investigators [242-244] used an optical fibre and a phototransistor situated under the tappet. Historically, Bona *et al.* [246] were the first researchers to monitor tappet rotation, where a pushrod was fitted inside the tappet and the rotation was obtained by means of a variable speed electric motor that caused the pushrod to rotate together with the tappet. On the other hand, a light reflectance arrangement was used by Pieprzak *et al.* [243] to investigate tappet rotation, where the light beam is aligned parallel to the axis of the tappet and focused on a portion of the tappet which is subdivided into reflective and non-reflective areas.

In recently published work, Mufti *et al.* [234] used a miniature magnetometer chip to measure tappet rotation. The sensor was fitted in the tappet-bore and detected a small slot that was machined into the tappet side. Although this method requires more modifications on the rig, this technique is less hazardous than using radioactive markers and is not affected by lubricants as compared to optical systems. The results showed that the tappet rotational speed generally increased with increase in camshaft speed and oil temperature. In addition, they reported that the rotation of all tappets in the engine may not behave similarly at the same speed under certain operating conditions. Dyson *et al.* [100] showed that during one cam revolution, the tappet rotational speed was not constant and will vary with the change of cam angle.

Researchers have mainly focused on understanding the link between tappet rotation, cam angle, oil temperature and camshaft speed. Very limited studies can be found focusing on the behaviour of tappet rotation under different oil formulations [235, 247]. Also, no work has been reported on the performance of tappet rotation under the effect of different coatings, thicknesses of tappets

and formulations with Molybdenum Dialkyl Dithiocarbamate (MoDTC) which has been found to be problematic to DLC wear [221, 226-230].

To address these gaps, a simple and effective technique has been employed in the Single Cam Rig (SCR) taken from a Ford engine. This technique does not require any changes or modifications on the SCR [234] while almost all the previous techniques are inapplicable as they required extensive modifications. According to [234], mounting the sensor and the magnet was a challenge due to lack of space on the single cam rig. Therefore, a new technique was developed as well as new positions for the sensor and the magnet were applied to overcome the limitations of the single cam rig employed. Details of this will be presented in the Chapter 4.

3.9.2 Tappet Clearance

The clearance between the follower and the camlobe (see Fig. 3-20) plays a considerable role in engine efficiency; incorrect clearance can negatively affect the tribological and tribochemical responses of the system. The incorrect tappet clearance can be defined as the clearance between the cam/follower tribopair which could be very small or very large. Small/large tappet clearance can cause inefficient performance of the engine valves (i.e. the valves may stay open or may not fully open/close). This would lead to valve leak (i.e. the leak can occur during compression and working stroke) and therefore engine power would be declined [248]. In addition, large tappet clearance can cause noise for the valvetrain which in turn would lead to increased wear and possible failure of the cam/follower system. Therefore, the clearance between the cam/follower tribopair is an important parameter that should be strictly taken into consideration during the design of an engine (direct acting tappet in particular) or in the process of maintenance (i.e. adjusting process for valve clearance). Selection of the thickness of the tappet will depend on the following factors; friction, wear, lubrication, noise, vibration and harshness (NVH). It is also worth mentioning that engine manufactures would consider further factors (such as the configuration/design of valvetrain, tappet thickness, valve lift, cam lift, etc.) before selecting the

correct/appropriate clearance. Tappet insert with variable clearance will affect the valve lift and as such the flow of air/exhaust in the combustion chambers of the engine. As a result, the engine power will be affected. However, cam/follower clearance will also affect wear, friction and NVH, possibly even leading to failure and inefficient performance of the intake/exhaust valves of the engine. Hence, it is important for engine manufacturers to understand the effect of the cam/follower clearance on friction, wear and tribochemical responses.

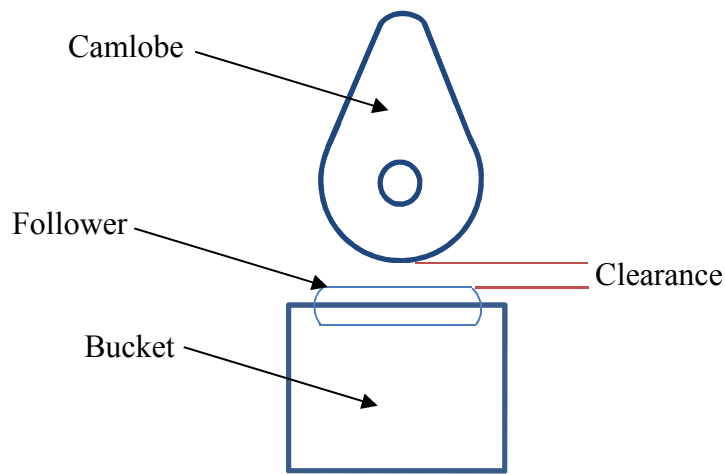


Figure 3-20 2D-schematic diagram of camlobe and follower

Author of this work believes that no reports have been published which address the impact of clearance on friction, wear and tribochemical responses in a valvetrain system. In this study, the first objective was to examine the friction and wear modes of the camlobes/tappets under the effect of tappet clearance and type of coating. The second objective was to map the tribochemical films across the camlobes as well as the tappets, with the tappet coating and clearance being the parameters of focus.

3.9.3 Tribochemistry and Wear of Camlobe

Essentially, “tribochemistry is a subject that brings together the disciplines of tribology, chemistry, physics, surface science and surface engineering to understand reaction processes occurring at lubricated contacts” [249]. The tribochemistry of an engine deals with the chemical reactions caused by different reasons, such as friction and wear, due to the interactions between surfaces in the presence of lubricants. These chemical reactions produce chemical tribofilms with particular characteristics.

Understanding the tribochemistry of the tribofilms, which mainly formed across the camlobe, will definitely help to prevent or reduce wear on the cam/follower tribopair. However, significant attention has been focused on the tribochemistry and wear of the tappet with little consideration of the camlobe. The reason may be from an idea that the tappet insert is always in contact with the camlobe but not all parts of the camlobe are connected with the tappet. Thus, the biggest wear was expected on inserts than on camlobes [62]. In terms of camlobe wear, the measurement methods were limited and classical. Also, the time duration of most tests was not sufficient to observe wear on camlobe. As a result, the knowledge of camlobe wear is still limited and unclear.

One of the objectives of this work is to study in detail the wear on camlobes with a newly developed single cam rig. As mentioned earlier, this study will also investigate the tribochemical films across the camlobes. Thus, by correlating the tribochemical behaviour of the tribofilms (that formed on the camlobes and tappets) to the wear profiles, more knowledge will be addressed regarding the nature of tribofilms formed across the camlobe, where these tribofilms typically has varying film thickness (i.e. different lubrication regimes), pressure, lubricant entrainment velocities and slide/roll ratio.

3.9.4 Sliding and Rolling Contacts

Sliding and rolling contacts are widely presented in different mechanical components such as cams, gears and roller bearings. The combination of

sliding/rolling motion can cause lubrication difficulties, high loads/applied stresses and film thickness variation. As a result, wear and plastic deformation can be observed which may lead to failure of the components. In the literature, however, most of the previous works have tended to focus mainly on pure sliding contacts, probably due to the fact that the pure sliding contacts are generally observed to be more severe than sliding/rolling contacts [124]. It should be noted that pure sliding contact, in most cases, does not necessarily simulate the actual contact in mechanical components as they mostly experience the combination of both motions (i.e. pure sliding and sliding/rolling). Thus, it is essential to investigate both the sliding and sliding/rolling contacts and to compare their tribological and tribochemical performance under mixed-boundary lubrication regimes.

The chemical composition of the tribofilms and/or tribofilm evolution is understood to vary with changing the type of contact (e.g. pure sliding contact + sliding/rolling contact). However, the understanding of the tribofilm formation towards changes in the tribological system, such as changing the type of contact (i.e. implying different SRR values) has not been given special attention. In the literature, the effect of sliding/rolling ratio on ZDDP tribofilm formation was previously investigated [122]. In addition, the tribofilm generation for a base oil and a fully formulated oil under the influence of sliding/rolling ratio was also examined [121]. Moreover, Khaemba *et al.* [119] studied the role of sliding/rolling ratio and surface roughness on the decomposition of MoDTC in a steel/steel system. However, in a DLC/Cl system, there is still limited understanding about how sliding/rolling ratio affects tribofilm build-up when using lubricants containing MoDTC additive.

3.10. Summary of Gaps in the Literature

- The behaviour of tappet rotation as a function of coating type, lubricant additives (especially MoDTC) and tappet clearance has not been given much needed attention.

- In general, the effect of tribochemistry on real cam/follower contacts has not been fully investigated.
- In particular, most studies have been focused on studying the behaviour of wear and tribochemistry of follower/tappet with little consideration on the camlobe.
- The impact of tappet clearance on friction, wear and tribochemical responses in a valvetrain system has not been clearly identified.
- Comparing sliding/rolling contact of DLC/cast iron systems to pure sliding contact, less focus on sliding/rolling contact has been reported.
- The link between sliding/rolling contacts, tribofilm build up and oil chemistry, in a DLC/cast iron system lubricated with MoDTC-type friction modifier, has not been clearly addressed.
- Wear performance between DLC coatings and MoDTC is still not fully understood. It is however essential to address how DLC coatings affect the interactions with MoDTC as a function of tappet clearance and type of contact.

Chapter 4. Experimental Methodology and Surface Analysis Techniques

4.1. Introduction

This chapter describes the experimental parts of this thesis study by covering several aspects:

- The tribometers used in the experimental work are described, namely MTM and SCR.
- A detail about the test materials, coatings and test lubricants are presented.
- A novel technique to measure tappet rotation are introduced.
- The methodology of the experimental work are described.
- A description of surface analysis techniques are reported.

4.2. Mini Traction Machine (MTM) Tribometer

The mini traction machine (MTM) in Fig. 4-1 was used to produce tribofilms under mixed-boundary lubrication conditions.

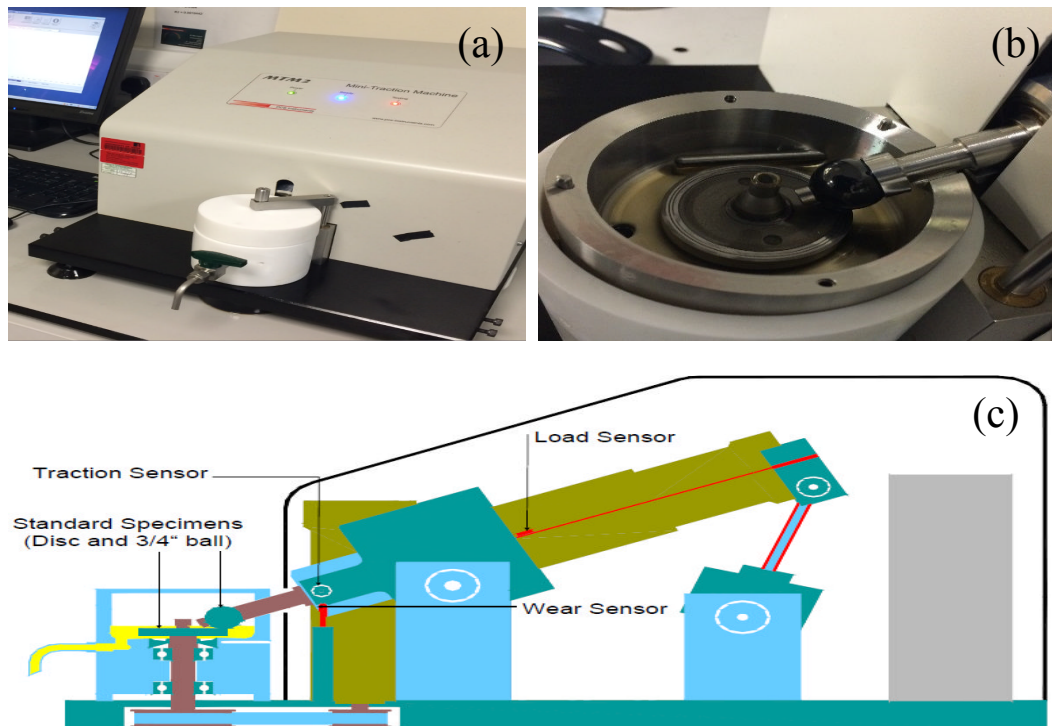


Figure 4-1 MTM tribometer (a) photograph of MTM (b) inside the test chamber (c) 2D schematic of MTM [250]

It consists of a 19.05 mm diameter ball rubbed against a 46 mm diameter disc and both were driven independently to allow for any desired sliding/rolling ratio (SRR). The tribopair (i.e. ball and disk) was submerged in the lubricant with a temperature controller to maintain the required value within ± 1 °C. The tribometer contains a load cell which attached to the ball drive to measure the friction. Wear, load and lubricant temperature can also be measured online by using several sensors [250, 251].

The MTM tribometer has a lid that covers the contact pair in order to keep a stable temperature in the tribometer and to avoid lubricant leakage. In addition, the MTM is controlled by a specific programme in a standard computer. This program can control the speed, temperature and load of the contact pair. It should be noted that MTM tribometer has a wide range of applications and can be used with different options such as (i) a pin-on-disc option (a stationary ball or pin loaded against the disc), (ii) a reciprocating option (cam and follower is the most common example) and (iii) electrical contact resistance (ECR) option [250, 251].

4.2.1 Test Materials and Coatings

Balls were made of alloy steel 16MnCr5 and discs were made of cast iron (CI). Balls were coated by commercial DLC coatings which contained 15 % hydrogen (a-C: 15H). The coating was deposited on the steel balls (by Oerlikon Balzers Ltd., UK.) using Plasma Enhanced Chemical Vapour Deposition (PECVD) process. From PECVD, a gas contained the elements of DLC coating (a-C: 15H) was supplied into the vacuum chamber and a discharge powered by an AC voltage was ignited. As a result, free carbon and hydrogen atoms (ions and radicals) were created and then reacted chemically with the substrate surface. This in return led to form the DLC coating on the steel balls. The selection of materials and coatings were based on the simulation process between MTM and SCR tribometers, which will be discussed in Chapter 9, with taking into account the commercial side. The detailed physical properties of the DLC coating, balls and discs are given in Table 4-1.

Table 4-1 Physical properties of balls, discs and DLC coating

	Balls	Discs	DLC coating
Specification	16MnCr5 Steel ^a	EN-GIL-250 Grey cast iron ^a	a-C: 15H ^b
Hardness	7.453-7.846 GPa	2.256-2.354 GPa	20-25 GPa
Roughness, R_q	0.02-0.05 μm	0.08-0.11 μm	0.02-0.05 μm
Reduced Young's modulus	207 GPa	110 GPa	160-200 GPa
Composition/ coating thickness	C 0.16, Si 0.20%, Mn 1.11%, P 0.011%, S 0.026%, Ni 0.07%, Cr 0.90%, Mo 0.01%, Cu 0.14%, Sn 0.10%, Al 0.022%, N 0.0101%	C 3.34%, Si 2.40%, Mn 0.49%, P 0.081%, S 0.060%, Mg 0.001%	1.5-3 μm

^a Balls and discs provided by PCS instruments, UK.

^b Commercial coatings provided by Oerlikon Balzers Ltd., UK.

4.2.2 Test Lubricants

The lubricants associated with the MTM tribometer are Group III mineral base oil and fully formulated oil, grade 5W30. All the oils were commercial and supplied by Total. Initially, several concentrations of MoDTC ranging from 0.1 wt % to 0.5 wt % were blended with the lubricants used in this study. However, considering the test duration, it was found that the effect of these low concentrations on friction reduction was insignificant and therefore difficult to discriminate between different oil formulations with regards to friction performance. For this reason, 1 wt% concentration of MoDTC was used in this work. With respect to lubricants containing ZDDP, the lubricant used was provided by Total with 1 wt% concentration of ZDDP. The key additive

components of each lubricant are described in Table 4-2. A representative photograph of lubricant oil samples is shown in Fig. 4-2. The base oil is a mixture of base oils and polymers (VI improvers and cold flow improvers). The fully formulated oil B contains detergents, dispersants, antioxidant, antiwear, viscosity index improvers as well as cold flow improvers. The detailed chemistry of the fully formulated oil B (i.e. O3) is provided by Total and shown in Table 4-3.

Table 4-2 Test lubricants

Annotations	Oil formulation
BO	Base oil B
O1	Base oil B + 1 wt% MoDTC
O2	Fully formulated oil B (free of ZDDP/MoDTC)
O3	Fully formulated oil B (free of MoDTC) + 1 wt% ZDDP
O4	Fully formulated oil B (free of ZDDP) + 1 wt % MoDTC
O5	Fully formulated oil B +1 wt% ZDDP + 1 wt% MoDTC

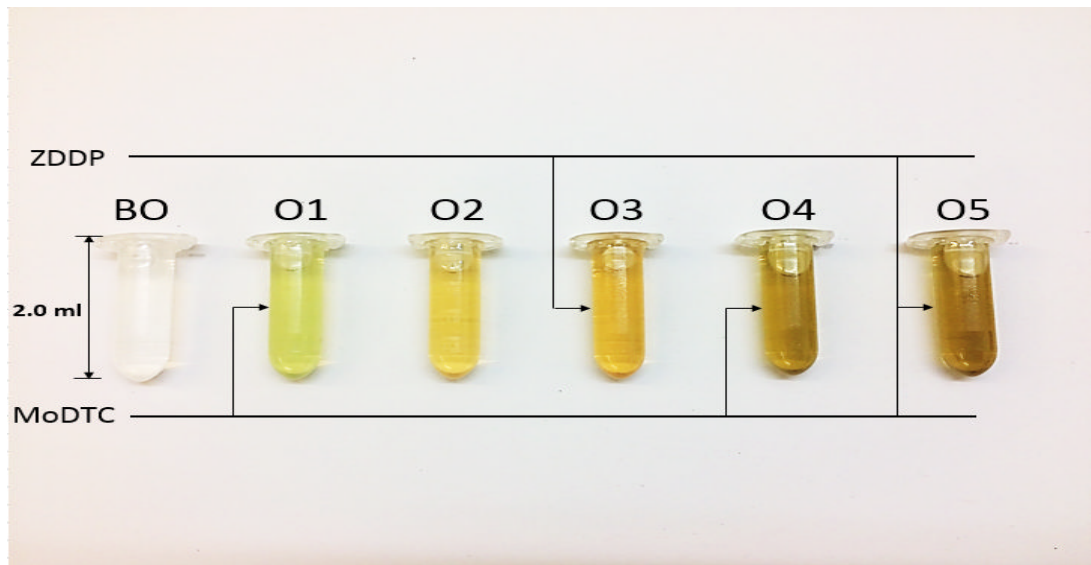


Figure 4-2 Photograph showing six representative oil samples

Table 4-3 General, physical and chemical characteristics

Characteristics		Fully formulated oil B	Unit
General characteristics			
SAE grade		5W30	N/A
API classification		SL/CF	N/A
Base oil type		Group 3	N/A
Physical characteristics			
Kinematic viscosity	At 40 °C	56,2	mm ² /s
	At 100 °C	9,84	mm ² /s
Viscosity index		163	-
Flash point		236	°C
Pour point		<-45	°C
Chemical characteristics			
Chemical Elements	Zn	1190	ppm
	Ca	3860	ppm
	Mg	<10	ppm
	B	<10	ppm
	P	1065	ppm
	Mo	0	ppm
	Ci	<30	ppm
	S of the lubricant	0,5	%
	S of the base oil	<0,05	%
Antiwear		ZDDPII	N/A
Friction modifier		No	N/A

4.2.3 Test Conditions

Initially, it was required to take the range of test parameters of the MTM tribometer into consideration because it explores the limitations of the tribometer and gives an attractive assistance during the experimental part and during the simulation process. The typical test parameter ranges of MTM tribometer are represented in Table 4-4. The test conditions employed in this study were: entrainment speed = 100 mm/s; temperature = 100 °C; sliding/rolling ratio = 50% and 200%; running-in duration = 30 mins; test duration = 6 hrs. Based on Hertzian contact pressure analysis and considering the test conditions (i.e. radius of the ball, the Young's modulus of the tribopair, entrainment speed, etc.), the contact load of 33.85 N gives a contact pressure of 0.75 GPa. This pressure was chosen in order to replicate a typical pressure at the cam nose in the cam/follower system. The entrainment speed with respect to the contacting surfaces was represented as $(u_b + u_d)/2$, where u_b is the speed of the ball while u_d is the speed of the disc. The sliding/rolling ratio was represented as the ratio of sliding speed $|u_b - u_d|$ to entrainment speed. However, SRR= 50% represents the sliding/rolling contact (this ratio is selected as a standard slipping ratio) while SRR = 200% represents the pure sliding contact (the ball was held stationary and the disc was allowed to rotate). The contact pressure values were however calculated based on the information mentioned in Table 4-5.

Table 4-4 Test parameters ranges of MTM tribometer

Parameter	Range
Load	0 to 75 N
Contact Pressures	0 to 1.25 GPa
Speed	-4 to 4 ms ⁻¹
Slide/Roll Ratio	0 to 200 %
Temperature Range	Ambient to 150 °C

Adapted from [250]

Table 4-5 Mechanical properties of samples

Property	Ball	Disc
Young modulus	207GPa	110GPa
Poisson ratio	0.3	0.211

4.2.4 Experimental Methodology / MTM

Figure 4-3 illustrates the experimental outline of the MTM tribometer. The samples were cleaned ultrasonically prior to the start of the test using acetone for at least 15 minutes. Further, the samples were wiped with a cotton bud soaked in isopropanol. Lastly, an airbrush with isopropanol was used to clean the samples from dust.

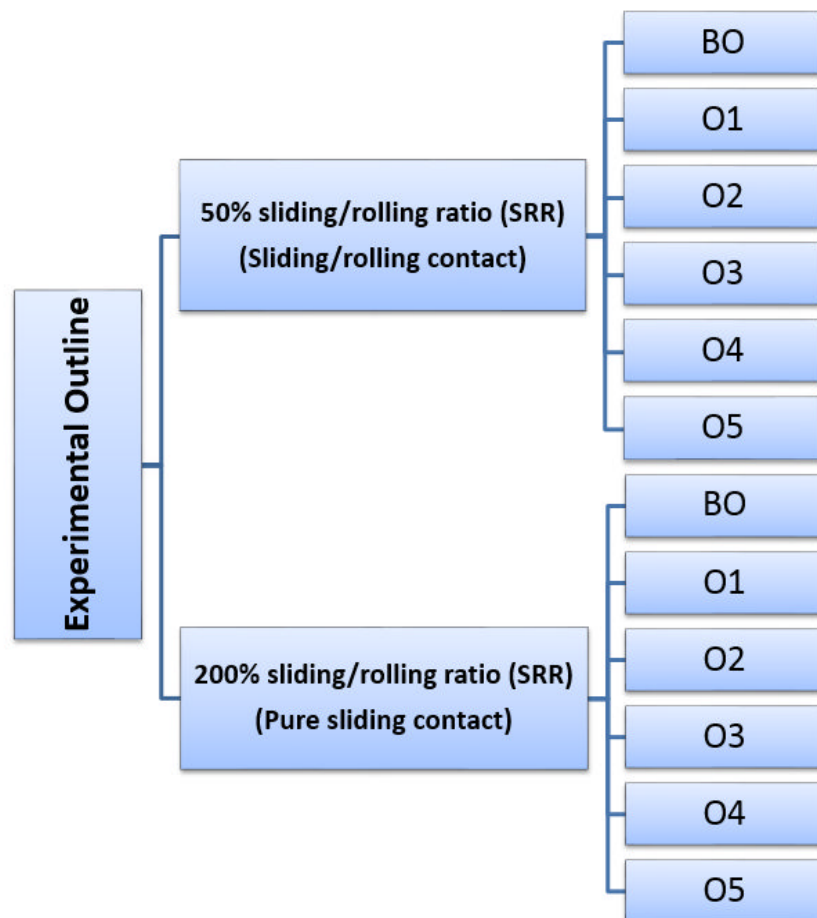


Figure 4-3 MTM experimental outline

Two types of tests were carried out in the MTM tribometer, (i) durability tests and (ii) Stribeck curve tests. Durability tests are used to observe the stability of the DLC/cast iron system over a period of time under the boundary lubrication regime. Stribeck curve tests are used to evaluate the friction properties of the DLC/cast iron system under mixed-boundary lubrication regimes. The durability test was calculated at 100 mm/s during the whole test duration (6.5 hrs) which is in the boundary lubrication regime. The Stribeck curve test was obtained by measuring friction over a range of entrainment speeds ranging from low to high speeds, 5 to 2000 mm/s. Film thickness develops with increasing entrainment speed, progressing from boundary lubrication regime at low speed through to mixed lubrication regime at high speed. Each test had eight steps, as described in Table 4-6.

Table 4-6 MTM test steps

NUMBER OF STEPS	STEP DESCRIPTION	COMMENTS
1	Running-in	Test duration 30 minutes Speed 100 mm/s
2	Stribeck test	Test duration 1-2 minutes Speed range 5-2000 mm/s
3	Durability test	Test duration 2 hours Speed 100 mm/s
4	Stribeck test	Test duration 1-2 minutes Speed range 5-2000 mm/s
5	Durability test	Test duration 2 hours Speed 100 mm/s
6	Stribeck test	Test duration 1-2 minutes Speed range 5-2000 mm/s
7	Durability test	Test duration 2 hours Speed 100 mm/s
8	Stribeck test	Test duration 1-2 minutes Speed range 5-2000 mm/s

From Equation 2-2 and Equation 2-3, the calculated Lambda ratio (λ) showed that the operating regime was boundary lubrication ($\lambda = 0.1$) for the durability test and mixed-boundary lubrication (ranging from $\lambda=0.1$ at low speed to $\lambda = 1.2$ at high speed) for the Stribeck curve tests. For BO and O1, however, the calculated Lambda ratio was not exceeding 0.9 at high speed implying a boundary lubrication regime throughout the Stribeck curve tests for these lubricants.

4.3. Single Cam Rig (SCR) Tribometer

The single cam rig tribometer in Fig. 4-4 was developed by Ofune *et al.* [76]. This was to simulate the real operating conditions of the cam/follower interface in an automotive engine. The rig was constructed from a cut down 1.25L ford Fiesta Zetec-SE engine with a double overhead camshaft (DOHC) and flat faced removable inserts/tappets in bucket arrangement. The calibration and development of the direct acting SCR tribometer have been described in detail previously [76]. Basically, the camshaft was driven through a mechanical coupling by a 2.2 kW ABB motor (i.e. non-fired mode). The system was able to operate at high speed (up to 3000 rpm) with limited noise and vibration. A high sensitivity torque transducer (RWT 421) was connected to the camshaft by means of flexible coupling to obtain speed and torque measurements. The calibration of the torque transducer has frequently been made by the manufacturer. However, an additional calibration was done in Leeds university [115]. A Hohner shaft encoder with a 720 pulse wheel of 25.4 mm diameter was affixed at the end of the 20 mm camshaft for cam angle triggering. The SCR was equipped with a heating system (HAAKE DC200) with a sensitivity of ± 0.10 °C to simulate the temperature close to real engine operating conditions. The lubricant bath consists of a 5 L reservoir which was filled with the set amount of the lubricant for the test. The flow rate of the lubricant was controlled by check valves connected to a 6 mm hose. The SCR tribometer consists of a box which covers the cam/follower area in order to keep a stable temperature in the tribometer and to avoid lubricant leakage. In addition, the SCR is also controlled by a standard computer which gives simplicity and accuracy during tests. The clearance/gap between the followers and base

circle of the camlobes was maintained around 0.11-0.58 mm. This was achieved by using standard production inserts with different thicknesses (i.e. 2.275, 2.575 and 2.75 mm). The centre of the tappet was slightly offset from the centre of the camlobe to facilitate rotation of tappet/bucket for friction torque reduction.

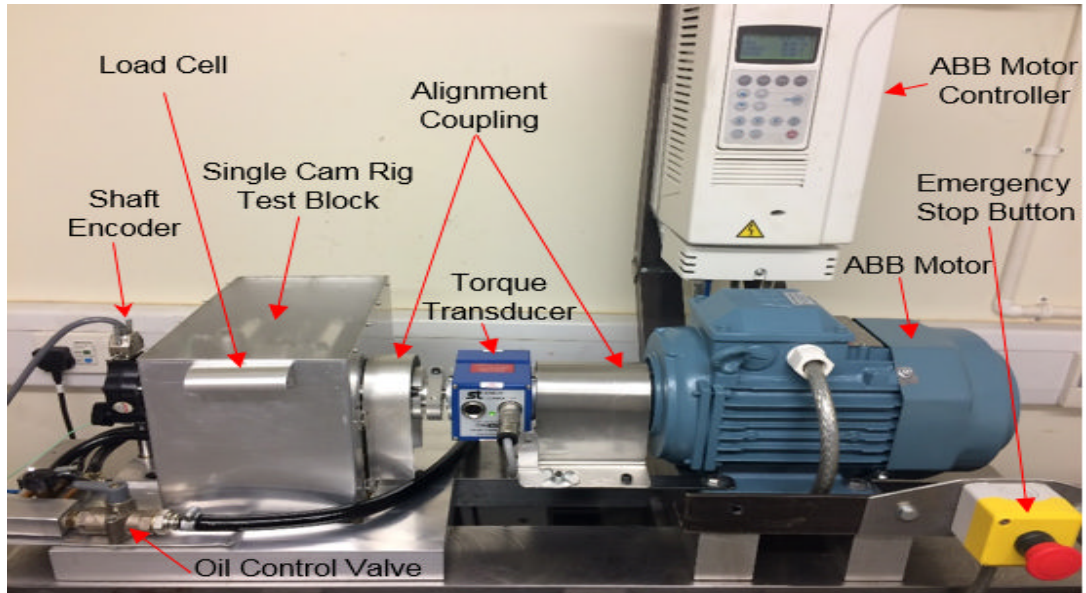


Figure 4-4 Single cam rig tribometer (SCR)

4.3.1 Test Materials and Coatings

Experiments were performed using standard production inserts made of steel. The inserts were coated with Mn-phosphate coating (MnPO_4) with thickness of 0.5-2.0 μm , where MnPO_4 coating is a commercial standard production surface coating for inserts. Diamond-Like Carbon coating (DLC) with thickness of 1.5-5.5 μm was also evaluated in the motored single cam rig. Similar to MTM samples, the DLC coating was deposited on the steel tappets (by Oerlikon Balzers Ltd., UK.) using Plasma Enhanced Chemical Vapour Deposition (PECVD) process. The surface roughness values were 0.25 μm and 0.02 μm for the MnPO_4 and DLC coating respectively. The camshaft is a standard production made from chromium chilled cast iron with R_a 0.15 μm . The tappet insert is made of 16MnCr5 steel (with thin film surface coating of Mn-Phosphate) with hardness of 60 – 70 HRC (typically harder than the camshaft). The hardness of camshaft was in the range of 50 – 55 HRC. In addition, the hardness of DLC coating was in the range of 15 – 25 GPa. For

the engine used in this work (1.25L ford Fiesta Zetec-SE), different tappet thicknesses ranging from 2 mm to 3.3 mm can be employed. However, as mentioned earlier, only three thicknesses of tappets were chosen for this study (2.275, 2.575 and 2.75 mm) which were commercially available and in line with the methodology of this work.

4.3.2 Test Lubricants

Two lubricants were used in the SCR tests (i.e. O3 and O5, from Table 4-2). Both of them were fully formulated oils containing 1wt% of Zinc DialkylDithioPhosphate (ZDDP). However, one of the fully formulated oils (i.e. O5) was blended with 1 wt% of Molybdenum Dialkyl Dithiocarbamate (MoDTC).

4.3.3 Test Conditions

A cam/follower design is very complex because there are many inter-related parameters that must be taken into account. These parameters experience a huge dynamic variation in load and applied stress at different engine operating conditions such as low speed, high speed, high temperature, full-load, no-fuel motoring and others [252]. Thus, it is essentially important to explore the range of operating conditions of a cam/follower system because it helps during the experimental work and the simulation process. Table 4-7 shows typical tribological and performance parameters of cam/follower mechanism for IC engines with a range of its operation conditions.

Table 4-7 Typical tribological and performance parameters for IC engines

Parameter	Cam / Follower
Temperature	80 – 150 °C
Speed	250 – 9000 rpm
Maximum Pressure/Loading	0.6 – 2.0 GPa
Minimum Film Thickness	0.1 – 0.15 µm
Power Losses	0.04 – 0.20 KW
Composite Surface Roughness	0.02 – 0.3 µm Ra

Adopted from [28]

The single cam rig tribometer offers a great opportunity to simulate the real operating conditions of cam/follower contact in an automotive engine taking into account the limitation of speed in the single cam rig (i.e. high speeds increase the vibration and the noise of the rig). The average friction torque was recorded at camshaft speeds of 300, 600, 1000, 1200, 1500, 1800 and 2100 rpm. The average friction torque was obtained by taking an average of the 200 data points obtained for each camshaft cycle (i.e. this corresponds to approximately 1 data point for every 1.8° of cam shaft rotation). The SCR has a typical contact load (1286 N) which in return results in a mean contact pressure of 0.75 GPa.

For MnPO₄ experiments, the oil temperature was maintained at 100 °C and 130 °C, as different test conditions. For DLC experiments, however, the test was only carried out at 100 °C due to limited availability of sensors used in tappet rotation measurement.

To evaluate the lubrication regime at the cam/follower interface, Dowson and Higginson equation for line contact was used [31]. For both coatings (i.e. MnPO₄ and DLC) and based on the speed range tested, the oil film thickness lies in the range of 0.05-0.21 μm. In addition, the calculated Lambda ratio (λ) was 0.21 at 300 rpm and around 3.12 at 2100 rpm (i.e. boundary/mixed regime). The SCR was set to run for a longer duration at low speeds, which is under predominantly boundary lubrication regime.

4.3.4 Tappet Rotation Measurement

A range of GMR sensors against magnets were investigated for sensing rotation of the tappet. Initially, a simple test rig (see Fig. 4-5) was designed (by ReSolve, UK) to help validate and tune the sensor-magnet setup. The test rig was used to evaluate the different sensor board-magnet combinations across varied geometric conditions. The relative orientation of the sensor and magnet was investigated to determine the best signal response while considering the machining and geometric constraints of the cam housing and tappet respectively. The sensor signal was monitored using a data acquisition

device (NI myDAQ, National Instruments, USA) while the speed of the motor (918D15112/1, Como Drills, UK) was varied from 0-400 rpm. For a vertical mounted sensor with the magnet configuration shown, a stable pulse train was generated across the entire speed range. This configuration was therefore selected for integration into the cam housing.

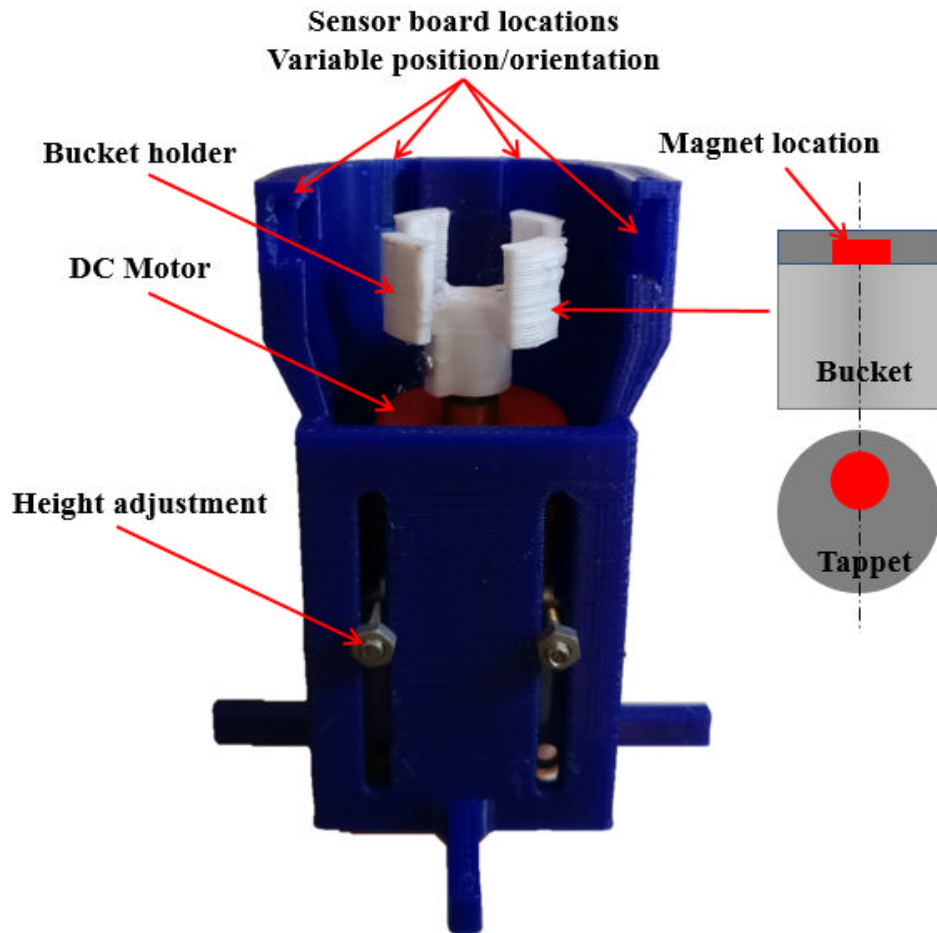


Figure 4-5 Tappet rotation test rig

The ADV001-00E north-south latching bipolar digital switch sensor (RHOPOINT components, UK) was found to give the highest sensitivity to the magnet/tappet magnetic field within a suitable form factor for integration into the tappet housing. The ADV001-00E was configured with a 5 V supply (myDAQ, National Instruments, Texas, USA) and a pull up resistor to generate a latch low (0 V) signal upon approach with a sufficient magnetic field and high reset (5 V) on presence of an opposing field.

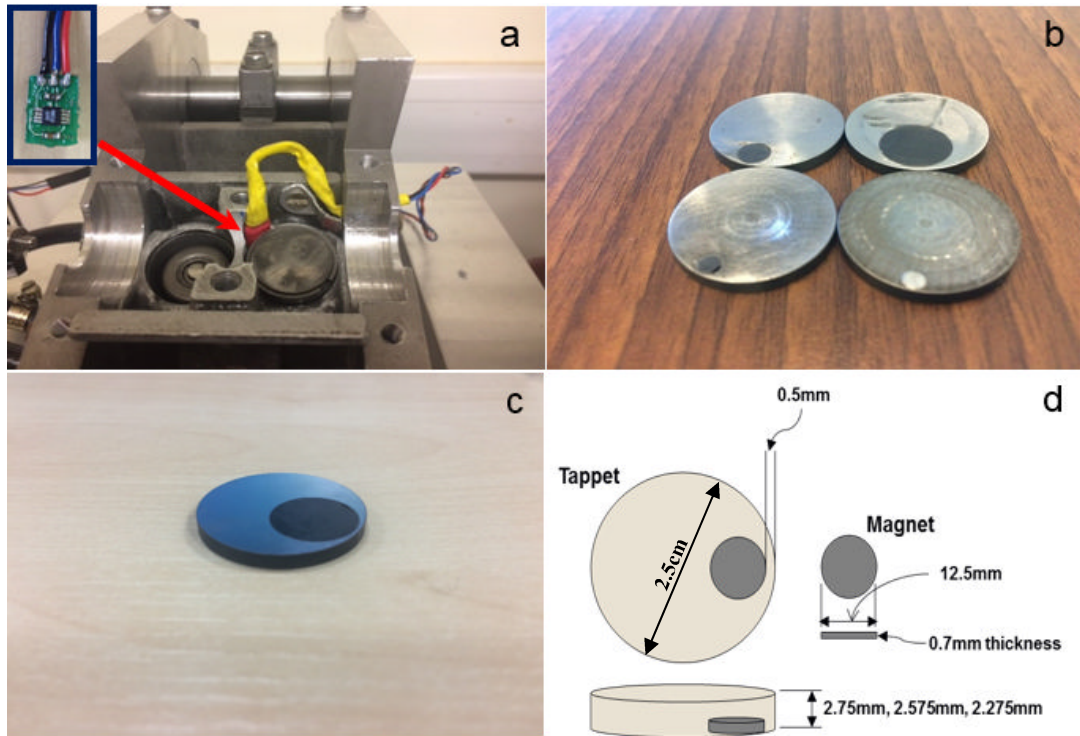


Figure 4-6 Sensor and magnet information: (a) sensor position on the single cam rig, (b) different sizes of magnets were initially tested, (c) a magnet force fitted onto the underside of a shim (d) magnet dimensions and position

As shown in Fig. 4-6a, the sensor was installed very close to the tappet/bucket and the wires (from the sensor) were routed out of the rig from the side. Different sizes of magnets (see Fig. 4-6b) were initially tested in order to select the right size magnet which has the ability to maintain a strong magnetic field at high temperatures. Therefore, the sensor was coupled with a split pole ferrite disc magnet (12249, RHOPOINT components, UK) which was machined eccentrically into the underside of the tappet (see Fig. 4-6c). A material from the tappet was extracted and the magnet (with thickness 0.7 mm) was force fitted onto the tappet. Magnet information (i.e. dimensions and its position on the tappet) are shown in Fig. 4-6d. The mass of tappet was checked with and without the magnet and the difference was negligible. Likewise, magnet position did not modify the normal rotation of the tappet. Latching behaviour of the sensor generated a robust pulse train with one cycle per revolution of the tappet allowing rotation count and speed determination. Measurements of tappet rotation were obtained using a data acquisition device and bespoke software (LabVIEW, National Instruments).

4.3.5 Experimental Methodology / SCR

Figure 4-7 shows the experimental outline of the single cam rig (SCR) tribometer. The test cycle included two sections: the running-in stage and the steady state stage, as shown in Fig. 4-8. A whole test contains six cycles (i.e. each cycle takes 12.5 hrs and the total time for each test is 75 hrs, without the running-in time). On the other hand, tappet rotation was recorded using an advanced data acquisition system. Accordingly, from the LabVIEW software, the rotation was obtained by calculating the number of counts (i.e. pulse counts) per second.

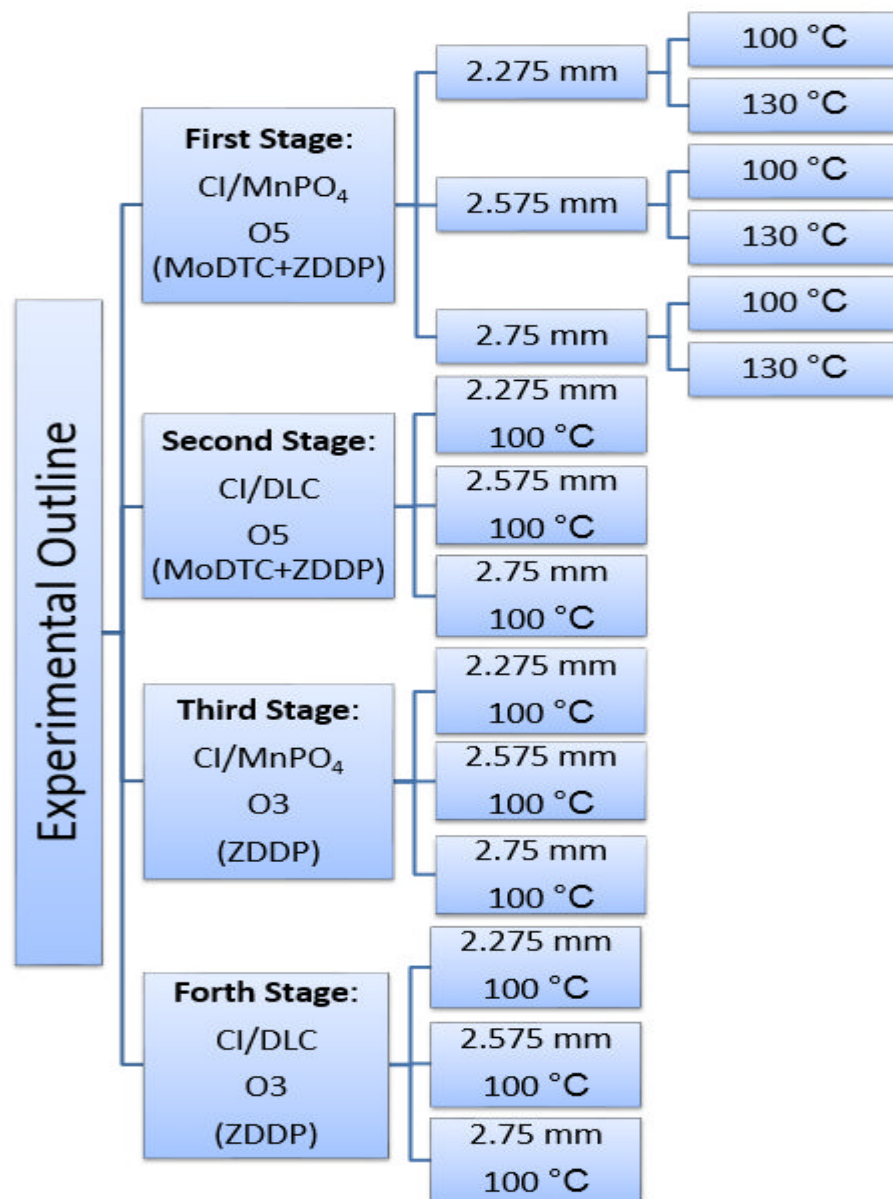


Figure 4-7 SCR experimental outline

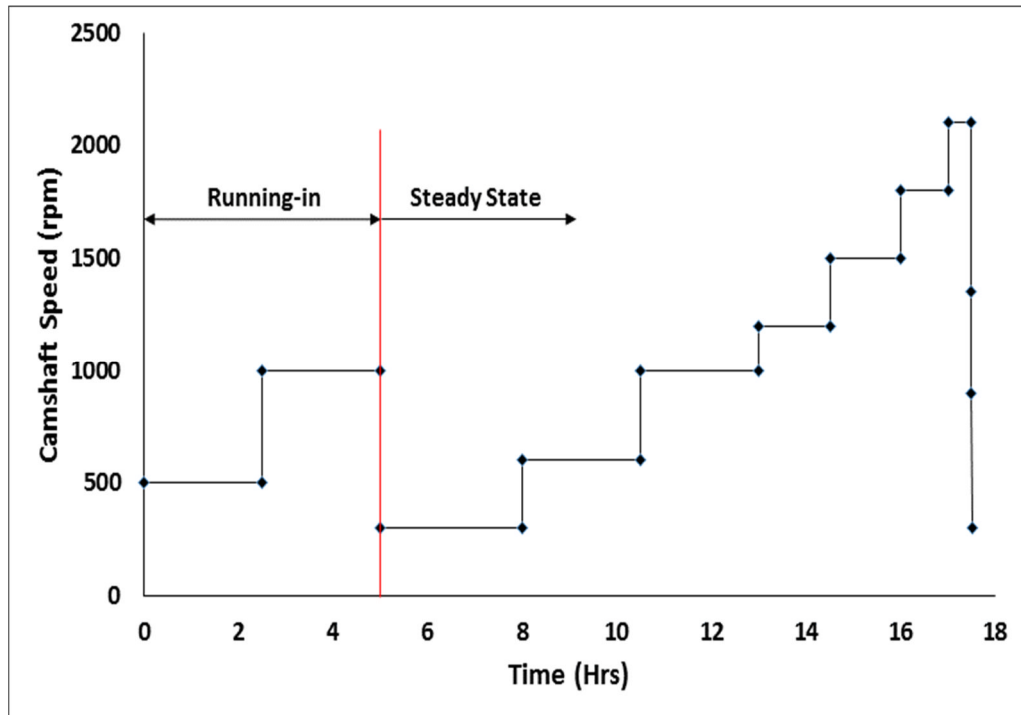


Figure 4-8 Single cam rig test cycle

4.4. Surface Analysis Techniques

Different surface analysis techniques were used in this study to characterise the topographical and chemical features of the formed tribofilm on the wear scar.

4.4.1 Optical Microscope

A Leica DM6000M Microscope was used for physical observation of DLC balls and CI discs. High quality 2D and 3D Images can be obtained from this microscope using LAS V3.8 software. The microscope helps to provide information on wear mechanisms (i.e. investigate the durability of coatings) as well as to measure the width of the wear scars formed on the ball/disc tribopair.

4.4.2 NPFLEX White Light Interferometer (WLI)

2D and 3D images of wear tracks generated on the MTM samples (i.e. ball and disc) and SCR samples (tappets only) were obtained by white light interferometry using NPFLEX from Bruker, UK. The results obtained from

NPFLEX were analysed using Vision64 software. Before NPFLEX analyses, in order to remove any physisorbed tribofilm formed on the wear scar, all samples were cleaned in acetone in an ultrasonic bath for at least 15 minutes. In addition, prior to the wear measurement, a droplet of ethylenediaminetetraacetic acid (EDTA) was used (by the method described in [253]) to remove the tribofilm from the analysed wear track. The droplet was removed with a cotton bud and the samples were cleaned with an airbrush filled with isopropanol. This was necessary to avoid any misleading wear measurements due to the transparent characteristics of the formed tribofilm [254]. Two-dimensional and three-dimensional images for the wear track were taken, and the average wear depth of different sections inside the wear track were calculated. The typical data of the cross sectional area of the wear scar, obtained from the Vision64 software, is given in Figure 4-9.

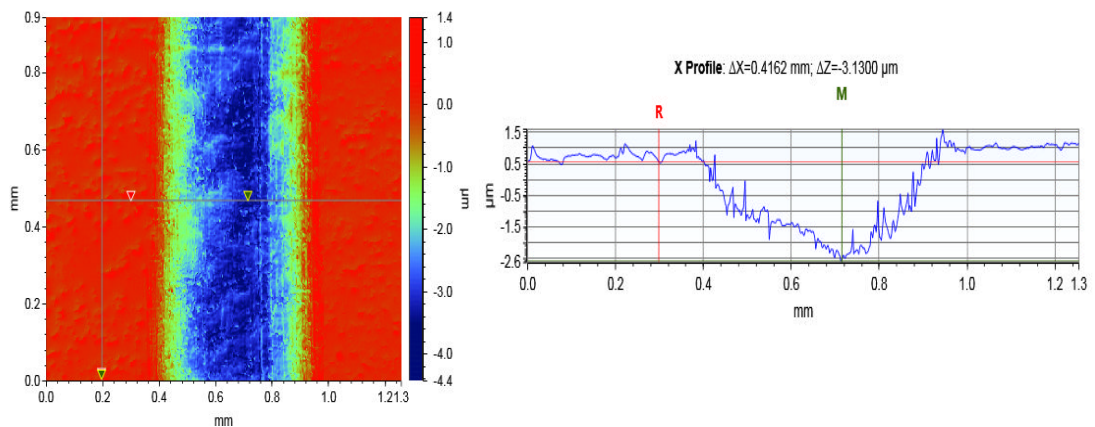


Figure 4-9 Typical NPFLEX wear measurements of the CI disc

4.4.3 Scanning Electron Microscope (SEM) / Energy Dispersive X-Ray (EDX)

In this work, a Zeiss EVO MA15 variable pressure SEM was used to analyse the worn surfaces and to investigate the durability of the coatings employed. An Oxford instrumented EDX (probes to 1 µm depth) with scan size of 80 mm² was incorporated into the SEM device to provide elemental composition of the different regions on the coated inserts. Energy-Dispersive X-ray (EDX) analyses of the inserts were obtained from inside and outside the wear tracks.

For all samples, it was essential to examine an unworn surface for comparison. Thus, SEM/EDX analyses were performed before and after the test.

From SEM (see Fig. 4-10), under vacuum conditions, high resolution images to nano-meter scales (nm) can be produced. These images were recorded at an accelerating voltage of 20 keV corresponding to a volume fraction analysis depth around 2-3 μm . Ideally, a beam of electrons are produced by an electron gun. These electrons will interact with the atoms of the test surface resulting in different signals. The radiation emitted can be collected by a detector and the signals will be shown on the television monitor screen [255]. These signals allow the identification of surface features and small particles present.

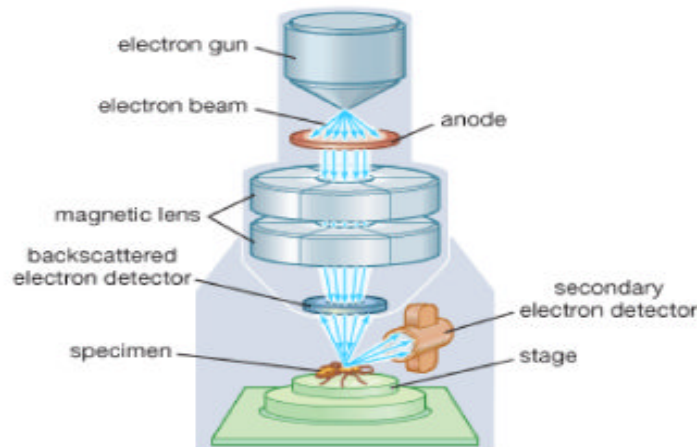


Figure 4-10 Schematic of Scanning Electron Microscope [256]

4.4.4 Focused Ion Beam (FIB) / Transmission Electron Microscopy (TEM)

The samples were prepared using FEI Nova200 dual beam SEM/FIB fitted with a Kleindiek micromanipulator for in situ lift-out. FIB technique is used to quantify the exact thickness, composition and morphology of any tribofilm formed on the worn samples. The FIB section is 15 microns by 5 microns with a final thickness of approximately 50 nm.

After FIB sample preparation, Transmission Electron Microscopy (TEM) analyses were performed. A beam of electrons is transmitted through an ultra-thin specimen and interacting with the specimen. Consequently, an image is formed from the interaction of the electrons transmitted through the specimen. TEM analysis was carried out using the FEI Titan Themis Cubed 300 operated at 300kV, fitted with Super-X EDX system with windowless 4-detector design, EDX data was analysed using Velox. TEM images were collected using the Gatan OneView 16 Megapixel CMOS digital camera. STEM images were collected under HAADF conditions. The TEM high resolution images were used to provide quantitative and qualitative information about the thickness of the tribofilms formed after the tribotest. Fig. 4-11 shows one of the typical FIB preparation sections for TEM.

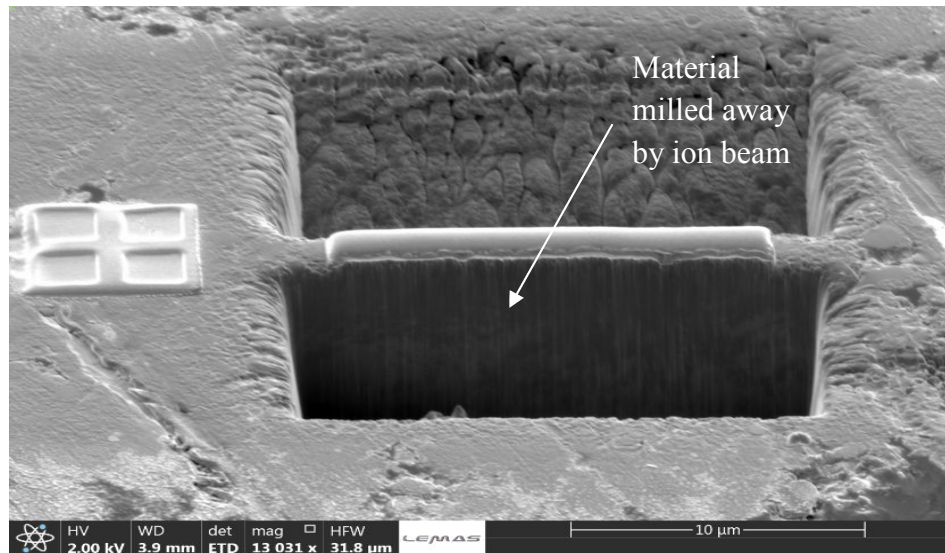
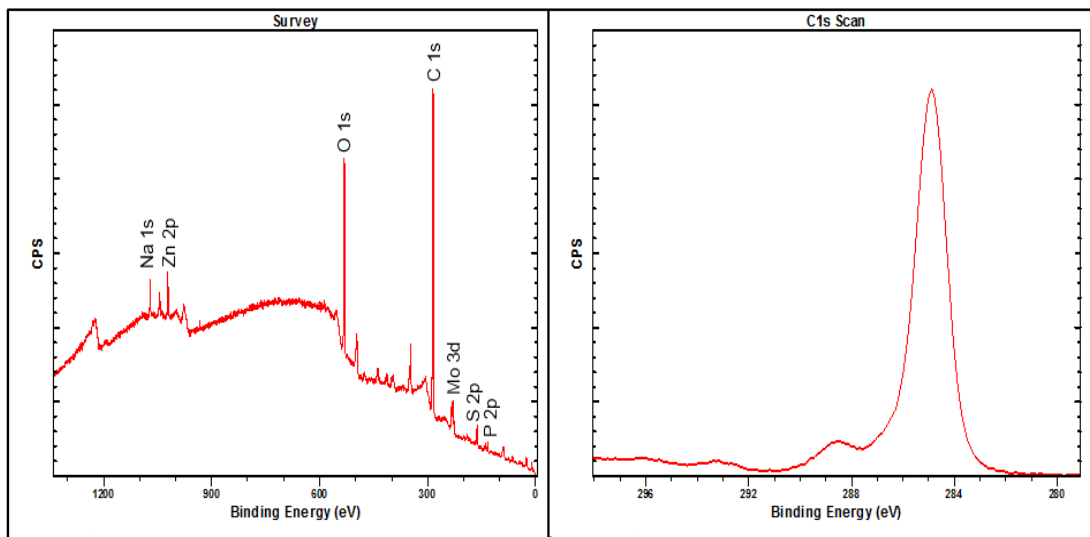


Figure 4-11 Typical FIB preparation section for TEM

4.4.5 X-ray Photoelectron Spectroscopy (XPS)

X-ray Photoelectron Spectroscopy (XPS) analysis was carried out in this study. XPS is a powerful technique extensively used for the surface analysis of materials. This technique allows the tribofilms chemistry to a depth of approximately 5 nm to be determined. XPS was performed at NEXUS facility nanoLAB with a Theta Probe MK (II). XPS depth profiling experiment was performed on worn samples using ion gun monatomic bombardment. For both tribometers, the XPS survey scan was used to determine the type of elements

present in the tribofilms. Typical survey and long scans obtained from the XPS instrument are presented in Fig. 4-12. However, before using XPS analysis, all samples were cleaned using n-heptane to remove residual oil and contaminants. The electrons were excited with a micro focused monochromatic aluminium K-alpha X-ray source of 1486.6eV. A handbook of XPS was used to identify most of the chemical species at the respective binding energies [257]. The XPS curves were processed using the CasaXPS software. The position of the major component of the C1s peak (284.8 eV) was considered as the reference for charge correction. The peak area ratio, full-width at half-maximum (FWHM), and difference between binding energies of the doublets were taken and found from literature and then applied to the data received. A linear background approximation was used to process the data in this study.



(a)

(b)

Figure 4-12 Typical survey scan (a) and long scan (b) obtained from XPS

4.4.6 Raman Spectroscopy

Raman spectroscopy has been commonly used to determine the structure/composition of the tribofilms generated in a tribocontact. In this study, a Renishaw inVia Raman spectrometer with 488 nm wavelength and 10% power filter was used to examine the structural modifications inside and

outside the wear track of all the samples. The laser power of 488 nm was essential to detect distinct MoS₂ peaks from MoDTC tribofilm [198]. For camlobes, the structural modifications of the tribofilms took place at seven locations using ASTM D6891 standard. This was also an attempt to map the tribochemical films across the camlobes and correlating this to the wear. Details of this will be discussed in the following section. Raman principle is based on the inelastic scattering of a monochromatic light [258]. This scattered light is split into component wavelengths or spectrum and detected on a charged-couple device (CCD) detector (see Fig. 4-13). This light interacts with the vibrations of the system resulting in a variable energy that shifts up and down. This shifting provides information about the test sample.

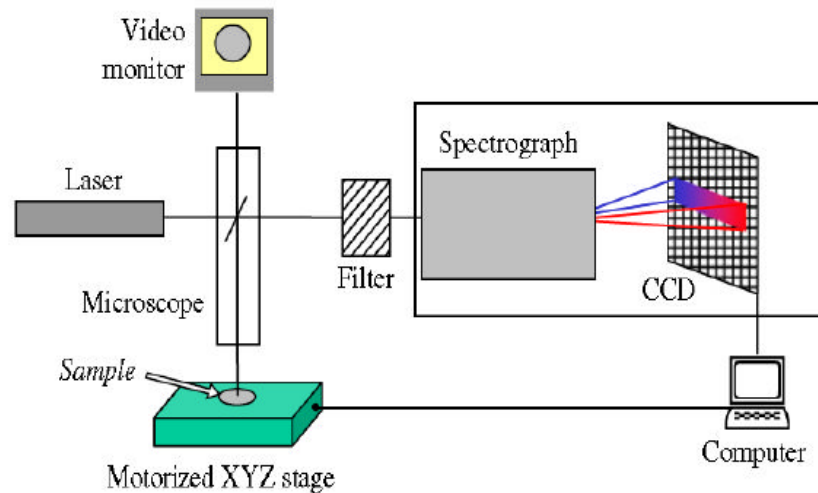


Figure 4-13 2D schematic representation of Raman spectroscopy [259]

4.4.7 Contact Profilometry

In this study, two dimensional measurements were conducted using the Talysurf 120L from Taylor Hobson. This technique was used to observe the depth of wear scar formed on camlobes. In addition, surface profile and surface roughness were analysed. The data was collected using Talysurf ultra software. In an attempt to link the wear of the camlobes with standard engine tests, wear examination took place at seven locations on the cam profile ($\pm 14^\circ$, $\pm 10^\circ$, $\pm 4^\circ$ and cam nose- 0°) (see Fig. 4-14), in accordance with ASTM D6891 standard (sequence IVA). This method was recently used by [76, 134]. The

cam nose (0°) was considered as the reference and other locations were indexed with respect to this location. However, all locations were measured with an angular digital dial and protractor which was affixed on the camlobes with an accuracy of $\pm 0.5^\circ$. For all seven selected locations, the contact pressure, lubricant entrainment velocity, load per unit length, cam lift profile, velocity profile and acceleration profile were evaluated by Ofune [115] to correlate these values to the wear mechanisms (see Table 4-8 and Fig. 4-15). This was done to understand the nature of tribofilms formed across the cam profile which typically, has varying pressure, film thickness, slide roll ratio and lubricant entrainment velocities. Moreover, at all locations, several traces were taken and the average was used as the wear scar for the camlobe. A typical cam nose profile pre-test and post-test is presented in Fig. 4-16.

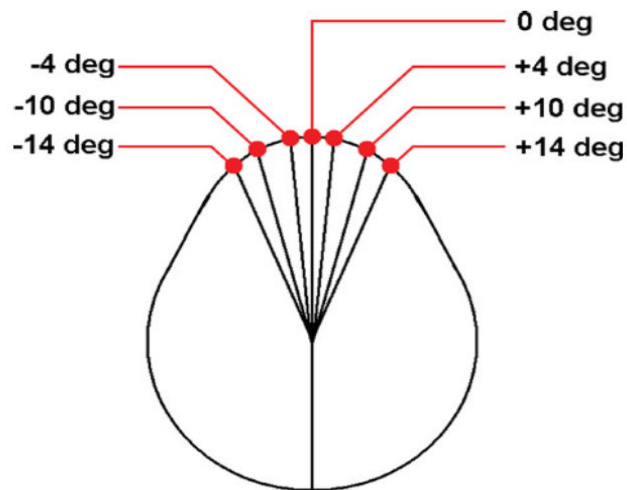


Figure 4-14 The seven positions of surface profilometer traces on the camlobes [134]

Table 4-8 Contact pressure across camlobe

Angle	Pressure
0° (cam nose)	0.76 GPa
$\pm 4^\circ$	0.70 GPa
$\pm 10^\circ$	0.62 GPa
$\pm 14^\circ$	0.59 GPa
180° (base circle)	0 GPa

Adapted from [115]

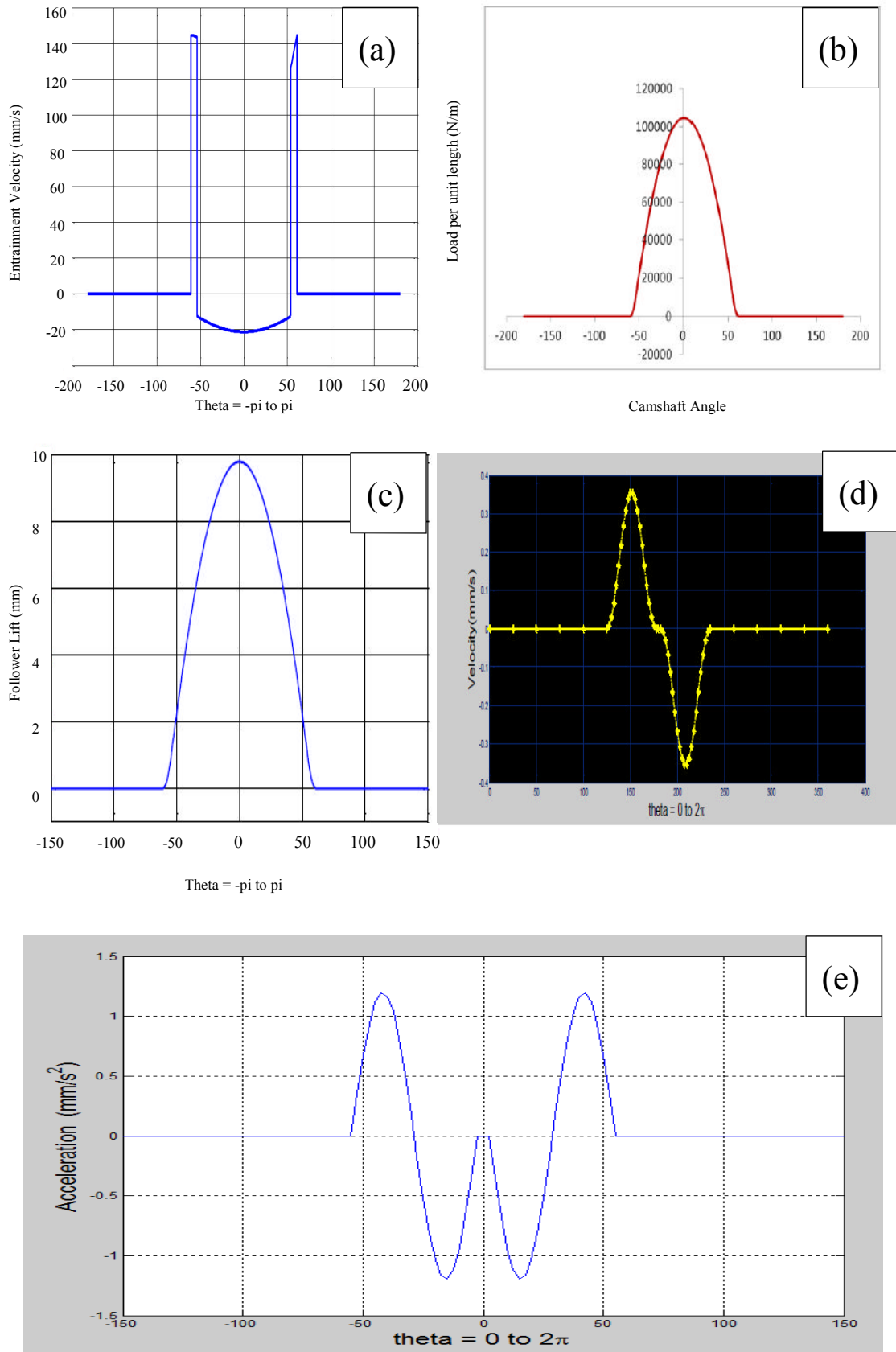
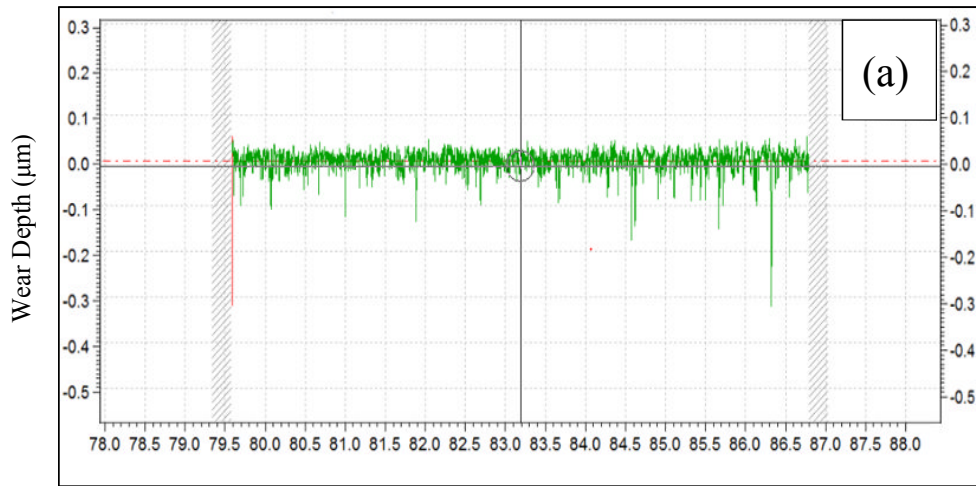
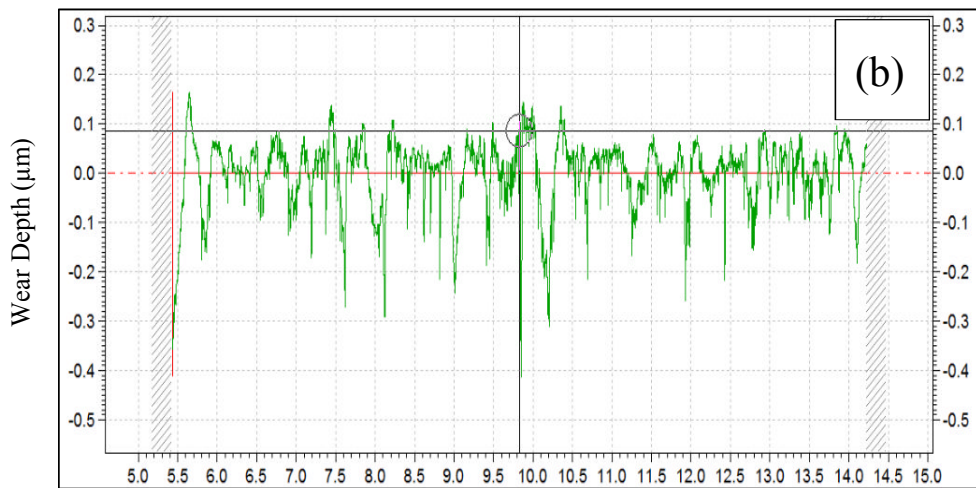


Figure 4-15 Calculations for: (a) lubricant entrainment velocity, (b) load per unit length, (c) cam lift profile, (d) velocity profile and (e) acceleration profile



Measurement across the cam nose (mm)



Measurement across the cam nose (mm)

Figure 4-16 Cam nose profile (a) pre-test and (b) post-test

Chapter 5. Mini Traction Machine (MTM): Investigation of Friction, Wear and Tribochemistry of Different Lubricant Formulations under Pure Sliding and Sliding/Rolling Contacts

5.1. Introduction

Diamond-Like Carbon (DLC)/cast iron (CI) systems have been widely investigated due to their important applications in engine components such as cylinders, pistons and more specifically for the cam/follower interface. In this chapter, results obtained from the Mini Traction Machine (MTM) are presented. The experiments address the effect of MoDTC under mixed-boundary lubrication conditions using a fully formulated oil containing Zinc DialkylDithioPhosphate (ZDDP), a fully formulated oil free from ZDDP and a Group III mineral base oil. Optical Microscopy and White Light Interferometry were used to observe the wear scar. In addition, Scanning Electron Microscopy (SEM), Energy-Dispersive X-ray (EDX), Raman spectroscopy and X-ray Photoelectron Spectroscopy (XPS) analyses were all performed on the tribofilms to understand the effect of type of contact on the tribochemical interactions between oil additives and the ball/disc interface.

5.2. Friction Results

5.2.1 The Correlation between SRR and Friction

The MTM durability test, which is mentioned in Chapter 4, is primarily essential to identify the stability of the system through a particular period. Figure 5-1 shows friction coefficient values during the whole test duration at 50% SRR and 200% SRR values. As mentioned earlier, MTM tests lasted for 6.5 hrs and were started with 30 minutes running-in followed by a Stribeck curve test for 1-2 minutes then a durability test for two hours. This procedure, except the running-in period, is repeated twice. The fluctuation in the data at 1800 s, 9000 s and 16200 s is where the Stribeck (speed-scanning) tests were done. In

general, all oils followed the same trend with time but there were quite clear fluctuations when SRR was 200% and this resulted from the severe conditions of the test. In other words, at 200%, the ball is stationary and that in turn offered more instability to the system. The steady state friction, under boundary lubrication, was presented as the average friction values of the last hour of each test. Accordingly, Fig. 5-2 shows the average of coefficients of friction for all oils at 50% SRR and 200% SRR. It can be seen that no systematic trend of friction coefficient was observed for both SRR values. However, this is found to be due to the influence of sliding/rolling ratio on surface chemistry. Details of this will be addressed later in this chapter.

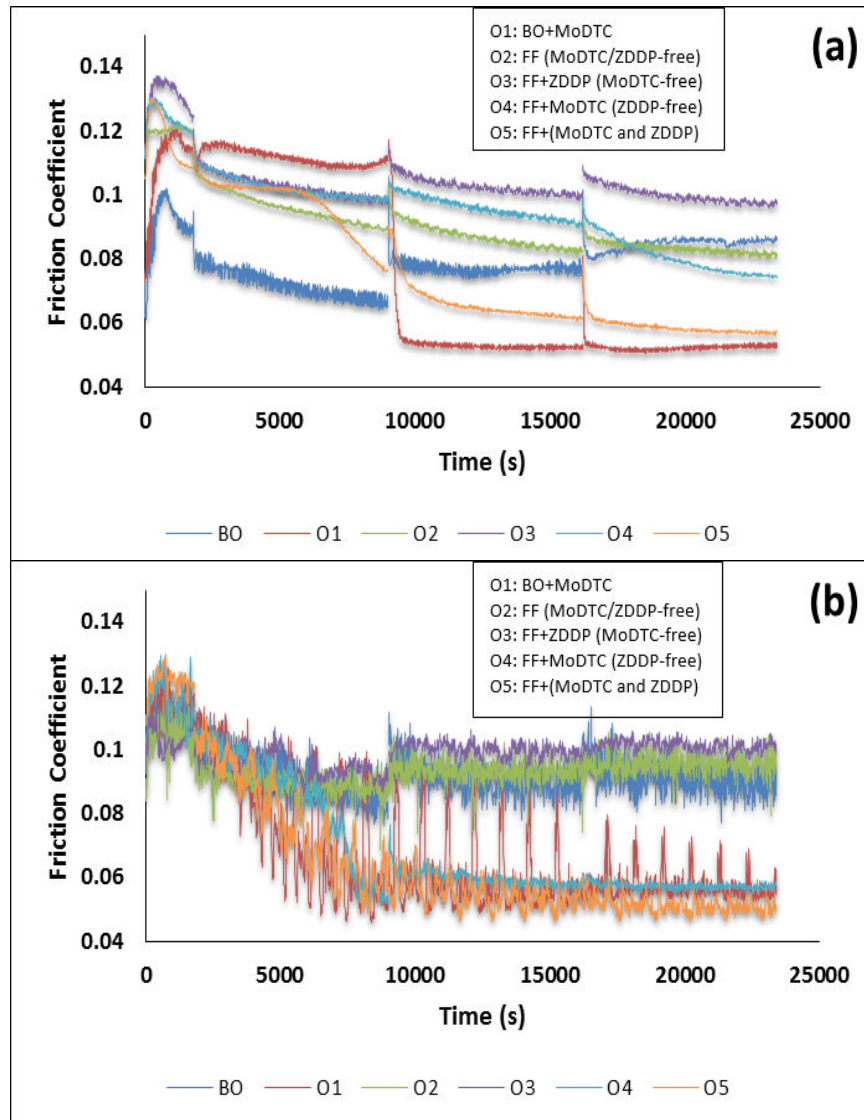


Figure 5-1 Friction coefficients for a CI/DLC system as a function of time: (a) at 50%SRR and (b) 200%SRR

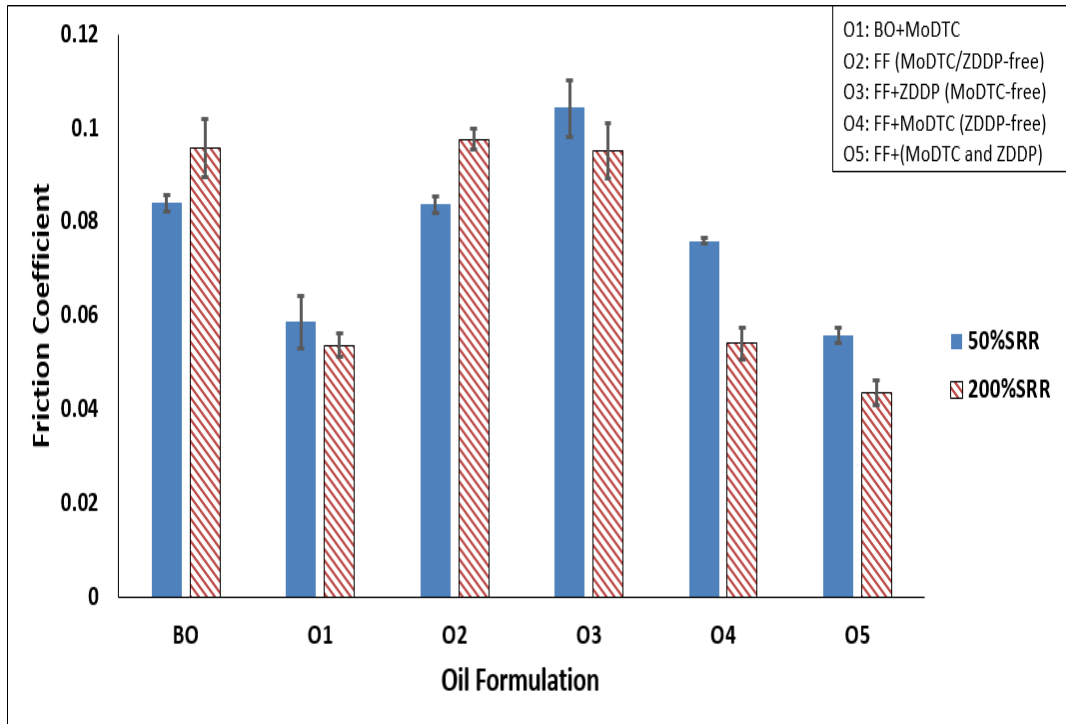


Figure 5-2 Average friction coefficient values for the last hour for all oils at 50% SRR and 200% SRR

5.2.2 The Correlation between SRR and Stribeck Curve Evaluation

The Stribeck curve evaluation gives an indication of the tribofilm build-up and the time to reach steady state conditions.

Fig. 5-3 and 5-4 show Stribeck curves for each oil as a function of time and mean speed under the sliding/rolling (50% SRR) and the pure sliding (200% SRR) conditions. A systematic trend of friction coefficient was seen for both SRR values over time. For example, comparing the first 30 minutes to the following 2 hrs of the tests, friction was generally higher at 50% SRR (i.e. sliding/rolling contact) than 200% SRR (i.e. pure sliding contact) for oils containing MoDTC. This suggests a slower build-up of tribofilms in sliding/rolling contacts compared to a pure sliding contact. For the lubricants with no MoDTC (BO, O2, O3), the change in friction over time was not significant at 200% SRR. However, at 50% SRR, for O2, a considerable change in friction over time was seen suggesting tribofilm evolution over a much longer timeframe.

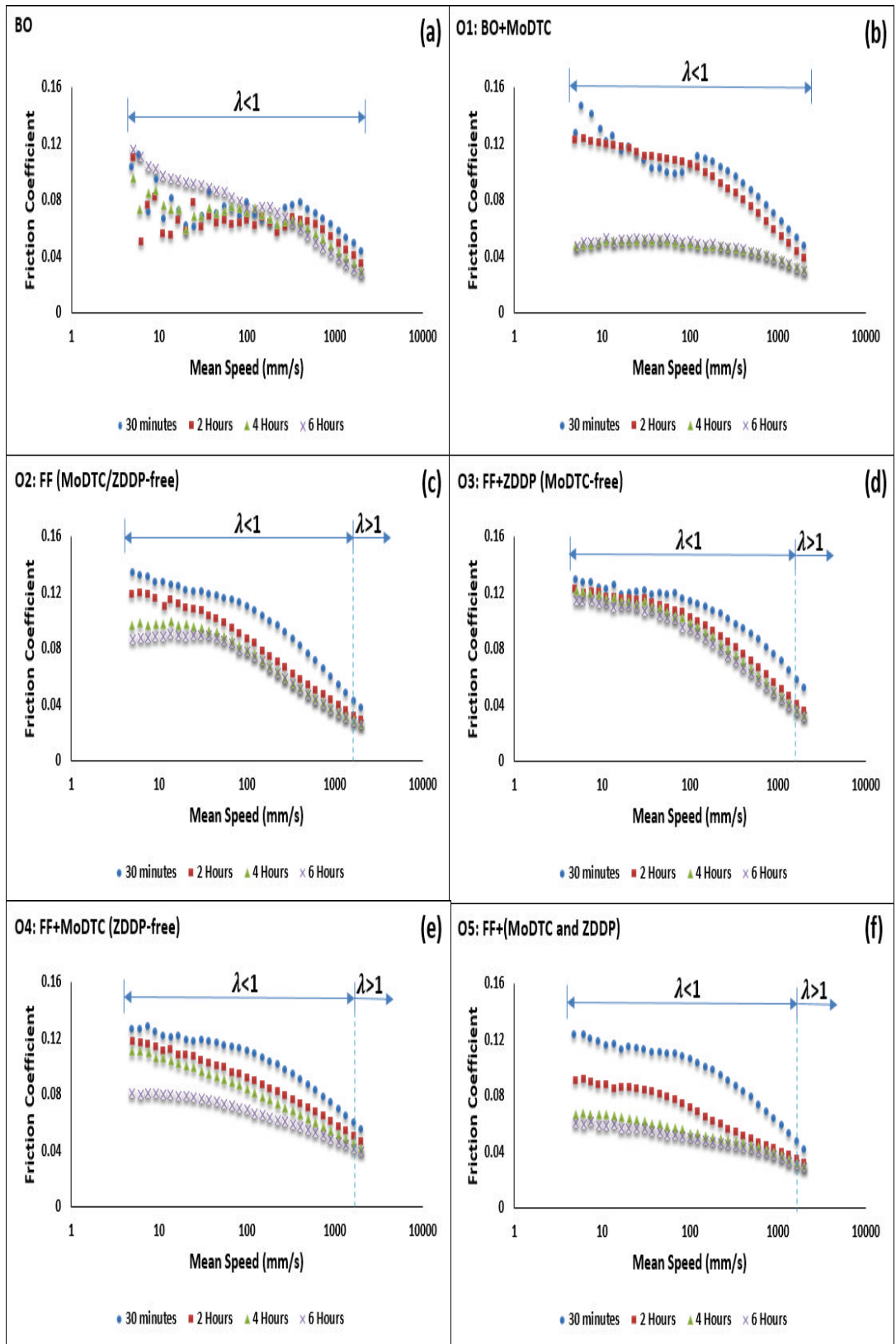


Figure 5-3 Stribeck curves for (a) BO, (b) O1, (c) O2, (d) O3, (e) O4 and (f) O5 as a function of time at 50% SRR

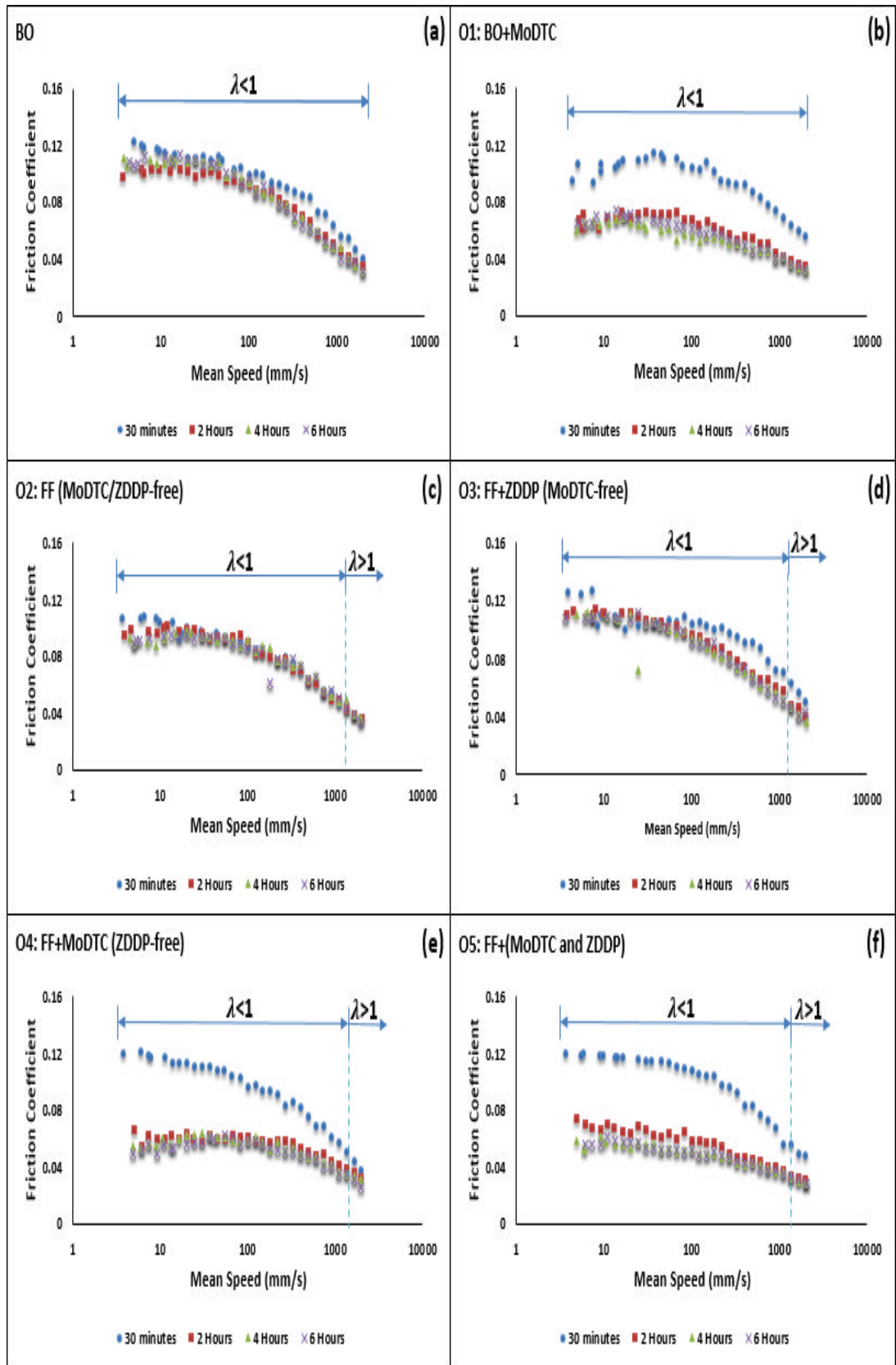


Figure 5-4 Stribeck curves for (a) BO, (b) O1, (c) O2, (d) O3, (e) O4 and (f) O5 as a function of time at 200% SRR

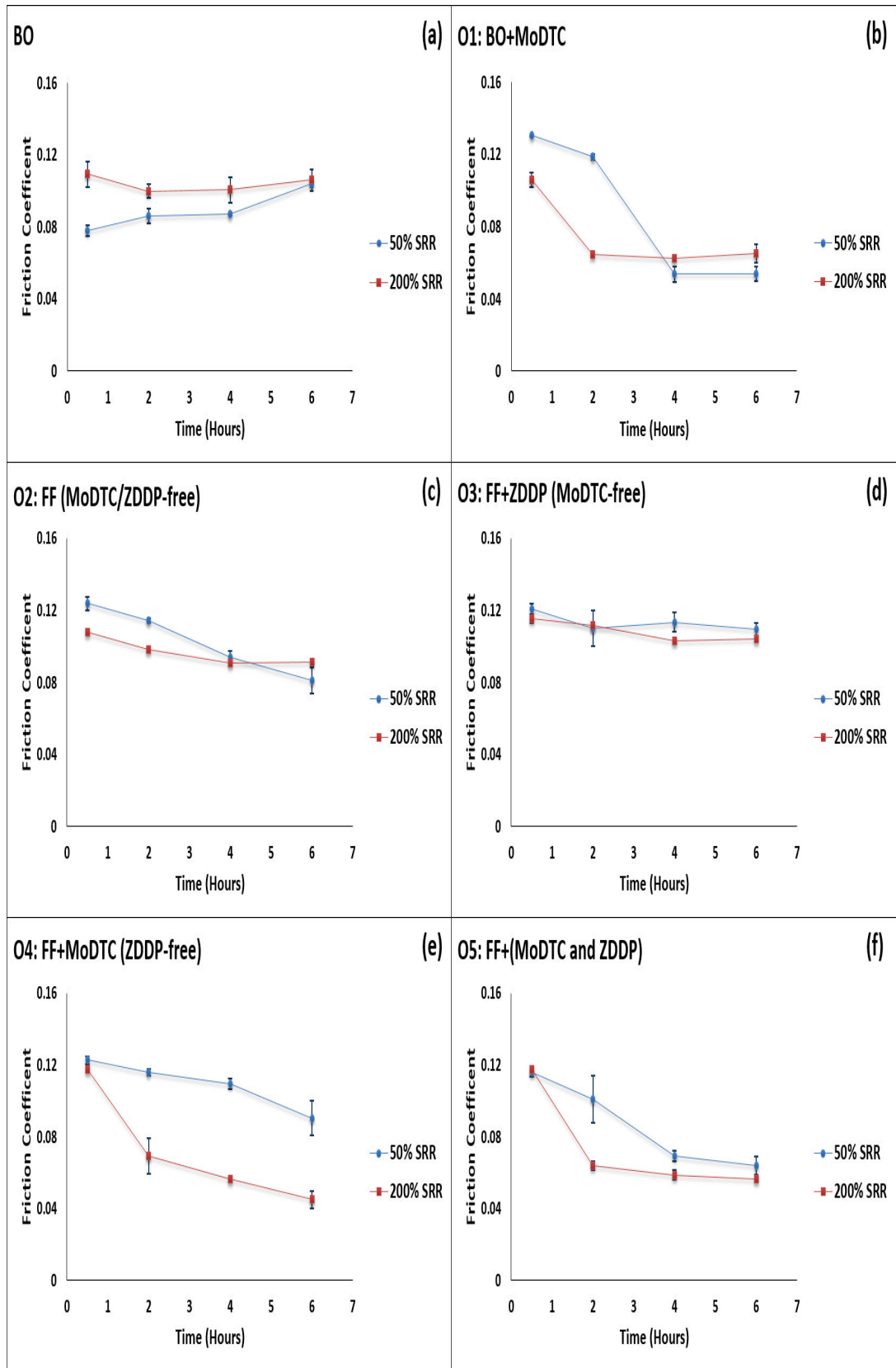


Figure 5-5 Friction coefficients for (a) BO, (b) O1, (c) O2, (d) O3, (e) O4 and (f) O5 at mean speed = 10 mm/s under 50% SRR and 200% SRR

In order to have a better picture of the SRR effect on the tribological behaviour of the lubricants under the boundary lubrication regime, friction coefficients for each oil were plotted (see Fig. 5-5) at 50% SRR and 200%. The speed of 10 mm/s was chosen to be representative of the boundary lubrication regime. From Fig. 5-5, it can be seen that SRR can play an important role in the frictional behaviour for the lubricants containing MoDTC (i.e. O1, O4 and O5). In particular, pure sliding contact enhanced the activation of MoDTC over time. It is also interesting to note that the lubricant with ZDDP only (i.e. O3) was not affected by different SRR values and the friction responses were comparable over time.

Table 5-1 Range of surface roughness for balls and discs at the end of each test

Oil Type	Roughness, R_q (μm)			
	50% SRR		200% SRR	
	Disc	Ball	Disc	Ball
BO	0.22-0.36	0.05-0.31	0.13-0.12	0.09-0.20
O1: BO+MoDTC	0.11-0.29	0.10-0.15	0.15-0.20	0.09-0.31
O2: FF(MoDTC/ZDDP-free)	0.19-0.21	0.03-0.16	0.20-0.22	0.09-0.32
O3: FF+ZDDP (MoDTC-free)	0.14-0.15	0.11-0.13	0.12-0.30	0.07-0.11
O4: FF+MoDTC(ZDDP-free)	0.13-0.27	0.04-0.13	0.23-0.37	0.03-0.11
O5: FF+(MoDTC+ZDDP)	0.11-0.17	0.12-0.16	0.13-0.20	0.09-0.33

The observed reduction or difference in friction between both contacts was expected to be influenced by change in surface roughness over time in addition to changes in surface chemistry. The surface roughness for balls and discs at the end of each test was investigated, as shown in Table 5-1. Comparing the surface roughness after the test to the initial roughness (see

Table 4-1), rougher surfaces were observed for both the discs and the balls after the tests. Nevertheless, friction reduction was reported over time for most oils. The tribological performance is more controlled by the contact type and the tribofilm formed on the ball/disc tribopair rather than the surface roughness. This means that the Lambda ratio progressively decreases as the tests progress and the lower friction is dominated by the action of the tribochemistry effect.

5.2.3 Range of Friction Values in the Boundary Lubrication Regime

Table 5-2 shows how the addition of MoDTC affects steady state friction values for the DLC/CI system when lubricated in base oil, fully formulated (FF) oil without ZDDP and fully formulated oil with ZDDP in the boundary lubrication regime. From Table 5-2, it is apparent that regardless of the type of contact, the addition of MoDTC to the oil formulations always improved the frictional properties of the DLC/CI system. In the case of fully formulated oil B containing ZDDP (i.e. O3 and O5), it can be seen that the positive effect of MoDTC on reducing friction was more pronounced for the pure sliding contact (i.e. more tangible friction reduction at 200% SRR than at 50% SRR when lubricated with fully formulated oil B containing ZDDP).

The range of friction values ($\Delta\mu$) is defined as the difference between the highest friction value (i.e. at the start of the test) for each test duration and the lowest friction value under the boundary lubrication regime (i.e. when $\lambda < 1$). $\Delta\mu$ values for all lubricants and for different time intervals throughout the tests are plotted in Fig. 5-6. From Fig. 5-6 (a), at 50% SRR, MoDTC offered the highest friction reduction for the first 2 hrs for O1 and O5 while the highest friction reduction was observed for O4 when the test ran for 4 hrs. Fig. 5-6 (b), at 200% SRR, the effect of MoDTC on friction reduction was considerable during the running-in period (i.e. initial 30 minutes). Interestingly, the range of friction values for the lubricant with ZDDP alone was quite constant and was not affected over time. It is clear that friction coefficient values were observed to vary quite considerably for most of the lubricants. This is quite an important finding as most of the modelling works assume a constant value for (μ) across

the boundary lubrication regime [254]. In practice, however, friction values may vary due to the changes in surface physical, chemical and mechanical properties. In addition, surface topography experiences significant modifications due to different surface phenomena which can lead to fluctuations in friction.

Table 5-2 Average of steady state friction in boundary lubrication at the last hour of each test

Average of steady state friction coefficients when $\lambda < 1$				
Oil Type	50% SRR		200% SRR	
	Without MoDTC	With MoDTC	Without MoDTC	With MoDTC
BO	0.08	0.05	0.09	0.06
FF (free of ZDDP)	0.08	0.07	0.09	0.06
FF + ZDDP	0.1	0.06	0.1	0.05

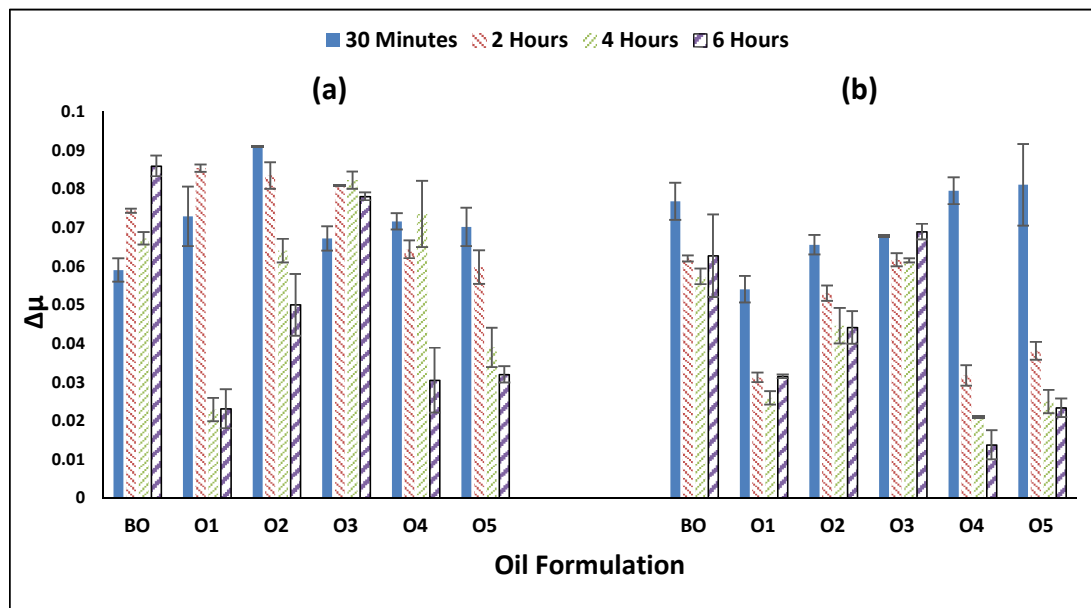


Figure 5-6 Range of friction values $\Delta\mu$ at $\lambda < 1$ for all oils: (a) at 50% SRR and (b) at 200% SRR

5.3. Wear Results

Post-test physical observation of CI discs and DLC balls (under both contacts) was initially carried out by optical microscopy.

Representative images of the wear track that formed on both the CI disk and the DLC coated ball are shown in Fig. 5-7 and Fig. 5-8. DLC balls however indicated a very shallow wear scar on all balls irrespective of the oil formulation which made the quantitative analysis of the wear scar on all DLC balls a challenge.

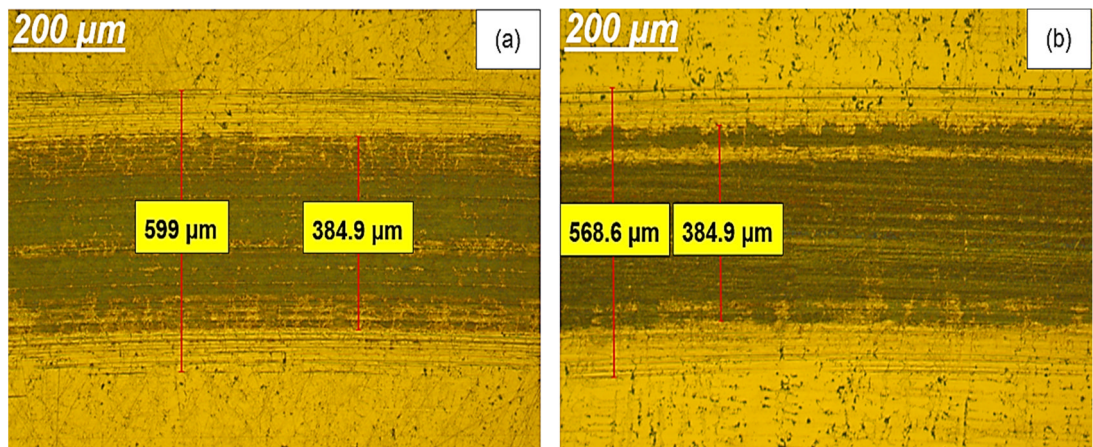


Figure 5-7 Representative optical images of the wear scar formed on uncoated cast iron discs (a) at 50%SRR (b) at 200%SRR

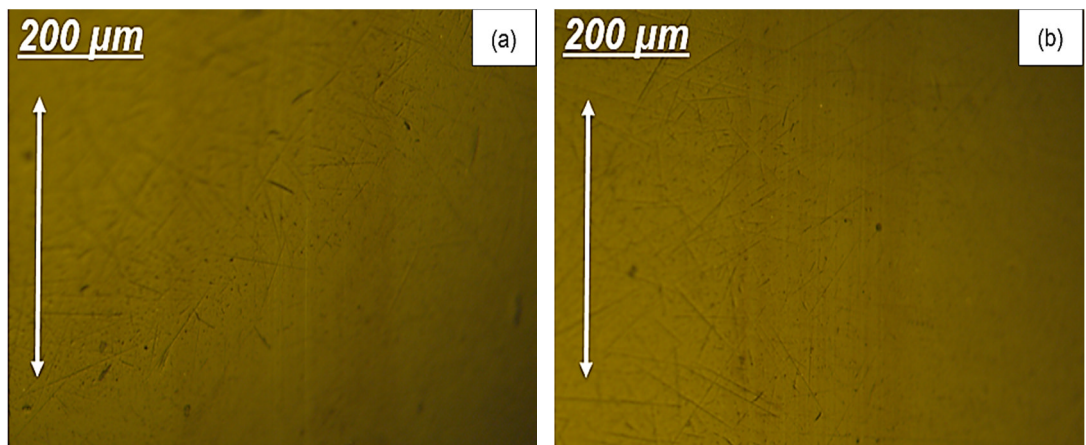


Figure 5-8 Representative optical images of the wear scar formed on DLC coated balls (a) at 50%SRR (b) at 200%SRR, the arrows on the left side of the images show sliding directions

In order to quantify the wear depth of the coated balls and CI disks, White Light Interferometer (WLI) was used. Representative images of the wear track that formed on both the CI disk and the DLC coated ball are shown in Fig. 5-9.

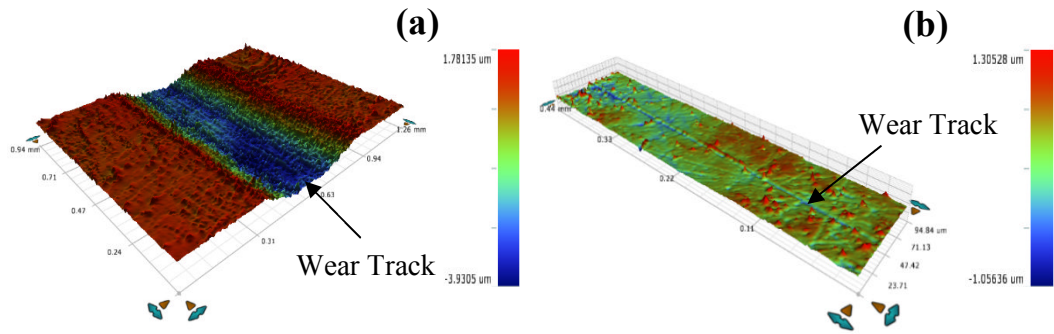


Figure 5-9 Representative interferometer images of the wear track that formed on: (a) uncoated cast iron disc and (b) DLC coated ball

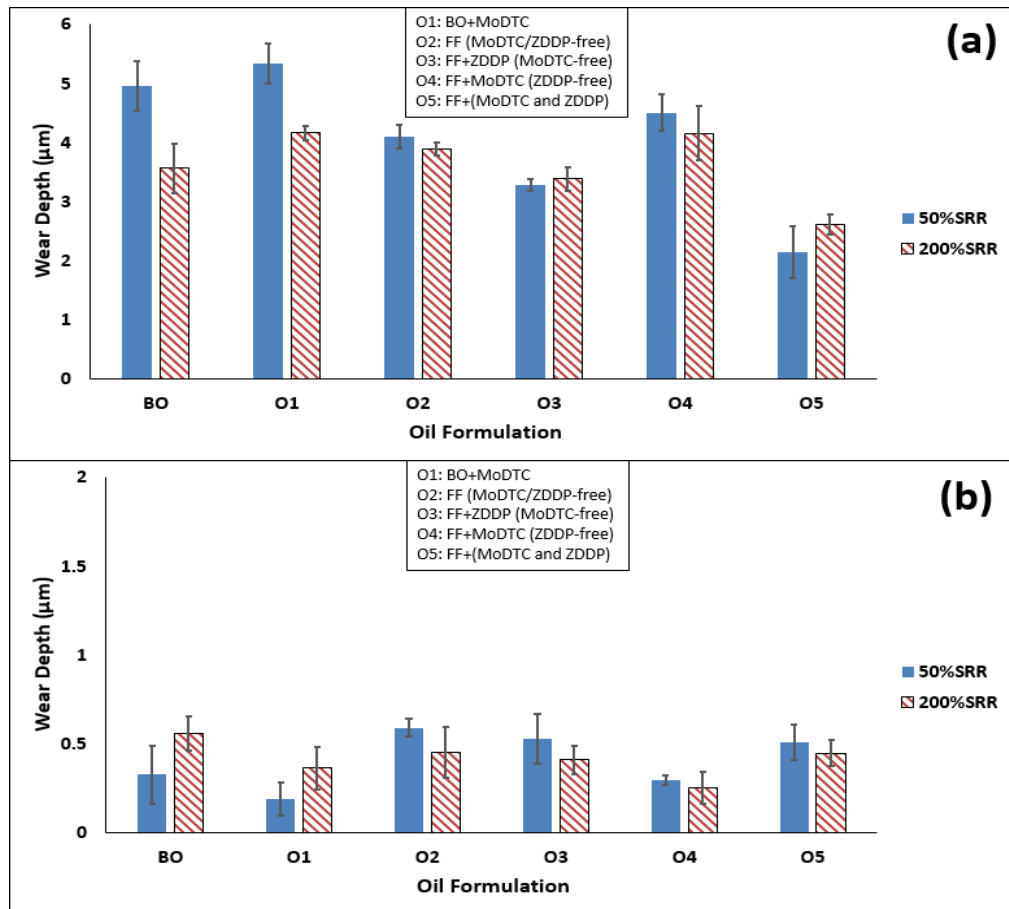


Figure 5-10 Average of wear depths that formed on: (a) uncoated cast iron discs and (b) DLC coated balls (note different wear depth scales)

Furthermore, wear depths for both the discs and the balls were evaluated and shown in Fig. 5-10. It is important to observe that no lubricants show extremely high wear on DLC coating. In addition, the uncoated cast iron discs exhibited more wear than the DLC coated balls, as expected, because of the large difference in hardness. This is in line with other published literature where they found lower wear of the DLC coated balls as compared to the uncoated disk [221, 260, 261].

5.4. Chemical Analysis of Tribofilm

5.4.1 SEM-EDX Results

From Fig. 5-11, SEM micrographs of the CI discs revealed that interactions took place among the oil formulation, type of contact, the disc surface and the DLC ball surface. However, the DLC balls were not clearly identified by SEM and the micrographs (not shown here) were seen to be similar under the effect of contact type and oil formulation.

EDX semi-quantification of CI discs and DLC balls (for Mo, Zn, P and S elements) is presented in Fig. 5-12. Essentially, the chemical composition of the tribofilms was found to vary with changing the type of contact and the oil formulation. Generally, greater Mo, Zn, S and P was reported on CI discs than DLC balls. This reveals that the tribofilm formed on the CI discs was thicker than the tribofilms formed on the DLC balls. Similar findings were seen by Raman spectroscopy and XPS.

Comparing sliding/rolling contact to pure sliding contact, the CI disk lubricated in O1 showed similar characteristics under both contacts. Nevertheless, low friction and good wear was observed under pure sliding contact. This clearly confirms that the tribological performance was not only controlled by the tribofilm formed on the surface but also by the contact type. Although quite similar amounts of Mo were detected on the CI discs (lubricated in O4) under both contacts, a clear reduction in friction was reported under pure sliding contact. For the DLC balls lubricated in O1, O4 and O5, only Mo was seen while no other elements (i.e. Zn, S and P) were detected under both contacts.

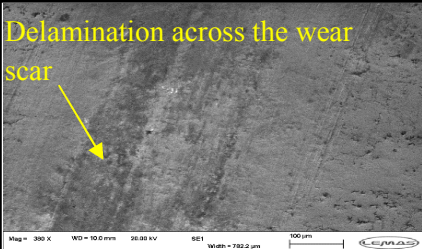

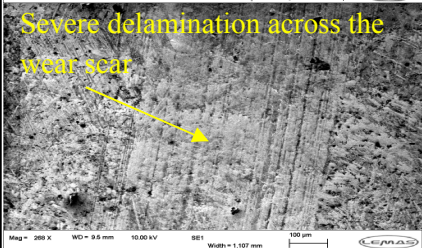
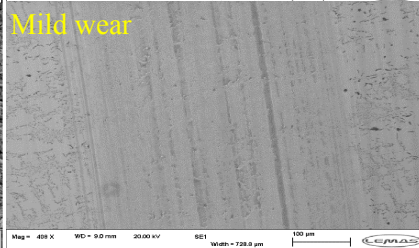
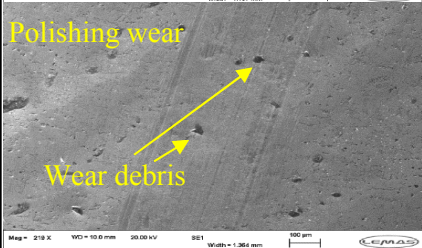
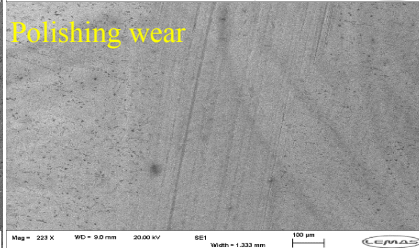
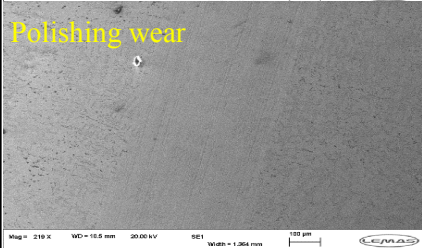
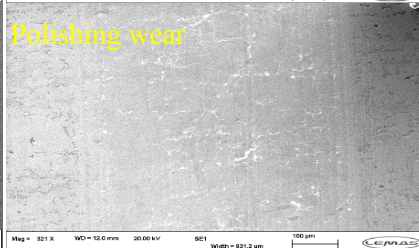
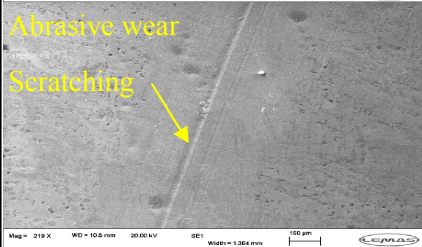
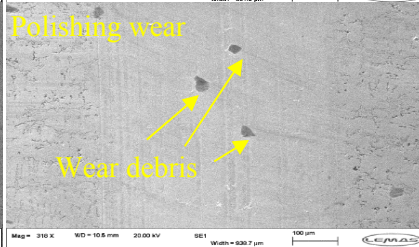
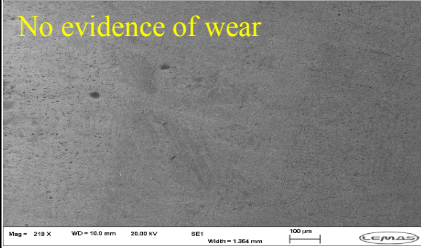

		Contact	
Oil	Sliding/rolling contact	Pure sliding contact	
BO	<p>Delamination across the wear scar</p>  <p>Mag = 300 X WD = 10.0 mm 20.00 kV SE1 Width = 732.2 µm</p>	<p>Polishing wear</p>  <p>Mag = 219 X WD = 10.5 mm 20.00 kV SE1 Width = 1.354 mm</p>	
O1	<p>Severe delamination across the wear scar</p>  <p>Mag = 269 X WD = 9.5 mm 10.00 kV SE1 Width = 1.107 mm</p>	<p>Mild wear</p>  <p>Mag = 498 X WD = 9.0 mm 20.00 kV SE1 Width = 729.9 µm</p>	
O2	<p>Polishing wear</p> <p>Wear debris</p>  <p>Mag = 219 X WD = 10.0 mm 20.00 kV SE1 Width = 1.354 mm</p>	<p>Polishing wear</p>  <p>Mag = 229 X WD = 9.0 mm 20.00 kV SE1 Width = 1.333 mm</p>	
O3	<p>Polishing wear</p>  <p>Mag = 219 X WD = 10.5 mm 20.00 kV SE1 Width = 1.354 mm</p>	<p>Polishing wear</p>  <p>Mag = 321 X WD = 12.0 mm 20.00 kV SE1 Width = 821.2 µm</p>	
O4	<p>Abrasive wear</p> <p>Scratching</p>  <p>Mag = 219 X WD = 10.5 mm 20.00 kV SE1 Width = 1.354 mm</p>	<p>Polishing wear</p> <p>Wear debris</p>  <p>Mag = 310 X WD = 10.5 mm 20.00 kV SE1 Width = 830.7 µm</p>	
O5	<p>No evidence of wear</p>  <p>Mag = 219 X WD = 10.0 mm 20.00 kV SE1 Width = 1.354 mm</p>	<p>Polishing wear</p>  <p>Mag = 321 X WD = 12.0 mm 20.00 kV SE1 Width = 821.2 µm</p>	

Figure 5-11 SEM micrographs of CI disks at end of test

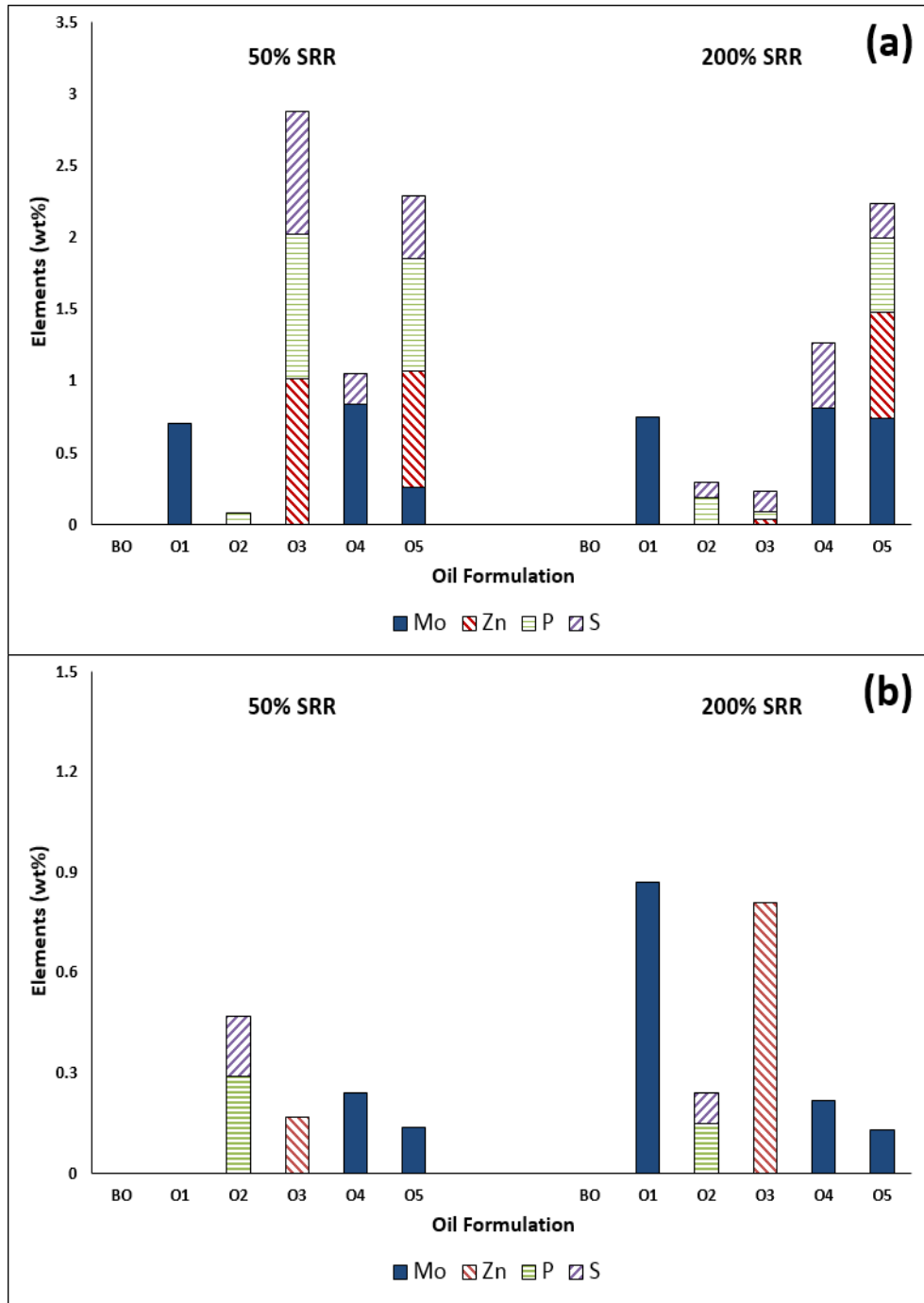


Figure 5-12 Data from regions inside the wear track under both contacts on: (a) uncoated cast iron discs and (b) DLC balls (note different wt% scales)

5.4.2 Raman Spectroscopy Results

Based on the literature, the expected shift in Raman spectroscopy for molybdenum disulfide (MoS_2) is reported at $383\text{-}410\text{ cm}^{-1}$, molybdenum trioxide (MoO_3) at $828\text{-}951\text{ cm}^{-1}$, carbon (C) at $1366\text{-}1596\text{ cm}^{-1}$, haematite (Fe_2O_3) at $120\text{-}310\text{ cm}^{-1}$ and magnetite (Fe_3O_4) at $670\text{-}680\text{ cm}^{-1}$ [15, 76, 201, 262, 263]. Raman spectra obtained from the CI discs under both contacts is shown in Fig. 5-13. Raman spectra are plotted on the same scale and have been shifted vertically for clarification purposes. For the CI discs lubricated with MoDTC additive (i.e. O1, O4 and O5), the Raman spectra under sliding/rolling contact indicated the presence of MoS_2 in the range of ($380\text{-}413\text{ cm}^{-1}$). For all lubricants containing MoDTC, MoO_3 was not detected by Raman spectroscopy. The broad peaks at $925\text{-}926\text{ cm}^{-1}$ were assigned to the iron (II) molybdate FeMoO_4 [119, 201, 202]. The iron molybdate is clearly detected when using O1 while there was little presence of FeMoO_4 when using O4 and O5. Due to the graphite normally present in the microstructure of the cast iron, peaks due to the formation of graphitic carbon are observed on the CI disc surface. The G and D peaks were around 1595 cm^{-1} and 1367 cm^{-1} respectively. However, carbon peaks were not clearly pronounced when using O1, O2 and O5 as compared to the CI discs lubricated in BO, O3 and O4. Fe_2O_3 peaks ($197\text{-}299\text{ cm}^{-1}$) were observed for BO, O1, O4 and O5. In addition, Fe_3O_4 was clearly detected in the range of ($671\text{-}685\text{ cm}^{-1}$) when using BO, O1, O3 and O4. In contrast, there was no presence of Fe_2O_3 and Fe_3O_4 for all lubricants under pure sliding contact.

Fig. 5-14 shows the intensity of MoS_2 and FeMoO_4 for all oils containing MoDTC (i.e. O1, O4 and O5) under both contacts. Comparing pure sliding contact to sliding/rolling contact, higher intensity of MoS_2 ($385\text{-}411\text{ cm}^{-1}$) was clearly observed. This is in agreement with the friction results (i.e. lower friction was reported for O1, O4 and O5 under pure sliding contact as compared to sliding/rolling contact). In addition, for pure sliding contact, FeMoO_4 (925 cm^{-1}) was only detected when using O1. Raman peaks due to the presence of carbon ($1595\text{ cm}^{-1}\text{-}1367\text{ cm}^{-1}$) were not observed when using O4 and O5.

For both contacts and for all lubricants used in this study, Raman spectra for the DLC balls have shown similar characteristics or film structures (i.e. no structural modifications have occurred), as shown in Fig. 5-15. Carbon peaks were the only peaks on the DLC ball surface. The G and D peaks were around 1550 cm^{-1} and 1370 cm^{-1} respectively. A broad G peak was detected due to the laser power of 488 nm used for the analysis [115, 264]. Also, for the G peak, under both contacts, the Raman spectra showed no difference in the value of the full-width at half-maximum (FWHM) and the value of the ratio H_D/H_G . This might suggest that no structural modification of the DLC balls has happened after 6.5 hours test duration. However, based on EDX results, Mo was detected in most DLC balls lubricated with MoDTC additive (i.e. O1, O4 and O5). Nevertheless, no MoS_2 and/or MoO_x peaks were observed on the DLC balls. This could either be due to a low amount of tribofilm formed or the surface sensitivity of the Raman Spectroscopy. Therefore, to confirm previous findings, all samples were examined using X-ray photoelectron spectroscopy (XPS). Details of this is discussed in the next section.

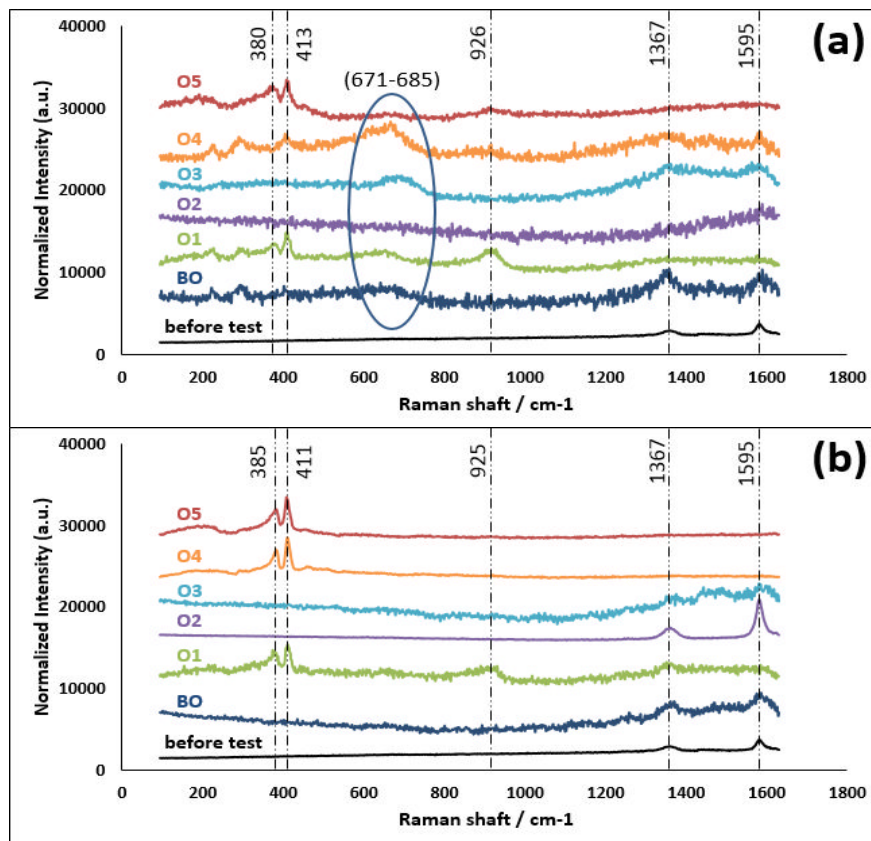


Figure 5-13 Raman spectroscopy for the CI discs under: (a) sliding/rolling contact, (b) pure sliding contact

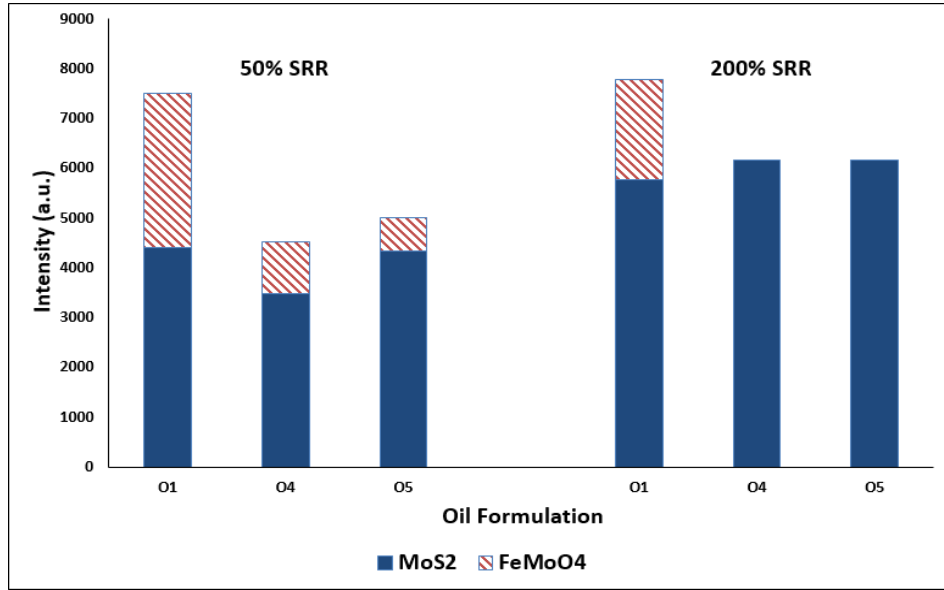


Figure 5-14 the intensity of MoS₂ and FeMoO₄ for the CI discs under both contacts

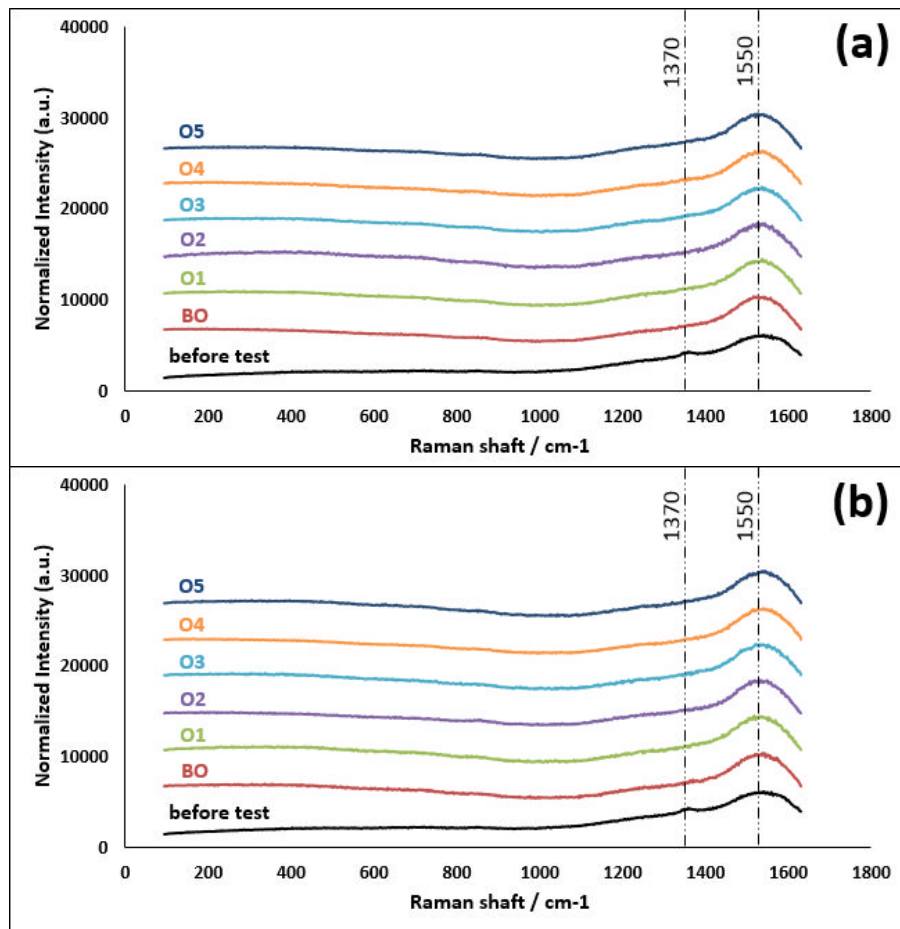


Figure 5-15 Raman spectroscopy for the DLC coated balls under: (a) sliding/rolling contact, (d) pure sliding contact

5.4.3 X-ray Photoelectron Spectroscopy Results

From previous XPS analyses, tribofilms of lubricants containing MoDTC showed Mo 3d peaks at 229, 232.3 and 235 eV [188, 194]. The tribofilms of lubricants containing MoDTC were thought to be composed of MoO₃ because of the presence of Mo 3d_{5/2} peak at 232.3 eV. The Mo 3d_{5/2} peak for FeMoO₄ is also reported at 232.3 eV [199, 200]. As molybdenum in MoO₃ and FeMoO₄ have the same oxidation state (+6), it is impossible to distinguish the two compounds (i.e. MoO₃ or FeMoO₄) from XPS analysis [201]. However, Raman spectroscopy is capable of clearly distinguishing molybdenum species, even if these species have the same oxidation state. Thus, MoO₃ or FeMoO₄ peaks were clearly distinguished from Raman analysis [202, 203]. In this work, Raman peaks belonging to FeMoO₄ were clearly observed but MoO₃ peaks were not detected at all. Therefore, for the XPS results, it was believed that the Mo 3d_{5/2} peaks are due to the presence of FeMoO₄ and not MoO₃ [201].

For both contacts, the fitted Mo 3d peaks obtained from the CI discs lubricated in oils containing MoDTC (i.e. O1, O4 and O5) are shown in Fig. 5-16. Unlike Raman results, it can be seen that regardless of the contact type, FeMoO₄ and MoS₂ were all identified in the tribofilms formed on the CI disks. For all lubricants, the MoS₂/FeMoO₄ ratio was higher under pure sliding contact compared to sliding/rolling contact. It is also evident that the quantity of Mo, as detected by the Mo 3d peak on the CI disk under pure sliding contact was higher for O5 compared to O1 and O4. That could explain the friction values which were found to be the lowest when using O5. From Fig. 5-16, it is also evident that FeMoO₄ was not detected on the disc before test, this confirms that FeMoO₄ come from the tribofilm, not the original surface. For both contacts, the XPS spectra of ZDDP derived species (Zn 2p and P 2p) formed on the CI disks using O3 and O5 are shown in Fig. 5-17. It can be seen that Zn-phosphate and ZnS/ZnO species were formed on the CI discs under both contacts.

Unlike the Raman spectra on the DLC balls, XPS spectra showed that FeMoO₄ and MoS₂ were generally observed on the tribofilms formed on the DLC balls. For both contacts, the fitted Mo 3d peaks obtained from the DLC balls lubricated in oils containing MoDTC (i.e. O1, O4 and O5) are shown in

Fig. 5-18. It was evident that the intensity of FeMoO₄ was higher under sliding/rolling contact as compared with the pure sliding contact. For O5, the amount of Mo 3d detected on the tribofilm formed on the DLC was higher under pure sliding compared to the sliding/rolling contact. This result validates the friction results obtained by the DLC ball under sliding/rolling contact. For both contacts, the XPS spectra of ZDDP derived species (Zn 2p and P 2p) formed on the DLC balls using O3 and O5 is shown in Fig. 5-19. It can be seen that the formation of the phosphate film was not affected by the presence of MoDTC. For O5, the amount of Zn 2p and P 2p detected on the DLC ball was slightly higher under pure sliding contact compared to the sliding/rolling contact. The obtained results could justify the wear performance of the DLC ball under pure sliding contact. For both contacts, the fully formulated lubricant (O5), which contains MoDTC and ZDDP, has shown the best tribological performance (i.e. lower friction and wear) of all the tested lubricants. XPS depth profiling for O5 only for both contacts was shown in Fig. 5-20. For clarification purposes, Fig.5-20 is plotted on different scales. For both contacts, the tribofilm formed on the CI discs was relatively thicker than the tribofilms formed on the DLC balls.

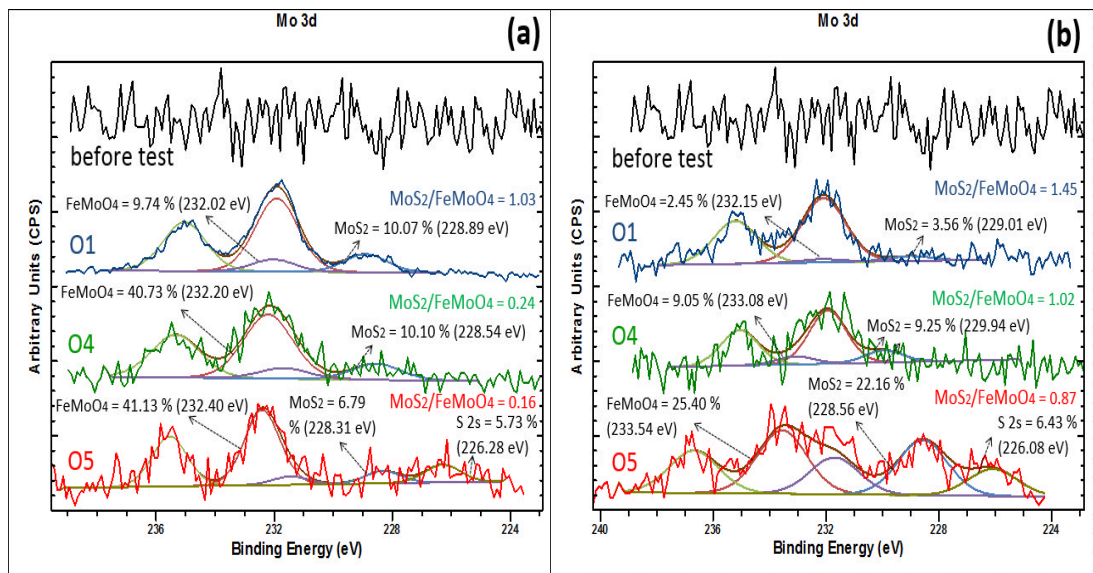


Figure 5-16 XPS spectra of the discs lubricated with MoDTC under: (a) sliding/rolling contact, (b) pure sliding contact

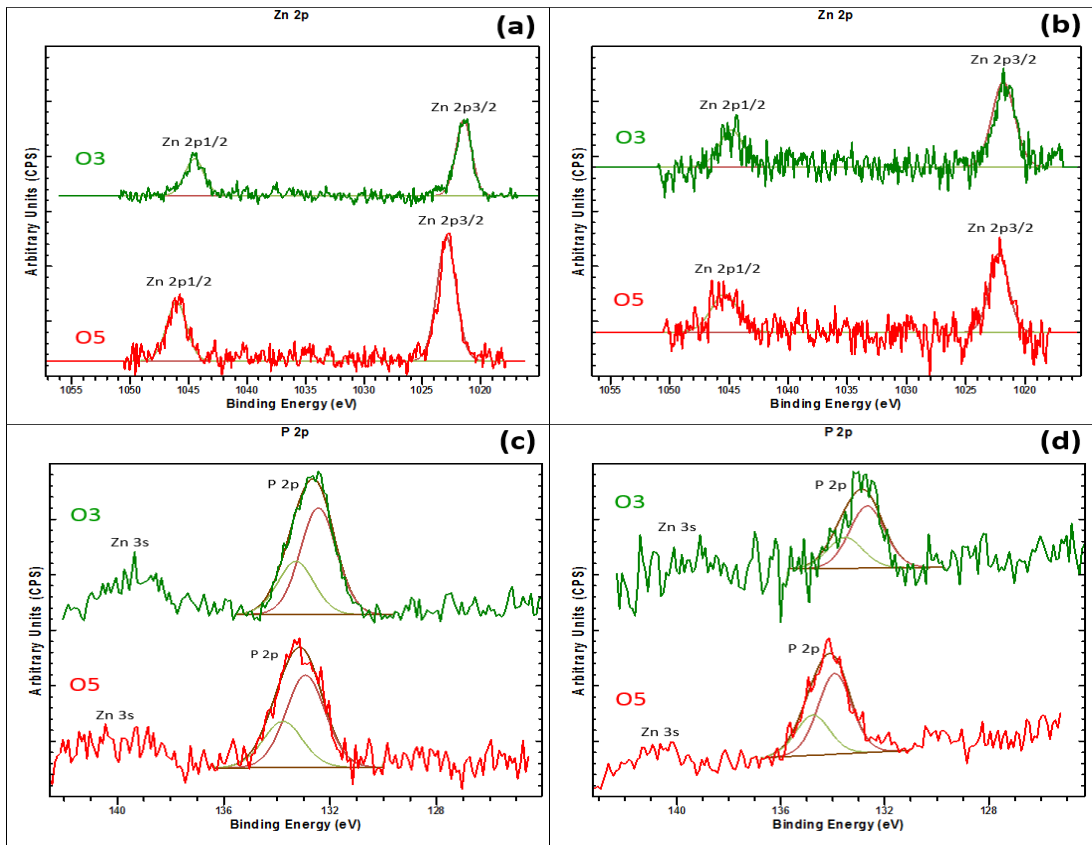


Figure 5-17 XPS spectra of the discs lubricated with ZDDP: (a) Zn 2p under sliding/rolling contact, (b) Zn 2p under pure sliding contact, (c) P 2p under sliding/rolling contact, (d) P 2p under pure sliding contact

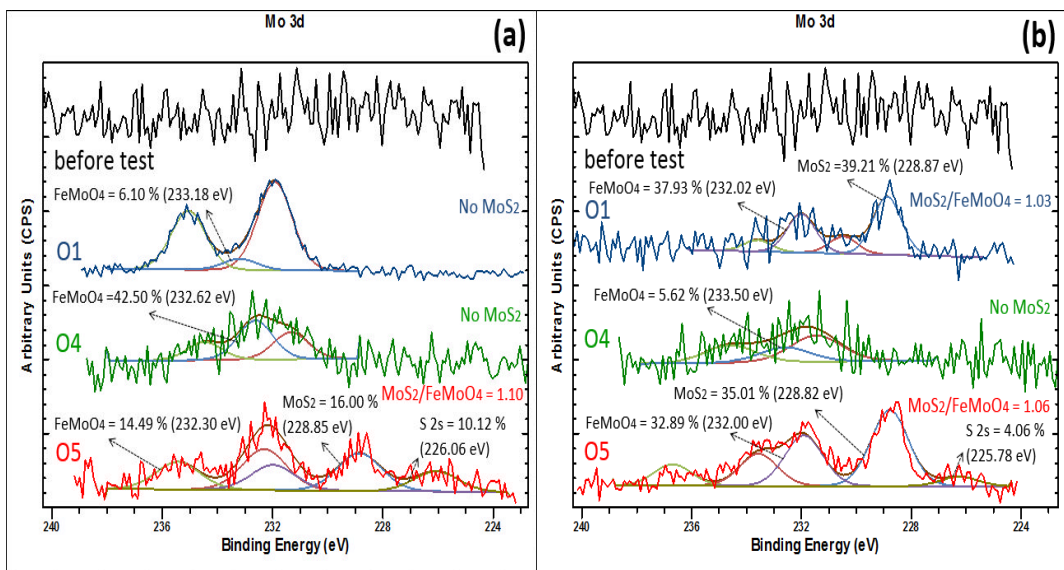


Figure 5-18 XPS spectra of the DLC coated balls lubricated with MoDTC under: (a) sliding/rolling contact, (b) pure sliding contact

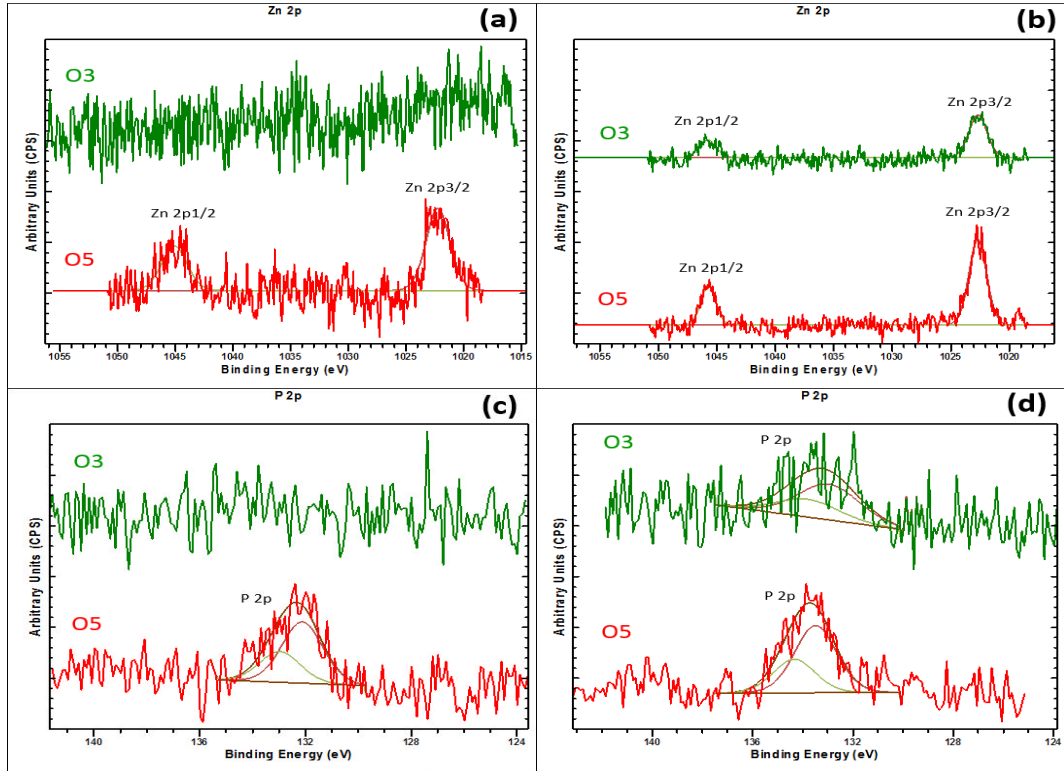


Figure 5-19 XPS spectra of the balls lubricated with ZDDP: (a) Zn 2p under sliding/rolling contact, (b) Zn 2p under pure sliding contact, (c) P 2p under sliding/rolling contact, (d) P 2p under pure sliding contact

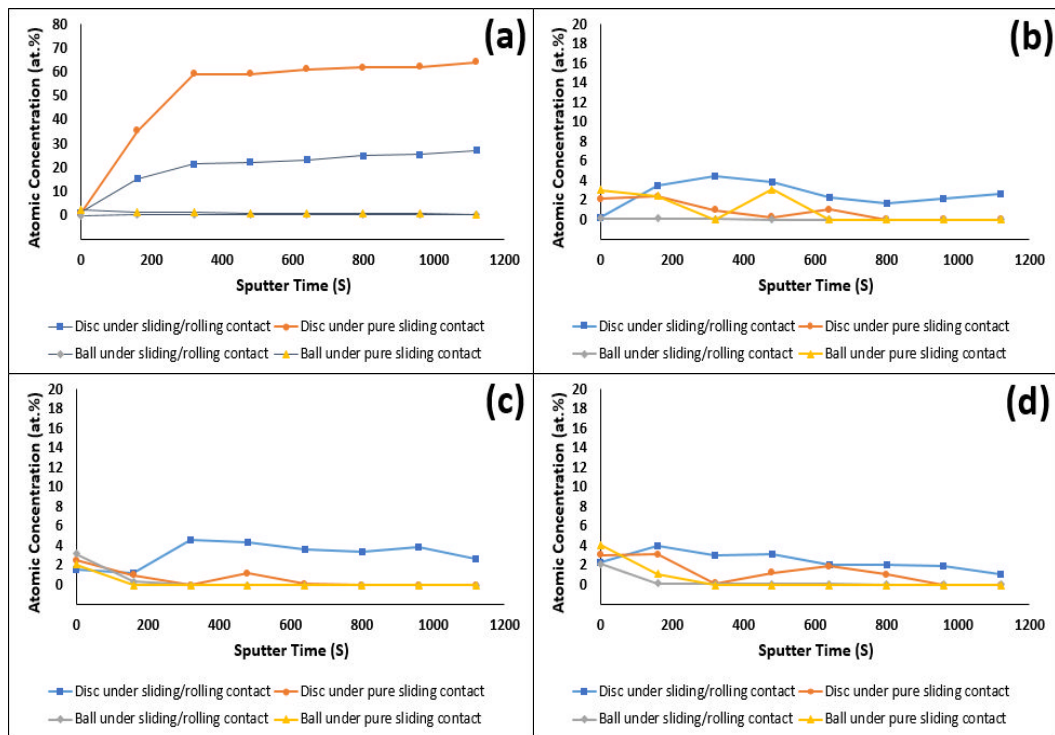


Figure 5-20 Depth profiles of the discs and balls lubricated in O5: (a) Fe, (b) Zn, (c) P, (d) Mo (note different at. % scales)

5.5. Effect of Oil Formulation and Contact Type on Stribeck Curve Evaluation

For 50% SRR (sliding/rolling contact) in Fig 5-3, it is clear that most of the lubricants showed a low friction coefficient of about 0.04 at high entrainment speed, characteristic of the mixed lubrication regime. The lubricant film provides partial separation; the contact load is shared between the contacting asperities and the film as a result of some mechanical interactions [16, 265]. At low entrainment speed, however, all of the lubricants showed higher friction, characteristic of the boundary lubrication regime, where extensive interactions occur and behaviour is characterised by the formation and removal of thin films of molecular proportions called tribofilms [28].

In the absence of additives, BO exhibited fluctuating friction values over varying entrainment speeds. MoDTC has no clear effect on friction reduction for the first 30 minutes of the tests; probably because the MoS₂ sheets need a sufficient time in order to be completely formed, as reported by Grossiord *et al.* [188] and Rai *et al.* [266]. BO gave the lowest friction among all other oil formulations for speeds ranging from 5 to 330 mm/s. Friction values were slightly reduced after 2 hrs of rubbing for all oil formulations and the reduction in friction was particularly significant for O5, probably due to a synergy between MoDTC and ZDDP. This is in line with the literature where MoDTC was found to be more effective when used together with the ZDDP and the combination of both was reported to significantly improve the tribological performance [197]. BO still exhibited fluctuating friction values after 2 hrs of rubbing, likely due to the absence of additives.

Early work [188, 192, 204] has shown that the MoDTC additive readily forms MoS₂ sheets under mixed-boundary lubrication regimes offering low friction on the tribological contacts. As a result, MoDTC played an essential role in reducing friction after 4 hrs of rubbing; O1 and O5 showed a higher friction reduction when compared to the rest of the oil formulations. Stable friction was reported after 6 hrs of rubbing. O3 gave the highest friction among all other oil formulations for speeds ranging from 5 to 530 mm/s. This is in line with the literature where tribofilms formed by ZDDP showed higher friction

performance [267]. In other words, ZDDP increases friction when added to the lubricant due to the formation of pad-like tribofilm.

For pure sliding (200% SRR) contact in Fig. 5-4, it is apparent that the effect of MoDTC and ZDDP in the first 30 minutes of rubbing is negligible. This is mainly because tribofilms of both additives need sufficient time to form on the surface. The lowest friction was about 0.03 which resulted from O2 and is characteristic of the mixed lubrication regime. One similarity between base oil and ZDDP alone was that BO and O3 gave the highest friction of about 0.1, probably due to the absence of additives in BO and the presence of ZDDP in O3. The effect of both MoDTC and ZDDP additives was more pronounced after 2 hrs of rubbing which led to a lower friction response. For this contact (i.e. pure sliding) O3 still showed the highest friction which was likely due to the presence of ZDDP additive.

5.6. Effect of MoDTC on Wear

From Fig. 5-10, cast iron (CI) discs showed relatively high wear when lubricated with O1 and O4 (i.e. MoDTC alone), suggesting an adverse effect of MoDTC in increasing wear of a ferrous counterpart rubbed against a DLC coating [221]. In line with the literature, the interaction between MoDTC and ZDDP at O5 gave the lowest wear to the CI disk [112]. ZDDP in O3, as expected, played a key role in reducing wear of the CI disk. In the absence of ZDDP (i.e. BO, O1, O2 and O4), sliding/rolling contact appears to exhibit more wear than pure sliding contact on the CI disks, suggesting that the wear reduction is not only controlled by the oil chemistry but also by the type of contact. That could be attributed to a slower build-up of tribofilms for the sliding/rolling contact compared to the pure sliding contact.

Some previous works [228-231] have reported high wear of DLC coatings in presence of MoDTC. In contrast, very limited studies showed reduction in wear of a DLC coating when lubricated with MoDTC additive. Vengudusamy *et al.* [221] observed that MoDTC reduces wear in most of his tests in DLC/DLC contact and a few tests in DLC/steel contacts. In this study, it is clear that no lubricants show extremely high wear on the DLC coating. For the

DLC balls lubricated with MoDTC additive, a ferrous surface (i.e. CI disc) was expected to help in increasing the wear of the DLC coating if iron oxide particles are presented in the DLC/cast iron interface [268]. However, in the absence of ZDDP, DLC coated balls showed quite low wear when MoDTC was present in the oil formulation (i.e. O1 and O4). Tung *et al.* [269] studied DLC/cast iron contacts and also reported that MoDTC reduces wear of a DLC coating in a formulated engine oil. There is however no evidence whether the formulated lubricants in Tung *et al.* [269] contained ZDDP or not, as this anti wear additive could suppress the effect of MoDTC on promoting wear of DLC coatings [230]. Comparing O3 with O2, the presence of ZDDP in the oil formulation reduced the wear of the DLC balls [261] but the wear reduction was not considerable. Sliding/rolling contacts for all formulated lubricants (except for BO and O1) exhibit relatively higher wear than pure sliding contact on the DLC coated balls. This suggests that the pure sliding contact probably facilitated the build-up of tribofilms on the interface which in return resulted in an enhanced lubrication and thus reduced wear of the DLC balls.

5.7. Effect of Contact Type on Tribofilm Evolution

The XPS analyses showed that a tribofilm on both tribopairs is formed under both contacts. Unlike recent work [119], it was found that the SRR values used in this study did affect the surface chemistry (i.e. tribofilm build-up was seen to be influenced by the change in SRR).

Table 5-3 summarises the effect of SRR on the tribofilms formed on the DLC coated balls (mainly when lubricated with O1 and O3). As can be seen from Table 5-3, for O1, the DLC ball under sliding/rolling contact mainly consisted of FeMoO₄. For the same oil under pure sliding contact, both MoS₂ and FeMoO₄ were detected on the DLC surface. This could justify the friction results where lower friction was reported under pure sliding contact as compared with the sliding/rolling contact. In addition, as the DLC ball under sliding/rolling contact mainly consisted of FeMoO₄, high wear was expected due to enhanced removal of tribofilms from the DLC ball. However, lower wear was reported on the DLC ball under sliding/rolling contact, suggesting that the

wear performance, in some cases, was controlled more by the type of contact than the oil formulation.

For O3 (FF+ZDDP), both Zn 2p and P 2p were observed on the DLC ball under pure sliding contact while no such compounds were detected on the DLC ball under sliding/rolling contact. Therefore, higher wear rate was reported for sliding/rolling contact than the pure sliding contact. On the other hand, for tribofilms formed on the CI discs, it can be seen that the MoS₂/FeMoO₄ ratio varies for the type of contact. In addition, it was found that MoS₂/FeMoO₄ ratio links to friction performance (i.e. the increasing of MoS₂/FeMoO₄ ratio reduces the coefficient of friction).

Table 5-3 Effect of SRR on the tribofilms detected on the DLC coated balls using XPS

	Sliding/rolling contact	Pure sliding contact
O1	Mo 3d (FeMoO ₄ only)	Mo 3d (FeMoO ₄ + MoS ₂)
O3	-	Zn 2p (Zn 2p _{1/2} + Zn2p _{3/2}) + P 2p

Generally, for most CI discs and DLC balls, there was a considerable variation in the chemical composition of the tribofilm that formed under both contacts. As a result, film thickness was seen to be influenced by the change in sliding/rolling ratio (SRR).

From Table 5-4 and Fig. 5-20, the film formed on the CI disc lubricated in O5 (FF+ZDDP+MoDTC) showed that concentrations of elements under pure sliding contact are significantly lower nearer to the substrate with high concentration of iron as compared to sliding/rolling contact. However, for DLC balls under both contacts, the depth profiles were fairly similar (i.e. both having thinner tribofilms). In addition, it can be observed that on cast iron, the thickness depends on sliding/rolling ratio whereas on DLC it does not.

Table 5-4 XPS quantification of tribofilms on the CI discs and DLC balls lubricated in O5

Sputter time:		C	Fe	O	Ca	Mo	Zn	P	S
1120s		1s%	2p%	1s%	2p%	3d%	2p%	2p%	2p%
Disc	50% SRR	20.7	27.2	37.7	5.9	1.0	2.5	2.7	2.0
	200% SRR	16.0	64.0	18.7	1.0	0	0	0	0
Ball	50% SRR	98.8	0	1.0	0	0	0	0	0
	200% SRR	97.7	0.1	1.6	0.4	0	0	0	0

5.8. Summary of Findings

The present chapter shows the tribological and tribochemical characteristics of a DLC/cast iron system with MoDTC-type friction modifier under sliding and rolling contacts. The main conclusions drawn from this work are:

- The sliding/rolling ratio affects friction, wear and tribochemistry in CI/DLC systems; pure sliding enhances MoDTC activation.
- Friction coefficient values were observed to vary across the boundary lubrication regime, unlike most modelling work which assume a constant value for coefficient of friction.
- The main MoDTC decomposition products are MoS₂ and FeMoO₄, not MoO₃. FeMoO₄ was identified as the reaction species, which is possibly responsible for the high friction.
- Tribofilm build-up is related to the sliding/rolling ratio (SRR). For instance, the DLC ball lubricated in base oil containing MoDTC (i.e. O1) created a film consisted of MoS₂ and FeMoO₄ under pure sliding contact while only FeMoO₄ was detected under sliding/rolling contact.

In addition, for pure sliding contact, Zn 2p and P 2p were observed on the DLC ball lubricated in the presence of ZDDP additive (i.e. O3 and O5) while no such compounds were detected on the DLC ball under sliding/rolling contact. All these variations are supported by the friction and wear results.

- MoS₂/FeMoO₄ ratio played a key role in the tribological performance of the CI discs. MoS₂/ FeMoO₄ for CI discs lubricated in the presence of MoDTC additive (i.e. O1, O4 and O5) was higher under pure sliding contact as compared with sliding/rolling contact. This correlates with the obtained friction results.
- Regardless of the contact type, no lubricants showed very high wear on the DLC coating. In addition, all DLC balls showed thinner films compared to CI discs, so the tribofilms were hard to detect by Raman technique.

Chapter 6. Single Cam Rig (SCR): Investigation of Friction and Wear of Cam/Follower Surfaces When Lubricated in a Fully Formulated Oil With and Without MoDTC-Type Friction Modifier

6.1. Introduction

This chapter addresses the effect of tappet clearance on the tribological performance of the camlobe/follower tribopair when lubricated in a fully formulated (FF) oil with and without Molybdenum Dialkyl Dithiocarbamate (MoDTC). White Light Interferometry and Talysurf contact profilometry were used to characterise the wear scar on the tappets and camlobes respectively. Torque profile, friction torque and wear data (as a function of tappet clearance, type of coating and oil formulation) are presented in this chapter.

6.2. Torque Profile Data

Representative torque profiles of different surfaces (at 300 rpm) were shown in Fig. 6-1. Basically, both coatings (MnPO_4 and DLC) were seen to have similar torque effect on the single cam rig system. A similar trend was also observed for all tappet thicknesses and camshaft speeds. From Fig 6-1, opening of the valves was presented by the higher positive profiles. In contrast, the return of the valves was presented by the lower negative section. It should be mentioned that if a system needs less work in order to open the valves, this would lead to significant friction benefits on the overall system.

Regardless of tappet clearance, the torque profiles showed close comparison between both coatings. Nevertheless, the torque profiles when using DLC coating were relatively decreased compared to inserts coated with Mn-phosphate. In addition, the lower thickness of tappets gave a lower torque profile. The reasons for these particular findings were discussed and explained later in this Chapter.

It is generally accepted that the torque benefits are directly proportional to less energy expended in operating an engine valvetrain system (mainly during

opening the valves). As a result, the torque benefits would then help to reduce energy that is lost due to friction.

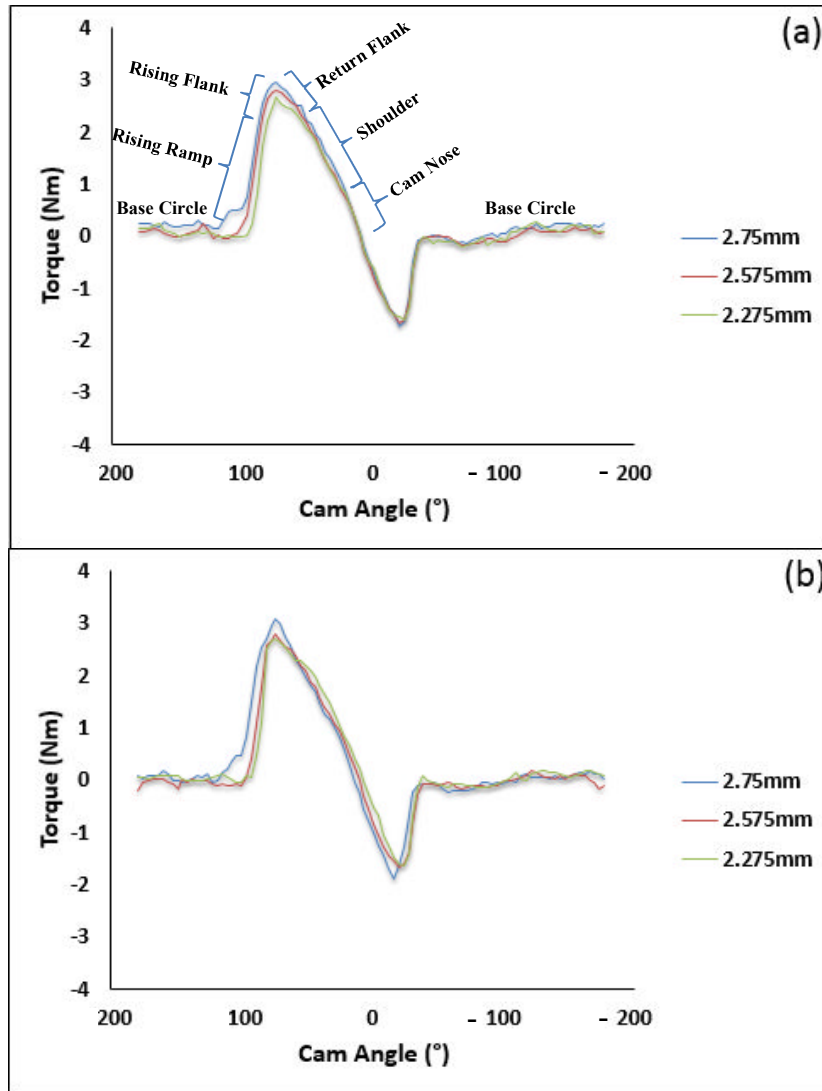


Figure 6-1 Torque profile of different tappet thicknesses at 300 rpm: (a) MnPO₄ inserts and (b) DLC inserts

6.3. Repeatability of Friction Torque Data

The single cam rig has proved to have good repeatability and high sensitivity to distinguish the frictional response of different coatings and fully formulated lubricants [76]. Representative friction data over 80 hrs test duration is shown in Fig. 6-2. The obtained friction data was stable and comparable for the whole test duration. Therefore, the average friction torque was calculated based on

all cycles (i.e. six test cycles). It is worth mentioning that this behaviour was seen for all coatings and speeds tested in this work. Nevertheless, all tests were performed twice at the same operating conditions with repeatable results.

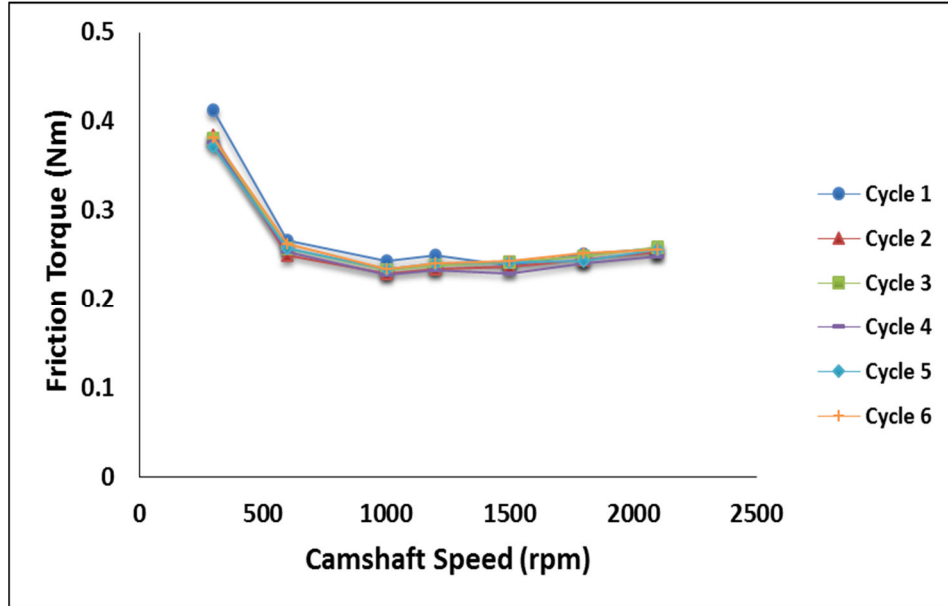


Figure 6-2 Repeatability of friction torque data for MnPO₄ insert (2.75mm tappet thickness) over 80 hrs test duration at 100 °C

6.4. First Stage and Second Stage Results

In both stages, MoDTC additive was blended with the fully formulated lubricant (i.e. O5). The only difference between both stages is the type of coating (i.e. the inserts of the first stage were coated with MnPO₄ coating while the inserts of the second stage were coated with DLC coating).

6.4.1 Friction Torque

6.4.1.1 Effect of Tappet Clearance and Camshaft Speed on Friction Torque

For Mn-phosphate tappets, the average friction torque as a function of tappet clearance and camshaft speed is shown in Fig. 6-3. As expected, the average friction torque generally reduced with increasing camshaft speed due to increased lubricant entrainment velocity into the cam/follower interface region. Similar results were reported previously [9, 75, 76, 85]. From the following

chapter, it has been reported that tappet rotation is affected by changing the clearance of the tappets. However, regardless of tappet rotation, the thickest tappet offered high friction torque. The thicker tappet experiences the lowest minimum film thickness and, as such justifies the high friction torque obtained. Figure 6-3 also shows the effect of temperature on the average friction torque. An increase in the average friction torque was observed with increasing lubricant temperature which is in agreement with previous works [66, 76, 270]. This is due to decreased oil viscosity (i.e. having a lower oil film thickness) under high temperatures leading to more asperity interactions.

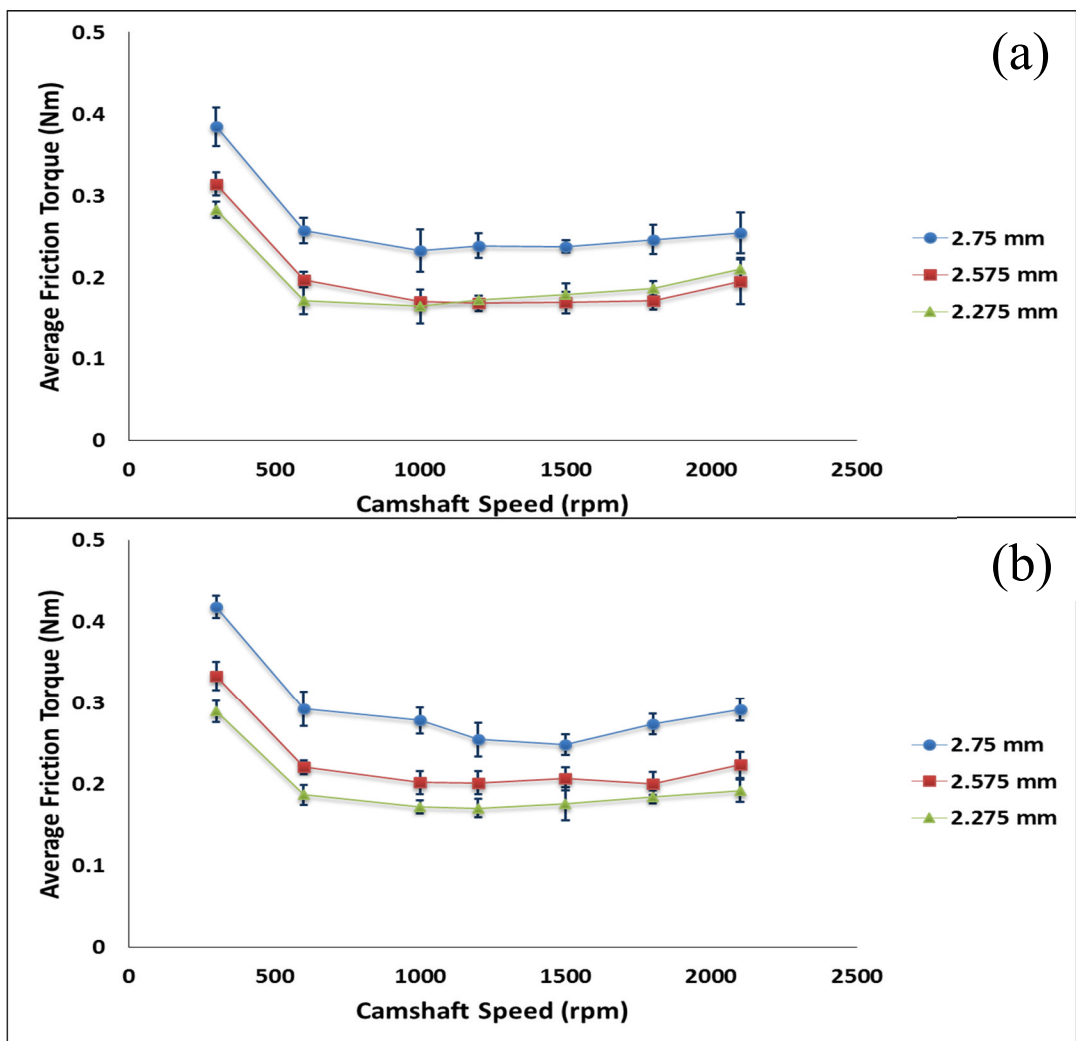


Figure 6-3 Average friction torque versus camshaft speed for MnPO₄ inserts at different thicknesses (a) at 100 °C, (b) at 130 °C

For both temperatures in Fig. 6-3, a high friction torque was observed at 300 rpm (lowest speed) due to the contact being in the boundary lubrication

regime, where more asperity-asperity interactions occur with the friction determined by the chemical and physical actions of thin films of molecular proportions [28]. The mixed lubrication regime is mainly represented at higher speeds where the lubricant film provides partial separation whereas the contact load is shared between the contacting asperities and the elastohydrodynamic lubrication film [16, 265]. Overall, the higher thickness of tappets gave a higher friction torque, suggesting a high asperity interaction at the cam/follower interface along with less reactivity to lubricant additives.

Based on the configuration of the SCR (taken from Ford engine), the action angle of cam half period is 56° (i.e. the valve lift typically occurs at 112° revolution). Changing the thickness of tappets varies the relative point of contact on the camlobe (see Fig. 6-4). Therefore, the highest thickness of tappet offers the maximum relative point on the contact, which in turn provides longer contact area between the camlobe and the follower.

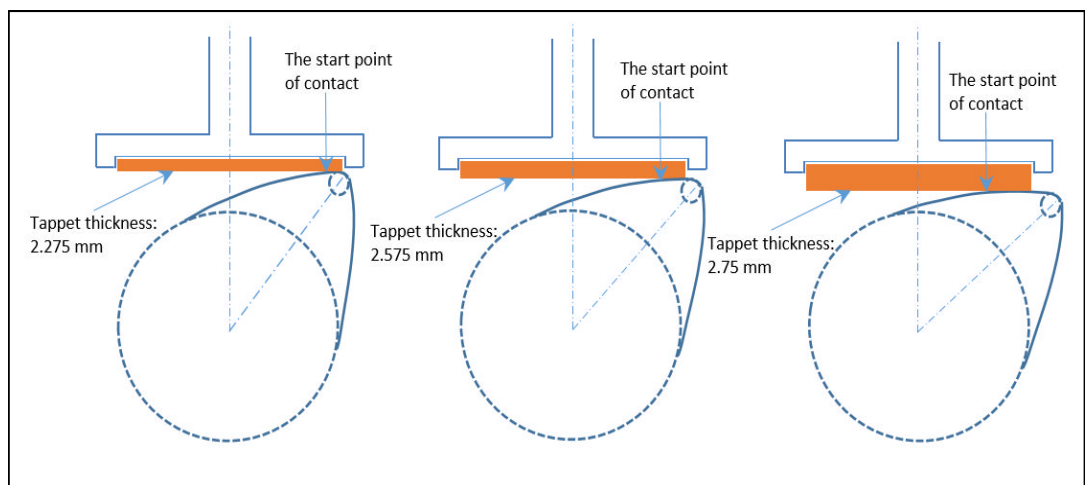


Figure 6-4 the start point of contact on the camlobe under different tappet thicknesses

Furthermore, based on Hooke's Law, $F=kx$ (where F : is the spring force, k : is the spring constant and x : is the deformation of the spring), it was clear that the thicker tappet will result in longer spring displacement and hence larger force (see Fig. 6-5). Thus, a higher friction torque was reported for the thicker tappet. This also confirms that the higher pressure due to use thicker tapper did not enhance the decomposition of MoDTC.

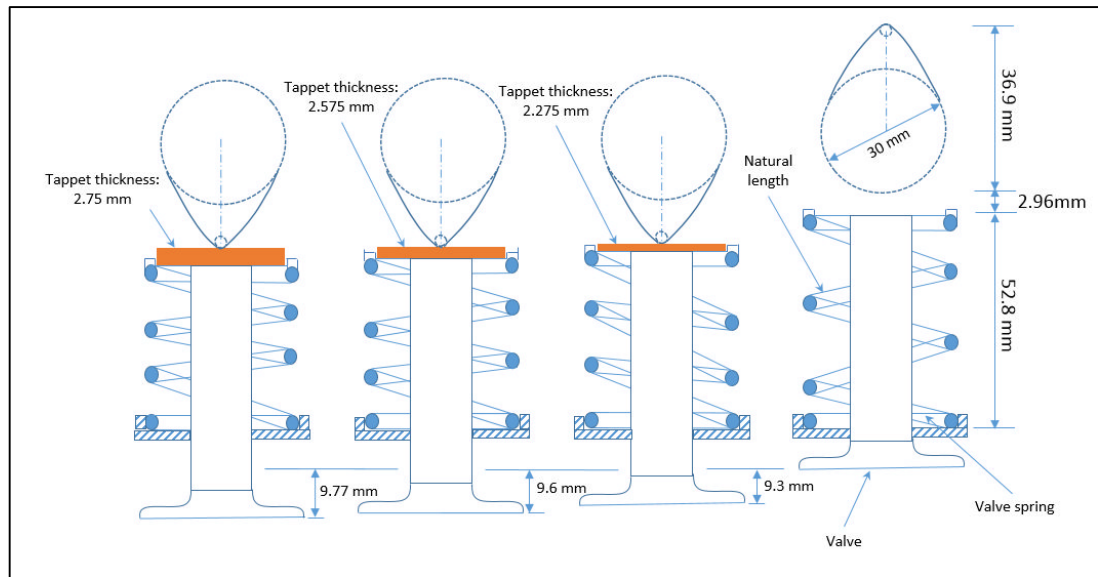


Figure 6-5 Effect of tappet thickness on valve spring

The valve lift can be related to the cam lift and the clearance between camlobe and follower using Equation 6-1:

$$\text{Valve lift} = \text{cam lift} - \text{clearance} \quad 6 - 1$$

The cam lift of the setup used in this work was 9.88 mm. The clearance between the followers and base circle of the camlobes depends on the tappet thickness. Thus, the clearance was measured, and reported around 0.11 mm for 2.75 mm tappet thickness, 0.28 mm for 2.575 mm tappet thickness and 0.58 mm for 2.275 mm tappet thickness. As a result, from Equation 6-1, different valve lift values were calculated and reported, as shown in Fig. 6-5. In other words, the valve lift values for 2.275 mm, 2.575 mm and 2.75 mm tappet thicknesses were reported around 9.3 mm, 9.6 mm and 9.77 mm respectively. The opening/closing ramp height for the cam used in this work was about 0.47 mm. For a real engine, however, the cam to tappet clearance is usually controlled to be 0.1 to 0.3 mm. Also, the selected clearance is not allowed to be bigger than the ramp height. It is also worth mentioning that the contact load for the spring and camlobe combinations is cyclic (constant) and is not expected to change for a particular rpm range. However, the thickness

would potentially change the instantaneous point of contact which in turn affects the slide-roll ratio and the tappet rotation, consequently affecting tribological performance.

6.4.1.2 Effect of Coating on Friction Torque

For DLC tappets in stage 2, the average friction torque as a function of tappet clearance and camshaft speed is shown in Fig. 6-6. Although the average friction torque of DLC tappets (as a function of tappet clearance) seems to be within the standard deviation, quite similar findings to those noticed on MnPO_4 tappets were observed regarding the effect of tappet clearance on friction performance (i.e. the tappet with higher thickness generally showed higher friction torque). This is best described referring back to Figure 6-4 where the percentage of the cycle (when the components are in contact) increases as the tappet clearance decreases. From Fig. 6-6, it should also be mentioned that no difference in the average friction torque of DLC tappets as a function of tappet clearance was observed in boundary lubrication regime. This is however opposite to those observed on MnPO_4 tappets.

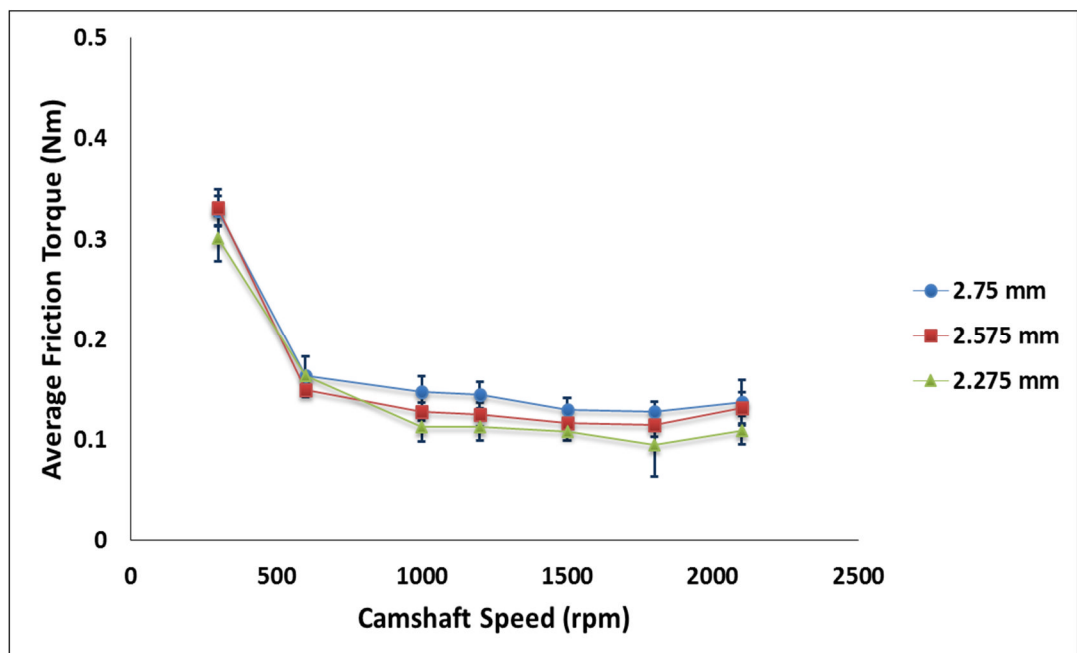


Figure 6-6 Average friction torque versus camshaft speed for DLC inserts at 100 °C

Furthermore, the average friction torque when using DLC coating was decreased compared to inserts coated with MnPO_4 . This was expected due to the high roughness of MnPO_4 tappet (which is a commercial standard production surface coating for inserts). The higher roughness of MnPO_4 coating gave rise to asperity interactions, and thereby led to high wear and friction [86]. Nevertheless, coating properties as well as the interactions between the coating, the counter-body and the lubricant are crucial to the friction/wear and tribochemical performance. Thus, the observed friction reduction could also be attributed to the behaviour of DLC coatings in the presence of additives including MoDTC, where DLC coatings offer friction reduction by forming MoDTC derived MoS_2 sheets on DLC surfaces [222-224].

6.4.2 Wear Evaluations

6.4.2.1 Tappets

Wear tracks on the tappet surface correspond to the rotation of the tappet and the interaction points during the cam cycle. For MnPO_4 inserts, the tappets with largest thickness showed the highest wear depth, as shown in Fig. 6-7. This suggests a higher interaction between the cam/follower tribopair with increasing tappet thickness. Accordingly, tappets with thickness of 2.275 mm have shown the lowest wear among the three thicknesses. However, noisy running was observed for the thinnest tappets, which could potentially result in higher wear of the valvetrain for longer test durations. From Fig. 6-7, the greatest wear depth was typically observed at the centre of the insert due to the contacts with the cam nose, flank, and shoulder and ramp regions. At the edge of the insert, however, there was no significant wear on the surface. As expected, and in line with previous findings [76, 271], the follower surface indicated concentric circles of the wear scar with different widths, as shown in Fig. 6-8. A potential reason for these concentric circles is the effect of tappet rotation which allows circumferential rubbing action to take place on the

surface of inserts. At higher temperature, the wear rate was mostly increased due to the effect of high temperatures on the lubricant viscosity.

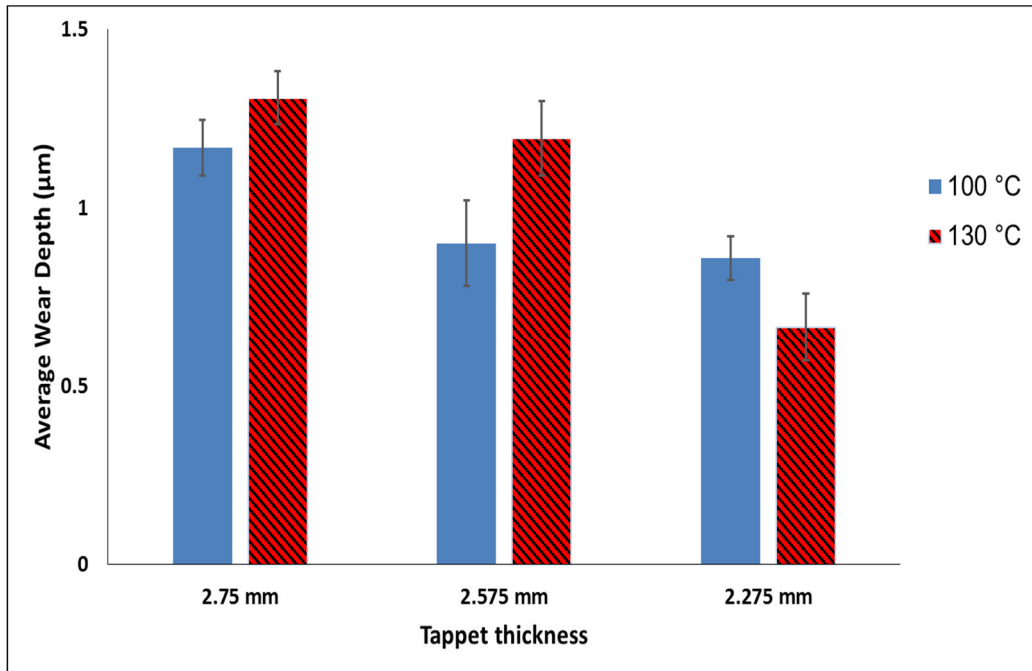


Figure 6-7 Average wear depth versus tappet thickness for MnPO₄ inserts at 100 °C and 130 °C

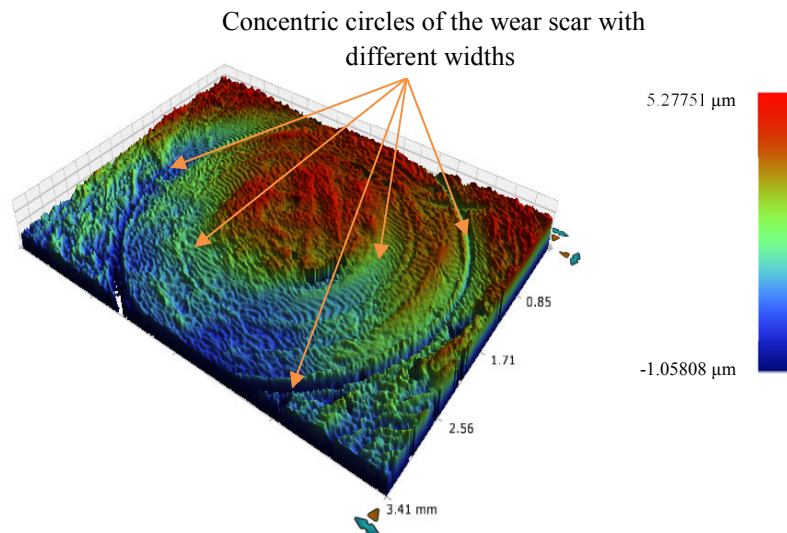


Figure 6-8 Typical wear scar of MnPO₄ tappet insert

For the second stage (i.e. tappets coated with DLC coating), Fig. 6-9 shows the average wear depth versus tappet clearance. Similar to the first stage, the high thickness of tappets showed the high wear rate. Thus, it is fair to conclude

that the wear performance of tappets is also more controlled by the tappet clearance rather than the type of coating. Further, the wear depth of the DLC insert was relatively lower than the wear depth of the MnPO_4 insert. This is however in contrast with the literature [226-231], where DLC coating was worn faster in the presence of MoDTC when rubbed against a ferrous counterpart. This discrepancy could be explained by the lubricant used in this study. As the lubricant contains 1%wt of ZDDP, this probably hinders the MoDTC potency in giving high wear to DLC coating in the DLC/ferrous combinations [231]. In addition to the properties of DLC coating (a-C- 15H), the differences in surface roughness between coatings were also believed to play a vital role on wear performance (i.e. DLC coating experienced low wear rate due to its low roughness). Likewise, from the following Chapter, the DLC coating was reported to offer a high rotation of inserts, this also in return would help to reduce wear of the DLC inserts by promoting lubricant retention in the contact.

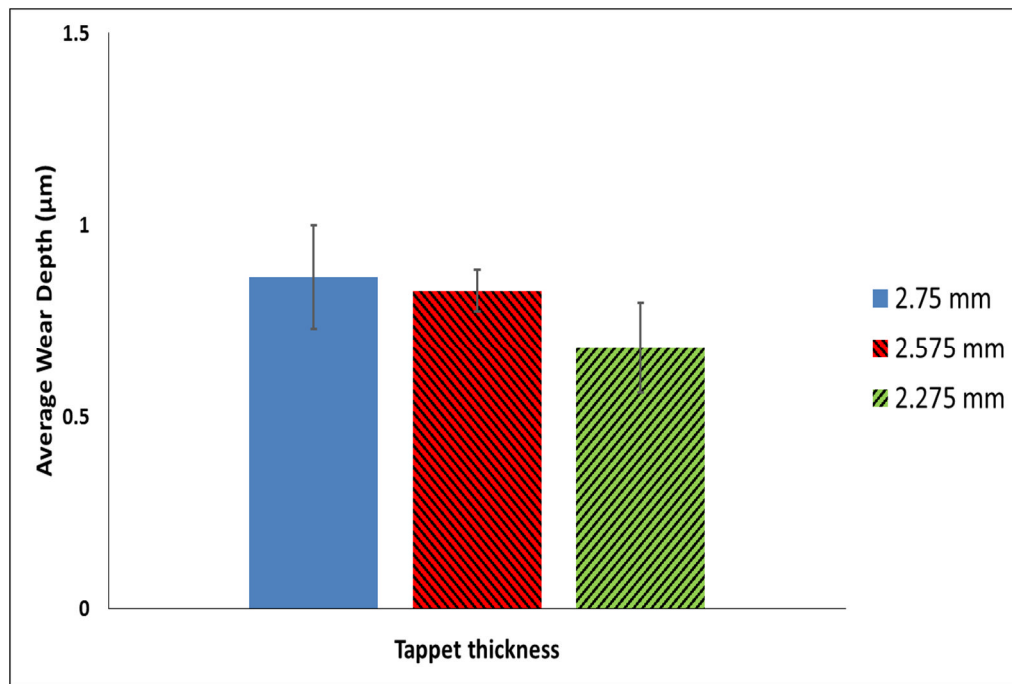


Figure 6-9 Average wear depth versus tappet thickness for DLC inserts at 100 °C

6.4.2.2 Camlobes

In line with standard engine tests, wear of the CI camlobes was reported at seven locations. However, as the cam half period (i.e. action angle) is at 56°,

different traces were also taken in the region between 14° and 56° (both sides). It is worth mentioning that the wear on this region was not considerable as compared to the wear on the selected seven locations.

For the first stage, the average wear depth across the camlobe (rubbing against Mn-phosphate inserts) at two temperatures (100 °C and 130 °C) is shown in Fig. 6-10.

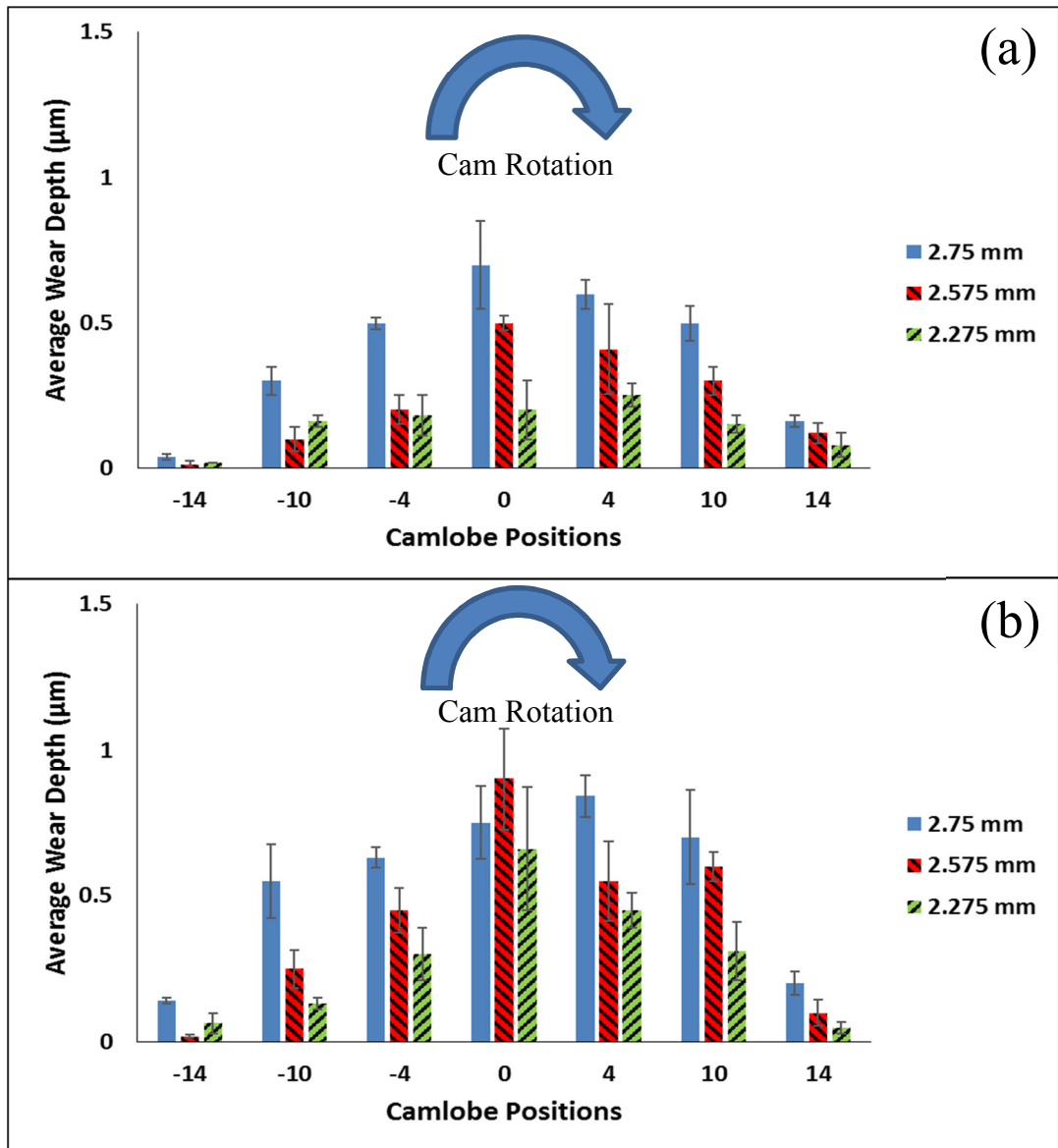


Figure 6-10 Average wear depth across the camlobe when interacting with MnPO₄ insert: (a) at 100 °C, (b) at 130 °C

For both temperatures, the high thickness of tappets generally showed the high wear depth on the camlobe surface. The cam nose is found to be a region of significant wear, especially toward the edges (i.e. sharp edges and worn tip) [272]. This is called edge loading which occurs due to high load/pressure on the nose (i.e. harsh conditions). For all thicknesses, a significant increase of wear was observed at two locations (cam nose and 4°), mainly due to the adverse effect of boundary lubrication and sliding action. Similar results showed that the camlobe wear was the highest near the camlobe nose [3]. In addition, camlobes mostly showed higher wear at the positive section (+14°, +10°, +4°) than the negative section and this behaviour is basically due to action of opening the valves [115]. A significant deformation of the CI camlobe surface occurred during the opening of the valve, probably due to greater energy/work which is expended during valve opening actions. Similar findings were reported previously [3, 76]. At higher temperature, the wear rate was generally increased which indicates that the durability (wear) of the Mn-phosphate coating is considerably lower at high temperature due to lower viscosity.

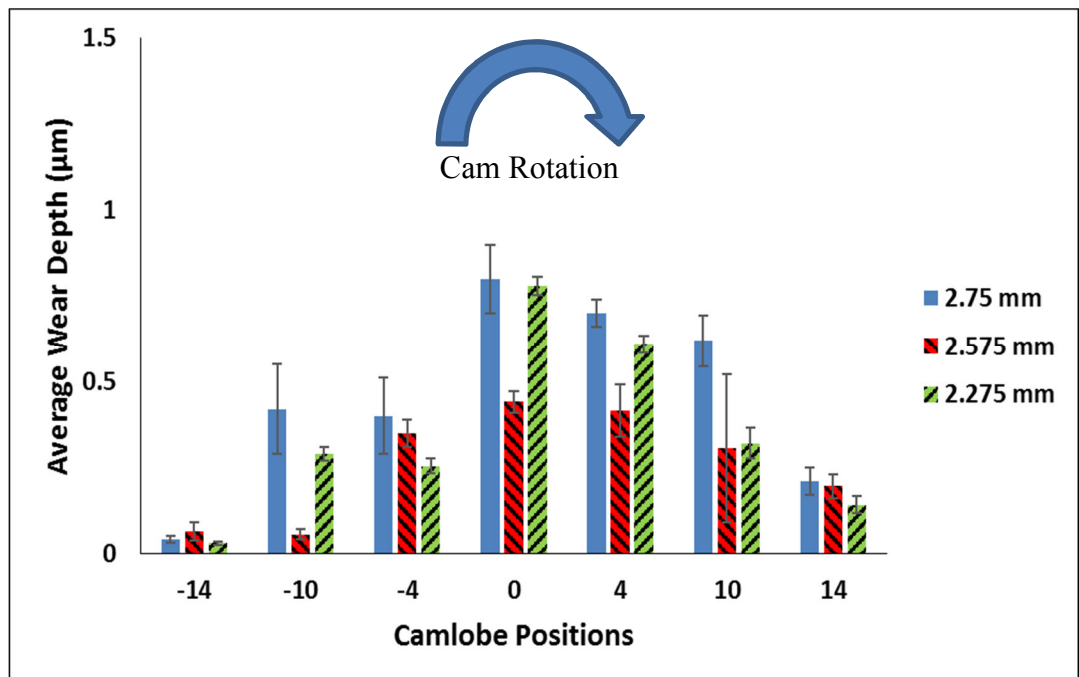


Figure 6-11 Average wear depth across the camlobe when interacting with DLC insert at 100 °C

For the second stage, the average wear depth across the camlobe (rubbing against DLC inserts) is shown in Fig. 6-11. A similar trend was observed under the effect of tappet clearance (i.e. the low clearance of tappets relatively showed high wear rate). It is interesting to note that regardless of the type of counterpart, wear rate is comparable for all camlobe positions. In other words, for both stages, wear distribution on camlobe positions was similar. Thus, it is interesting to report that wear of the camlobe is not mainly affected by the type of tappet. This is similar to findings by Ofune *et al.* [115]. Nevertheless, the wear depth of the CI camlobe rubbed against a DLC insert was generally higher than the wear depth of the CI camlobe rubbed against a MnPO_4 insert. This is mainly due to the differences in hardness and surface roughness between coatings. Also, it is believed to be related to the tribochemistry of the interface which will be discussed in detail in the Chapter 8 and Chapter 9.

6.5. Third Stage and Fourth Stage Results

The fully formulated (FF) lubricant in both stages is free of MoDTC (i.e. O3). Also, as mentioned earlier in Chapter 4, the inserts of the third stage were coated with MnPO_4 coating while the inserts of the fourth stage were coated with DLC coating.

6.5.1 Friction Torque

For both stages, the average friction torque as a function of tappet clearance and camshaft speed is shown in Fig. 6-12. Similar to previous stages (i.e. stage 1 and stage 2), the average friction torque generally reduced with increasing camshaft speed due to increased lubricant entrainment velocity into the cam/follower interface region. For both temperatures, as expected, a high friction torque was reported at the lowest speed (300 rpm) due to the contact being in the boundary lubrication regime. In contrast, the mixed lubrication regime is mainly observed at higher speeds.

For both stages (i.e. in the absence of MoDTC), the higher thickness of tappets also provided a higher friction torque, where the thicker tappet

experiences the lowest minimum film thickness. However, for the third stage (i.e. tappets coated with Mn-phosphate), it can be seen that the tappet with 2.575 mm thickness showed the lowest average friction torque. It was suggested that the tappet rotation is one of the main reasons for this particular findings. Details of this will be discussed in Chapter 9.

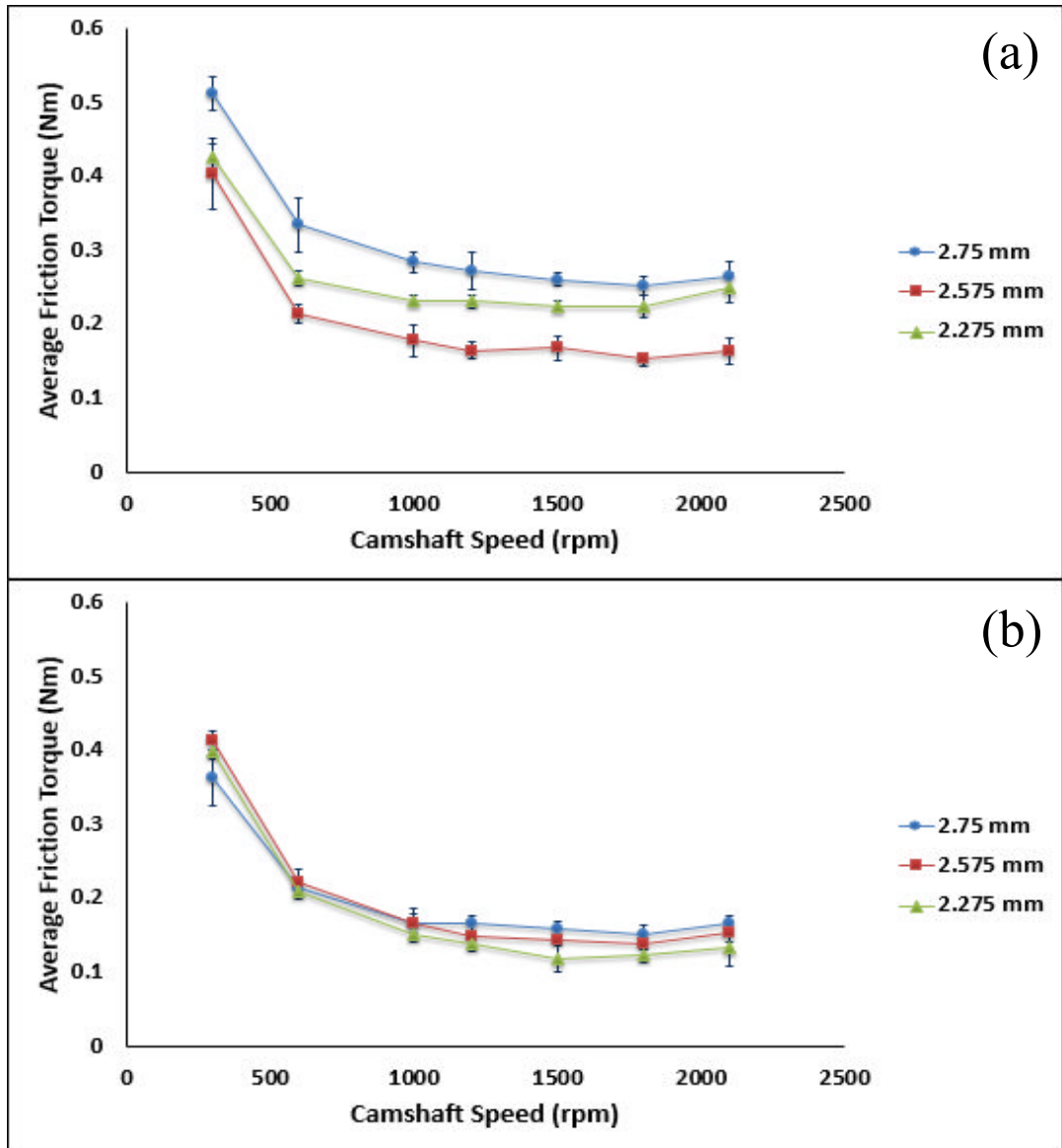


Figure 6-12 Average friction torque versus camshaft speed at 100 °C: (a) third stage (MnPO₄ inserts), (b) fourth stage (DLC inserts)

6.5.2 Wear Evaluations

In the absence of MoDTC, Fig. 6-13 shows the average wear depth versus tappet clearance for the third stage and fourth stage. Unlike the previous

stages, it can be seen that the tappets with thicknesses of 2.75 mm and 2.275 mm showed the high wear rate with close comparison of the wear that formed on the surface. The tappet thickness of 2.575 mm for both stages, however, showed the lowest wear rate. This was linked to the rotation of tappet with this thickness which helped to reduce not only the friction but also the wear rate. Details of this will be presented in the following Chapter. In addition, similar to the previous stages (i.e. the first stage and second stage), regardless of MoDTC additive, the wear that formed on the DLC inserts was generally seen to have less wear as compared to the inserts coated with MnPO₄. This is mainly due to the differences in surface roughness between coatings which was believed to play a vital role on wear performance.

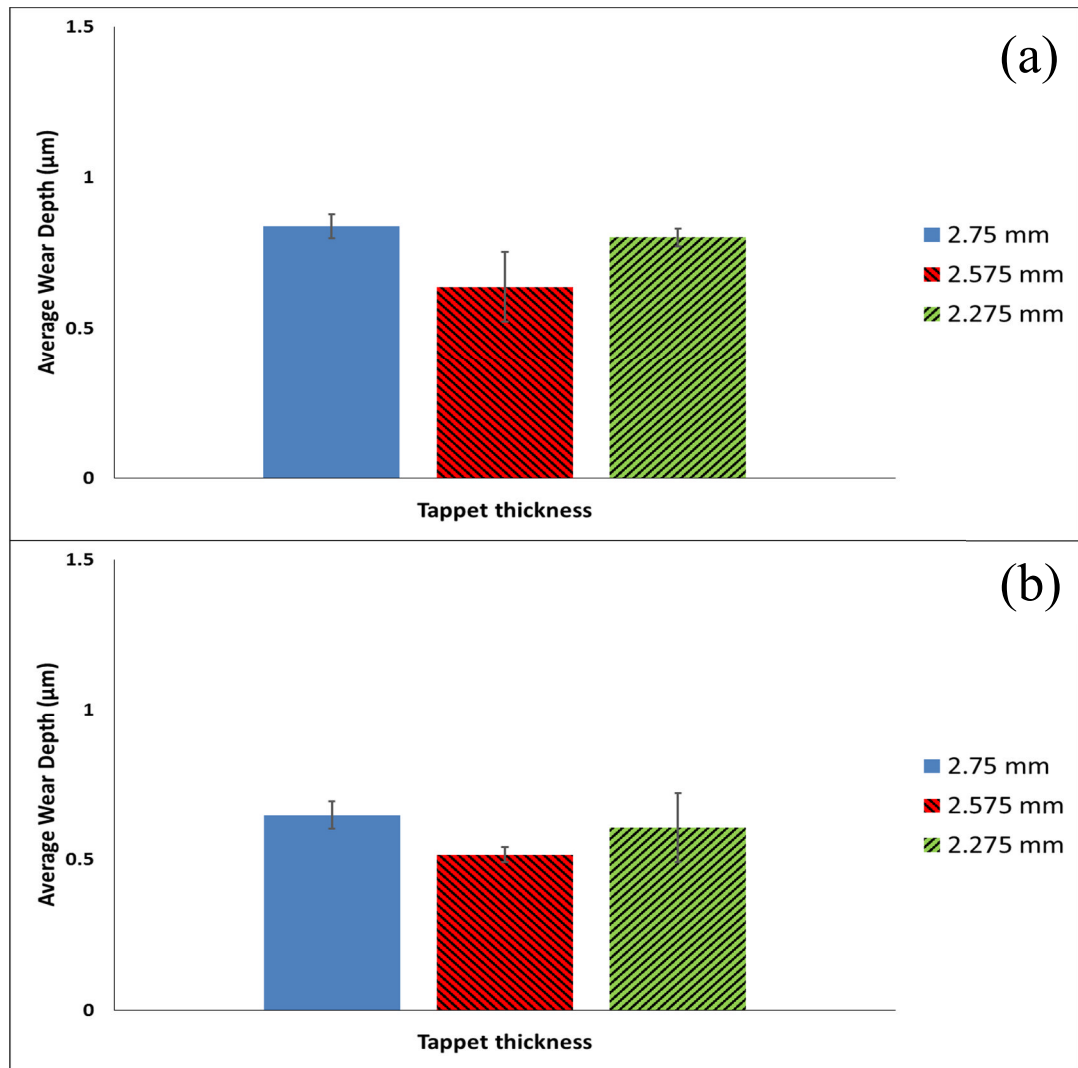


Figure 6-13 Average wear depth versus tappet thickness at 100 °C: (a) third stage (MnPO₄ inserts), (b) fourth stage (DLC inserts)

For camlobes, the average wear depth across the camlobe (rubbing against Mn-phosphate and DLC inserts) at 100 °C is shown in Fig. 6-14. For both stages, when the camlobe rubbed against an insert with thickness of 2.275 mm, the cam nose is found to be a region of significant wear. For the camlobe rubbed against inserts with thicknesses of 2.75 mm and 2.575 mm, however, the higher wear was observed at 4°. Furthermore, similar to previous stages, camlobes showed higher wear at the positive section (+14°, +10°, +4°) than the negative section, which is mainly due to action of opening the valves [115]. Moreover, the wear depth of the CI camlobe rubbed against a DLC insert was generally higher than the wear depth of the CI camlobe rubbed against a MnPO₄ insert.

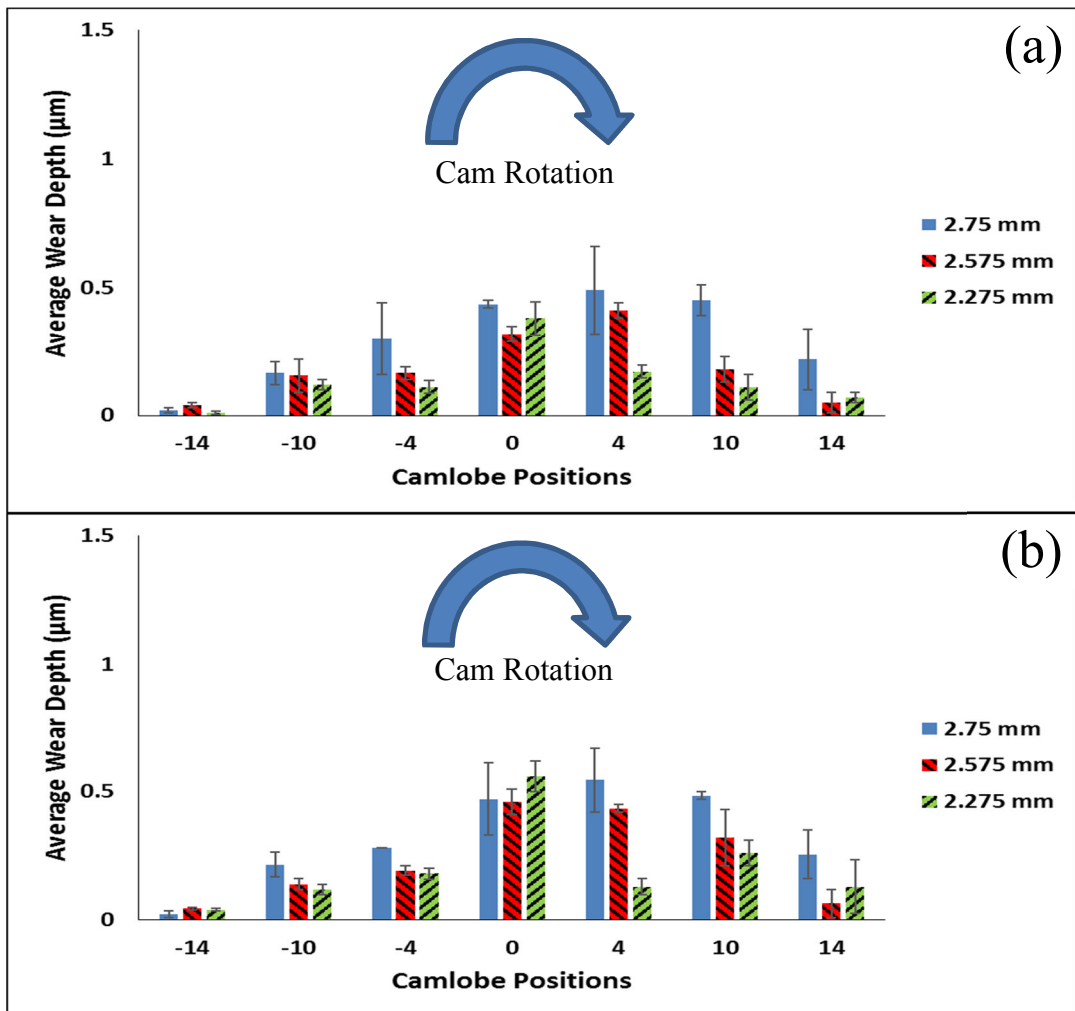


Figure 6-14 Average wear depth across the camlobe: (a) third stage (when interacting with MnPO₄ inserts), (b) fourth stage (when interacting with DLC inserts)

6.6. The Comparison of Tribological Performance for All Stages

For all tappet thicknesses, the first stage and second stage (i.e. MnPO_4 and DLC inserts lubricated with MoDTC) showed low friction compared to the third stage and fourth stage (i.e. MnPO_4 and DLC inserts lubricated in a lubricant free of MoDTC). This was expected as the MoDTC additive provides low friction under boundary lubrication by forming MoS_2 low friction sheets on the tribological contact [112, 188-191]. For the first, second and fourth stages, the higher thickness of tappets showed a higher friction torque. However, for the third stage, regardless of the coating type, it was found that the tappet with 2.575 mm thickness showed the lowest average friction torque. This was correlated to the behaviour of tappet rotation when using tappets with thickness of 2.575 mm.

In terms of wear, for camlobes under all stages, regardless of MoDTC additive, the wear depth of the CI camlobe rubbed against a DLC insert was generally higher than the wear depth of the CI camlobe rubbed against a MnPO_4 insert. This suggests that the DLC insert is harder than the MnPO_4 insert, which in turn, the DLC insert promoted high wear on the camlobe surface. In general, two locations (cam nose and 4°) are found to be a region of significant wear for most stages. Furthermore, for all stages, regardless of MoDTC additive and type of coating, camlobes showed higher wear at the positive section ($+14^\circ$, $+10^\circ$, $+4^\circ$) than the negative section.

For the wear detected on tappets, it can be observed that regardless of coating type and oil formulation, the high thickness of tappets showed the high wear rate. However, for the third stage and fourth stage, the tappet thickness of 2.575 mm showed the lowest wear rate. In addition, the first stage and second stage (i.e. MnPO_4 and DLC inserts lubricated with MoDTC) showed relatively high wear compared to the third stage and fourth stage (i.e. MnPO_4 and DLC inserts lubricated in a lubricant free of MoDTC). Similar findings [226-231] have reported high wear of DLC coatings in presence of MoDTC.

6.7. Summary of Findings

The main conclusions drawn from this chapter are given below:

- In both coatings, the tappet with smaller clearance in the first stage and second stage resulted in higher friction and wear, suggesting a high interaction between the cam/follower tribopair with increasing tappet thickness.
- Although less friction and wear was achieved using tappets with thickness of 2.275 mm, noisy running was observed. This possibly can cause an increase in the valvetrain wear for longer test durations.
- In both coatings, the tappet with thickness of 2.575 mm in the third stage and fourth stage resulted in lower friction and wear as compared to other thicknesses. This will be linked to the behaviour of tappet rotation with thickness of 2.575 mm.
- The clearance between the base circle and the follower plays a key role in engines efficiency and durability. For all stages, tappets with a thickness of 2.575 mm (0.285 mm clearance) might be considered the best selection among the three thicknesses. This thickness showed less friction and wear as compared to 2.75 mm tappet thickness. Also, it showed lower vibration, less noise and reduced wear for longer test durations as compared to 2.275 mm tappet thickness.
- Comparing DLC inserts to MnPO₄ inserts, a considerable reduction in the friction torque and wear was observed. This was expected due to the high roughness of MnPO₄ tappet (which is a commercial standard production surface coating for inserts).
- For stage 1 and stage 2, adding MoDTC to the lubricant helped in friction reduction but it was one of the main reason to promote high wear rate on the surface.
- In terms of camlobes wear, two locations (cam nose and 4°) were found to be regions of significant wear for most stages. In addition, comparing the wear across the camlobe, the selected seven locations showed the highest wear while the wear of the other locations was not considerable.

Chapter 7. Single Cam Rig (SCR): Investigation of Tappet Rotation When Lubricated in a Fully Formulated Oil With and Without MoDTC-Type Friction Modifier

7.1. Introduction

This chapter presents the tappet rotation results when lubricated in a fully formulated (FF) oil with and without MoDTC-type friction modifier. To the best of the authors' knowledge, no studies have reported the rotation of tappet as a function of different coatings, thicknesses of tappets and oil additives such as MoDTC additive which has been reported to be detrimental to the wear of some DLCs.

7.2. Repeatability of Tappet Rotation Data

The technique developed in this work showed good repeatability and high sensitivity to distinguish tappet rotational speed under different temperatures, coatings and thicknesses. Initially, the repeatability of the tappet rotation during an 80 hr test was investigated. Fig. 7-1 compares the number of counts/rotations (per second) at the end of the time for each cycle. In general, it can be seen that the number of counts, for all speeds, gradually increases with increase in the number of test cycles (i.e. longer test duration). This believed to be due to running-in which suggests that the surface of the tappet becomes smoother over time which could potentially lead to a better conformity of the two surfaces in contact. This in return promotes the rotation of the tappet over time.

To have a better picture of the effect of test duration on tappet rotation, a representative set of data at 1200 rpm over six test cycles is shown in Fig. 7-2. A considerable increase of the tappet rotation was observed for the first four cycles. However, tappet rotational speed became fairly stable and comparable for the last three cycles. Consequently, the average tappet speed was generally calculated based on the last three cycles (i.e. steady state rotation).

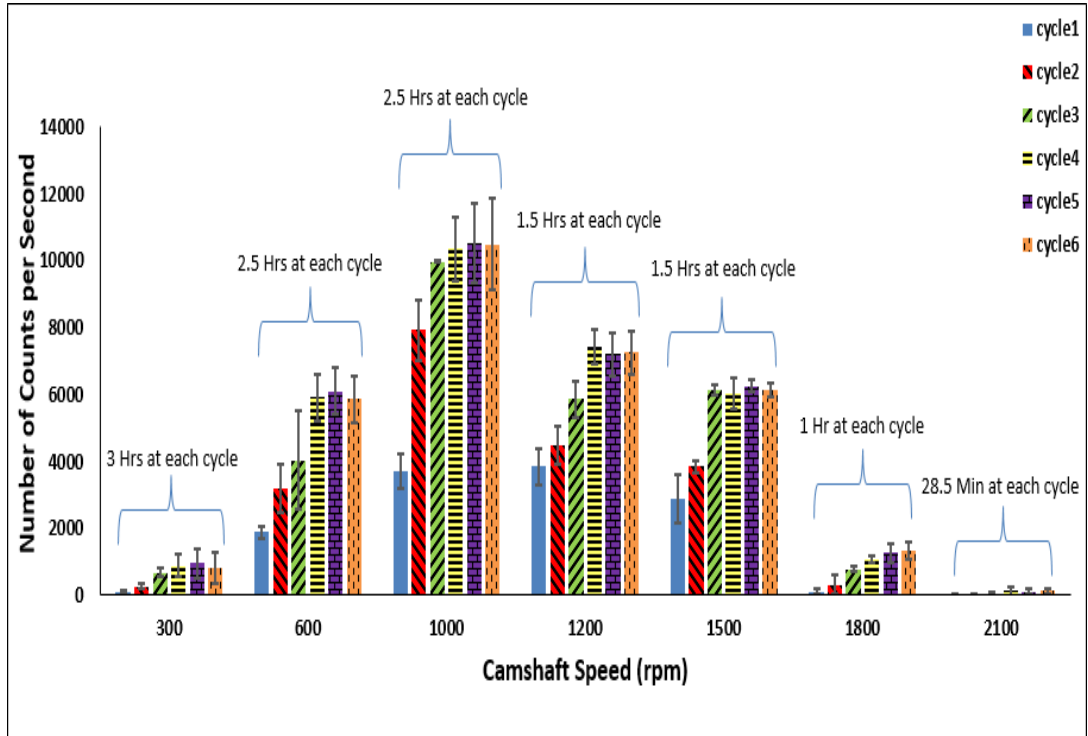


Figure 7-1 Number of counts for MnPO₄ insert with thickness of 2.75mm during an 80 hour test

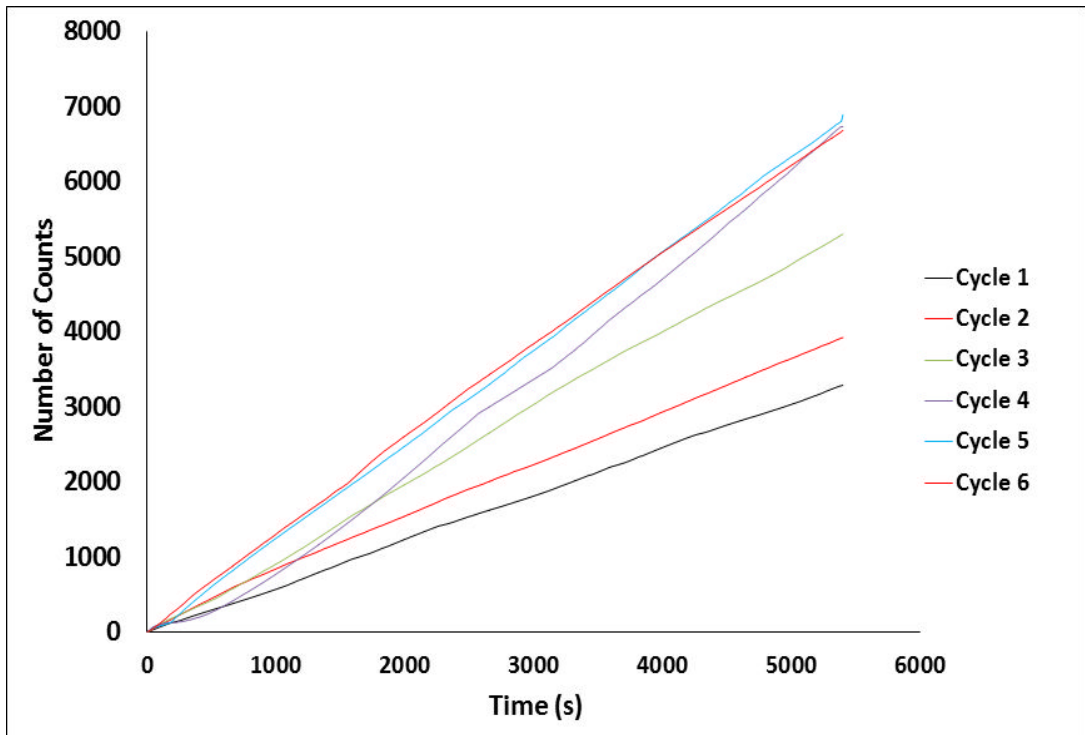


Figure 7-2 Repeatability of tappet rotation for MnPO₄ insert with thickness of 2.75mm at 1200 rpm

7.3. First Stage and Second Stage Results

7.3.1 Effect of Tappet Clearance and Camshaft Speed on Tappet Rotation

For the tappets coated with Mn-phosphate (i.e. the first stage), the effect of tappet clearance and camshaft speed on the average tappet rotation is shown in Fig. 7-3. In general, tappets with higher thickness showed higher rotation. This could be due to an enhanced interaction between the cam/follower interface when reducing the clearance between the follower and base circle of the camlobe (i.e. increasing the tappet thickness).

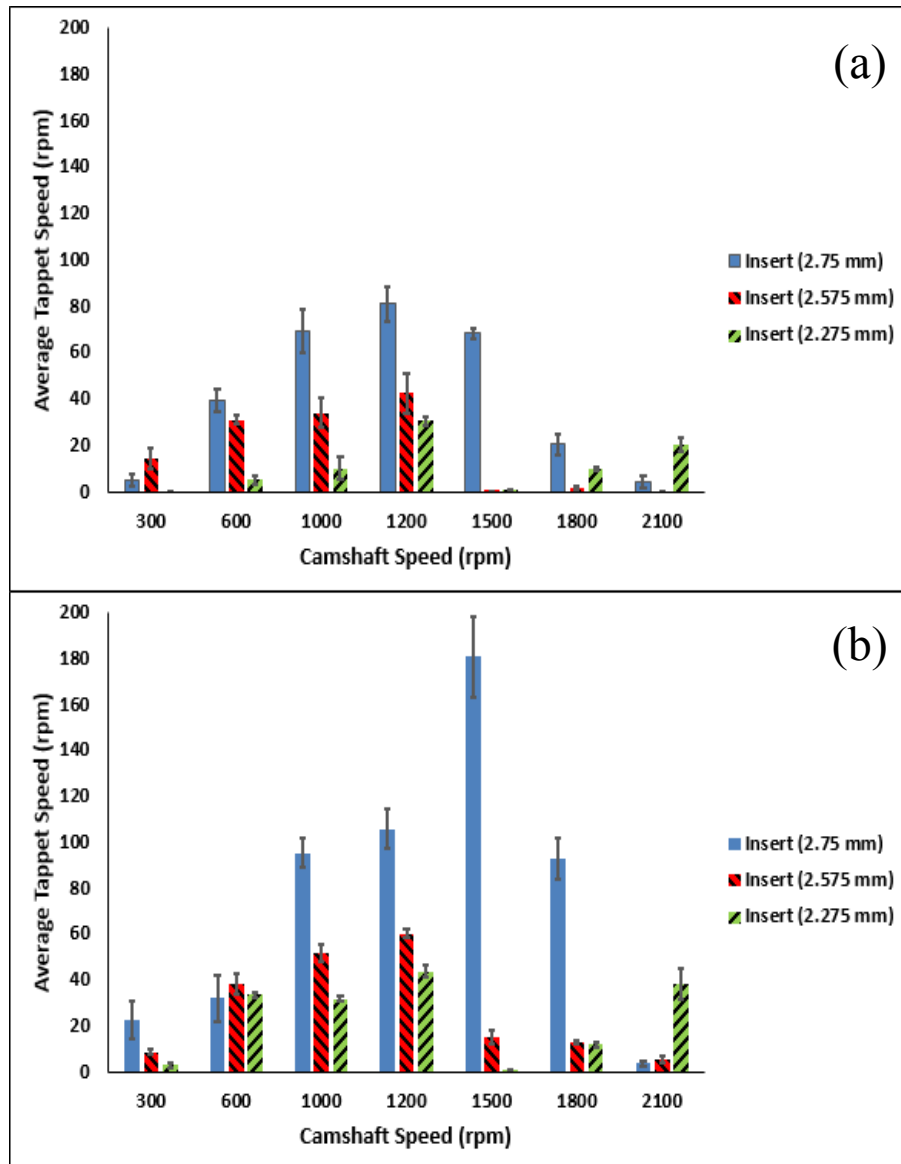


Figure 7-3 Average tappet rotation versus camshaft speed for MnPO₄ inserts at different thicknesses: (a) at 100 °C, (b) at 130 °C

In addition, based on the configuration of the SCR, the valve lift typically occurs at 112° revolution (i.e. the action angle of cam half period is 56°). Using different tappet thicknesses affects the relative point of contact on the camlobe. In other word, this relative point of contact varies with different variation of the tappet clearance. Therefore, the highest thickness of tappet offers the maximum relative point on contact, which in turn provides longer contact area between the camlobe and the follower. This would lead to a higher tappet rotation with the thicker tappet.

Also, from Fig. 7-3a, the highest rotation of 2.75 mm insert was observed at 1200 rpm. For this thickness, the tappet speed is directly related to the camshaft speeds of up to 1200 rpm. For speeds more than 1200 rpm, the tappet rotation was decreased gradually and the lowest rotation was at 2100 rpm. Similar results were reported in the literature [234, 241]; they found less rotation in some tappets for camshaft speeds more than 1050 rpm [234] or 2000 rpm [241]. A potential reason for this particular behaviour could be an increase in slip at the cam/follower interface with increase of the camshaft speed.

For 2.575 mm thickness, the tappet speed was also increased and the highest rotation was at 1000 rpm. However, the rotation was negligible at camshaft speeds between 1500 and 2100 rpm. For 2.275 mm, there was no rotation at 300 rpm while the highest rotation was at 1200 rpm. Comparing all thicknesses, it is interesting to note that the rotation of tappet was considerable at 2100 rpm when using tappet with the thickness of 2.275 mm. This suggests that a lower slip rate (at the tribocontact) can be achieved with a higher clearance between the cam/follower tribopair.

Figure 7-3 also shows the effect of temperature on the average tappet rotation. From Fig. 7-3b, it can be seen that the rise of the oil inlet temperature to 130°C clearly increases tappet rotation. This is due to decrease in the oil viscosity, resulting in more mixed to boundary interaction, which lead to the increase in friction at the cam/follower interface. This in return promotes the rotation of the tappet.

Similar results regarding the effect of temperature on the tappet rotation were reported previously [234, 235, 247]. However, Monteil *et al.* [241] reported that the tappet rotation is slightly dependent on the temperature while oil pressure has the major influence on the tappet rotation.

7.3.2 Effect of Coating on Tappet Rotation

MnPO₄ and DLC coatings are widely used in cam/follower systems [84]. In particular, DLC coatings are considered as good candidates for reducing friction and improving durability of automotive engines [93]. Therefore, investigating the effect of both coatings on tappet rotation was one of the main concerns in this work. Accordingly, for the second stage, the DLC coating was applied for all tappet thicknesses, as shown in Fig. 7-4.

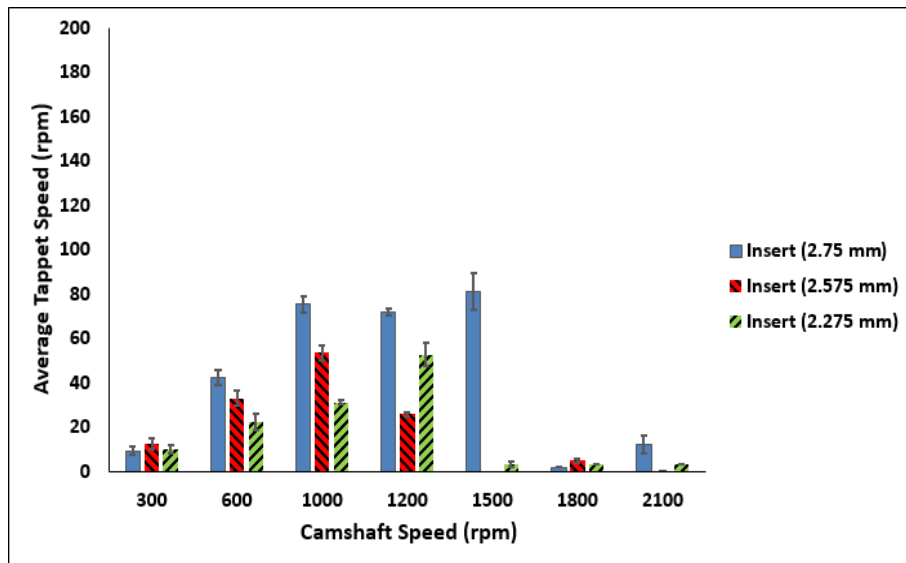


Figure 7-4 Average tappet rotation versus camshaft speed for DLC inserts at 100 °C

Regardless of type of coating, similar findings were seen regarding the effect of tappet clearance on tappet speed (i.e. tappet with higher thickness generally showed higher rotation). It is apparent that regardless of the type of the coating, the tappet speed is mainly controlled by the tappet clearance. Generally, it was found that the tappet rotation for DLC inserts was higher than the inserts coated with MnPO₄. A representative comparison of tappet speed

between both coatings (i.e. DLC and MnPO₄) is shown in Fig. 7-5. In general, the tappet speed for DLC insert was also increased gradually with the increase in camshaft speed and the highest rotation was at 1500 rpm. For all thicknesses and coatings, the highest tappet rotation was seen to vary with different type of coating and the tappet thickness. Thus, it is fair to conclude that the highest tappet rotation was found to be influenced not only by the camshaft speed but also by the type of coating and the tappet clearance. From Fig. 7-5, it can be seen that for all camshaft speeds (except for 1200 rpm and 1800 rpm), the tappet rotation for DLC insert was higher than the insert coated with MnPO₄. Similar results were generally observed for all thicknesses of the DLC tappets. The higher tappet rotation of DLC coated inserts is most likely one of the main reasons that helped in reducing friction and increasing the anti-wear properties of the DLC inserts. However, the reason for this behaviour is understood to be mainly due to surface roughness. MnPO₄ is rougher than the DLC and the polycrystalline surfaces of MnPO₄ resist any motion particularly those due to tappet rotation. Another important aspect is better running-in properties of DLC surfaces than the Mn-phosphate coating which gives rise to increased tappet rotation at boundary/mixed lubrication regimes [115]. Another reason, based on Newton's second law of motion, the resist torque is high when using DLC coating and that in return assists to promote the rotation of tappet.

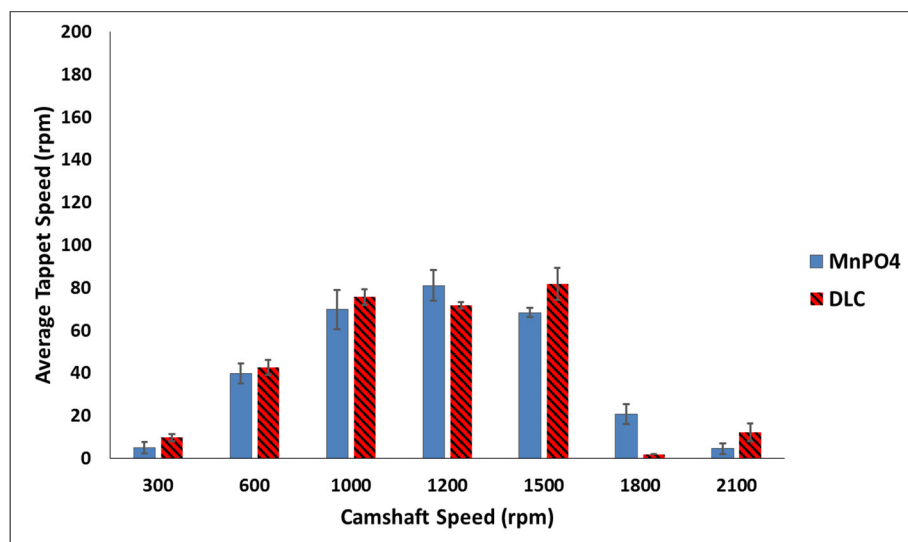


Figure 7-5 Effect of coatings on the rotation of 2.75mm tappet thickness at 100 °C

7.4. Third Stage and Fourth Stage Results

7.4.1 Effect of Tappet Clearance and Camshaft Speed on Tappet Rotation

In the absence of MoDTC, Figure 7-6 shows the effect of tappet clearance and camshaft speed on the average tappet rotation. In both stages (i.e. third stage and fourth stage), tappets with thickness of 2.575 mm generally showed higher rotation. This clearly justifies the low friction and low wear obtained from the tappet thickness of 2.575 mm.

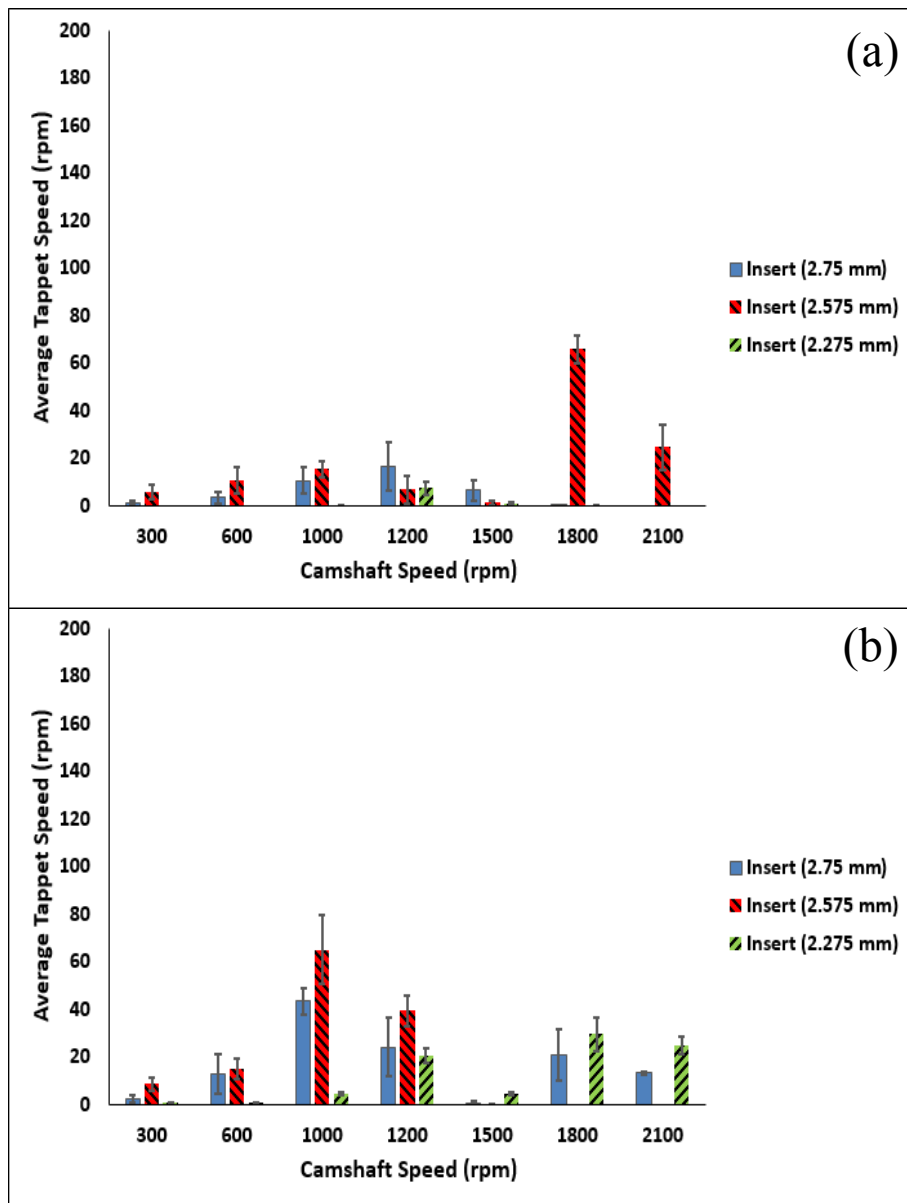


Figure 7-6 Average tappet rotation versus camshaft speed at 100 °C: (a) third stage (MnPO₄ inserts), (b) fourth stage (DLC inserts)

From Fig. 7-6a, the third stage, the highest rotation of 2.575 mm insert was observed at 1800 rpm. For this thickness, the tappet speed is directly related to the camshaft speeds of up to 1000 rpm. For speeds more than 1000 rpm, the tappet rotation was decreased gradually and the lowest rotation was at 1500 rpm. For 2.75 mm, the tappet speed is directly related to the camshaft speeds of up to 1200 rpm. For speeds more than 1200 rpm, the tappet rotation was also decreased gradually and the lowest rotation was at 1800 rpm and 2100 rpm. In addition, for 2.275 mm, the rotation was negligible at all camshaft speeds (except for 1200 rpm and 1500 rpm).

In the fourth stage (see Fig. 7-6b), for 2.575 mm and 2.75 mm, the highest rotation was seen at 1000 rpm. For speeds more than 1000 rpm, the tappet rotation was clearly decreased. However, for 2.575 mm, the rotation was negligible at 1800 rpm and 2100 rpm. In addition, it should be mentioned that the tappet rotation, for thickness of 2.275 mm, was seen to be not considerable at low camshaft speeds (i.e. 300 rpm and 600 rpm) and the highest rotation was reported at 1800 rpm.

7.4.2 Effect of Coating on Tappet Rotation

Figure 7-6 also shows the effect of coating type on tappet rotation under the absence of MoDTC additive. In both coatings, similar findings were observed regarding the effect of tappet clearance on tappet speed (i.e. tappet with thickness of 2.575 mm generally showed higher rotation). In addition, similar to the first stage and second stage results, it can be seen that the tappet rotation for DLC inserts was higher than the inserts coated with MnPO_4 . This is obviously helped in reducing friction and increasing the anti-wear properties of the DLC inserts.

7.5. The Comparison of Tappet Rotation for All Stages

Comparing the first stage (i.e. MnPO₄ insert lubricated with MoDTC) to the third stage (i.e. MnPO₄ insert lubricated in a lubricant free of MoDTC), it can be noticed that regardless of tappet clearance, a higher tappet rotation was reported with the first stage. This means that the MoDTC additive was helped in increasing tappet rotation. As the MoDTC was reported to form MoS₂ low friction sheets on the tribological contact [112, 188-191], these sheets were suggested to provide a better conformity of the two surfaces in contact which in return increases the rotation of the tappet.

In addition, comparing the second stage (i.e. DLC insert lubricated with MoDTC) to the fourth stage (i.e. DLC insert lubricated in a lubricant free of MoDTC), it can also be observed that the tappet rotation was higher with the second stage. This confirms the findings from the first stage and second stage (i.e. the MoDTC additive promotes the rotation of the tappet). For the first stage and second stage, it should be noted that tappets with higher thickness showed higher rotation. This could be due to an improved interaction between the cam/follower interfaces when increasing the tappet thickness. However, for the third stage and fourth stage, tappets with thickness of 2.575 mm generally showed higher rotation.

Furthermore, comparing MnPO₄ coating (used in the first stage and third stage) to DLC coating (used in second stage and fourth stage), it can be seen that the tappet rotation for MnPO₄ inserts was lower than the inserts coated with DLC. This is obviously led to increase friction and wear of the MnPO₄ inserts.

It is worthwhile to mention that any ridges/grooves on the surface of the insert can directly affect tappet rotation behaviour. Thus, a smoother surface of DLC inserts gave higher tappet rotation than the MnPO₄ inserts with a rougher surface.

7.6. Summary of Findings

The following conclusions are drawn based on the adaption of the single cam rig to measure tappet rotation when lubricated with fully formulated oil containing 1wt % MoDTC or free from MoDTC:

- The technique developed in this study facilitates evaluation of tappet rotation with good repeatability and high sensitivity to distinguish tappet rotational speed under different temperatures, coatings and thicknesses.
- Based on the findings in this chapter, we have discovered that tappet rotation is controlled by the following factors in order of impact;
 - Clearance between the camlobe and the tappet (i.e. coating clearance).
 - Temperature and speed.
 - Surface roughness of the tappet or type of coating.
- For the first stage and second stage, regardless of coating type, the thickest tappets showed high rotation, suggesting that the tribological performance is more controlled by the clearance between the follower and the camlobe rather than the type of coating or tappet rotation. However, for the third stage and fourth stage, tappets with thickness of 2.575 mm generally showed higher rotation.
- Regardless of tappet clearance, a higher tappet rotation was reported when lubricated with fully formulated oil containing 1wt % MoDTC, suggesting that MoS₂ sheets were led to a better conformity of the cam/follower surfaces which then helped in increasing the rotation of the tappet.
- The tappet rotation for DLC inserts was higher than the inserts coated with MnPO₄. This is clearly helped in reducing friction and increasing the anti-wear properties of the DLC inserts.

Chapter 8. Tribochemistry Evaluation of Tribofilms Formed from Single Cam Rig (SCR) Tribometer When Lubricated in a Fully Formulated Oil With and Without MoDTC-Type Friction Modifier

8.1. Introduction

This chapter reports the tribochemical performance of cam/follower surfaces when lubricated in a fully formulated (FF) oil with and without MoDTC. Scanning Electron Microscopy (SEM) was used on both (i.e. camlobes and tappets) for wear assessment as well as to assess the durability of coatings used on the tappets. Energy-Dispersive X-ray (EDX), Raman spectroscopy, X-ray Photoelectron Spectroscopy (XPS) and Focused Ion Beam (FIB)/Transmission Electron Microscopy (TEM) analyses were all performed on the tribofilms to understand the tribochemical interactions between oil additives and the cam/follower interface.

8.2. First Stage and Second Stage

8.2.1 SEM-EDX Results

For both stages, SEM micrographs in Fig. 8-1, revealed that interactions took place between oil additives, the camlobe surface and the coating insert surface. Unlike the camlobes, the wear scar of the inserts for both coatings (i.e. MnPO_4 and DLC) was clearly identified by SEM.

Figure 8-1 also shows the effect of tappet clearance on the tribofilms formed on the cam/follower surfaces. For both coatings, confirming friction and wear results, the thickest tappet showed high interactions with the camlobe surface and the oil additive. EDX semi-quantification of Cl camlobes and coated steel inserts (2.75 mm) is presented in Table 8-1. In addition, the elemental composition of the Cl camlobes and the coated steel inserts (2.575 mm and 2.275 mm) is presented in Table 8-2.

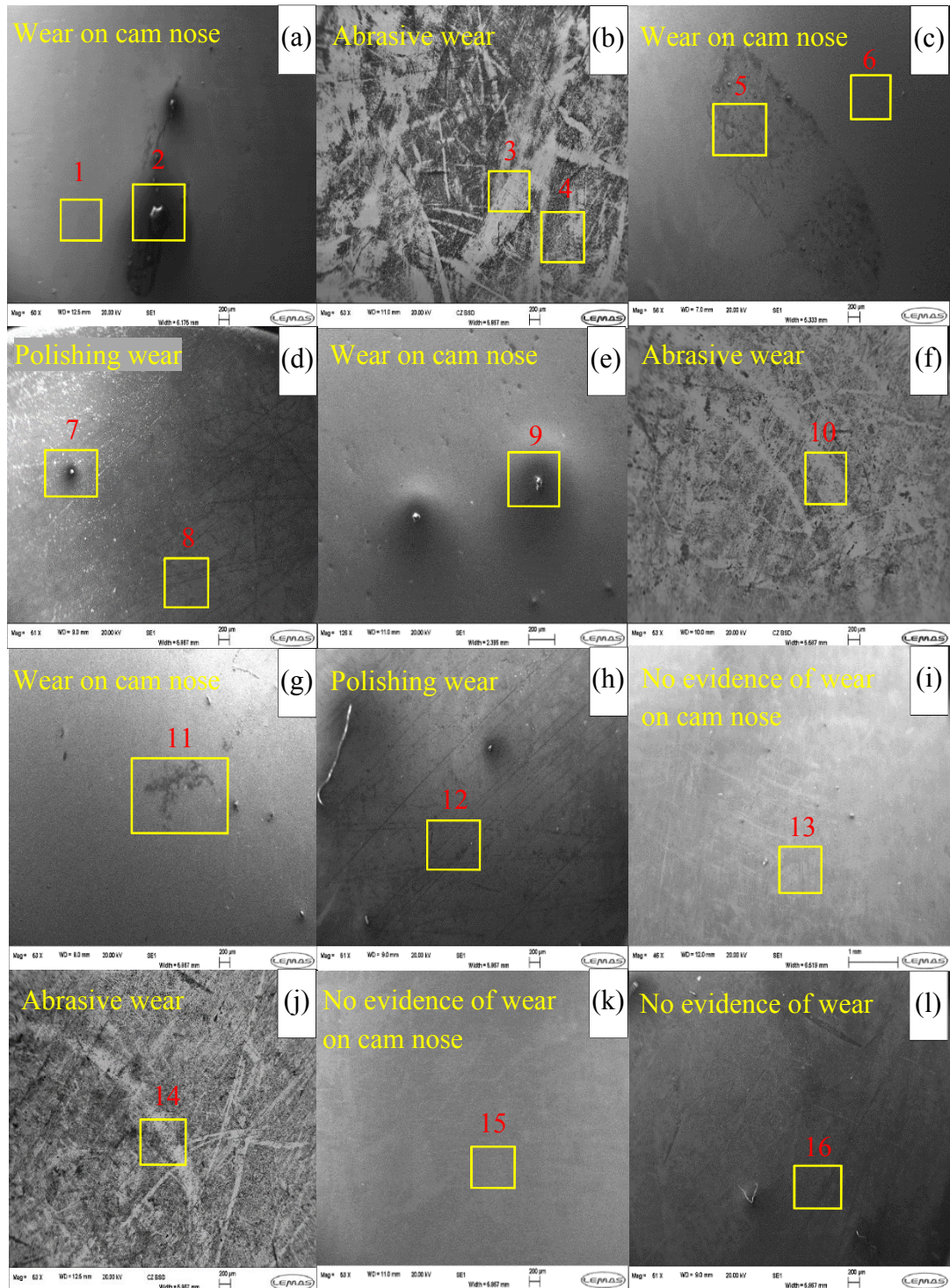


Figure 8-1 Scanning electron micrograph (SEM) at 100 °C: (a) CI camlobe rubbed against (2.75 mm) MnPO₄ shim, (b) MnPO₄ shim with thickness 2.75 mm, (c) CI camlobe rubbed against (2.75 mm) DLC shim, (d) DLC shim with thickness 2.75 mm, (e) CI camlobe rubbed against (2.575 mm) MnPO₄ shim, (f) MnPO₄ shim with thickness 2.575 mm (g) CI camlobe rubbed against (2.575 mm) DLC shim, (h) DLC shim with thickness 2.575 mm (i) CI camlobe rubbed against (2.275 mm) MnPO₄ shim, (j) MnPO₄ shim with thickness 2.275 mm, (k) CI camlobe rubbed against (2.275 mm) DLC shim, (l) DLC shim with thickness 2.275 mm

The CI camlobe in Fig. 8-1a, showed the presence of phosphorus on both regions (i.e. region 1 and 2) on the cam nose. This can be derived either from the elements of the lubricant or the coating of the insert (i.e. due to rubbing action from the camlobe to the MnPO_4 insert). At region 1, little or no changes were observed in carbon, oxygen and iron concentrations as compared to a pre-test CI camlobe suggesting minimal chemical reactions took place with the lubricant additives. Nevertheless, low levels of Mo, Zn and S were observed in both regions, implying a heterogeneous distribution of the lubricant derived films on the camlobe surface.

From Fig. 8-1b and Table 8-1, the iron concentration inside the wear track (i.e. region 3) was high and the MnPO_4 coating appeared to be stripped off from the surface thereby exposing the 16MnCr5 steel substrate. This may be due to load/pressure variations, flash temperatures and reactivity/or interaction with the MoDTC additive on the substrate [115]. At region 4, the MnPO_4 coating is partially removed, revealing that the coating was not fully affected by the chemical reactions (thermally activated) outside the wear track. However, lubricant additive-derived elements of Mo, Zn, S, P and Ca were observed inside and outside the wear track with different concentrations, implying a heterogeneous distribution of tribofilm on MnPO_4 insert after 80 hrs of testing. The CI camlobe in Fig. 8-1c, showed scoring marks with high levels of carbon in both region 5 and region 6 as compared to a pre-test CI camlobe. These marks were not only seen on the cam nose but also on the cam flank (both sides). It is also important to note that there was no detection of Zn in these regions. In addition, at region 6, sulfur and phosphorus were not observed on the surface. This supports the wear results where the absence of the lubricant antiwear properties on the CI camlobe surface led to an abrasive wear process. Furthermore, high level of Molybdenum was observed on the CI camlobe rubbed against DLC shim (at region 5 and 6) when compared to the CI camlobe rubbed against MnPO_4 shim (region 1 and 2). Consequently, the friction torque was less when the CI camlobe was interacting with the DLC insert.

The DLC insert in Fig. 8-1d, showed low levels of carbon with high levels of iron in both regions (region 7 and 8) as compared to a pre-test DLC shim. This

could be due to thinning of DLC coating resulting from wear. In addition, high level of Mo, S and Zn detected in the wear scar could be related to additive-derived elements leading to low friction and wear. This is also in line with the obtained friction and wear results.

Table 8-1 EDX semi-quantification of CI camlobes and coated inserts (2.75mm)

CI camlobe rubbed against MnPO ₄ insert	CI camlobe		Element (wt %)									
			Cr	C	P	S	Zn	Mn	Mo	Fe	O	Others
	Before Test		0.60	8.57	-	-	-	0.96	-	87.84	1.06	0.97
	After Test	Region 1	0.63	7.73	0.17	0.34	0.36	0.92	0.31	86.68	1.33	1.35
		Region 2	-	75.79	0.19	0.16	0.07	-	0.01	11.22	11.83	0.73
	MnPO ₄ insert		Element (wt %)									
			Cr	C	P	S	Zn	Mn	Mo	Fe	O	Others
	Before Test		0.68	6.36	15.46	-	-	14.24	-	21.96	39.61	1.69
	After Test	Region 3	1.49	5.31	0.59	0.03	0.37	0.56	0.44	87.81	2.98	0.42
		Region 4	1.67	6.50	8.12	0.09	0.39	6.16	0.22	54.21	22.09	0.55
CI camlobe rubbed against DLC insert	CI camlobe		Element (wt %)									
			Cr	C	P	S	Zn	Mn	Mo	Fe	O	Others
	Before Test		0.60	8.57	-	-	-	0.96	-	87.84	1.06	0.97
	After Test	Region 5	0.39	44.07	0.43	0.26	-	0.66	1.04	38.80	12.08	2.27
		Region 6	0.55	26.63	-	-	-	0.74	1.75	66.24	3.33	0.76
	DLC insert		Element (wt %)									
			Cr	C	P	S	Zn	Mn	Mo	Fe	O	Others
	Before Test		28.15	71.45	-	-	-	-	-	0.20	-	0.20
	After Test	Region 7	48.00	47.23	-	0.15	0.21	-	0.88	3.42	-	0.11
		Region 8	43.59	53.14	-	0.12	0.29	-	0.84	1.84	-	0.18

The DLC inserts were supporting a polishing wear process (i.e. the wear produced a smooth burnished appearance on the surface) [271]. The polishing wear process which is caused by mild abrasive wear was observed by the White Light Interferometer, as shown in Fig. 8-2a. It should be mentioned that this process was not observed on the DLC insert with thickness of 2.275 mm. For all MnPO₄ inserts, however, the surface appears fairly rough (R_a is about 0.47 μm for the thinnest tappet and 1.7 μm for the thickest tappet) compared to MnPO₄ insert before test (R_a 0.25 μm). The surface was consisting of ridges/grooves on the surface of the insert. This is equally supporting an abrasive wear process for MnPO₄ inserts (i.e. significant abrasive marks on MnPO₄ inserts were observed by the White Light Interferometer, as shown in Fig. 8-2b).

Table 8-2 EDX semi-quantification of CI camlobes and coated inserts (2.575mm and 2.275 mm)

	CI camlobe	Element (wt %)									
		Cr	C	P	S	Zn	Mn	Mo	Fe	O	Others
CI camlobe rubbed against MnPO ₄ insert	Region 9	0.46	32.21	0.27	0.57	0.37	0.80	1.17	58.61	3.97	1.57
	Region 13	0.41	10.54	0.39	0.61	0.77	0.53	1.02	81.08	3.61	1.04
	MnPO ₄ insert	Element (wt %)									
		Cr	C	P	S	Zn	Mn	Mo	Fe	O	Others
	Region 10	1.59	6.19	5.33	0.08	-	0.37	1.17	80.35	4.64	0.28
	Region 14	1.81	9.51	7.06	-	0.04	0.99	1.03	74.66	4.69	0.21
CI camlobe rubbed against DLC insert	DLC insert	Element (wt %)									
		Cr	C	P	S	Zn	Mn	Mo	Fe	O	Others
	Region 11	0.70	26.37	0.06	0.16	-	0.88	0.91	67.06	3.16	0.70
	Region 15	0.64	18.65	-	-	-	0.87	1.37	72.65	5.37	0.45
	Region 12	45.68	51.63	0.14	0.04	-	-	0.10	2.41	-	-
	Region 16	30.14	65.89	-	-	-	-	0.76	1.78	-	1.43

The tribofilm derived on tappet inserts was generally seen to be affected by changing the clearance of tappet. For example, from Fig. 8-1j, inside the wear track (see region 14), the MnPO_4 with thickness of 2.275 mm showed high levels of P, Zn and C and low levels of Fe as compared to the MnPO_4 tappets with thickness of 2.75 mm and 2.575 mm (i.e. region 3 and 10). That could explain the lowest wear obtained by the thinnest tappets of 2.275 mm. The results were also supported by Raman spectroscopy (presented in the next section), where MnPO_4 coating (with tappet thickness of 2.575 mm and 2.75 mm) was reported to be fully stripped off from the steel substrate.

On the other hand, from Fig. 8-1l (region 16), the DLC insert with thickness of 2.275 mm, showed the highest levels of carbon with the lowest levels of iron as compared to the DLC tappets with thickness of 2.75 mm and 2.575 mm (i.e. region 7, 8 and 12). This also supports the wear results (i.e. the wear rate clearly reduced on the DLC insert with thickness of 2.275 mm). It is important to note that detecting high levels of carbon with low levels of iron on the DLC insert indicates that the DLC coating still exists and is not stripped off from the steel substrate. This in return helps to reduce wear on the DLC surface.

The tribofilm derived on camlobes was also reported to be varied when the camlobes rubbed against different tappet clearances. For example, from Fig. 8-1e and 8-1i, the CI camlobe rubbing against MnPO_4 insert with thickness of 2.575 mm and 2.275mm, showed high levels of Mo, Zn, P and S in both regions (i.e. region 9 and 13) as compared to the CI camlobe rubbing against MnPO_4 insert with thickness of 2.75 mm (i.e. region 1 and 2). This reveals a heterogeneous distribution of the lubricant derived tribofilms on the camlobe surface when rubbing against thinnest tappets. It should be mentioned that there was no evidence of wear on the cam nose and cam flank when CI camlobe rubbed against MnPO_4 with thickness of 2.275 mm. From Fig. 8-1k, the CI camlobe rubbing against DLC insert with thickness of 2.275 mm, showed a smooth surface with low levels of carbon as compared to the CI camlobes rubbing against DLC inserts with thickness of 2.75 mm and 2.575 mm (i.e. region 5, 6 and 11). This smooth surface was observed on both regions (i.e. the cam nose and the cam flank), with no evidence of wear on all regions of the camlobe. This could validate the lower friction and wear values

obtained by CI camlobe rubbing against DLC insert with thickness of 2.275 mm.

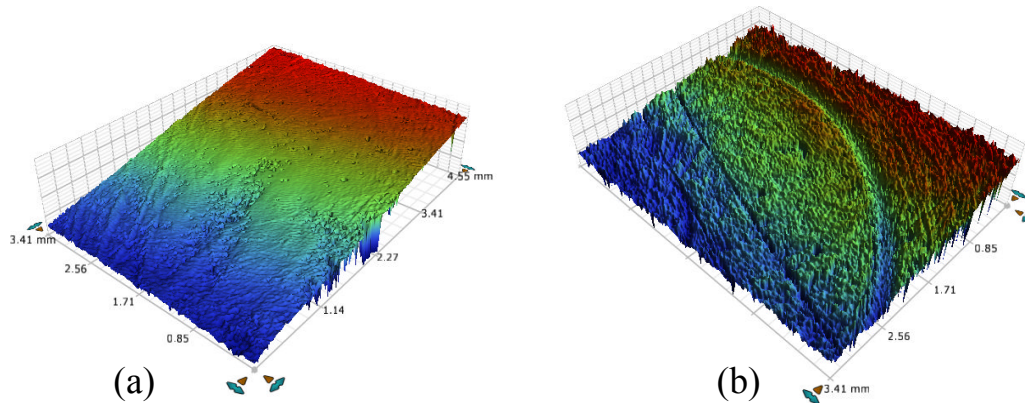


Figure 8-2 Typical wear process on tappet inserts (a) polishing process (b) abrasive process

8.2.2 Raman Spectroscopy Results

Essentially, Raman peaks for molybdenum disulfide (MoS_2) were reported at $383\text{--}410\text{ cm}^{-1}$, carbon (C) at $1366\text{--}1596\text{ cm}^{-1}$, phosphate (PO_4^{3-}) at $949\text{--}970\text{ cm}^{-1}$, haematite (Fe_2O_3) at $120\text{--}310\text{ cm}^{-1}$ and magnetite (Fe_3O_4) at $670\text{--}680\text{ cm}^{-1}$ [15, 76, 201, 262, 263]. For the first stage, the Raman spectra from CI camlobes (rubbed against MnPO_4 inserts with different thicknesses) are shown in Fig. 8-3. The spectra are plotted on the same scale and have been shifted vertically for clarification purposes.

In general, similar Raman peaks were observed for all tappet thicknesses. The results indicate the presence of MoS_2 ($385\text{--}410\text{ cm}^{-1}$) at all regions ($+14^\circ$, 0° cam nose, -14°). In addition, as graphite flakes are normally present in the microstructure of the cast iron, clear carbon peaks were detected on the camlobe before the test. The G and D peaks were around 1581 cm^{-1} and 1367 cm^{-1} respectively. The G peak represents the graphite and D peak represents the disorder in graphite [113].

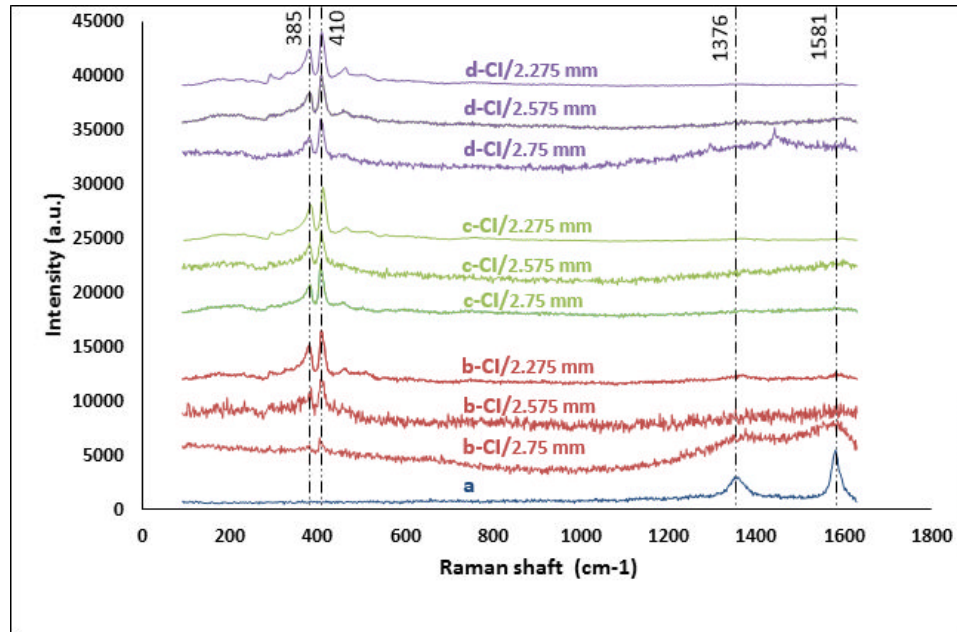


Figure 8-3 Raman spectroscopy for the CI camlobes (rubbed against MnPO₄ inserts) at 100 °C: (a) before test, (b) at cam nose, (c) +14° from cam nose, (d) -14° from cam nose

It was understood that the tribofilm derived across the camlobe (mainly at the seven specified locations) might vary due to the differences in contact pressure, load and lubricant entrainment velocity at the contact of the asperities. In particular, MoS₂ sheets were generally seen to be varied across the seven specified locations on the camlobe. From Fig. 8-3, MoS₂ peaks at the cam nose (for the CI camlobe rubbed against 2.75 mm MnPO₄) were not as pronounced as MoS₂ peaks detected on the cam flanks, suggesting that MoDTC-derived tribofilm was comparatively thin on the cam nose. That is why the cam nose was seen to have a significant wear. Also, from Fig. 8-3, it can be seen that carbon peaks were only observed at the cam nose (for the CI camlobe rubbed against 2.75 mm MnPO₄) and the D and G peaks were not found in the spectrum taken from +14° and -14° positions inside the wear scar of the camlobe suggesting that the graphite flakes, which are normally present in the microstructure of the cast iron, did not participate in the formation of the transfer layer on these particular positions or the transfer layer from the counterpart (i.e. MnPO₄ insert) developed a thick deposition film on the cam flank (both sides), which in return made the carbon/graphite flakes peaks from

the cam flank undetectable. Figure 8-4 shows the Raman spectra obtained from MnPO₄ inserts with different thicknesses.

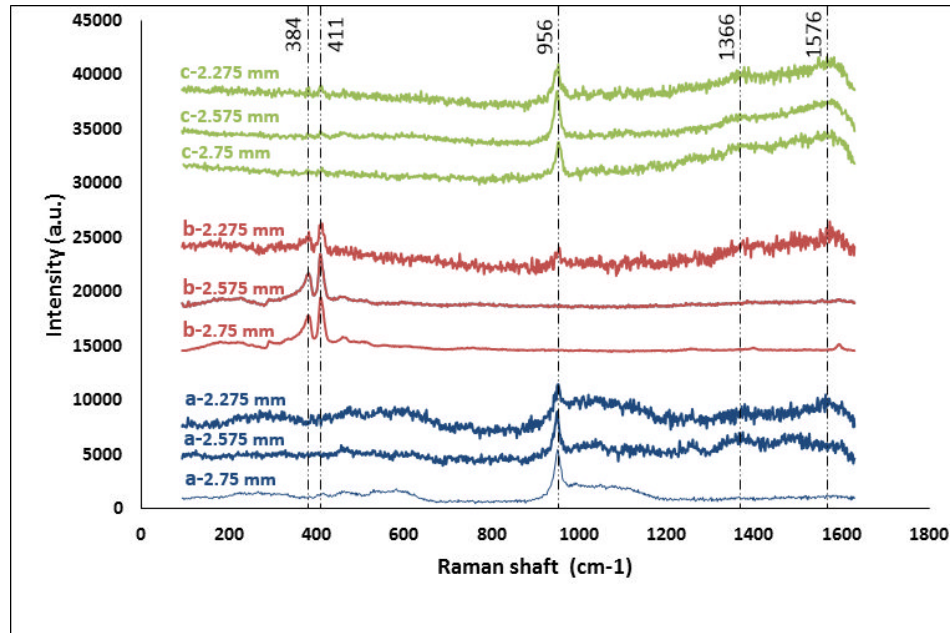


Figure 8-4 Raman spectroscopy for the MnPO₄ inserts at 100 °C: (a) before test, (b) inside wear track, (c) outside wear track

The Raman shift clearly indicated the presence of phosphate (956 cm⁻¹) outside the wear track for all thicknesses. However, for thickness of 2.75 mm and 2.575 mm, no phosphate was observed inside the wear track, suggesting that the MnPO₄ coating is either stripped off from the steel substrate or that the phosphate within the wear track is covered by deposited MoS₂ from the oil. Peaks attributed to the formation of graphitic carbon were mainly observed outside the wear track, which confirms that there is a transfer of material from the camlobe to the MnPO₄ insert. It is however possible that the detected carbon could be from trapped oil (i.e. MnPO₄ is a porous coating and oil could be trapped between MnPO₄ crystals). For thickness of 2.275 mm, carbon peaks were detected inside and outside the wear track. This could be related to the low wear rate seen on the thinnest tappet. Confirming EDX results, distinct MoS₂ peaks were observed for all thicknesses inside the wear track at 384 cm⁻¹ (E_{2g}¹ peak) and 411 cm⁻¹ (A_{1g} peak), whereas little or no MoS₂ peaks were observed outside the wear track, suggesting a higher amount of film

formed inside the wear track. In addition, higher MoS₂ peak intensity was observed inside the wear track as tappet thickness increases which could indicate more MoS₂ film formed inside the wear track. That could be related to higher pressure at the interface (for higher tappet thickness) resulting in an enhanced MoDTC decomposition.

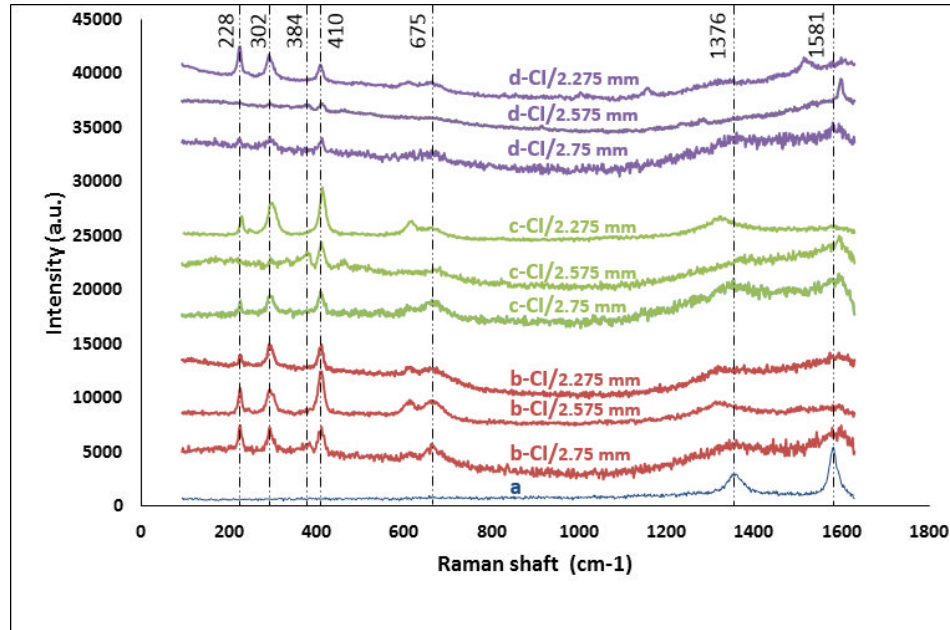


Figure 8-5 Raman spectroscopy for the CI camlobes (rubbed against DLC inserts) at 100 °C: (a) before test, (b) at cam nose, (c) +14° from cam nose, (d) -14° from cam nose

For the second stage, the results from Raman spectroscopy for the CI camlobes (rubbed against DLC inserts with different thicknesses) are shown in Fig. 8-5. In general, the spectra clearly indicate the presence of MoS₂ (386-413 cm⁻¹) and Fe₃O₄ (675 cm⁻¹) at all regions. Also, the additional peaks, 228 and 302 cm⁻¹ were believed to be attributed to the formation of iron oxide (Fe₂O₃) [198]. Furthermore, carbon peaks at 1376 and 1581 cm⁻¹ assigned to the formation of amorphous carbon were generally detected for all regions on the camlobe (i.e. cam nose and cam flank). Figure 8-6 shows the Raman spectra obtained from the DLC inserts with different thicknesses.

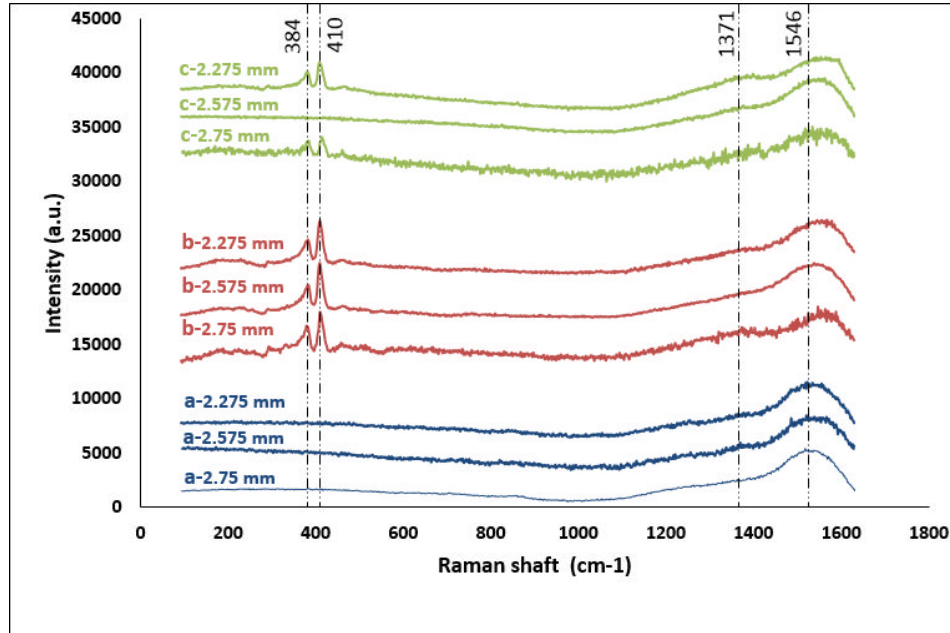


Figure 8-6 Raman spectroscopy for the DLC inserts at 100 °C: (a) before test, (b) inside wear track, (c) outside wear track

The presence of MoS₂ (384-413 cm⁻¹) is mostly evident inside and outside the wear track. As can be seen, sharper MoS₂ peaks were detected inside wear track as compared to outside wear track. This indicates that MoDTC-derived tribofilm was fairly thin outside wear track and that tribological contact promotes formation of MoS₂ on the wear scar. It is worth mentioning that the presence of MoS₂ outside wear track could be due to the thermal decomposition of MoDTC as opposed to tribochemical reactions. The broad peak in the range of 140-250 cm⁻¹ inside wear track was attributed to stress-induced disorder in MoS₂ crystal structure [201]. As expected, regardless of tappet thickness, Raman peaks related to the presence of carbon were clearly observed inside and outside the wear track of the DLC inserts. On the other hand, it is worth mentioning that neither MoO_x peaks nor iron (II) molybdate (FeMoO₄) peaks were observed on any surfaces of camlobes and followers.

8.2.3 X-ray Photoelectron Spectroscopy Results

XPS was used to scan different positions on each camlobe and tappet. This surface sensitive technique can examine the very top layer of the surface (5

nm depth). High-resolution scans for elements of interest (Mo, Zn, P, S and O) were obtained. Figure 8-7 presents the XPS spectra of the tribofilms formed on the CI camlobes (mainly on the cam nose) rubbed against tappets coated with MnPO_4 and DLC coatings. It can be seen that oil additives were decomposed and formed on the tribofilms formed on the CI camlobes. This in return helped to dominate the tribological behaviour of the cam/follower tribopair.

From Fig. 8-7, the corresponding XPS spectra of S 2p peaks were clearly detected on the camlobe that rubbed against Mn-phosphate insert while no such peaks were observed with the camlobe rubbed against DLC insert. In addition, the amount of Zn 2p detected on the tribofilm formed on the camlobe was higher when rubbed against Mn-phosphate insert compared to the camlobe rubbed against DLC insert.

As Zn 3s and P 2p binding energies own an exceptional advantage of not been altered by severe chemical shifts, the difference in binding energy between them was used as a complementary means for the determination of polyphosphate chain length in tribological systems [115, 273]. Long chain phosphate glasses was introduced by the larger binding energy differences between Zn 3s and P 2p (i.e. $\Delta \text{Zn 3s} - \text{P 2p}$). From Fig. 8-7, $\Delta \text{Zn 3s} - \text{P 2p}$ exposes that the tribofilms are composed of relatively long chain calcium phosphates at the camlobe rubbed against MnPO_4 insert as compared to the camlobe rubbed against DLC insert.

From Raman analysis, as mentioned earlier, MoO_x and iron (II) molybdate (FeMoO_4) peaks were not detected on the cam/follower tribopair. From XPS, however, it was believed that the Mo $3d_{5/2}$ peaks that detected on the surface were due to the presence of MoO_3 and not FeMoO_4 . Accordingly, MoS_2 and MoO_3 peaks were clearly seen on the tribofilms formed on camlobes. Based on the literature [90, 96, 112], the increasing of $\text{MoS}_2/\text{MoO}_3$ ratio reduces the coefficient of friction. From Fig. 8-7, it was reported that the $\text{MoS}_2/\text{MoO}_3$ ratio for the camlobe rubbed against DLC insert is higher than the $\text{MoS}_2/\text{MoO}_3$ ratio for the camlobe rubbed against MnPO_4 insert. That could validate the friction results obtained by the camlobe rubbed against DLC insert.

The O1s peaks consisted of the bridging oxygen (BO), non-bridging oxygen (NBO) and metallic oxides (MO). The corresponding binding energies of the bridging oxygen (BO), non-bridging oxygen (NBO) and metallic oxides (MO) are $533.04 \pm 0.25 \text{ eV}$, $532.25 \pm 0.5 \text{ eV}$ and $530.80 \pm 0.3 \text{ eV}$ respectively. BO is an oxygen atom that forms covalent bonds between two phosphate groups (i.e. P–O–P bond). NBO is an oxygen atom that is within a terminating phosphate ($-\text{PO}_x$). The area ratio of the BO/NBO is also used for the determination of phosphate chain length even though the difference between the linewidth of the peaks and the chemical shift may not be entirely distinguishable [115, 134, 273]. A greater BO/NBO is also supporting a long chain polyphosphate which can be used to determine the polymeric number (n) by the following Equation.

$$\frac{BO}{NBO} = \frac{(n-1)}{2(n+1)} \quad \text{Equation 8-1}$$

Both parameters (BO/NBO and $\Delta \text{ Zn } 3s\text{-P } 2p$) were used to observe the phosphate films formed on camlobes and tappets. Table 8-3 shows the link among the wear performance, BO/NBO, $\Delta \text{ Zn } 3s\text{-P } 2p$ and $\text{P } 2p/\text{Zn } 3s$ across the seven specified locations on the camlobe rubbed against MnPO_4 insert with thickness of 2.75 mm. It can be seen that both parameters (BO/NBO and $\Delta \text{ Zn } 3s\text{-P } 2p$) were reported to be higher at the cam nose compared to the cam flank (both sides). This suggests that the tribofilm formed on the cam nose was composed of long chain calcium phosphates as compared to the tribofilm formed on cam flank in both sides.

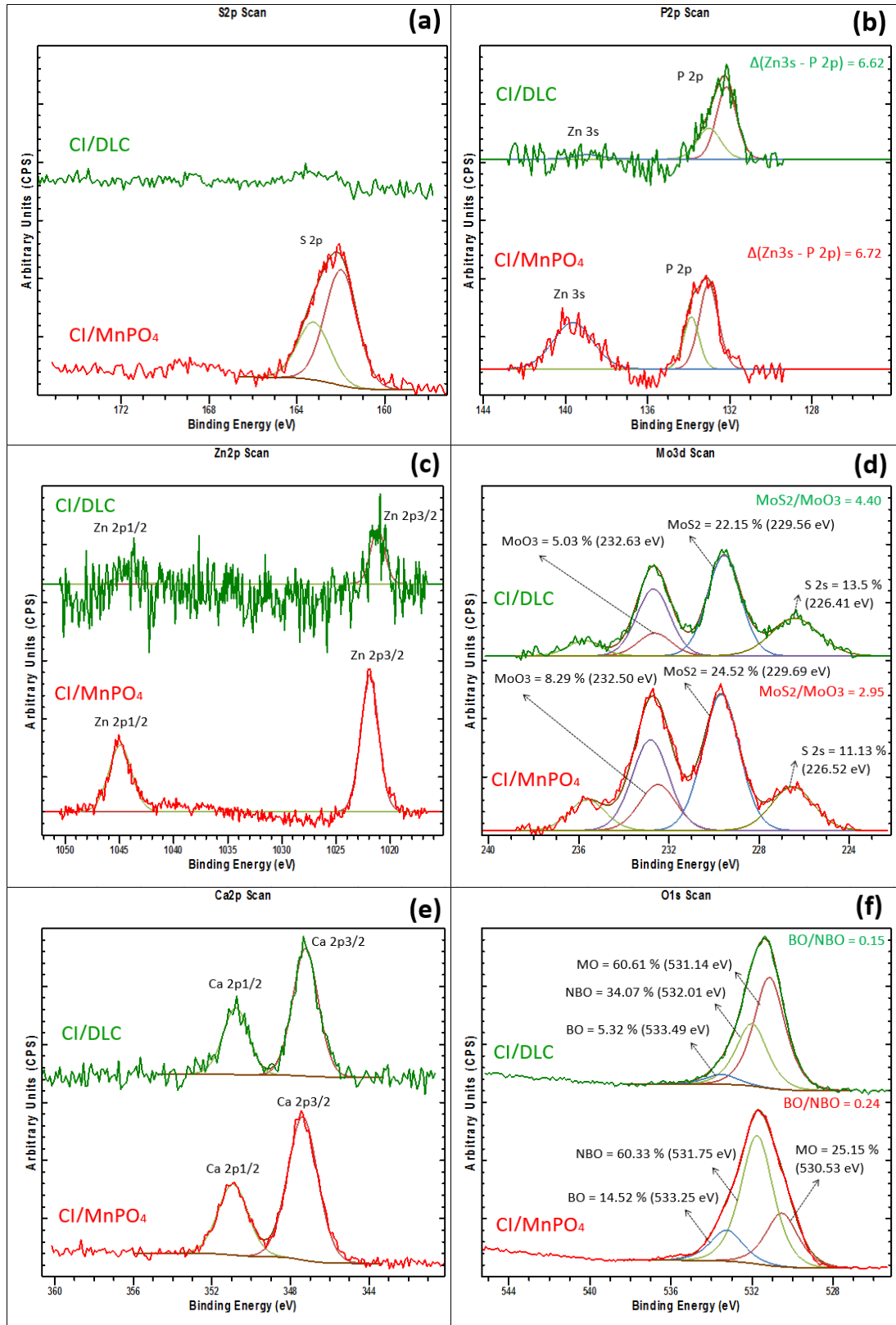


Figure 8-7 XPS analysis of cast iron camlobes rubbed against tappets coated with MnPO₄ and DLC coatings at 100 °C: (a) S 2p peaks, (b) P 2p peaks, (c) Zn 2p peaks, (d) Mo 3d peaks, (e) Ca 2p peaks and (f) O 1s peaks

Table 8-3 Wear depth, BO/NBO area ratio, $\Delta(\text{Zn } 3s - \text{P } 2p)$ (eV), and P 2p/Zn 3s area ratio for the seven specified positions on CI camlobe rubbing against MnPO_4 insert with thickness of 2.75 mm at 100 °C

Angular Position (°)	Wear Depth (um)	BO/NBO	$\Delta(\text{Zn } 3s - \text{P } 2p)(\text{eV})$	P 2p/Zn 3s
- 14	0.04	0.15	6.49	4.75
- 10	0.3	0.20	6.60	3.17
- 4	0.5	0.20	6.58	2.58
0	0.7	0.24	6.72	2.31
+ 4	0.6	0.11	6.70	5.02
+ 10	0.5	0.21	6.54	2.72
+ 14	0.16	0.12	6.50	2.30

Table 8-4 Binding energies of XPS spectra of Zn 3s, P 2p, S 2p, MoS_2 and MoO_3 , and spectra at two temperatures (100 °C and 130 °C) and the corresponding species formed on top surface of camlobes rubbed against tappets with different thicknesses

T (°C)	Camlobe rubbed against tappets with different thickness	Binding Energies (eV)				
		Zn 3s	P 2p	S 2p	MoS_2	MoO_3
100	2.75 mm	139.65	133.03	161.98	229.69	232.50
	2.575 mm	137.46	132.87	-	-	-
	2.275 mm	139.86	133.14	162.38	230.00	232.48
130	2.75 mm	139.92	133.27	162.13	229.57	232.60
	2.575 mm	140.00	132.87	162.04	229.44	232.46
	2.275 mm	139.79	132.98	162.18	229.69	232.50

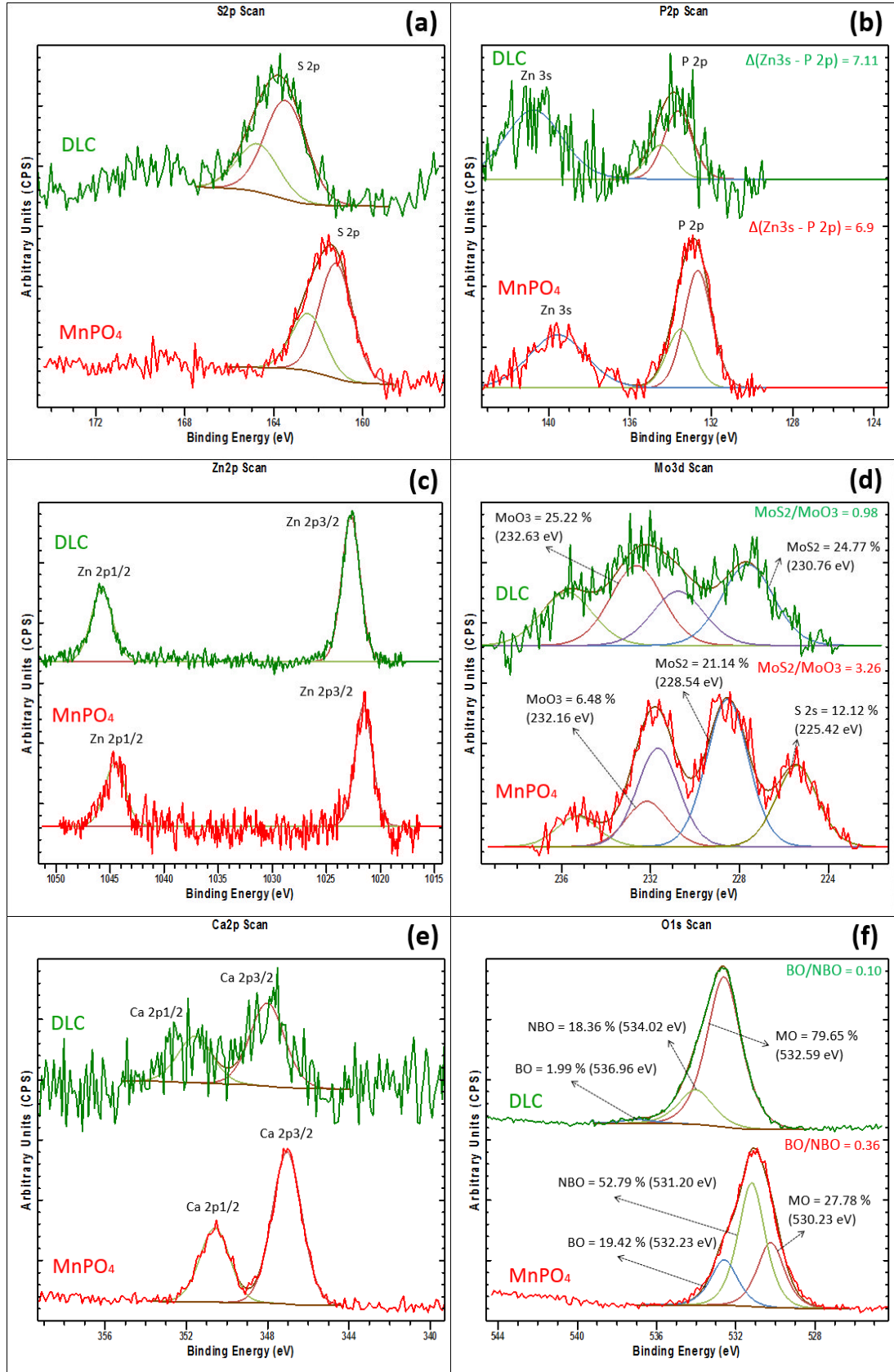


Figure 8-8 XPS analysis of steel tappets coated with MnPO₄ and DLC coatings at 100 °C: (a) S 2p peaks, (b) P 2p peaks, (c) Zn 2p peaks, (d) Mo 3d peaks, (e) Ca 2p peaks and (f) O 1s peaks

In addition to that, Table 8-4 shows the binding energies of XPS spectra for the camlobes under the effect of tappet thickness and temperature. It can be seen that regardless of tappet thickness and lubricant temperature, oil additives were all observed on the tribofilms formed on the camlobes. However, it was evident that the S 2p, MoS₂ and MoO₃ peaks were not detected on the camlobe when rubbed against MnPO₄ insert with thickness of 2.575 mm at 100 °C. Figure 8-8 shows the XPS spectra of the tribofilms formed on the tappets coated with MnPO₄ and DLC coatings. Evaluations of Δ Zn 3s - P 2p showed that the tribofilms are composed of relatively long chain calcium phosphates at the DLC insert as compared to the MnPO₄ insert. Unlike Raman results, regardless of tappet coating, MoO₃ peaks were also observed on the tribofilms formed on the surface.

Furthermore, it was found that the MoS₂/MoO₃ ratio for the DLC insert is lower than the MoS₂/MoO₃ ratio for the MnPO₄ insert. Nevertheless, lower friction was observed on DLC surfaces. This was attributed to the effect of surface roughness and tappet rotation on friction performance (i.e. DLC inserts have lower roughness and higher rotation as compared to MnPO₄ inserts). The O1s peaks were also consisted of the bridging oxygen (BO), non-bridging oxygen (NBO) and metallic oxides (MO). The ratio of bridging oxygen to non-bridging oxygen in the polyphosphate glass was calculated by dividing the intensity of BO and NBO peaks obtained from XPS analysis. Results for BO/NBO area ratio, Δ Zn 3s-P 2p and P 2p/Zn 3S inside and outside the wear track (for the tappets coated with MnPO₄ and DLC coatings) were presented in Table 8-5.

For MnPO₄ insert, no Zn 3s and P 2p were detected outside wear track. For DLC insert, however, both peaks (i.e. Zn 3s and P 2p) were detected inside and outside the wear track with relatively slight difference in BO/NBO and Δ Zn 3s-P 2p. Inside wear track, Δ Zn 3s-P 2p was reported to be lower as compared to the outside wear track, revealing that the tribofilm formed inside wear track composed of short chain calcium phosphates as compared to the tribofilm formed outside wear track. In addition to that, Table 8-6 presents the binding energies of XPS spectra for the steel tappets under the effect of tappet thickness and temperature. It was evident that regardless of tappet thickness and type of coating, oil additives were all observed on the tribofilms formed on

the tappets. A representative survey scan on the tribofilms formed on the cam/follower tribopair is presented in Fig. 8-9. In general, the tribofilm is mainly rich in oxygen. Also, it can be noticed that both ZDDP and MoDTC were clearly observed on both tribopairs (i.e. Cl camlobe/MnPO₄ insert system).

Table 8-5 BO/NBO area ratio, Δ (Zn 3s- P 2p) (eV), and P 2p/Zn 3s area ratio for MnPO₄ and DLC inserts inside and outside the wear track at 100 °C

Insert coating	Position on insert	BO/NBO	Δ (Zn 3s – P 2p)(eV)	P 2p/Zn 3s
MnPO₄	Inside wear track	0.36	7.11	2.78
	Outside wear track	0.26	-	-
DLC	Inside wear track	0.10	6.90	1.26
	Outside wear track	0.08	7.09	3.12

Table 8-6 Binding energies of XPS spectra of Zn 3s, P 2p, S 2p, MoS₂ and MoO₃, and the corresponding species formed on top surface of MnPO₄ and DLC inserts inside the wear track at 100 °C

Insert coating	Insert thickness	Binding Energies (eV)				
		Zn 3s	P 2p	S 2p	MoS ₂	MoO ₃
MnPO₄	2.75 mm	139.57	132.67	161.23	228.54	232.16
	2.575 mm	139.31	132.35	160.89	228.23	231.87
	2.275 mm	139.32	132.39	160.89	228.39	231.77
DLC	2.75 mm	140.86	133.76	163.47	230.76	232.63
	2.575 mm	141.82	134.73	164.63	229.21	232.34
	2.275 mm	141.23	133.99	163.03	230.02	233.15

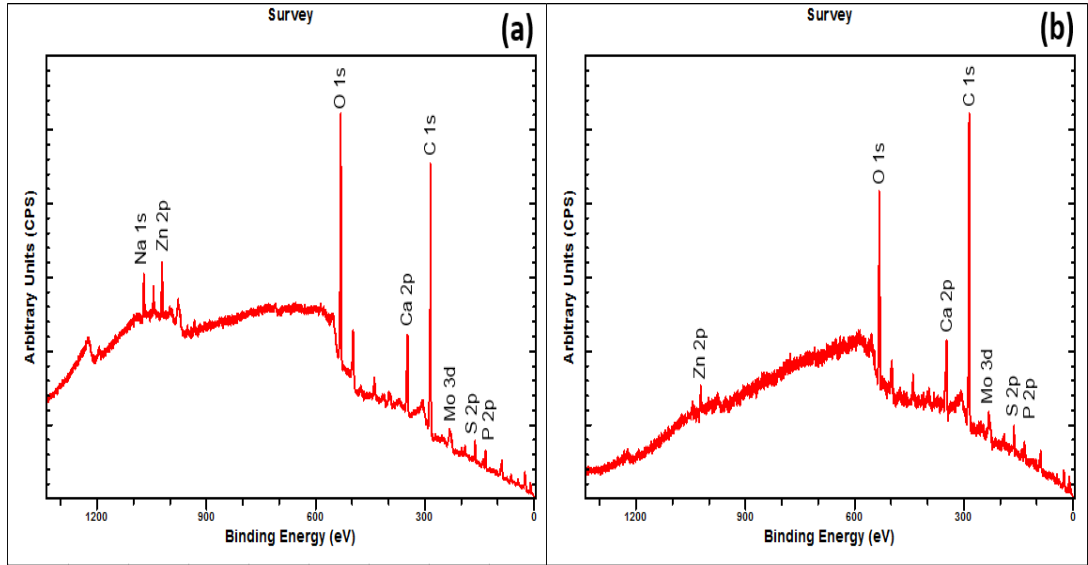


Figure 8-9 XPS survey scan for the tribofilms formed on the: (a) CI camlobe rubbed against (b) MnPO₄ insert with thickness of 2.75 mm

8.2.4 FIB-SEM Results

Figure 8-10 shows the thicknesses of tribofilms formed on cam/follower tribopair. It can be seen that the thickness of the tribofilm formed on the camlobe rubbed against MnPO₄ (32-43 nm) insert and the MnPO₄ insert (48-49 nm) is considerably lower than those observed on the camlobe rubbed against DLC insert (38-58 nm) and the DLC insert (51-67 nm). In addition, regardless of type of coating, it was reported that the thickness of the tribofilm formed on the tappets was higher than those observed on the camlobes.

The lubricant used in the first stage and second stage (i.e. O5) produced a very thin film at the cam nose while thick tribofilm was formed at the cam flank (both sides). Similar trend was generally observed for all tappets (i.e. thinner film was detected at the centre of the inserts compared to several spots near the edge of the insert). This could be correlated to the removal action due to high pressure rubbing action (from the ramp, flank, shoulder and nose) of the camlobe at the centre of the insert. Likewise, the observed difference in thickness between both tribopairs could support a removal and formation process, which is probably because of load/pressure variations, flash temperatures and interaction with the lubricant. It is worth mentioning that good dispersed tribofilms reduce the wear rates. Zhang *et al.* [274] reported

that the film thickness appears to be one of the causes of the differences in wear.

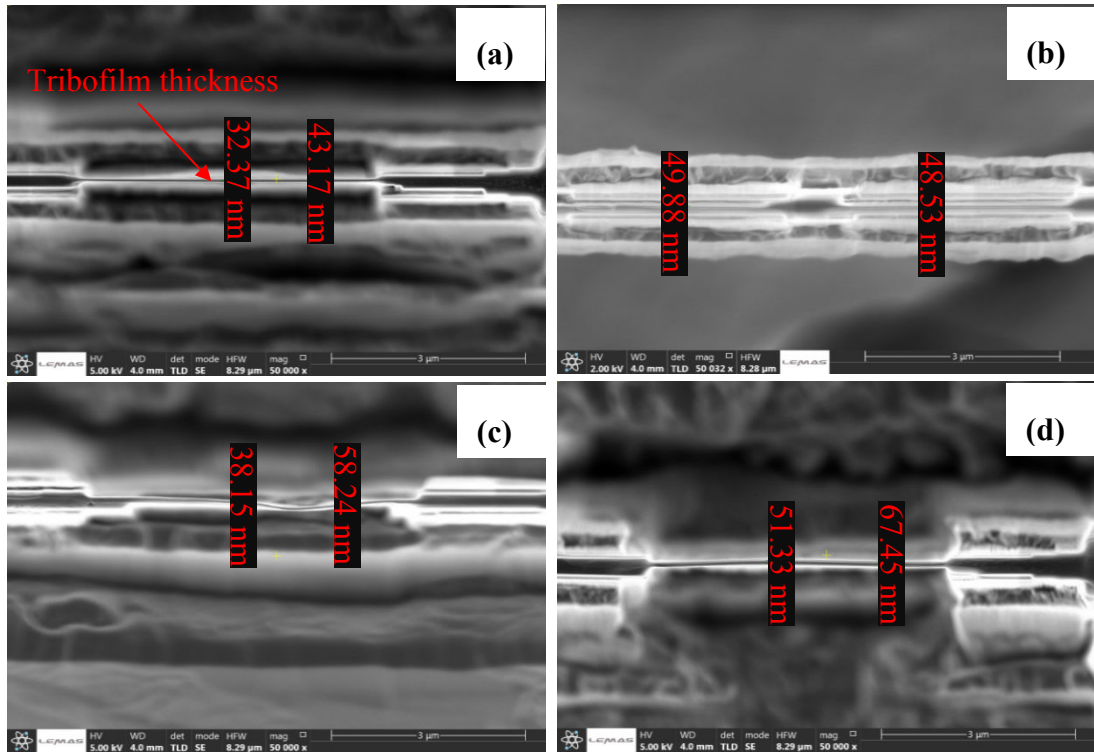


Figure 8-10 FIB-SEM showing tribofilm thickness for: (a) camlobe rubbed against MnPO₄ insert, (b) MnPO₄ insert, (c) camlobe rubbed against DLC insert and (d) DLC insert

8.2.5 TEM Results

For both stages, Fig. 8-11 shows the characterisation on the surfaces of the camlobes rubbed against inserts coated with MnPO₄ and DLC coatings. As earlier supported by FIB-SEM, the thickness of the tribofilm formed on the camlobe rubbed against MnPO₄ insert is noticeably lower than those observed on the camlobe rubbed against DLC insert.

For the camlobe rubbed against MnPO₄ insert, the tribofilm was mainly made of Fe, Zn, Mo, P and S. However, confirming XPS results, sulfur (S) was not detected on the camlobe that rubbed against DLC insert. The tribofilm was mainly consisted of Zn, Mo, P and C. The platinum layer is coming from the deposition prior to cutting in the FIB-SEM.

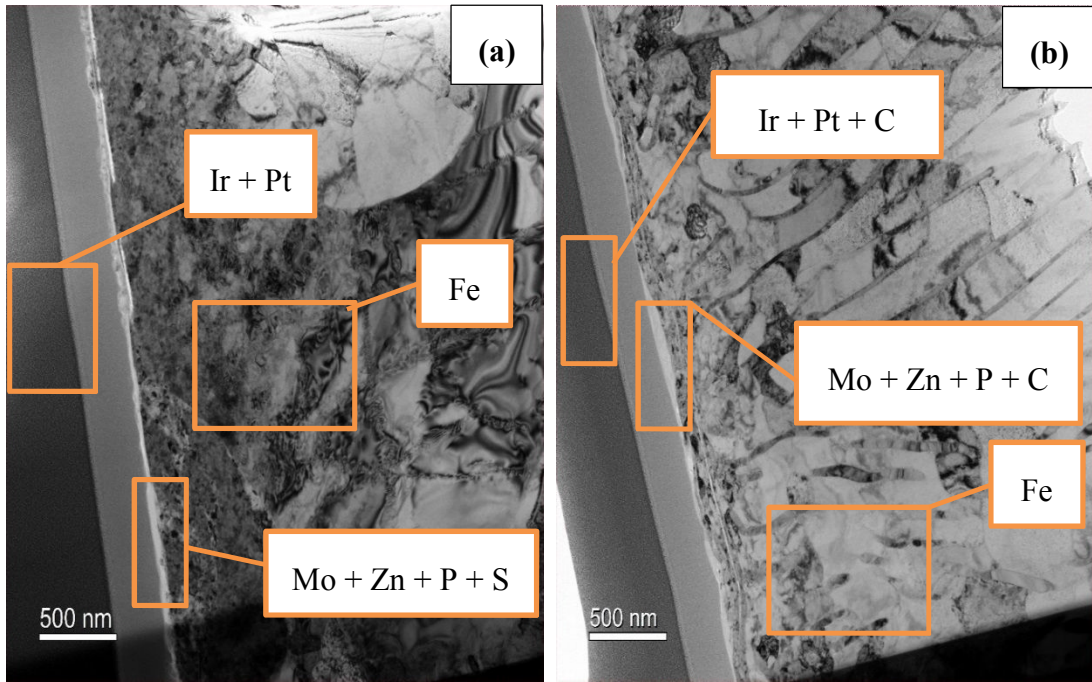


Figure 8-11 TEM images showing tribofilm at cam nose rubbed at: (a) MnPO_4 insert and (b) DLC insert

Figure 8-12 presents the characterisation on the surfaces of the MnPO_4 inserts and DLC inserts. Different tribofilms were observed on both inserts. This change in the structure of the tribofilm on the surface definitely has a significant effect on the wear.

For MnPO_4 insert (i.e. stage 1), the tribofilm was mainly made of Zn, Mo, S, Al and Fe. The Al originates from the modified cylinder head and the Fe are from the wear of the insert surface. However, unlike XPS results, P was not detected on the surface of MnPO_4 insert. Gallium is the source of the device while copper is the grid which enable the samples to be held in place. Platinum was also detected on top of the layers as a protective platinum layer that deposited on the inserts by FIB.

For DLC insert (i.e. stage 2), the tribofilm was mainly consisted of Mo, Zn, S, P and C. The coating layers from top to bottom were detected to be C, Cr and Fe (substrate), respectively. The white region is mainly of carbon (i.e. carbon layer) while the interlayer was made of CrC.

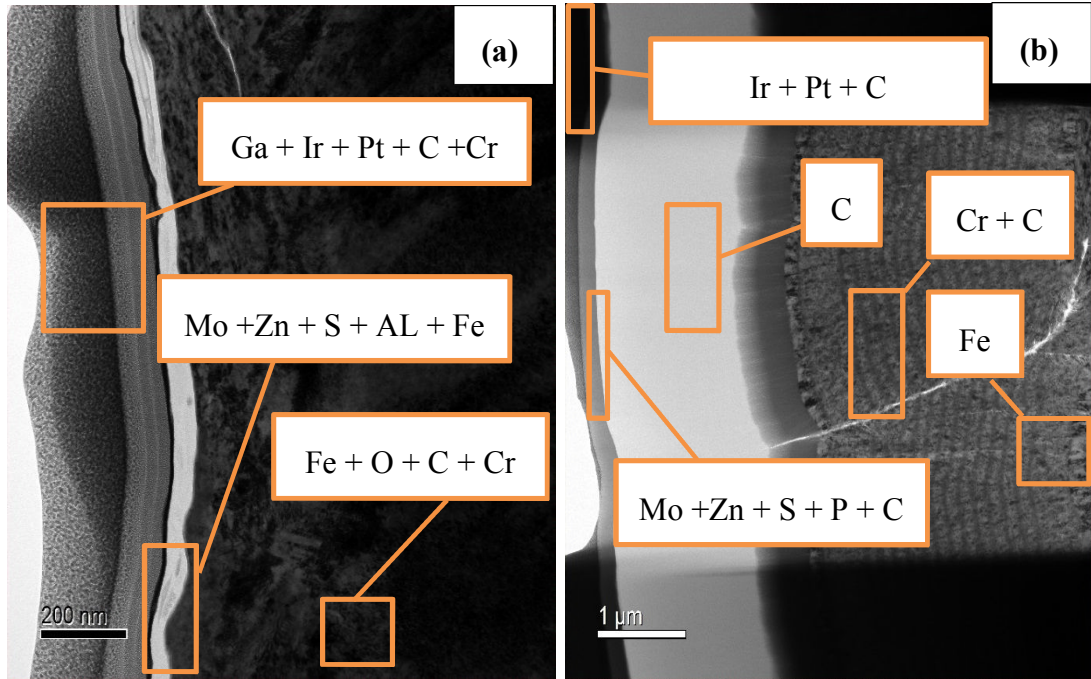


Figure 8-12 TEM images showing tribofilm at: (a) MnPO₄ insert and (b) DLC insert

8.3. Third Stage and Fourth Stage

8.3.1 SEM-EDX Results

Figure 8-13 shows SEM micrographs for the CI camlobes, MnPO₄ inserts and DLC inserts under the absence of MoDTC additive. Similar to the first stage and second stage, the wear scar on the camlobes was not detected by SEM while the wear scar on the inserts for both coatings (i.e. MnPO₄ and DLC) was clearly identified by SEM. Regardless of type of coating, it is worth mentioning that the thickest tappet does not necessarily shows high interactions with the camlobe surface and the oil additive. Thus, in some cases, wear rate was found to be low for the thickest tappet. This confirms the friction and wear results obtained from the third stage and the fourth stage. EDX semi-quantification of CI camlobes and coated steel inserts (2.75 mm) is presented in Table 8-7. Furthermore, in order to evaluate the effect of tappet thickness on tribofilm formation, the elemental composition of the CI camlobes and the coated steel inserts (2.575 mm and 2.275 mm) is presented in Table 8-8.

From Fig. 8-13a, the CI camlobe revealed the presence of P, S and Zn on both regions (i.e. region 1 and 2) on the cam nose as they were derived from

the elements of the lubricant, confirming a heterogeneous distribution of the lubricant derived films on the camlobe surface. Similar composition was seen on the cam flank (both sides). Comparing to a pre-test CI camlobe, relatively high changes in carbon, oxygen and iron concentrations were observed at region 1. This confirms that chemical reactions were taking place with the lubricant additives (mainly ZDDP). From Fig. 8-13b and Table 8-7, inside the wear track (i.e. region 3), Fe was considerably high at region 3 compared to region 4 (i.e. outside wear track) and a pre-test MnPO₄ insert. Nevertheless, the coating was not stripped off from the surface. Outside the wear track, at region 4, the MnPO₄ coating was not affected by the chemical reactions that occurred between the lubricant, the CI camlobe and the MnPO₄ insert. Nevertheless, Zn, S, and P were all seen outside the wear track with different concentrations. From Fig. 8-13c, the CI camlobe in both region 5 and region 6 showed similar distribution of the lubricant derived films on the cam nose surface and even on cam flank surface (both sides). However, P was not detected at region 6 as well as this region was reported with high levels of Zn and S as compared to those elements at region 5.

For the fourth stage, the DLC insert in Fig. 8-13d, inside the wear track (i.e. region 7), showed no S and Zn in the wear scar as compared to the region outside the wear track (i.e. region 8). This is in line with the obtained friction and wear results.

Similar to the first stage and second stage, changing the clearance of tappet affected the tribofilm formed on the cam/follower tribopair. From Fig. 8-13j, at region 14, the MnPO₄ with thickness of 2.275 mm low levels of P and high levels of Fe as compared to the MnPO₄ tappets with thickness of 2.75 mm and 2.575 mm (i.e. region 3 and 10). That correlates the high wear that obtained by the tappets with the thinnest thickness. In contrast, from Fig. 8-13l (region 16), the DLC insert with thickness of 2.275 mm, showed the highest levels of carbon with the lowest levels of iron as compared to the DLC tappets with thickness of 2.75 mm and 2.575 mm (i.e. region 7, 8 and 12). The obtained findings clearly reduces the wear rate on the DLC insert with thickness of 2.275 mm.

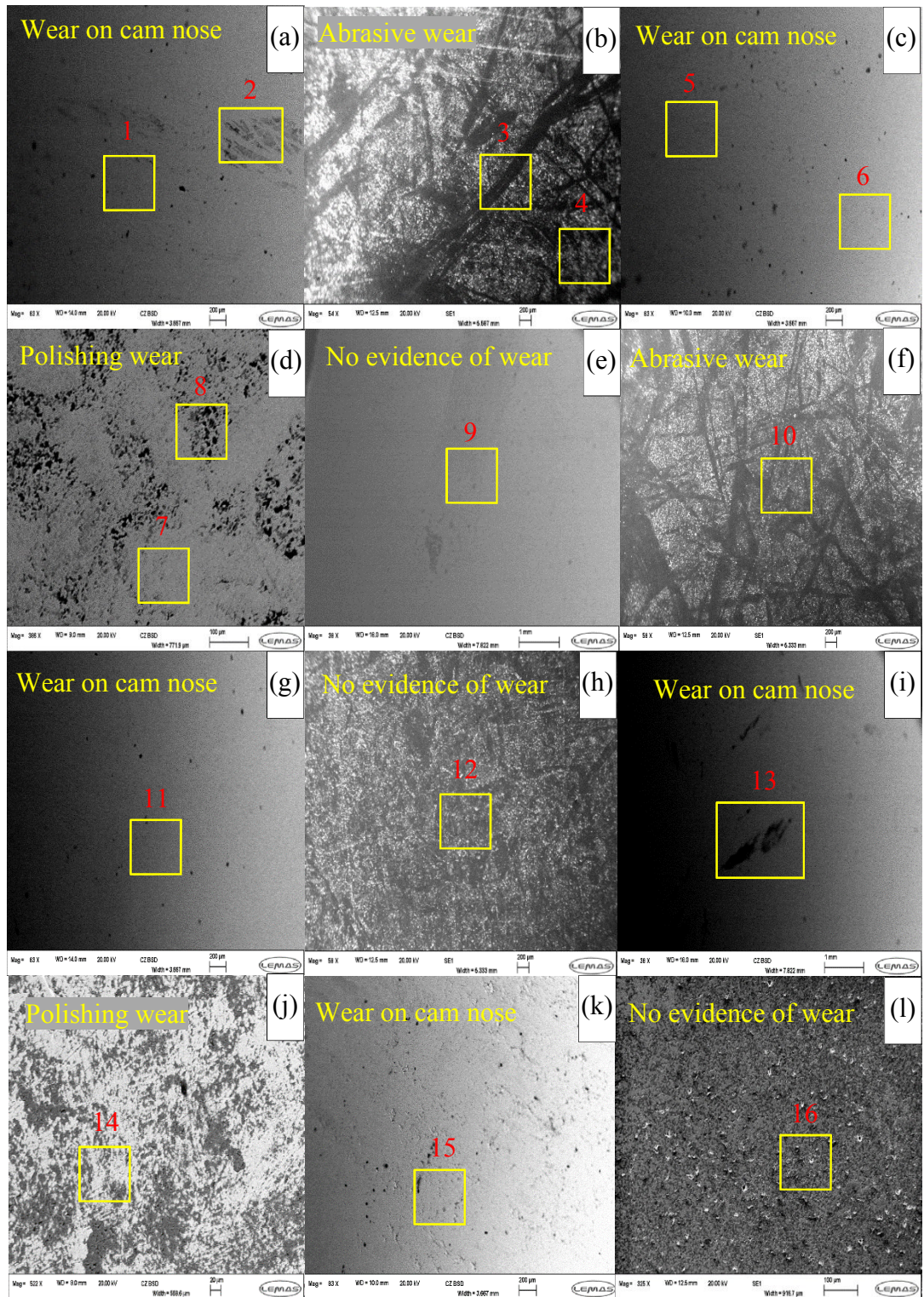


Figure 8-13 Scanning Electron micrograph (SEM) at 100 °C: (a) CI camlobe rubbed against (2.75 mm) MnPO₄ shim, (b) MnPO₄ shim with thickness 2.75 mm, (c) CI camlobe rubbed against (2.75 mm) DLC shim, (d) DLC shim with thickness 2.75 mm, (e) CI camlobe rubbed against (2.575 mm) MnPO₄ shim, (f) MnPO₄ shim with thickness 2.575 mm (g) CI camlobe rubbed against (2.575 mm) DLC shim, (h) DLC shim with thickness 2.575 mm (i) CI camlobe rubbed against (2.275 mm) MnPO₄ shim, (j) MnPO₄ shim with thickness 2.275 mm, (k) CI camlobe rubbed against (2.275 mm) DLC shim, (l) DLC shim with thickness 2.275 mm

For the camlobes, the tribofilm derived was seen to be relatively similar when the camlobes rubbed against different tappet thicknesses. In general, the DLC inserts, with thickness of 2.575 mm and 2.275 mm, showed no evidence of wear. However, it should be mentioned that a polishing process was only observed on the DLC insert with thickness of 2.75 mm. For all MnPO₄ inserts, an abrasive wear process was seen on all MnPO₄ inserts.

Table 8-7 EDX semi-quantification of CI camlobes and coated inserts (2.75mm)

CI camlobe rubbed against MnPO ₄ insert		Element (wt %)									
		Cr	C	P	S	Zn	Mn	Mo	Fe	O	Others
Before Test		0.60	8.57	-	-	-	0.96	-	87.84	1.06	0.97
After Test	Region 1	0.6	23.4	0.2	0.2	0.5	0.8	-	71.8	-	2.4
	Region 2	0.5	24.4	0.5	0.5	1.5	0.9	-	65.6	4.2	1.9
MnPO ₄ insert		Element (wt %)									
		Cr	C	P	S	Zn	Mn	Mo	Fe	O	Others
Before Test		0.68	6.36	15.46	-	-	14.24	-	21.96	39.61	1.69
After Test	Region 3	1.8	5.4	7.0	0.2	0.4	5.1	-	59.7	19.4	1.1
	Region 4	2.0	5.7	7.4	0.2	0.7	5.6	-	56.9	20.1	1.3
CI camlobe rubbed against DLC insert		Element (wt %)									
		Cr	C	P	S	Zn	Mn	Mo	Fe	O	Others
Before Test		0.60	8.57	-	-	-	0.96	-	87.84	1.06	0.97
After Test	Region 5	0.5	26.2	0.5	0.9	0.9	0.6	-	49.3	17.2	3.5
	Region 6	0.3	29.7	-	1.6	0.7	0.6	-	38.2	23.7	4.3
DLC insert		Element (wt %)									
		Cr	C	P	S	Zn	Mn	Mo	Fe	O	Others
Before Test		28.15	71.45	-	-	-	-	-	0.20	-	0.20
After Test	Region 7	25.1	74.4	-	0.1	-	-	-	-	-	0.3
	Region 8	24.7	75.0	0.1	0.1	0.1	-	-	-	-	-

Under the absence of MoDTC, the tribofilm formed on the cam/follower tribopair was also found to be affected by changing the thickness of tappet affected. From Fig. 8-13j, the MnPO₄ with thickness of 2.275 mm low levels of P and high levels of Fe at region 14 as compared to the MnPO₄ tappets with

thickness of 2.75 mm and 2.575 mm at region 3 and 10. That correlates the high wear that obtained by the tappets with the thinnest thickness. However, from Fig. 8-13I, the DLC insert with thickness of 2.275 mm at region 16 presented the highest levels of carbon with the lowest levels of iron as compared to the DLC tappets with thickness of 2.75 mm and 2.575 mm at region 7, 8 and 12. The obtained results evidently reduces the wear rate on the DLC insert with thickness of 2.275 mm.

Table 8-8 EDX semi-quantification of CI camlobes and coated inserts (2.575mm and 2.275 mm) at 100 °C

	CI camlobe	Element (wt %)									
		Cr	C	P	S	Zn	Mn	Mo	Fe	O	Others
CI camlobe rubbed against MnPO ₄	Region 9	0.6	17.8	0.5	0.2	1.1	1.0	-	72.4	4.0	2.3
	Region 13	0.3	23.7	0.3	-	0.7	0.4	-	66.7	5.5	2.1
	MnPO ₄ insert	Element (wt %)									
		Cr	C	P	S	Zn	Mn	Mo	Fe	O	Others
	Region 10	1.8	8.0	7.6	-	-	8.2	-	52.8	20.8	1.0
	Region 14	1.4	17.2	0.9	0.3	0.8	0.8	-	71.8	6.6	0.5
CI camlobe rubbed against DLC	CI camlobe	Element (wt %)									
		Cr	C	P	S	Zn	Mn	Mo	Fe	O	Others
	Region 11	0.2	64.1	0.2	0.2	0.4	0.2	-	19.5	14.1	0.9
	Region 15	0.6	25.9	0.6	0.4	1.0	0.7	-	58.5	10.8	1.7
	DLC insert	Element (wt %)									
		Cr	C	P	S	Zn	Mn	Mo	Fe	O	Others
Region 12	21.4	78.2	-	-	-	-	-	0.2	-	0.3	
Region 16	27.5	72.0	0.1	-	-	-	-	0.3	-	0.2	

8.3.2 Raman Spectroscopy Results

For O3 (i.e. under the absence of MoDTC), the Raman spectra from CI camlobes (rubbed against MnPO₄ inserts with different thicknesses) are shown in Fig. 8-14. The spectra are also plotted on the same scale and have been shifted vertically for clarification purposes. It can be seen that for all tappet thicknesses, similar Raman peaks were observed. As mentioned

earlier, the carbon peaks were detected on the camlobe before the test. The G and D peaks were around 1581 cm^{-1} and 1376 cm^{-1} respectively. After the test, however, the D and G peaks were not clearly seen on the thinnest tappets suggesting that the graphite flakes, which are normally present in the microstructure of the cast iron, did not participate in the formation of the transfer layer on these particular positions. In addition, from Fig. 8-14, the peaks at 677 cm^{-1} were attributed to the formation of iron oxide (Fe_3O_4).

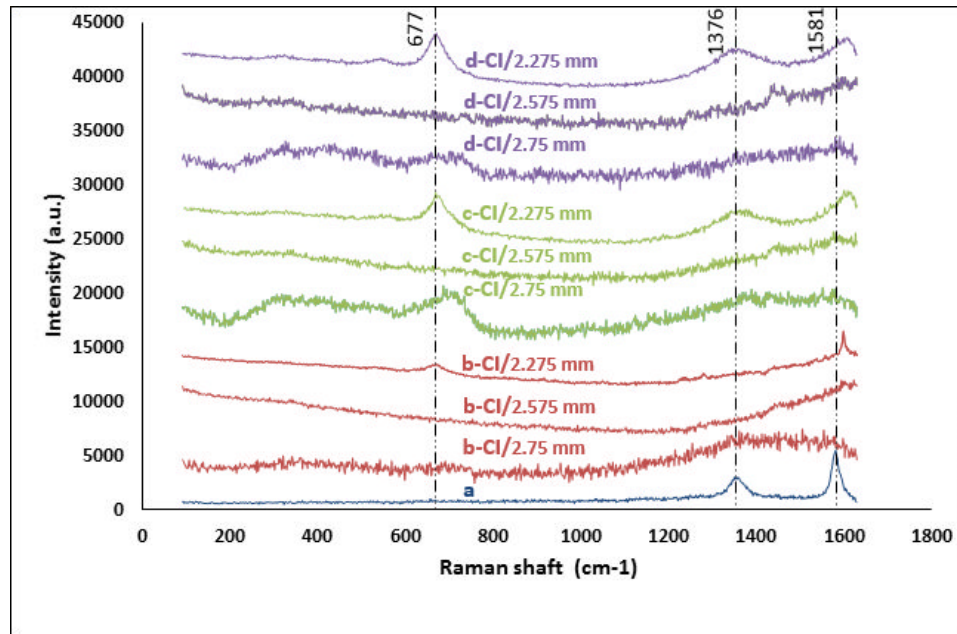


Figure 8-14 Raman spectroscopy for the CI camlobes (rubbed against MnPO_4 inserts) at $100\text{ }^\circ\text{C}$: (a) before test, (b) at cam nose, (c) $+14^\circ$ from cam nose, (d) -14° from cam nose

The Raman spectra for MnPO_4 inserts with different thicknesses is shown in Fig. 8-15. The Raman shift generally showed the presence of phosphate (956 cm^{-1}) inside and outside the wear track for all thicknesses. This confirms that the MnPO_4 coating was not stripped off from the steel substrate. After test, carbon peaks were generally detected inside and outside the wear track. This also confirms that there is a transfer of material from the camlobe to the MnPO_4 insert.

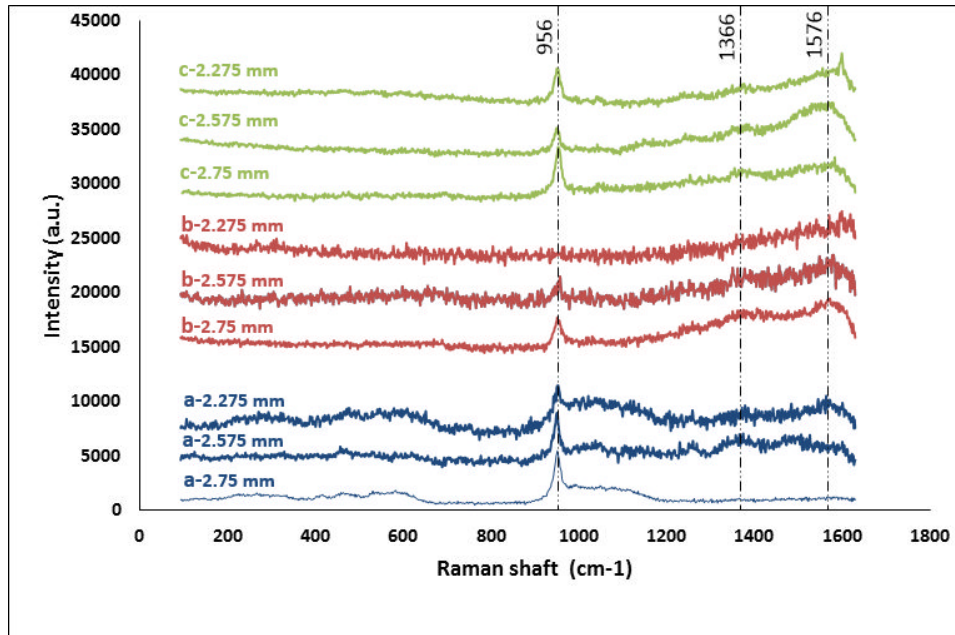


Figure 8-15 Raman spectroscopy for the MnPO₄ inserts at 100 °C: (a) before test, (b) inside wear track, (c) outside wear track

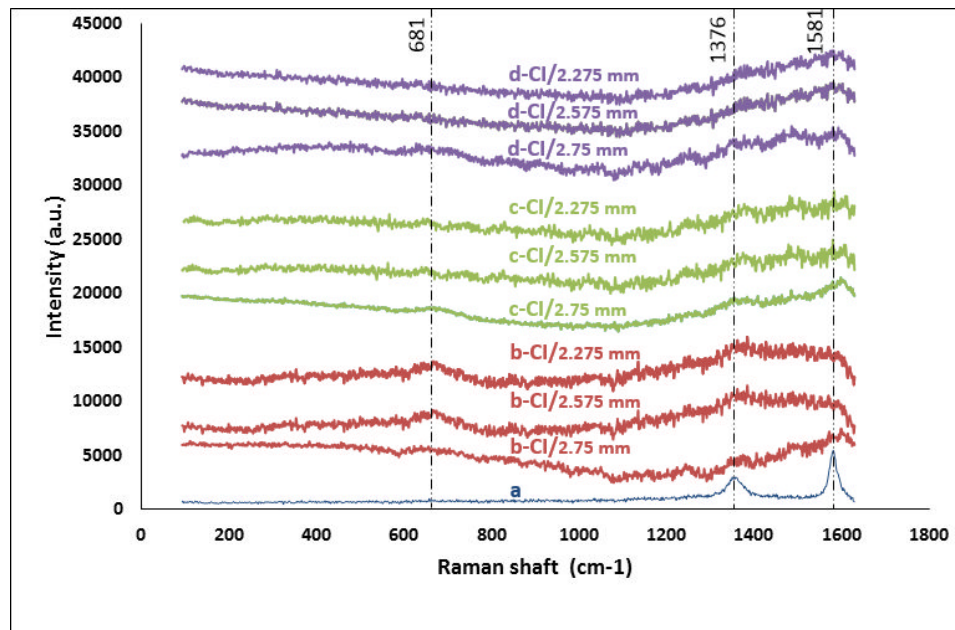


Figure 8-16 Raman spectroscopy for the Cl camlobes (rubbed against DLC inserts) at 100 °C: (a) before test, (b) at cam nose, (c) +14° from cam nose, (d) -14° from cam nose

Fig. 8-16 shows the Raman spectroscopy for the Cl camlobes (rubbed against DLC inserts with different thicknesses). For thickness 2.575 mm and 2.275 mm, the peaks at 681 cm⁻¹ were attributed to the formation of Fe₃O₄. Carbon

peaks at 1376 and 1581 cm^{-1} were generally detected for all regions on the camlobe (i.e. cam nose and cam flank). The Raman spectra obtained from the DLC inserts with different thicknesses is presented in Fig. 8-17. Regardless of tappet thickness, it can be seen that the Raman peaks related to the presence of carbon were the only peaks that detected inside and outside the wear track of the DLC inserts. For the third stage and fourth stage, as the lubricant is free of MoDTC, MoO_x and iron (II) molybdate (FeMoO_4) peaks were also not observed on any surfaces of camlobes and followers.

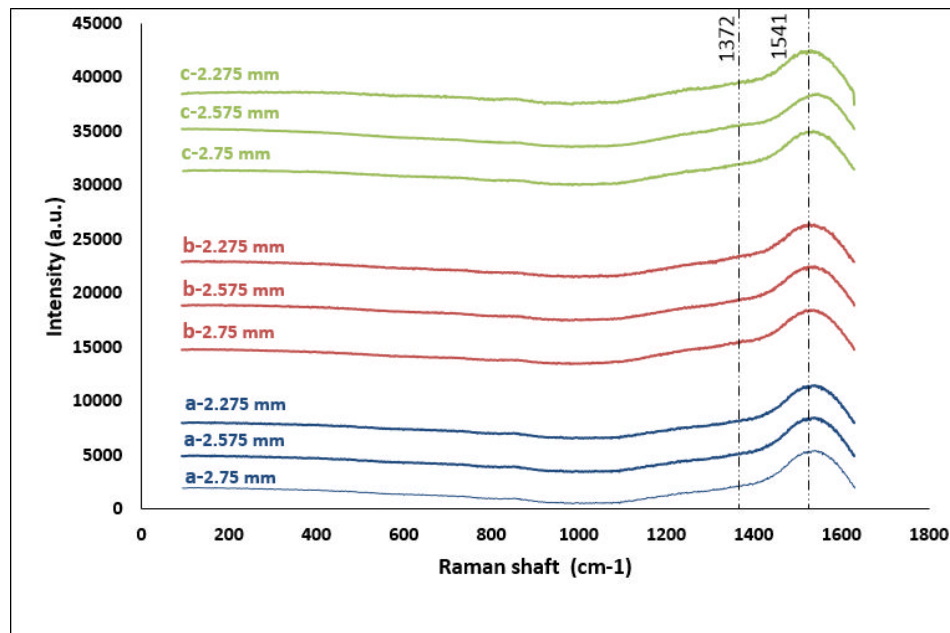


Figure 8-17 Raman spectroscopy for the DLC inserts at 100 °C: (a) before test, (b) inside wear track, (c) outside wear track

8.3.3 X-ray Photoelectron Spectroscopy Results

Under the absence of MoDTC, the XPS spectra of the tribofilms formed on the CI camlobes rubbed against tappets coated with MnPO_4 and DLC coatings is shown in Fig. 8-18. Regardless of coating type, the S 2p, Zn 3s, P 2p and Zn 2p peaks were clearly observed on the camlobes that rubbed against the steel inserts. However, the amount of P 2p detected on the tribofilm formed on the camlobe was higher when rubbed against DLC insert compared to the camlobe rubbed against MnPO_4 insert. In addition, Δ Zn 3s - P 2p shows that the tribofilms are composed of fairly long chain calcium phosphates at the

camlobe rubbed against MnPO₄ insert as compared to the camlobe rubbed against DLC insert. This result was also confirmed by the BO/NBO ratio which found to be higher for the camlobe that rubbed against Mn-Phosphate insert (i.e. a greater BO/NBO also supports a long chain polyphosphate). Table 8-9 presents the binding energies of XPS spectra for the camlobes under the effect of tappet thickness and coating. Regardless of tappet thickness and coating type, oil additives were all detected on the tribofilms formed on the camlobes. However, it was evident that the S 2p peak was not seen on the camlobe when rubbed against MnPO₄ insert with thickness of 2.275 mm. The S 2p peak was also not observed on the camlobe when rubbed against DLC insert with thickness of 2.575 mm.

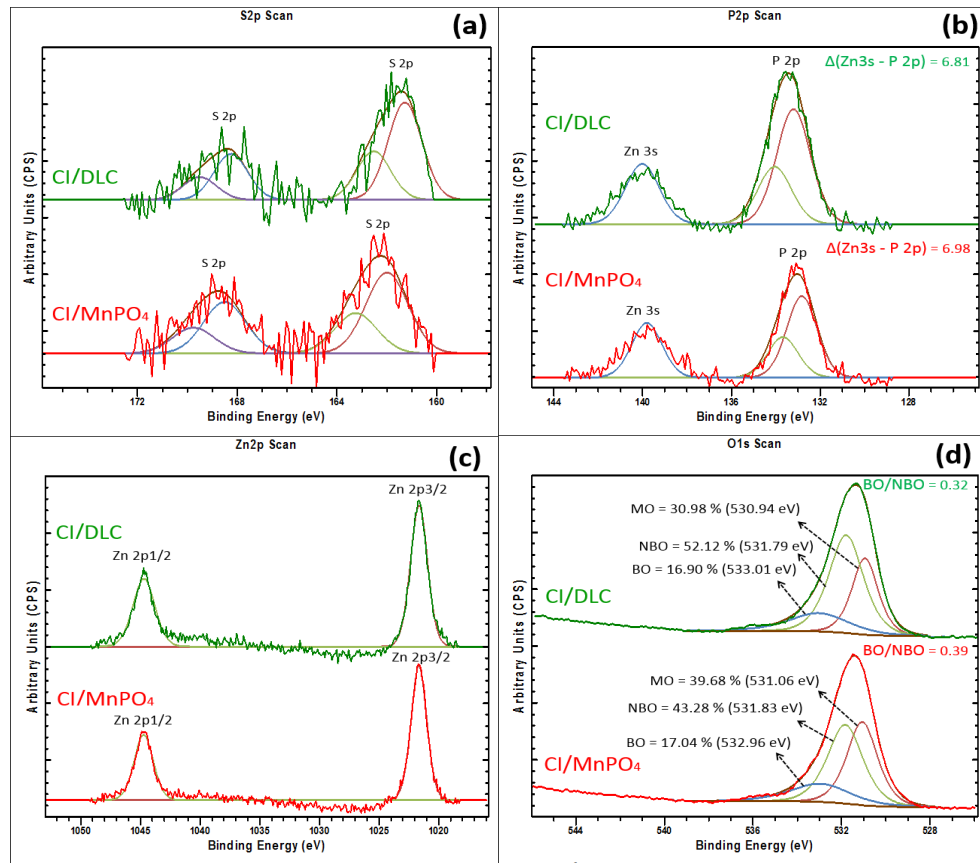


Figure 8-18 XPS analysis of cast iron camlobes rubbed against tappets coated with MnPO₄ and DLC coatings at 100 °C: (a) S 2p peaks, (b) P 2p peaks, (c) Zn 2p peaks, (d) O 1s peaks

Figure 8-19 presents the XPS spectra of the tribofilms formed on the tappets coated with MnPO₄ and DLC coatings

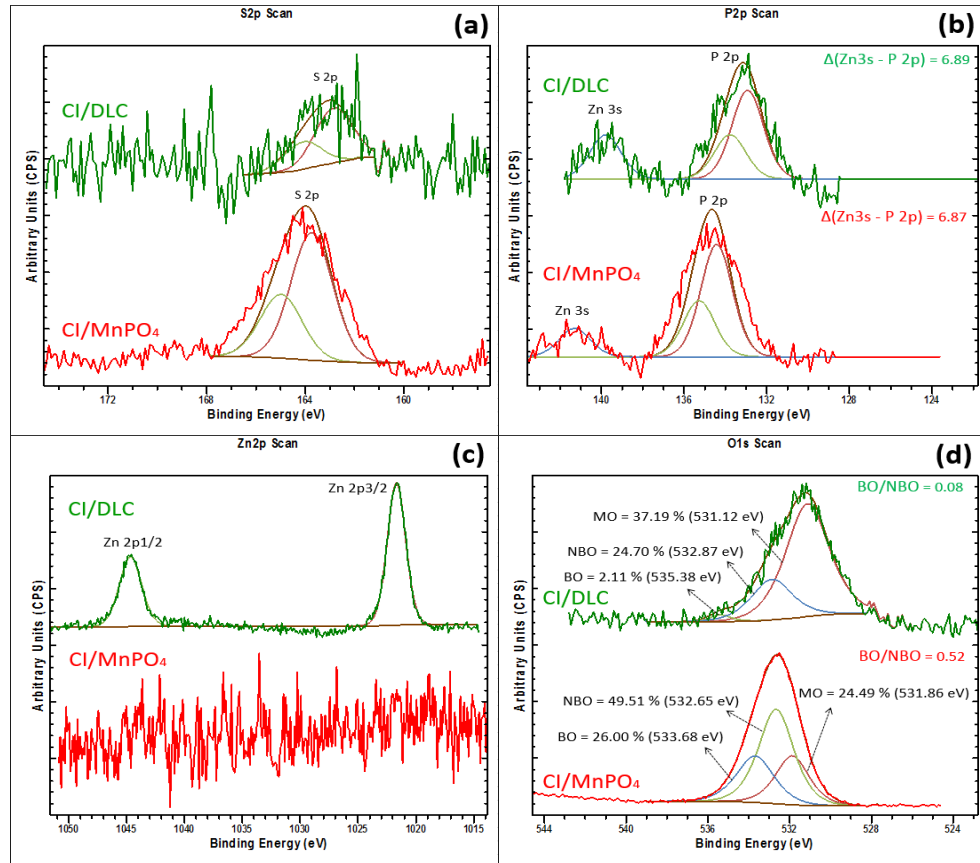


Figure 8-19 XPS analysis of steel tappets coated with MnPO₄ and DLC coatings at 100 °C: (a) S 2p peaks, (b) P 2p peaks, (c) Zn 2p peaks, (d) O 1s peaks

It can be seen that the amount of S 2p detected on the tribofilm formed on the MnPO₄ insert was higher compared to the DLC insert. In addition, evaluations of Δ Zn 3s - P 2p showed that the tribofilms at the DLC and MnPO₄ inserts have similar long chain calcium phosphates. However, the BO/NBO ratio clearly revealed that the tribofilm formed on the DLC insert have longer chain calcium phosphates as compared with the tribofilm formed on the MnPO₄ insert.

Moreover, the BO/NBO, Δ Zn 3s-P 2p and P 2p/Zn 3s inside and outside the wear track for the tappets coated with MnPO₄ and DLC coatings are presented in Table 8-10.

Table 8-9 Binding energies of XPS spectra of Mo, Zn 3s, P 2p and S 2p formed on top surface of camlobes rubbed against tappets with different thicknesses and coatings at 100 °C

		Binding Energies (eV)			
		Insert thickness			
		Mo	Zn 3s	P 2p	S 2p
MnPO₄	2.75 mm	531.06	139.81	132.83	162.00
	2.575 mm	532.45	141.39	134.44	162.09
	2.275 mm	530.81	140.08	133.11	-
DLC	2.75 mm	530.94	140.01	133.20	161.28
	2.575 mm	530.20	139.02	132.05	-
	2.275 mm	531.11	140.09	133.11	162.00

Table 8-10 BO/NBO area ratio, $\Delta(\text{Zn } 3s - \text{P } 2p)$ (eV), and P 2p/Zn 3s area ratio for MnPO₄ and DLC inserts inside and outside the wear track at 100 °C

Insert coating	Position on insert	BO/NBO	$\Delta(\text{Zn } 3s - \text{P } 2p)$ (eV)	P 2p/Zn 3s
MnPO₄	Inside wear track	0.52	6.87	10.35
	Outside wear track	0.41	6.06	4.80
DLC	Inside wear track	0.08	6.89	5.27
	Outside wear track	0.02	-	-

From Table 8-10, for DLC insert (i.e. stage 4), no Zn 3s and P 2p wear detected outside wear track. For MnPO₄ insert, however, both peaks (i.e. Zn 3s and P 2p) were detected inside and outside the wear track. In addition, for MnPO₄ insert (i.e. stage 3), $\Delta \text{Zn } 3s\text{-P } 2p$ and BO/NBO were seen to be higher inside the wear track as compared to the outside wear track, suggesting that

the tribofilm formed inside wear track composed of long chain calcium phosphates as compared to the tribofilm formed outside wear track. Table 8-11 shows the binding energies of XPS spectra for the inserts under the effect of tappet thickness and coating. Regardless of tappet thickness and coating type, oil additives were also reported on all the tribofilms that formed on the tappets.

Table 8-11 Binding energies of XPS spectra of Mo, Zn 3s, P 2p and S 2p formed on top surface of tappets with different thicknesses and coatings at 100 °C

	Insert thickness	Binding Energies (eV)			
		Mo	Zn 3s	P 2p	S 2p
MnPO₄	2.75 mm	531.86	141.30	134.43	163.73
	2.575 mm	529.83	139.89	133.15	162.09
	2.275 mm	531.37	140.05	133.23	164.84
DLC	2.75 mm	531.12	139.81	132.92	162.85
	2.575 mm	530.40	140.01	133.20	162.84
	2.275 mm	532.64	141.37	134.31	163.81

8.3.4 FIB-SEM Results

Under the absence of MoDTC, representative thickness of tribofilm formed on cam/follower tribopair is presented in Fig. 8-20. Unlike the first stage and second stage, it was evident that the thickness of the tribofilm formed on the camlobe rubbed against MnPO₄ (45-62 nm) insert is relatively higher than those observed on the camlobe rubbed against DLC insert (40-45 nm).

For the tappets, it is clearly evident that the tribofilm formed on the DLC insert is thicker than the tribofilm formed on the Mn-phosphate (MnPO₄) insert. The lubricant used in the third stage and fourth stage (i.e. O3) also produced a thin film at the centre of the inserts while thick tribofilm was formed at different

areas near the insert edge. For the camlobes, however, the thickness of the tribofilm was relatively comparable across the camlobe, namely on the nose and the cam flank (both sides).

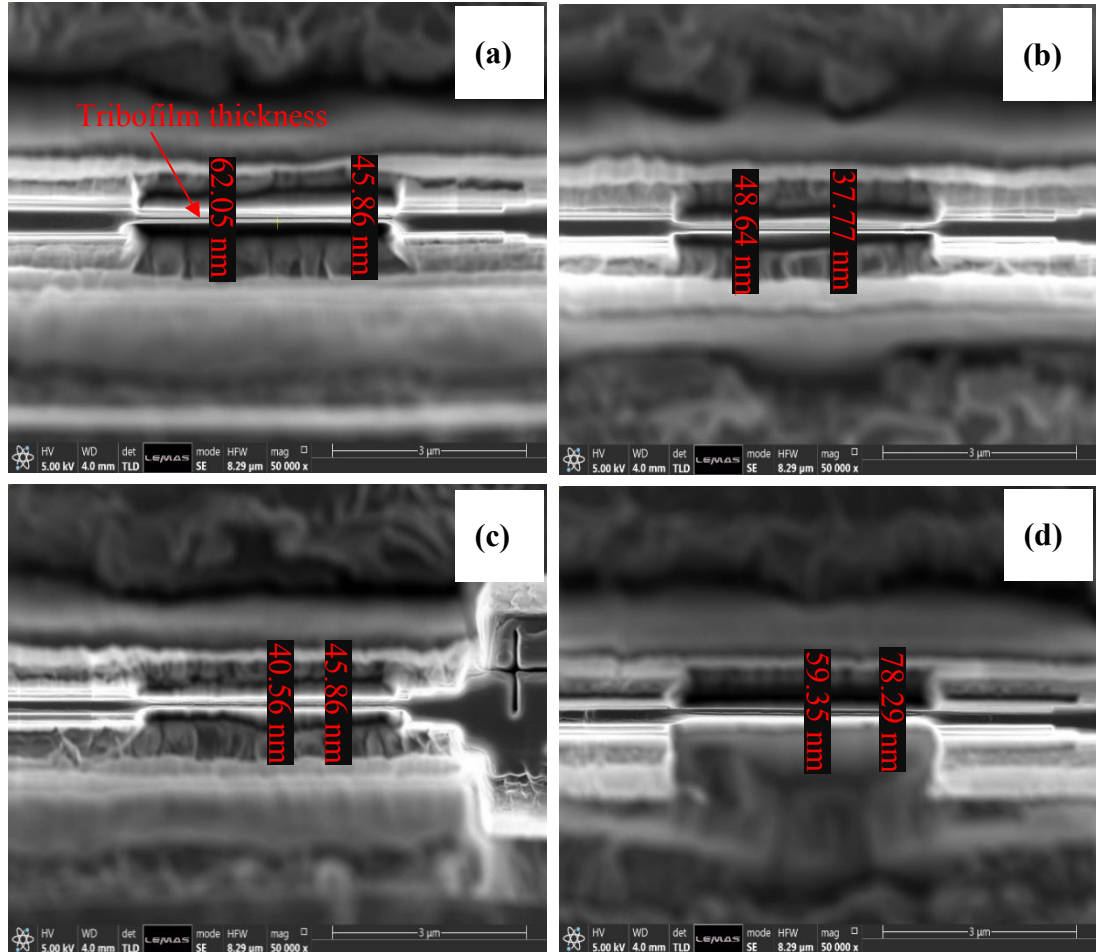


Figure 8-20 FIB-SEM showing tribofilm thickness for: (a) camlobe rubbed against MnPO₄ insert, (b) MnPO₄ insert, (c) camlobe rubbed against DLC insert and (d) DLC insert

8.3.5 TEM Results

The characterisation on the surfaces of the camlobes rubbed inserts coated with MnPO₄ and DLC coatings is shown in Fig. 8-21. For the camlobe rubbed against MnPO₄ insert, the tribofilm was mainly consisted of P, S, Zn, Cr and Ca. AS mentioned earlier, the platinum layer is coming from the deposition prior to cutting in the FIB-SEM. For the camlobe rubbed against DLC insert, the tribofilm was generally made of P, S, Zn and Cr.

For tappets, Fig. 8-22 and Fig. 8-23 show the EDX mapping on the surfaces of the MnPO_4 inserts and DLC inserts respectively. For MnPO_4 insert (i.e. stage 3), the tribofilm was mainly made of Zn, S and P and the substrate was mainly rich in iron. In addition, circular spots of chromium were detected on the substrate. Platinum was also detected on top of the layers as a protective platinum layer that deposited on the inserts by FIB. For DLC insert (i.e. stage 4), the tribofilm was mainly made of S, P, Cr and C. Confirming XPS results, Zn was also not detected on the surface of DLC insert. The coating layers from top to bottom were also reported to be C, Cr and Fe (substrate), respectively.

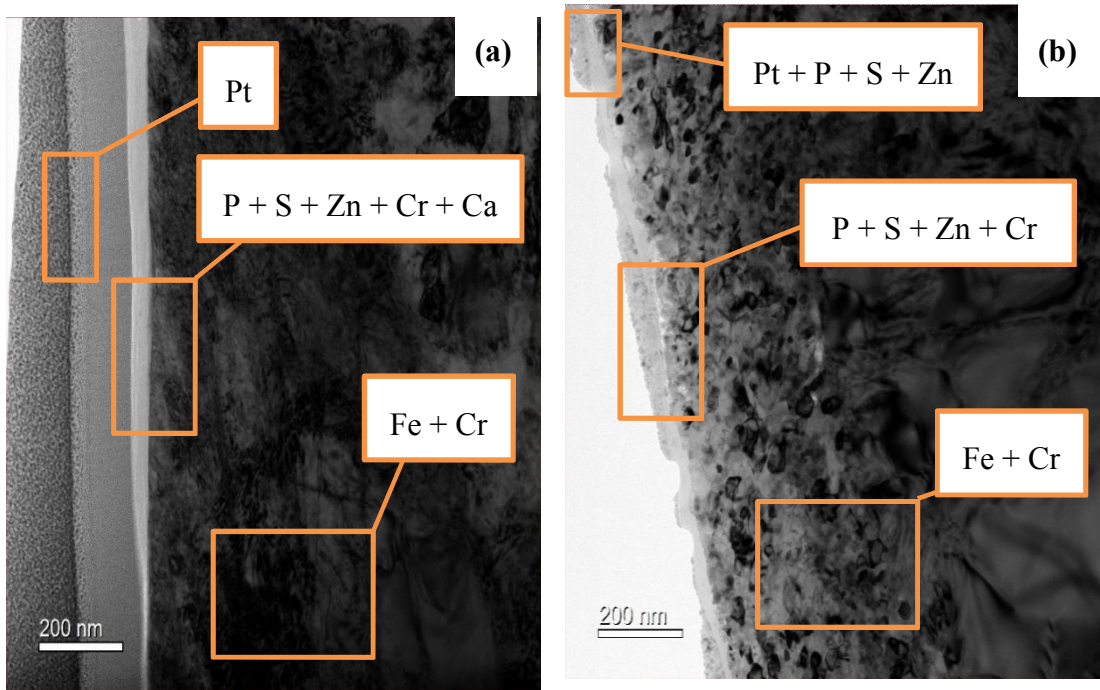


Figure 8-21 TEM images showing tribofilm at camlobe rubbed at: (a) MnPO_4 insert and (b) DLC insert

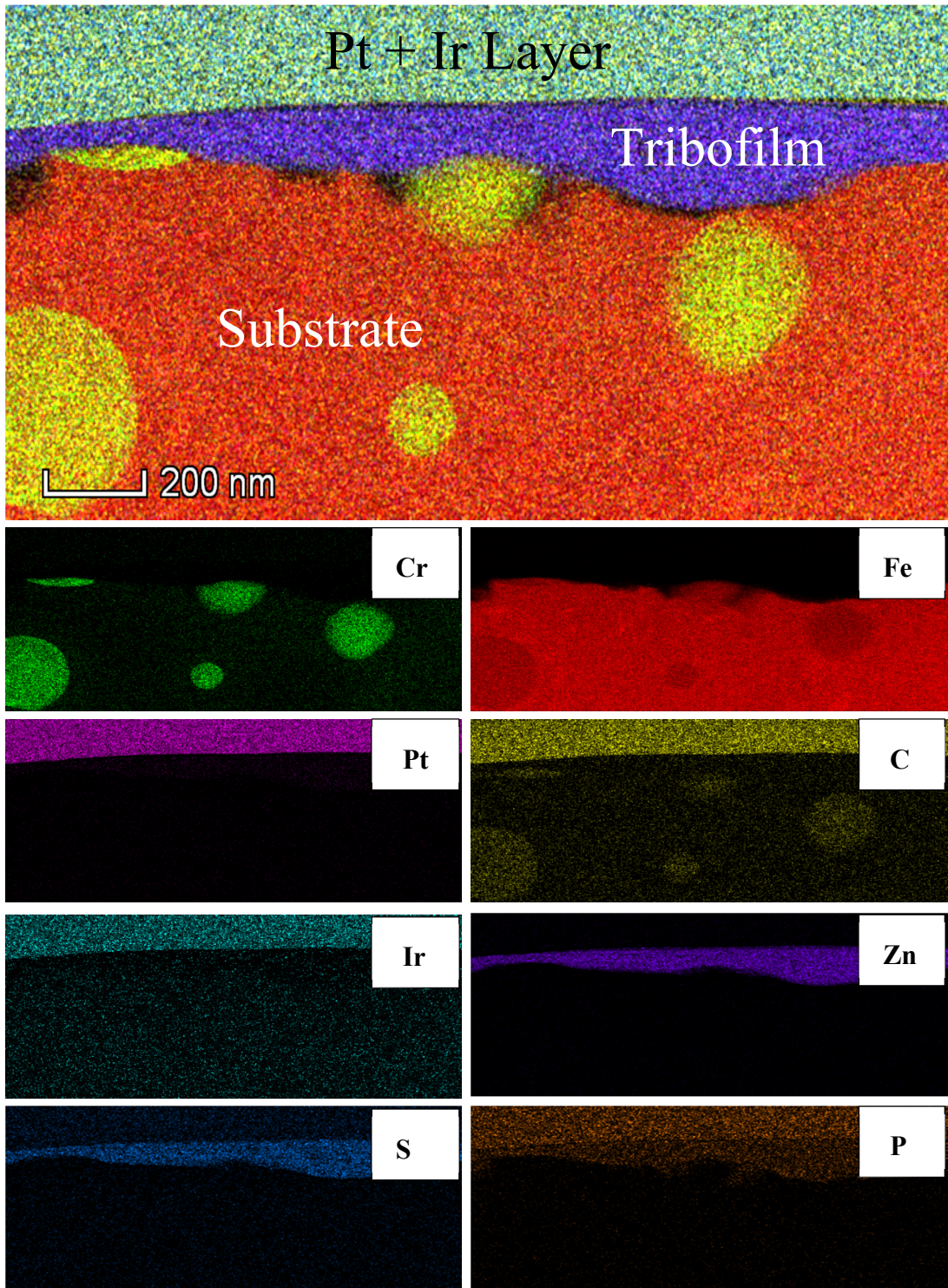


Figure 8-22 TEM mapping showing tribofilm at MnPO₄ insert

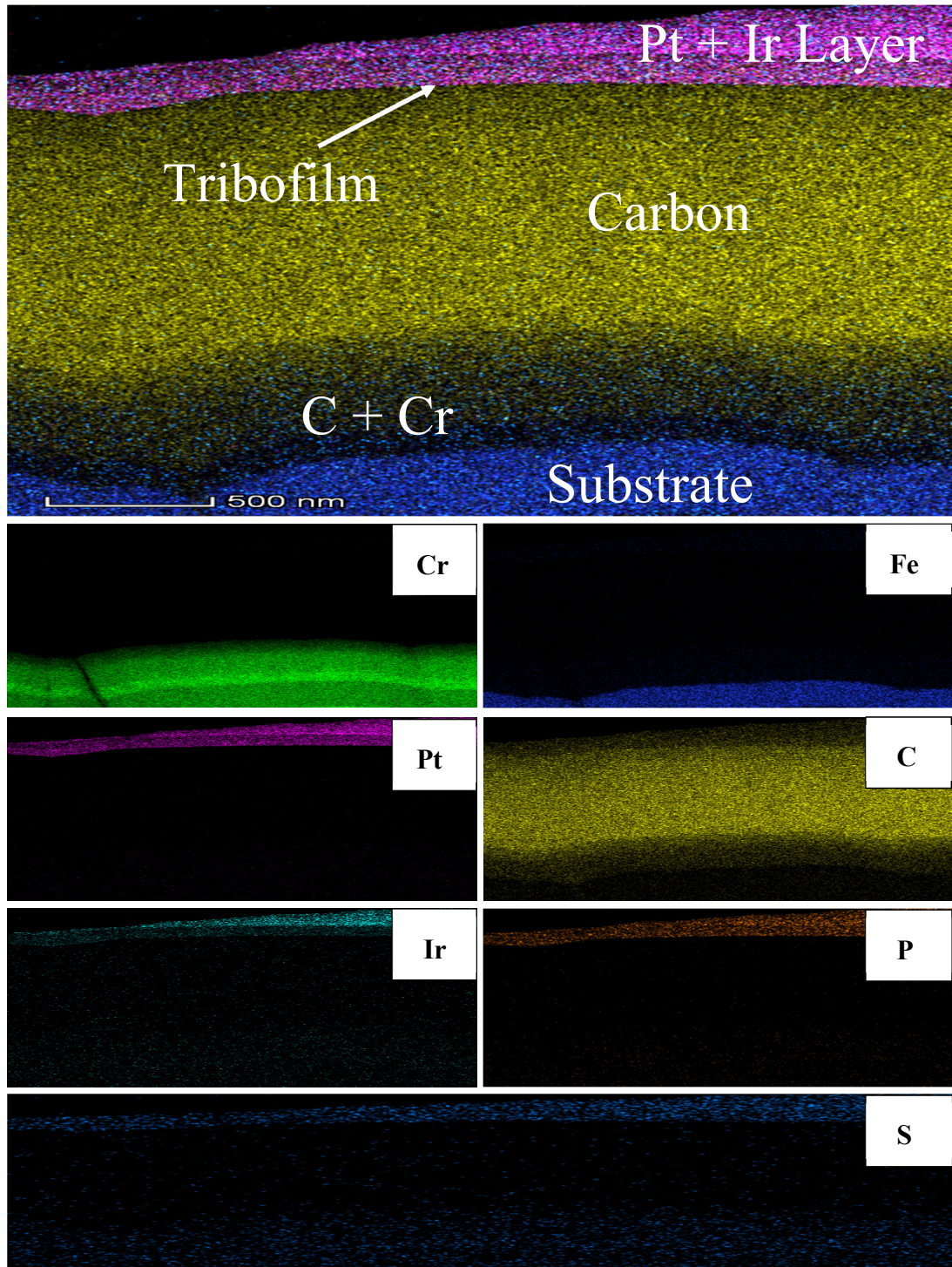


Figure 8-23 TEM mapping showing tribofilm at DLC insert

8.4. Summary of Findings

Several surface analysis techniques were performed on the tribofilms to understand the tribochemical interactions between oil additives and the

cam/follower interface. The main conclusions drawn from this chapter are given below:

- Results revealed that the tribofilm derived from camlobes and tappets were confirmed to be varied as a function of tappet clearance and cam profile.
- For the first stage and second stage, DLC inserts showed a smoother surface, supporting a polishing wear. However, this process was not observed on the DLC insert with thickness of 2.275 mm. For all MnPO₄ inserts, however, the surface appears fairly rough (R_a is about 0.47 μm for the thinnest tappet and 1.7 μm for the thickest tappet) compared to MnPO₄ insert before test (R_a 0.25 μm). The surface was consisting of ridges/grooves on the surface of the insert. This is equally supporting an abrasive wear process for MnPO₄ inserts.
- For the third stage and fourth stage, it should be mentioned that polishing process was only observed on the DLC insert with thickness of 2.75 mm. For all MnPO₄ inserts, an abrasive wear process was seen on all MnPO₄ inserts.
- Higher MoS₂ peak intensity was observed inside the wear track as tappet clearance decreases which could indicate more MoS₂ film formed inside the wear track. That could be related to higher pressure at the interface (for higher tappet thickness) resulting in an enhanced MoDTC decomposition.
- The lubricant used in the first stage and second stage (i.e. O5) produced a very thin film at the cam nose while thick tribofilm was formed at the cam flank (both sides). Similar trend was observed for all tappets (i.e. thinner film was detected at the centre of the inserts compared to several spots near the edge of the insert).
- The lubricant used in the third stage and fourth stage (i.e. O3) also produced a thin film at the centre of the inserts while thick tribofilm was formed at different areas near the insert edge. For the camlobes, however, the thickness of the tribofilm was relatively comparable across the camlobe, namely on the nose and the cam flank (both sides).

- In the presence of MoDTC, the thickness of the tribofilm formed on the camlobe rubbed against MnPO₄ (32-43 nm) insert and the MnPO₄ insert (48-49 nm) is relatively lower than those observed on the camlobe rubbed against DLC insert (38-58 nm) and the DLC insert (51-67 nm).
- In the absence of MoDTC, the thickness of the tribofilm formed on the camlobe rubbed against MnPO₄ (45-62 nm) insert is fairly higher than those observed on the camlobe rubbed against DLC insert (40-45 nm). For the tappets, the tribofilm formed on the DLC insert is thicker than the tribofilm formed on the Mn-phosphate (MnPO₄) insert.
- Tribochemical analysis showed that MoS₂ tribofilm was formed on non-ferrous surfaces (i.e. MnPO₄ and DLC surfaces).

Chapter 9. Discussion

9.1. Introduction

In this chapter, the results presented in Chapters 5, 6, 7 and 8 are discussed. The findings are assessed and compared with other published literature. The discussion is split into three main sections. The first section discusses the characteristics of tribofilm formed on the surface and its relation to current published studies. In addition, the effect of sliding/rolling ratio (SSR) on MoDTC tribofilm and friction are discussed. The first section also covers the effect of MoDTC on friction and wear. The second section discusses the coating performance, chemistry and thickness of tribofilm formed in the SCR and the newly developed tappet rotation technique. The third section links and discusses the correlation between MTM and SCR tribometers. Also, optimisation of friction and wear behaviour and its link to fuel economy is also presented in the third section.

9.2. Characteristics of MoDTC Tribofilm

The tribofilms formed from lubricants containing MoDTC are generally composed of low friction sheets of MoS₂ [112, 188-191]. The presence of MoS_x ($x > 2$) compounds has also been reported. These compounds are typically formed at lower temperatures than MoS₂ compounds. A recrystallization of MoS_x has been reported to form MoS₂ at high temperatures [275]. In other words, MoS_x is considered as an intermediate compound in the formation of MoS₂, where the transformation from MoS_x ($x > 2$) to MoS₂ is dependent on shear stress and temperature [198].

The presence of MoO_x in MoDTC lubricant has also been reported. Bouchet *et al.* [90] and Haque *et al.* [96] have used XPS surface analytical technique to observe MoS₂ and MoO₃ compounds in the MoDTC tribofilm. They also found that the increasing of MoS₂/MoO₃ ratio reduces the coefficient of friction. In this study, MoS₂ and MoO₃ compounds were clearly seen on the tribofilms formed on camlobes and followers. Iron (II) molybdate (FeMoO₄) is also reported as a product of MoDTC decomposition [201]. This is new reaction pathway of MoDTC additive which was identified by using Raman

spectroscopy. In the literature, the formation of FeMoO_4 was reported at 120 °C, due to a reaction of molybdenum compounds with iron oxides [276, 277]. In addition, iron (II) molybdate (FeMoO_4) can also be formed at room temperature via mechanical milling [278]. Recently, the formation of FeMoO_4 was reported, at 20 °C and 100 °C, on steel/steel system; FeMoO_4 was formed during thermal degradation of lubricants containing MoDTC in the presence of Fe_3O_4 and during tribotests on MoS_2 coated discs [198]. This however confirms that the tribochemical reaction was not essentially driven by temperature (i.e. the reactions are not thermally-activated). In this study, the formation of iron (II) molybdate (FeMoO_4) has also been observed at 100 °C using Raman and XPS techniques. It should be mentioned that, for the first time, FeMoO_4 was reported to form on DLC/CI system, not on steel/steel system as it was the case in [198]. The formation of FeMoO_4 is believed to be referred to a reaction of molybdenum compounds with iron oxides on cast iron and DLC surfaces.

9.3. Effect of Sliding/Rolling Ratio (SSR) on MoDTC Tribofilm

In the literature, the effect of contact type (mainly unidirectional linear sliding contact and sliding/rolling contact) on the decomposition of MoDTC were investigated. In general, it was found that MoDTC tribofilm was similar in both contacts except for a few cases where the type of contact affected the decomposition of MoDTC on the surface [198]. In results presented in Chapter 5, it was observed that changing the test conditions (e.g. the type of contact) can affect the decomposition of MoDTC on the surface. For example, in pure sliding contact, MoDTC additive was reported to form MoS_2 and FeMoO_4 on the DLC ball. For sliding/rolling contact, however, only FeMoO_4 and Fe_2O_3 was observed on the surface. This reveals that the coverage of adsorbed MoDTC is higher in a pure sliding contact than in a sliding/rolling contact. In other words, a pure sliding contact enhances MoDTC tribofilm coverage. A schematic diagram showing the effect of contact type on MoDTC decomposition is illustrated in Fig. 9-1. From Fig. 9-1b, as MoDTC was removed from the sliding/rolling contact due to the rotation of the ball, the

nascent surface was exposed to oxidation. This can explain the presence of Fe_2O_3 in sliding/rolling contact.

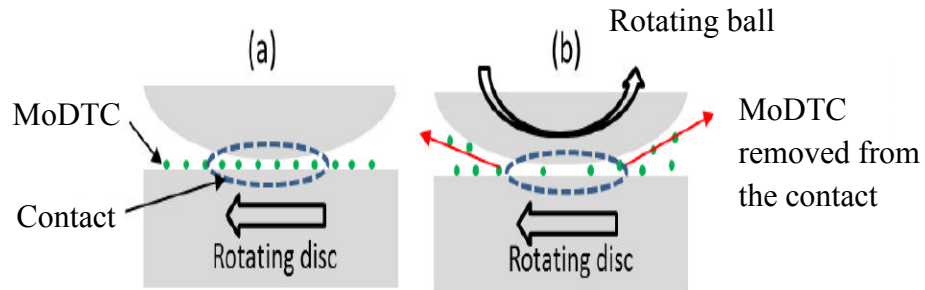


Figure 9-1 2D Schematic diagram showing adsorbed MoDTC in (a) unidirectional linear sliding contact and (b) sliding/rolling contact [198]

9.4. Effect of Sliding/Rolling Ratio (SSR) on Friction

Literature findings reported that an increase of friction can be obtained with increase in sliding/rolling ratio (SRR). Vengudusamy *et al.* [124] showed that the increase of the boundary friction was insignificant between 30% and 50% while it was substantial when SRR was 200%. Khaemba *et al.* [119] reported that boundary friction increases when increasing SRR from 100% to 200%. In addition, Brandao *et al.* [118] found that an increase in SRR (from 10% to 50%) increases elastohydrodynamic friction.

In this study, however, results obtained from MTM tribometer showed otherwise, where no systematic trend of friction coefficient was observed for both contacts (sliding/rolling and pure sliding). This was attributed to the influence of sliding/rolling ratio on surface chemistry, where the change in SRR was reported to influence the tribofilm build-up.

9.5. Effect of MoDTC on Friction and Wear

MoDTC additive was reported to produce MoS_2 friction sheets which result in low friction under boundary lubrication [119, 201, 231]. This is in agreement with the results obtained from this study. It should be mentioned, however, adding MoDTC to the lubricant caused high friction at the beginning of the test then followed by a rapid drop to low friction values. A similar trend was also

observed with some literature [190, 198, 279]. In order to explain this behaviour, Morina *et al.* [279] studied the chemical composition of wear scars at the beginning of the test (i.e. before friction drop). As a result, different elements such as Fe, O, S, C and N were detected on the wear scars before the friction drop. This confirms that the MoS₂ sheets (which are responsible for friction reduction) are not formed yet and thus need a sufficient time in order to be completely formed, as reported by Grossiord *et al.* [188] and Rai *et al.* [266].

In terms of wear, most literature [226-231] reported high wear on DLC coatings in the presence of MoDTC. A high concentration of MoDTC can promote wear of the DLC coating in oils without ZDDP [230]. In addition, MoO₃ compound (formed from MoDTC additive) was reported to react with DLC coating and this compound was responsible for the increase of wear of DLC coating [229]. Haque *et al.* [226] also observed that the presence of MoDTC gives high wear in a DLC/steel contact. This is in agreement with the wear results obtained from this study. Similarly, the wear detected on cast iron discs and cast iron camlobes was relatively high when lubricated with oils containing MoDTC alone. This confirms the adverse effect of MoDTC in increasing wear of a ferrous counterpart rubbed against a DLC coating (i.e. DLC ball and DLC tappet) [221]. This is essentially due to the formation of molybdenum-containing compounds in the presence of ferrous counterparts leading to oxidation and accelerated wear of the DLC coating [231]. The higher wear observed on the CI surface could also be explained by the absence of MoDTC tribofilms during the running-in process.

In terms of type of contact, the rolling motion derived from the sliding/rolling contact was reported to promote the removal of MoDTC [198]. Suzuki [280] proposed that a good adhesion of MoS₂ can be achieved with high sliding/rolling ratios (more sliding) due to high tensile stress. In this work, sliding/rolling contacts for lubricants containing MoDTC mostly exhibited higher wear for the DLC coated balls than pure sliding contact. This suggests that the pure sliding contact experienced high tensile stress and thereby provided better adherence of MoDTC than in sliding/rolling contact. As a result, this led to enhanced tribofilms build up (i.e. enhanced the reaction with

MoDTC) in pure sliding contact and resulted in an improved lubrication and therefore reduced wear of the DLC balls.

9.6. Coating Performance on SCR

In valvetrain systems, the friction or power consumption can be reduced by using coated tappets and even coated camlobes. In this study, a considerable reduction in friction and wear was achieved by changing the coating of the tappet from $MnPO_4$ (commercial standard production surface coating) to diamond-like carbon coating (DLC). This can be explained by the high roughness of $MnPO_4$ surface which gave rise to asperity interactions, and thus can lead to high wear and friction [86]. This can also be due the differences in hardness between coatings. In other words, DLC coating is harder than $MnPO_4$ coating and that in turn helped in reducing wear of DLC tappets.

In general, high hardness showed an improvement of the fatigue resistance and ploughing on interacting components [79]. For the same rig used in this study, it was reported by Ofune *et al.* [115] that using high hardness coatings (i.e. higher than the hardness of the DLC coating that used in this current work) will not conform to the rig configuration. Likewise, high hardness coatings cause high friction, high noise and need more time to break in. Nevertheless, in order to improve wear using a particular coating, a balance between hardness and oil formulation should be taken into consideration.



Although it was reported that DLC coatings offer friction reduction under the presence of MoDTC, a reduction in friction due to the interaction between ZDDP and DLC coating was also observed when lubricated in a lubricant free of MoDTC. This is in agreement with some literature, where ZDDP helps to decrease the friction [167]. This is however unlike some literature, where ZDDP was reported otherwise [52, 160, 168-171]. Nevertheless, it should be noted that a lubricant with MoDTC and ZDDP additives can provide lower friction on the DLC coating, than ZDDP alone [225].

As presented in Chapter 6, the wear of DLC coating was lower than the wear of tappets coated with $MnPO_4$. Similar findings were reported in the literature, where low wear of DLC coatings was observed in presence of MoDTC [221,

268]. It is worthwhile to mention that the lubricant used in this study was not only containing MoDTC but also ZDDP. This is most likely one of the potential reasons that helped to reduce wear on DLC coating [231].

Based on the results obtained from this study, and in addition to the properties of each coating (MnPO₄ or DLC), it was found that the surface roughness and hardness typically affects the friction response of SCR. Also, the hardness of the follower affects the wear on the camlobe, as shown in Table 9-1. It is however important to mention that a particular coating with high hardness will easily promote high wear on the counterpart (i.e. the camlobe). This was confirmed by the results presented in Chapter 6.

Table 9-1 Effect of surface roughness and hardness on coating performance

Type of coating	Hardness	Surface roughness	Friction	Wear	Wear on counterpart
MnPO₄					
	Low	High	High	High	Low
DLC					
	High	Low	Low	Low	High

In general, the coating performance is not only controlled by surface roughness or hardness of the coating but also controlled by the properties of coating, oil formulation and material of counterpart. Also, tribochemical reactions between the coating, the counterpart and the lubricant play a key role on controlling the performance of coating. Therefore, all these factors should be taken into consideration in order to understand and/or improve a tribological system.

9.7. Chemistry and Thickness of Tribofilm on SCR

The films formed on the cam/follower tribopair was observed to vary with the oil formulation and type of coating. In general, a considerable distribution of tribofilms was observed. That distribution in return helped to protect the surface from plastic deformation of the asperity. As the lubricants used in this work contained detergents and dispersants, these additives were promoted the distribution of the tribofilm on the surface [115].

In this study, it was observed that the distribution of the tribofilms was also dependent on the position of the sample (for both camlobes and tappets). For example, from FIB-SEM, regardless of MoDTC additive and type of coating, a very thin film was observed at the cam nose (a region of significant rubbing) while thick tribofilm was formed at the cam flank (both sides). This was also confirmed by observing the depth profile using XPS technique (not shown here). At cam nose, with a long time high energetic monoatomic etching, major change is detected and the tribofilm derived from MoDTC and ZDDP additives was fairly thin.

For tappets, thinner tribofilm was also formed at the centre of the inserts (a region of significant rubbing) compared to several spots near the edge of the insert. This was also confirmed by FIB-SEM technique which suggests a removal action due to high pressure rubbing action (from the ramp, flank, shoulder and nose) of the camlobe at the centre of the insert, flash temperatures and interaction with the lubricant. At the edges, the XPS depth profile for the tappets (not shown here) showed that the tribofilm is thicker at the centre. Fig. 9-2 shows a 3D schematic diagram of the tribofilm distribution on cam/follower tribopair.

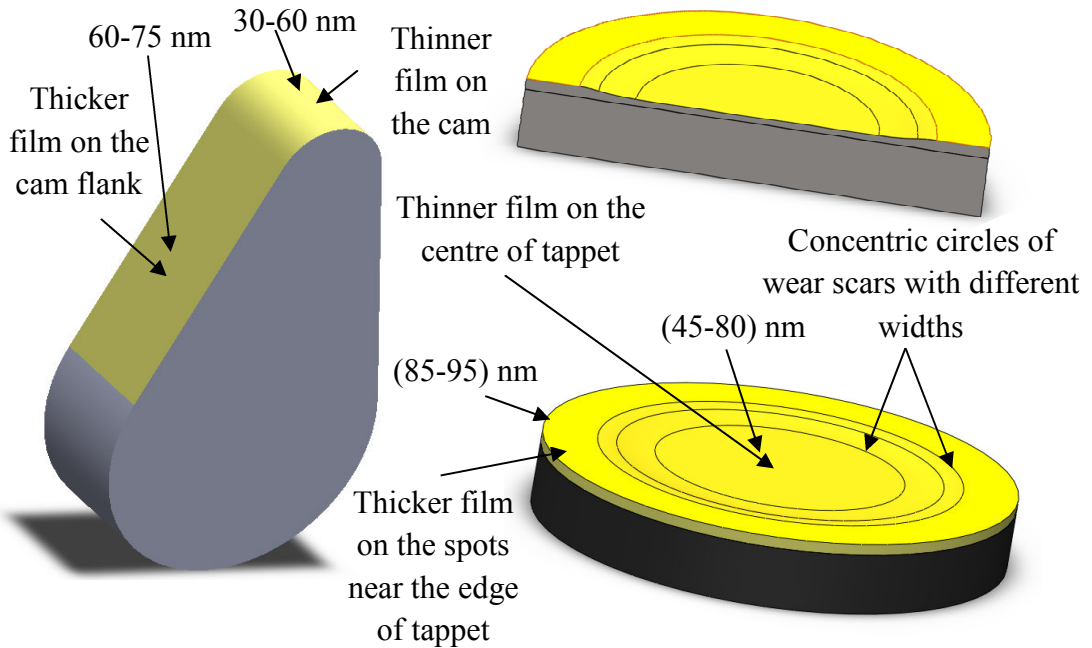


Figure 9-2 3D schematic diagram showing the tribofilm distribution on cam/follower tribopair

DLC tribofilms are reported to be different from those obtained on ferrous surfaces [75]. In fact, no interaction occurs in some cases [281]. However, results obtained from this study showed otherwise. The tribofilms formed on DLC and ferrous surfaces (i.e. cast iron camlobe) are reported to be relatively similar. TEM and XPS analysis of the DLC films showed that the films were mainly consisted of Mo, Zn, S, P and C. The coating layers from top to bottom were detected and the substrate was composed of C, Cr and Fe while the interlayer was made of CrC.

For the ferrous counterpart (i.e. camlobe rubbed against DLC insert), the tribofilm was mainly made of Fe, Zn, Mo and P. In other words, sulfur (S) was the only element that did not detect on the ferrous surface. From FIB-SEM, however, it should be noted that the thickness of the tribofilm formed on DLC tappets was fairly higher than those observed on CI camlobes and even MnPO_4 tappets.

9.8. Effect of Tribofilm Formation on Tappet Rotation

Initially, many cam rigs have been developed for valvetrain studies [9, 62, 63, 65, 75, 76, 85, 100-103]. A large number of works have also been conducted on valvetrain systems in order to investigate the behaviour of tappet rotation. Some researchers [238-240] have developed models to evaluate tappet rotation while most others have developed different experimental techniques [235, 241-247]. However, most of these techniques require extensive modifications on the rig. Also, it is important to mention that almost all these studies have captured only the effect of tappet rotation on speed, cam angle and oil temperature. It is however necessary to observe the behaviour of tappet rotation when the inserts lubricated with different oil formulations (e.g. with and without MoDTC).

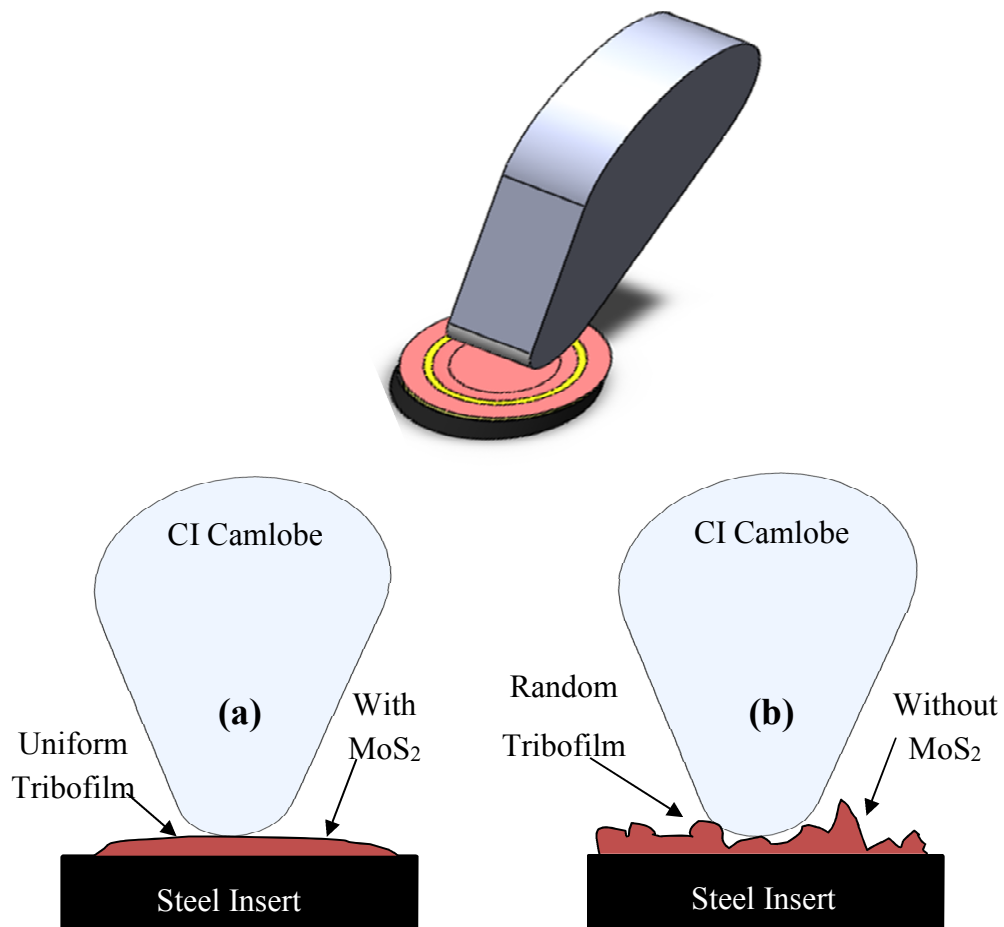


Figure 9-3 Schematic diagram of cam/follower tribopair (a) when the insert is lubricated with MoDTC (b) without MoDTC

In a 24h run-in tappet, Mufti *et al.* [235] reported that adding a friction modifier to the lubricant has no clear effect on tappet rotation speed. However, they did not mention whether the friction modifier that they used in their lubricant was MoDTC additive or not. In any case, this is in contrast with the results obtained from this study (presented in Chapter 7). In fact, it was found that MoDTC plays a key role in promoting tappet rotation. In other words, MoS₂ sheets (which come from MoDTC) were suggested to form a uniform layer on the surface during the rotation, as shown in Fig. 9-3. This uniform layer provided a better conformity between cam and tappet surfaces and that in return helped to increase tappet rotation in the presence of MoDTC. In contrast, a random layer was suggested to form on the surface in the absence of MoS₂ sheets (i.e. the absence of MoDTC), as shown in Fig. 9-3. This random layer offers low conformity between the cam/follower tribopair and in turn resists any motion mainly those due to tappet rotation.

9.9. The Link between MTM and SCR Tribometers

To give room for comparison, similar test conditions such as operating temperature, contact pressure, load, lubricant, material and coating combination were used in both tribometers. In addition, as the cam follower system has sliding/rolling and pure sliding motions, MTM tribometer was used in this work in order to produce both motions. Based on the similarities in test conditions, materials and motions, the simulation process between the contact pair (ball and disc) in the MTM tribometer and the contact pair (cam and follower) in the single cam rig tribometer is understood to be applicable, as shown in Table 9-2.

The purpose of the simulation is however to identify the differences and similarities between both tribometers in terms of tribological and tribochemical performance. Therefore, if the results are relatively similar (i.e. MTM results support SCR results), then MTM tribometer can be used in future to simulate the SCR. This would offer low cost tests with short time and to use low amount of lubricants. Also, the use of MTM can reduce tests on valvetrain rigs which in return could lead to lower costs for original equipment manufacturers.

For the MTM tribometer, the coated DLC ball was representing the coated steel follower while the uncoated CI disc was representing the uncoated CI camshaft. It is worth mentioning, however, based on the samples manufacturer, it was impossible to use balls made of cast iron as the heavier ball would damage the holder of the ball. Therefore, CI disc was representing the CI camshaft, not the ball.

Table 9-2 Similarities and differences between MTM and SCR

	Similarities	Differences
MTM and SCR tribometers	contact pressure, load, lubricant, lubrication regime, temperature, material, coating and type of contact	Test duration: MTM (6.30 hrs) SCR (80 hrs)

9.9.1 Tribological Comparison

9.9.1.1 Friction Performance

The author of this work believes that no works have compared the friction obtained from SCR tribometer and MTM tribometer. This is mainly due to the difference in scales between both tribometers in which the friction parameters are obtained. Scale differences are also appeared between the SCR and other tribometers. Nonetheless, Gangopadhyay *et al.* [75] compared the friction and wear characteristics between reciprocating tribometers and SCR systems. More recently, the comparison of friction and wear between the SCR tribometer and pin on plate (PoP) tribometer was done at the University of Leeds [115]. It is important to mention that PoP tribometer only experiences pure sliding contact, where this contact can be mainly found on the cam nose. As cam/follower tribopairs experience different sliding and rolling motions, evaluation of sliding/rolling contact is crucial. Therefore, the mini traction machine was used in this study.

Fig. 9-4 shows the friction analysis for both tribometers when lubricated with O5 (i.e. under the presence of MoDTC) and O3 (i.e. under the absence of

MoDTC). As already presented in Chapter 4, two types of coatings ($MnPO_4$ and DLC) for the steel follower were used in the SCR while only DLC coating for the steel ball was used in the MTM. Therefore, from SCR results, the first stage and the third stage (i.e. when the follower coated with Mn-Phosphate coating) have not been included in the comparison.

For Fig. 9-4, the single cam rig (SCR) friction torque was calculated as the average of the three tappet thicknesses. Furthermore, the MTM friction coefficient was reported as the average of pure sliding contact and sliding/rolling contact.

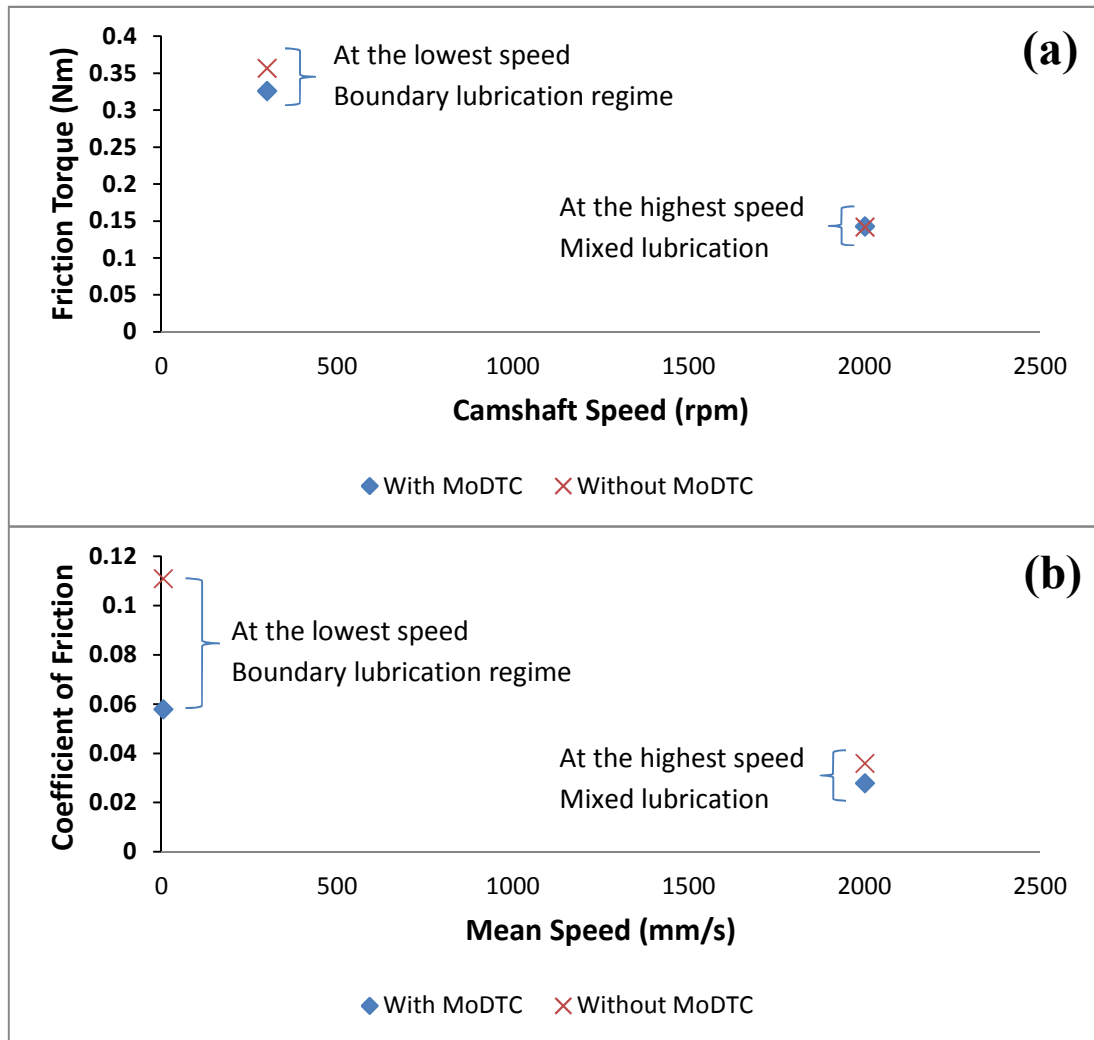


Figure 9-4 Friction analysis as a function of MoDTC for (a) SCR tribometer
(b) MTM tribometer

From Fig. 9-4, regardless of MoDTC additive, it can be seen that both tribometers were experienced boundary lubrication regime at the lowest

speed (300 rpm for the SCR and 5 mm/s for the MTM). These findings are in agreement with those obtained in [115]. This confirms that MTM tribometer, in boundary lubricated regime, offers good reliability of the level of representation for simulation of SCR tribometer. At the highest speed (2100 rpm for the SCR and 2000 mm/s for the MTM), the regime for both tribometers was mixed lubrication. From this work, the differences in widths between both tribometers are negligible as compared to those reported by Ofune *et al.* [115] for the same coating DLC (a: C-H). This implies that the results obtained from MTM are more realistic than those obtained from PoP.

Fig. 9-4 also shows the friction analysis for both tribometers as a function of MoDTC. It is worth mentioning that adding MoDTC in both tribometers has helped to reduce the friction in the system. MoDTC additive contains Mo-S compounds; these compounds form MoS₂ low friction sheets on the tribological contact [112, 188-191].

9.9.1.2 Wear Performance

Fig. 9-5 shows the wear comparison between both tribometers when lubricated with MoDTC additive (i.e. O5) and without MoDTC additive (i.e. O3). The same methodology was used for comparing the wear performance under both tribometers (i.e. the SCR wear depth was calculated as the average of the three tappet thicknesses while the MTM wear depth was reported as the average of pure sliding and sliding/rolling contacts).

From Fig. 9-5, it can be seen that CI camlobes experienced lower wear than CI discs. This is in a partial agreement to those obtained by [115], where they found that the highest wear was observed with the PoP (i.e. the wear was more severe on the pins than the camlobes). However, DLC shim showed higher wear than DLC balls. Also, from this work, the differences in widths between the disc and camlobe were generally more than those observed between the pin and the camlobe [115]. This could be due to the difference in the oil formulations that used in both studies. From Fig. 9-5, although longer test duration (80 hrs) was carried out in the SCR and this in turn might help to

increase wear as compared to a shorter test duration (6:30 hrs) that performed on the MTM tribometer, the highest wear depth was observed on the CI disk while the lowest wear was observed on the DLC ball.

Fig. 9-5 also shows the effect of MoDTC on wear performance for both tribometers. It can be seen that MoDTC promoted high wear on CI camlobe/DLC shim tribopair. Similar trend was reported in some literature [221, 226-230], where DLC coatings wear faster in the presence of MoDTC when rubbed against a ferrous counterpart. For MTM tribometer, however, DLC coated balls and CI disks showed relatively low wear when MoDTC was present in the oil formulation. Similar findings were reported by Tung *et al.* [269], where MoDTC was found to reduce wear of a DLC coating in a formulated engine oil.

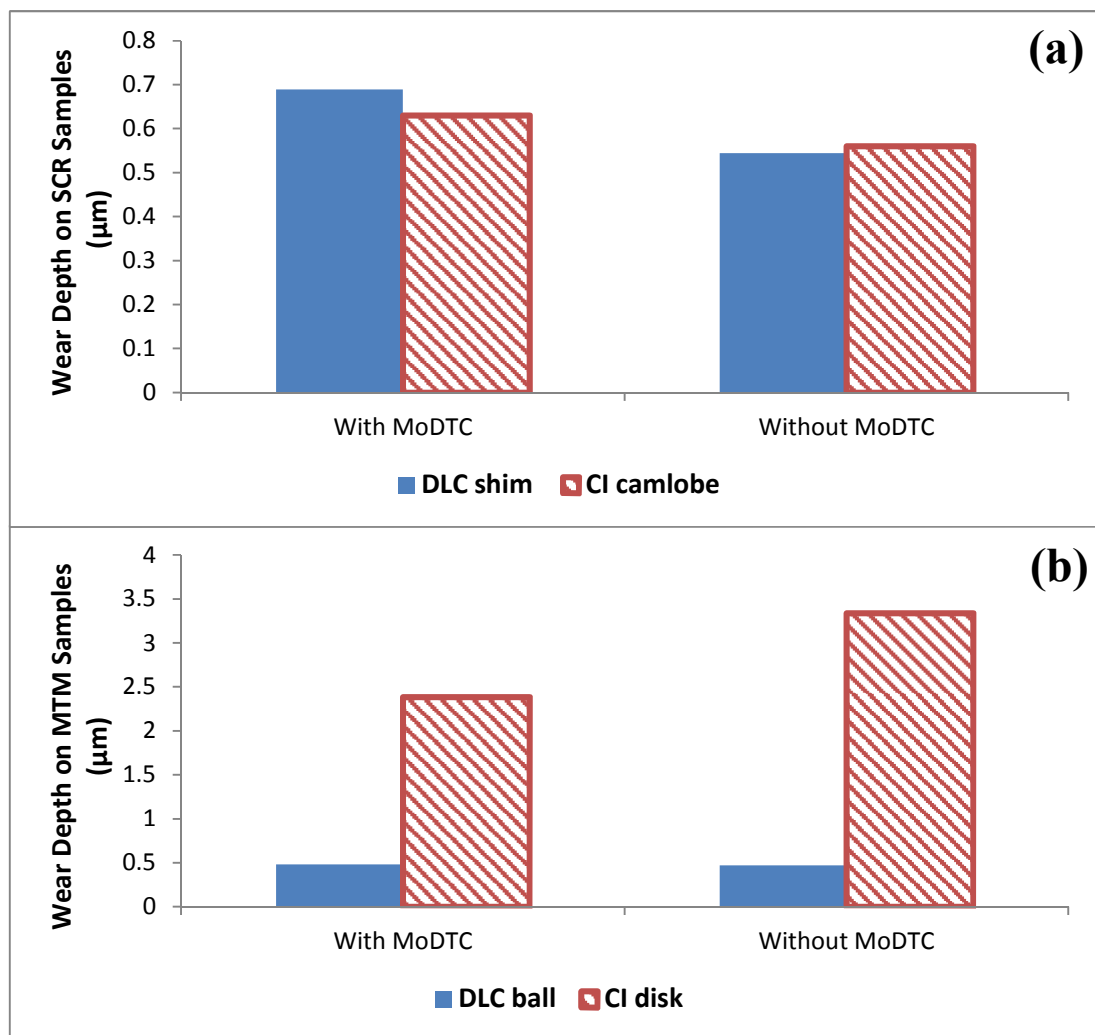
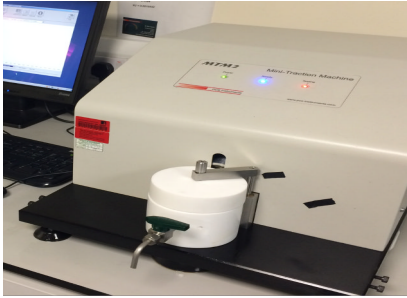
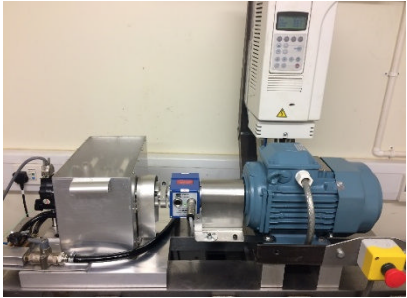


Figure 9-5 Wear analysis as a function of MoDTC for (a) SCR tribometer (b) MTM tribometer (note different scales)

9.9.2 Tribochemical Comparison

The comparison of the tribofilm from mini traction machine and single cam rig tribometers can be summarised as shown in Table 9-3.

Table 9-3 Showing the comparison of the tribofilm from mini traction machine and single cam rig tribometers when lubricated in a lubricant containing MoDTC and ZDDP (i.e. O5)

Mini Traction Machine tribometer		Single Cam Rig Tribometer	
			
Insert/Surface Coating	Tribofilm	Insert/Surface Coating	Tribofilm
CI Disks	Films composed of calcium phosphate, FeMoO ₄ , MoS ₂ , Fe ₂ O ₃ , Fe ₃ O ₄ , ZnS and P	CI Camlobes	Films composed of calcium phosphate, MoO ₃ , MoS ₂ , Fe ₂ O ₃ , ZnS and P
DLC Coated Balls	Films composed of calcium phosphate, FeMoO ₄ , MoS ₂ , ZnS and P	DLC Coated Shims	Films composed of calcium phosphate, CrC, MoO ₃ , MoS ₂ , ZnS and P
The tribofilm varies with changing the type of contact and the oil formulation.		The tribofilm varies as a function of tappet thickness, cam profile and oil formulation.	
The tribofilm formed on the CI discs was thicker than the tribofilms formed on the DLC balls.		The thickness of the tribofilm formed on the MnPO ₄ insert and the camlobe rubbed against MnPO ₄ insert is lower than those observed on the camlobe rubbed against DLC insert and the DLC insert.	

As can be seen, although the SCR tests are much longer than MTM tests, the tribofilm formed on both tribometers are fairly similar. This is in a partial agreement with the findings obtained by Ofune *et al.* [115]. From this study, there were two major differences between both tribometers. Firstly, as molybdenum in MoO₃ and FeMoO₄ have the same oxidation state (+6), it is impossible to distinguish the two compounds from the XPS analysis, due to overlapping peaks [201]. Nonetheless, Raman spectroscopy was used to distinguish between MoO₃ and FeMoO₄ [202, 203]. Therefore, unlike MTM tests, Mo 3d_{5/2} peaks that detected on the surface of SCR samples were due to the presence of MoO₃ and not FeMoO₄. Secondly, the tribofilm is dispersed differently based on the position of the tribofilm (i.e. the tribofilm were well dispersed at the centre of the camlobe/follower due to rubbing from cam flank/shoulder/ramp and nose). It is also worth mentioning that the tribofilms that formed on camlobes have relatively offered similar distribution like the pure sliding contact obtained on the mini traction machine tribometer.

9.10.Optimising Friction and Wear

Initially, six lubricant formulations were used in the MTM tribometer. It was observed that the fully formulated lubricant containing MoDTC and ZDDP (i.e. O5) exhibited the lowest friction and lowest wear among all other oil formulations. This is mainly due to the synergy between MoDTC and ZDDP. Compared with O3 (i.e. the lubricant contained ZDDP, not MoDTC), the fully formulated oil that composed of MoDTC and ZDDP (i.e. O5) showed a 30-43 % reduction range in friction. This is in agreement with the literature [112, 197, 204, 205], where MoDTC and ZDDP are reported to be more effective when used together.

According to Ofune *et al.* [115], a well-designed test in a valvetrain rig can offer a huge monetary savings. The friction responses obtained from valvetrain rigs are reported to be very similar to those observed in fired tests [282], especially at low speed, constant and cyclic test conditions [283]. For SCR tests, the DLC coating offered low friction and low wear when compared with MnPO₄ coating. The DLC coating was used to achieve 5-36% reduction

in friction (over the entire engine speed tested) when compared with MnPO_4 coating. These results are in line with the works of [110, 115, 284, 285]. This in return indicates a fuel saving effect. Using the same scale from a work of [285], a 0.5-1.6 % fuel economy can be estimated when the inserts are coated with DLC.

In terms of oil formulation, two lubricants (i.e. O3 and O5) were used in SCR tests. Comparing O5 (with MoDTC) to O3 (without MoDTC), a 3-35 % reduction range in friction was experienced over the speeds tested when lubricated with MoDTC additive. These benefits are in line with those obtained from MTM tribometer and also with those from the literature. A 0.3-1.7 % fuel economy can be achieved with O5.

In terms of tappet clearance, the thicker tappet (i.e. 2.75 mm) showed more friction and wear as compared to 2.575 mm tappet thickness. In fact, an 18-27 % increase in friction range was reported with the thicker tappet. This in turn implies a negative effect on fuel economy. Tappet with thickness of 2.275 mm showed the lowest friction and lowest wear among the three thicknesses. Compared to tappet thickness of 2.575 mm, a 10-15 % reduction in friction range was achieved for tappet thickness of 2.275 mm. However, during the tests, tappet with thickness of 2.275 mm showed higher vibration, more noise and possible more wear for longer test durations as compared to 2.275 mm tappet thickness.

As a result, tappet with thickness of 2.575 mm is considered to provide the better tribological performance. A representative diagram showing a summary of the optimum performance that observed from both tribometers is shown in Fig. 9-6.

Based on the results, it is understood that the tests obtained from both tribometers are crucial to provide better understating of valvetrain systems in terms of oil formulation and coating performance, tappet rotation and tappet thickness. This in return would lead to the ability of developing the real engines and the ability of avoiding any failure that could possibly occur on engine components.

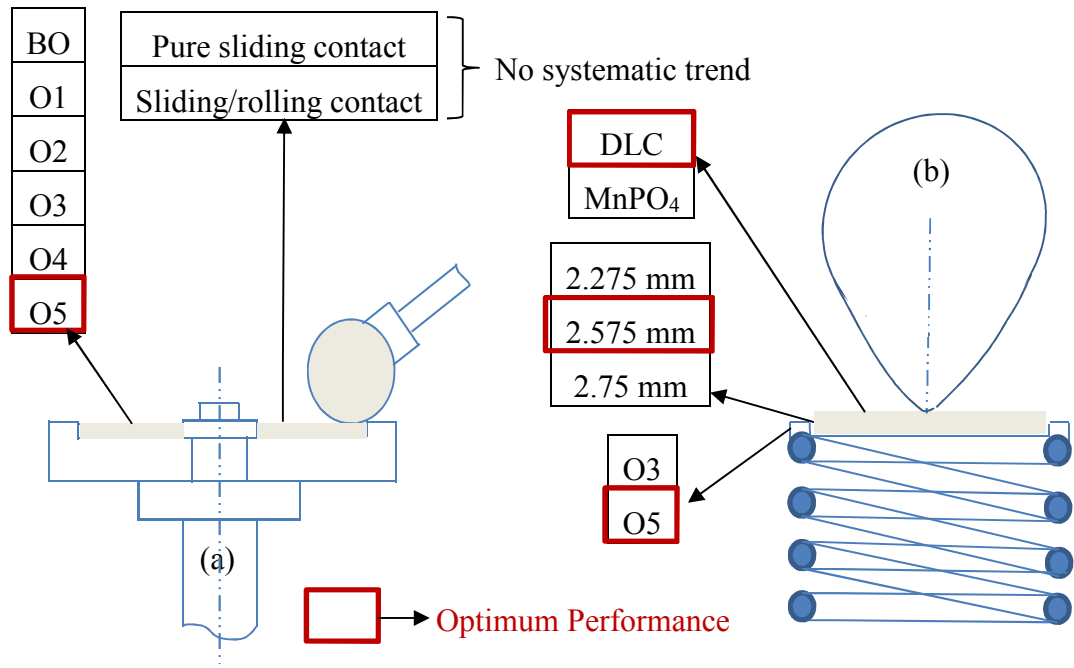


Figure 9-6 2D schematic diagram showing the optimum performance for (a) MTM and (b) SCR

Chapter 10. Conclusions and Future Work

10.1. Introduction

The work presented in this thesis has been concerned with both single cam rig (SCR) tribometer and mini traction machine (MTM) tribometer studies under the presence and absence of MoDTC friction modifier. The MTM tribometer has included six oil formulations and two types of contacts (i.e. pure sliding contact and sliding/rolling contact). The SCR tribometer has included four stages. These stages were different in type of coating (i.e. MnPO_4 and DLC) and oil formulation (i.e. with and without MoDTC). In addition, measuring tappet rotation was one of the novel contributions of this thesis. Furthermore, the link between both tribometers were also addressed.

10.2. Overall Conclusions

10.2.1 Mini Traction Machine (MTM)

- The tribological and tribochemical performance of DLC/cast iron system was mainly controlled by the oil formulation and the contact type.
- Pure sliding contact was found to enhance MoDTC activation. In other words, the sliding/rolling ratio affects the tribological and tribochemical performance of CI/DLC systems.
- Friction coefficients values were reported to differ across the boundary lubrication regime. This is however unlike most of modelling works which assume a constant value for coefficient of friction.
- Surface roughness did not play an essential role in friction reduction. Although rougher surfaces were reported for both tribopair after the test, reduction in friction was seen for most balls and discs under both contacts. This confirms that the tribological performance is more controlled by the contact type and the tribofilm formed on the ball/disc tribopair rather than the surface roughness.

- MoS₂ and FeMoO₄ (but not MoO₃) are the main decomposition products for MoDTC. FeMoO₄ was identified as the reaction species which is possibly responsible for the high friction as opposed to MoO₃.
- Tribofilm build-up links to the sliding/rolling ratio (SRR). The DLC ball lubricated in base oil containing MoDTC (i.e. O1) was consisted of MoS₂ and FeMoO₄ under pure sliding contact while only FeMoO₄ was detected under sliding/rolling contact. In addition, for pure sliding contact, Zn 2p and P 2p were observed on the DLC ball lubricated in the presence of ZDDP additive (i.e. O3 and O5) while no such compounds were detected on the DLC ball under sliding/rolling contact. All these variations justified the friction and wear results obtained.
- The ratio between MoS₂/FeMoO₄ played a key role in the tribological performance of the CI discs. MoS₂/ FeMoO₄ for CI discs lubricated in the presence of MoDTC additive (i.e. O1, O4 and O5) was higher under pure sliding contact as compared with sliding/rolling contact. This justifies the obtained friction results.
- For both contacts (i.e. sliding/rolling and pure sliding), no lubricants show extremely high wear on DLC coating. Also, as all DLC balls have showed thinner films compared to CI discs, the tribofilms were hard to be detected by Raman technique.

10.2.2 Single Cam Rig (SCR)

- The novel technique developed in the current work facilities evaluation of tappet rotational speed under different temperatures, coatings and thicknesses.
- Tappet rotation is controlled by the following factors in order of impact; clearance between the camlobe and the tappet (i.e. coating thickness), temperature and speed as well as surface roughness of the tappet or type of coating.
- The thickest tappets showed high rotation, implying that the tribological performance is more controlled by the clearance rather

than the type of coating or tappet rotation. However, for the third stage and fourth stage, tappets with thickness of 2.575 mm showed higher rotation.

- A higher tappet rotation was observed when lubricated with fully formulated oil containing 1wt % MoDTC, suggesting that MoS₂ sheets led to a more conformity of the cam/follower surfaces which then helped in increasing the rotation of the tappet.
- The tappet rotation for DLC inserts was higher than the inserts coated with MnPO₄. This in return helped in reducing friction and increasing the anti-wear properties of the DLC inserts.
- In terms of friction and wear, the thicker tappet in the first stage and second stage resulted in higher friction and wear, suggesting a high interaction between the cam/follower tribopair with increasing tappet thickness. Although less friction and wear was achieved using tappets with thickness of 2.275 mm, noisy running was observed. This possibly can cause an increase in the valvetrain wear for longer test durations.
- The tappet with thickness of 2.575 mm in the third stage and fourth stage resulted in lower friction and wear as compared to other thicknesses.
- Tappet with thickness of 2.575 mm (0.285 mm clearance) might be considered the best selection among the three thicknesses. This thickness showed less friction and wear as compared to 2.75 mm tappet thickness. Furthermore, it showed lower vibration, less noise and reduced wear for longer test durations as compared to 2.275 mm tappet thickness.
- Adding MoDTC to the lubricant helped in friction reduction for all stages but it was one of the main reason to promote high wear rate on the surface.
- Two locations in camlobe (cam nose and 4°) are found to be a region of significant wear. In addition, the selected seven locations showed the highest wear while the wear of the other locations was not considerable.

- The tribofilm derived from camlobes and tappets were seen to be varied as a function of tappet clearance and cam profile.
- DLC inserts showed a smoother surface, supporting a polishing wear. However, this process was not reported on the DLC insert with thickness of 2.275 mm. For all MnPO₄ inserts, however, the surface appears fairly rough (R_a is about 0.47 μm for the thinnest tappet and 1.7 μm for the thickest tappet) compared to MnPO₄ insert before test (R_a 0.25 μm). The surface was consisting of ridges/grooves on the surface of the insert. This is equally supporting an abrasive wear process for MnPO₄ inserts.
- For the third stage and fourth stage, polishing process was only observed on the DLC insert with thickness of 2.75 mm while an abrasive wear process was seen on all MnPO₄ inserts.
- Inside the wear track, higher MoS₂ peak intensity was observed as tappet thickness increases which could indicate more MoS₂ film formed inside the wear track. Suggesting a higher pressure at the interface (for higher tappet thickness) resulting in an enhanced MoDTC decomposition.
- O5 produced a very thin film at the cam nose while thick tribofilm was formed at the cam flank (both sides). For all tappets, thinner film was detected at the centre of the inserts compared to several spots near the edge of the insert.
- O3 also produced a thin film at the centre of the inserts while thick tribofilm was formed at different areas near the insert edge. For the camlobes, however, the thickness of the tribofilm was relatively comparable across the camlobe, namely on the nose and the cam flank (both sides).
- The thickness of the tribofilm (under the presence of MoDTC) formed on the camlobe rubbed against MnPO₄ (32-43 nm) insert and the MnPO₄ insert (48-49 nm) is lower than those observed on the camlobe rubbed against DLC insert (38-58 nm) and the DLC insert (51-67 nm).

- The thickness of the tribofilm (under the absence of MoDTC) formed on the camlobe rubbed against MnPO₄ (45-62 nm) insert is higher than those observed on the camlobe rubbed against DLC insert (40-45 nm). For the tappets, the tribofilm formed on the DLC insert is thicker than the tribofilm formed on the Mn-phosphate (MnPO₄) insert.
- The results obtained from SCR tribometer closely support those in the MTM tribometer. It was reported that the average friction and wear results were comparable for both tribometers. The tribofilm formed on both tribometers are quite similar. However, For MTM tribometer, Mo 3d_{5/2} peaks that detected on the surface were due to the presence of FeMoO₄ and not MoO₃.

10.3.Suggestions for Future Work

Some suggestions are proposed to continue in the field of this research:

- It is recommended to repeat the same methodology used in the MTM tribometer but with steel/steel interface. That would provide more information about sliding/rolling ratio, friction, wear and tribochemistry in steel/steel systems. Further tests should also be carried at different coating, surface roughness and hardness to provide a better insight on how these factors affect the tribological performance of CI/DLC and steel/steel systems.
- Single cam rig development can be made by adding some modifications to the rig and its components. This in return would improve the tribological and tribochemical understanding of the system.
- It is suggested to develop new friction modifiers and/or apply organic friction modifiers to replace the MoDTC. This would provide low friction and controllable wear with environmentally friendly additives.
- The obtained results in this work are only valid for a-C: 15H coating and MnPO₄ coating. Applying different types of DLC or using DLC with varying degrees of hydrogenation, to be more compatible with

current Mo additive technology, could lead to an optimised DLC coated system with an optimum tribological performance.

- Modelling of the single cam rig tribology (i.e. friction and wear models) is crucial. In order to build an accurate friction and wear models, focusing on the tribochemical films is also essential. Based on the literature, limited studies were found regarding the development of tribochemistry models. Ghanbarzadeh *et al.* [286] developed a tribofilm growth model based on local properties of contact on rough surfaces. This model can consider the effect of antiwear tribofilm on the localised wear of boundary lubricated systems. In addition, Bosman and Schipper [287] also evaluated the growth of the tribofilm and its removal using a diffusion reaction. However, further models can be developed to give a better simulation for valvetrain tribochemistry.
- In the present research, the developed technique for measuring tappet rotation was proved to provide a good comparison and repeatability of results and can be considered to be an important research tool for engine manufacturers. Therefore, this technique can be used to evaluate different coatings, oil formulations and materials. Also, some theoretical contents and/or theoretical validation are recommended for future work, such as mathematic model and theoretical arithmetic.
- Controlling tappet rotation is one of the main aspects in the current work. However, this aspect is not accomplished, mainly due to time constraints. Future studies should therefore focus on controlling tappet rotation, which could be achieved by modifying the single cam rig (for example, applying a mechanical system on the rig in order to control tappet rotation). Essentially, controlling tappet rotation means the ability of changing the rotation of tappet at any time (such as the ability to increase the rotation at low speeds and decrease it at high speeds). This in return help to reduce wear and friction of valvetrain systems. Further studies can also be focused on the effect of tribochemistry on tappet rotation.

List of References

- [1] "Climate Change Act 2008. (c.27). London. Parliament of the United Kingdom," 26/11/2008 2008.
- [2] "Low Carbon Vehicles-Driving the UK's Transport Revolution. Report published by the I.Mech.E.," 25th May 2009.
- [3] J. Durham and A. Kidson, "The effects of low sulfated ash, phosphorus and sulfur oils on camshaft/tappet tribocouples with various diamond-like-carbon coated tappets in motored and fired engines," *Lubrication Science*, vol. 26, pp. 411-427, 2014.
- [4] K. Holmberg, P. Andersson, and A. Erdemir, "Global energy consumption due to friction in passenger cars," *Tribology International*, vol. 47, pp. 221-234, 3// 2012.
- [5] B. Andersson, "Paper XVIII (iii) Company Perspectives in Vehicle Tribology-Volvo," *Tribology Series*, vol. 18, pp. 503-506, 1991.
- [6] C. M. Taylor, *Engine tribology* vol. 26: Elsevier, 1993.
- [7] F. Mariasiu, "EFFECTS OF LUBRICATING OIL CHARACTERISTICS ON VALVE TRAIN SYSTEM FRICTION LOSSES," *Research Journal of Agricultural Science*, vol. 44, pp. 281-288, 2012.
- [8] T. E. Kiovsky, N. C. Yates, and J. R. Bales, "Fuel efficient lubricants and the effect of special base oils," *Lubrication engineering*, vol. 50, 1994.
- [9] A. Gangopadhyay and D. G. McWatt, "The Effect of Novel Surface Textures on Tappet Shims on Valvetrain Friction and Wear," *Tribology Transactions*, vol. 51, pp. 221-230, 2008/03/25 2008.
- [10] J. E. Booth, T. J. Harvey, R. J. K. Wood, and H. E. G. Powrie, "Scuffing detection of TU3 cam-follower contacts by electrostatic charge condition monitoring," *Tribology International*, vol. 43, pp. 113-128, 2010.
- [11] C. Taylor, "Automobile engine tribology—design considerations for efficiency and durability," *Wear*, vol. 221, pp. 1-8, 1998.

- [12] R. C. Coy, "Practical applications of lubrication models in engines1," *Tribology International*, vol. 31, pp. 563-571, 10// 1998.
- [13] C. Taylor, "Fluid film lubrication in automobile valve trains," *Proceedings of the Institution of Mechanical Engineers, Part J: Journal of Engineering Tribology*, vol. 208, pp. 221-234, 1994.
- [14] A. Comfort, "An introduction to heavy-duty diesel engine frictional losses and lubricant properties affecting fuel economy-Part I," *SAE Technical Paper 0148-7191*, 2003.
- [15] K. Mistry, A. Morina, and A. Neville, "Single cam tribometer for evaluating tribological parameters and tribochemistry of DLC coated valve train follower," *Tribology-Materials, Surfaces & Interfaces*, vol. 6, pp. 31-37, 2012.
- [16] M. Priest, "Introducion to Tribology and real surfaces," vol. 1, pp. 1-76, 2011.
- [17] R. Wakelin, "Tribology: The friction, lubrication, and wear of moving parts," *Annual Review of Materials Science*, vol. 4, pp. 221-253, 1974.
- [18] D. M. Beloiu, "Modeling and Analysis of Valve Train, Part I- Conventional Systems," *SAE Technical Paper*2010.
- [19] H. Czichos, "Tribology. A systems approach to the science and technology of friction, lubrication and wear," *Elsevier Scientific Publishing Co.*, 1978, p. 414, 1978.
- [20] Z. Szeri Andras, "Fluid film lubrication: Theory and design," ed: *Cambridge University Press*, 1998.
- [21] T. Mang, K. Bobzin, and T. Bartels, *Industrial tribology: tribosystems, friction, wear and surface engineering, lubrication: John Wiley & Sons*, 2011.
- [22] S. Shaffer, "Tribology 101 – Introduction to the Basics of Tribology," *Bruker*2013.
- [23] D. Dowson and D. Dowson, *History of tribology: Longman London*, 1979.

- [24] J. R. Davis, Surface engineering for corrosion and wear resistance: ASM international, 2001.
- [25] G. Stachowiak and A. W. Batchelor, Engineering tribology: Butterworth-Heinemann, 2013.
- [26] P. D. H. Hirani, "Module 3, wear mechanisms," 2014.
- [27] A. Lansdown, Lubrication: a practical guide to lubricant selection: Elsevier, 2013.
- [28] M. Priest and C. M. Taylor, "Automobile engine tribology — approaching the surface," Wear, vol. 241, pp. 193-203, 7/31/ 2000.
- [29] B. J. Hamrock and D. Dowson, "Ball bearing lubrication: the elastohydrodynamics of elliptical contacts," 1981.
- [30] M. Niinomi, Metals for biomedical devices: Elsevier, 2010.
- [31] M. B. Peterson, W. O. Winer, and A. S. o. M. E. R. C. o. Lubrication, Wear Control Handbook: American Society of Mechanical Engineers, 1980.
- [32] J. P. Davim, Tribology in Manufacturing Technology: Springer, 2012.
- [33] R. S. Dwyer-Jouce, "Tribological design data," University of Sheffield, Institution on Mechanical Engineers, pp. 1-21, 1995.
- [34] B. J. Hamrock, S. R. Schmid, and B. O. Jacobson, Fundamentals of Fluid Film Lubrication: CRC Press, 2004.
- [35] "ATC Lubricant additives and the environment," vol. document 49 (revision 1), 2007.
- [36] R. M. Mortier and S. T. Orszulik. (1997). Chemistry and technology of lubricants. Available: <http://dx.doi.org/10.1007/978-94-017-1021-3>
- [37] G. E. Totten, S. Westbrook, and R. Shah, "Fuels and lubricants handbook: technology, properties, performance, and testing," Training, vol. 2007, pp. 08-21, 2003.
- [38] S. P. Srivastava, Advances in lubricant additives and tribology: Tech Books International, 2009.

- [39] B. Bhushan, *Modern Tribology Handbook, Two Volume Set*: Crc Press, 2000.
- [40] Z. Pawlak, *Tribochemistry of lubricating oils vol. 45*: Elsevier, 2003.
- [41] H. M. Wells and J. E. Southcombe, *The Theory and Practice of Lubrication: The "germ" Process*: Central House, 1920.
- [42] R. V. Kerley, "A history of aircraft piston engine lubricants," SAE Technical Paper 0148-7191, 1981.
- [43] G. C. Smith, "Surface analytical science and automotive lubrication," *Journal of Physics D: Applied Physics*, vol. 33, p. R187, 2000.
- [44] H. Spikes, "The history and mechanisms of ZDDP," *Tribology letters*, vol. 17, pp. 469-489, 2004.
- [45] L. R. Rudnick, *Lubricant additives: chemistry and applications*: CRC Press, 2009.
- [46] D. P. Wei, "Future directions of fundamental research in additive tribochemistry," *Lubrication Science*, vol. 7, pp. 211-232, 1995.
- [47] Q. Xue and W. Liu, "Tribochemistry and the development of AW and EP oil additives—a review," *Lubrication Science*, vol. 7, pp. 81-92, 1994.
- [48] M. De Barros, J. Bouchet, I. Raoult, T. Le Mogne, J. Martin, M. Kasrai, et al., "Friction reduction by metal sulfides in boundary lubrication studied by XPS and XANES analyses," *Wear*, vol. 254, pp. 863-870, 2003.
- [49] M. Ahmed Ali, H. Xianjun, L. Mai, C. Bicheng, R. Turkson, and C. Qingping, *Reducing Frictional Power Losses and Improving the Scuffing Resistance in Automotive Engines Using Hybrid Nanomaterials as Nano-Lubricant Additives vol. 364*, 2016.
- [50] R. S. Dwyer-Jouce, *Tribological design data*, University of Sheffiled, 1997.
- [51] K. Johnson, "Normal contact of elastic solids: Hertz theory," *Contact mechanics*, pp. 84-106, 1985.

- [52] S. Kosarieh, "Tribochemistry of boundary lubricated DLC/steel interfaces and their influence in tribological performance," Doctor of philosophy, School of mechanical engineering, Leeds University, 2013.
- [53] R. W. Bruce, Handbook of Lubrication and Tribology, Volume II: Theory and Design vol. 2: CRC Press, 2012.
- [54] D. Dowson, P. Harrison, C. Taylor, and G. Zhu, "Experimental observation of lubricant film state between a cam and bucket follower using the electrical resistivity technique," in Proceedings of the Japan international tribology conference, 1990, pp. 119-124.
- [55] R. Norton, Cam design and manufacturing handbook: Industrial Press, 2009.
- [56] R. Taylor and R. Coy, "Improved fuel efficiency by lubricant design: a review," Proceedings of the Institution of Mechanical Engineers, Part J: Journal of Engineering Tribology, vol. 214, pp. 1-15, 2000.
- [57] S. Korcek, J. Sorab, M. Johnson, and R. Jensen, "Automotive lubricants for the next millennium," Industrial Lubrication and tribology, vol. 52, pp. 209-220, 2000.
- [58] Y. Wang, Introduction to Engine Valvetrains: SAE International, 2007.
- [59] S. C. Tung and M. L. McMillan, "Automotive tribology overview of current advances and challenges for the future," Tribology International, vol. 37, pp. 517-536, 7// 2004.
- [60] T. Gilles, Automotive Engines: Diagnosis, Repair, Rebuilding: Cengage Learning, 2010.
- [61] I.-S. Suh and R. H. Lyon, "An investigation of valve train noise for the sound quality of IC engines," SAE Technical Paper 0148-7191, 1999.
- [62] A. Gangopadhyay, E. Soltis, and M. D. Johnson, "Valvetrain friction and wear: Influence of surface engineering and lubricants," Proceedings of the Institution of Mechanical Engineers, Part J: Journal of Engineering Tribology, vol. 218, pp. 147-156, 2004.

- [63] T. Kanzaki, N. Hara, A. Mori, and K. Ohtsubo, "Advantage of lightweight valve train component on engines," SAE Technical Paper 0148-7191, 1998.
- [64] A. Gangopadhyay, D. Mc Watt, P. Willermet, G. M. Crosbie, and R. L. Allor, "Effects of Composition and Surface Finish of Silicon Nitride Tappet Inserts on Valvetrain Friction," in Tribology Series. vol. Volume 36, M. P. C. M. T. P. E. T. H. C. C. G. D. Y. B. L. F. J. M. G. D. Dowson and A. A. Lubrecht, Eds., ed: Elsevier, 1999, pp. 635-644.
- [65] A. K. Gangopadhyay, R. CARTER III, S. Simko, H. Gao, K. Bjornen, and E. Black, "Valvetrain friction and wear performance with fresh and used low-phosphorous engine oils," Tribology Transactions, vol. 50, pp. 350-360, 2007.
- [66] R. A. Mufti and M. Priest, "Experimental and theoretical study of instantaneous engine valve train friction," Journal of tribology, vol. 125, pp. 628-637, 2003.
- [67] N. Nayak, P. A. Lakshminarayanan, M. K. G. Babu, and A. D. Dani, "Predictions of cam follower wear in diesel engines," Wear, vol. 260, pp. 181-192, 1// 2006.
- [68] H. A. Rothbart and D. L. Klipp, Cam design handbook vol. 394: McGraw-Hill New York, 2004.
- [69] Y. Enomoto and T. Yamamoto, "New materials in automotive tribology," Tribology Letters, vol. 5, pp. 13-24, 1998.
- [70] T. S. Eyre, R. F. Iles, and D. W. Gasson, "Wear characteristics of flake and nodular graphite cast iron," Wear, vol. 13, pp. 229-245, 1969/04/01 1969.
- [71] S. Jahanmir, "Examination of wear mechanisms in automotive camshafts," Wear, vol. 108, pp. 235-254, 1986/04/01 1986.
- [72] E. P. Becker, "Trends in tribological materials and engine technology," Tribology International, vol. 37, pp. 569-575, 7// 2004.
- [73] A. Dyson, "Scuffing - a review," Tribology International, vol. 8, pp. 77-87, 1975/04/01 1975.

- [74] M. Kano and I. Tanimoto, "Wear mechanism of high wear-resistant materials for automotive valve trains," *Wear*, vol. 151, pp. 229-243, 1991/12/20 1991.
- [75] A. Gangopadhyay, K. Sinha, D. Uy, D. G. McWatt, R. J. Zdrodowski, and S. J. Simko, "Friction, wear, and surface film formation characteristics of diamond-like carbon thin coating in valvetrain application," *Tribology Transactions*, vol. 54, pp. 104-114, 2010.
- [76] M. Ofune, P. Banks, A. Morina, and A. Neville, "Development of valve train rig for assessment of cam/follower tribochemistry," *Tribology International*, vol. 93, pp. 733-744, 2015.
- [77] A. Neville, A. Morina, T. Haque, and M. Voong, "Compatibility between tribological surfaces and lubricant additives—How friction and wear reduction can be controlled by surface/lube synergies," *Tribology International*, vol. 40, pp. 1680-1695, 10// 2007.
- [78] J. Michalski, J. Marszalek, and K. Kubiak, "An experimental study of diesel engine cam and follower wear with particular reference to the properties of the materials," *Wear*, vol. 240, pp. 168-179, 5// 2000.
- [79] M. Kano and Y. Kimura, "Quantitative analysis of cam follower wear in relation to various material properties," *Wear*, vol. 162–164, Part B, pp. 897-905, 4/13/ 1993.
- [80] K. Kitamura, H. Takebayashi, M. Ikeda, and H. M. Percoulis, "Development of ceramic cam roller follower for engine application," *SAE Technical Paper*1997.
- [81] J. Braza, R. Licht, and E. Lilley, "Ceramic cam roller follower simulation tests and evaluation," *Tribology transactions*, vol. 35, pp. 595-602, 1992.
- [82] S. Fukuoka, N. Hara, A. Mori, and K. Ohtsubo, "Friction loss reduction by new lighter valve train system," *JSAE Review*, vol. 18, pp. 107-111, 4// 1997.
- [83] T. Hasegawa, *Tribology Research Trends*: Nova Science Publishers, 2008.

- [84] S. C. Cha and A. Erdemir, *Coating Technology for Vehicle Applications*: Springer, 2015.
- [85] A. Gangopadhyay, D. G. McWatt, R. J. Zdrodowski, S. J. Simko, S. Matera, K. Sheffer, et al., "Valvetrain friction reduction through thin film coatings and polishing," *Tribology transactions*, vol. 55, pp. 99-108, 2012.
- [86] B. J. Taylor and T. S. Eyre, "A review of piston ring and cylinder liner materials," *Tribology International*, vol. 12, pp. 79-89, 1979/04/01 1979.
- [87] P. Kodali, K. Walter, and M. Nastasi, "Investigation of mechanical and tribological properties of amorphous diamond-like carbon coatings," *Tribology international*, vol. 30, pp. 591-598, 1997.
- [88] H. Ronkainen, S. Varjus, and K. Holmberg, "Friction and wear properties in dry, water-and oil-lubricated DLC against alumina and DLC against steel contacts," *Wear*, vol. 222, pp. 120-128, 1998.
- [89] C. Donnet and A. Grill, "Friction control of diamond-like carbon coatings," *Surface and Coatings Technology*, vol. 94–95, pp. 456-462, 10// 1997.
- [90] M. I. de Barros'Bouchet, J. M. Martin, T. Le-Mogne, and B. Vacher, "Boundary lubrication mechanisms of carbon coatings by MoDTC and ZDDP additives," *Tribology International*, vol. 38, pp. 257-264, 3// 2005.
- [91] J. Fontaine, C. Donnet, A. Grill, and T. LeMogne, "Tribochemistry between hydrogen and diamond-like carbon films," *Surface and Coatings Technology*, vol. 146–147, pp. 286-291, 9// 2001.
- [92] A. Gangopadhyay, R. Zdrodowski, and S. Simko, "Interactions of diamond-like carbon coatings with fully formulated engine oils," *Tribology Transactions*, vol. 57, pp. 503-514, 2014.
- [93] S. Lawes, M. Fitzpatrick, and S. V. Hainsworth, "Evaluation of the tribological properties of DLC for engine applications," *Journal of Physics D: Applied Physics*, vol. 40, p. 5427, 2007.
- [94] T. Eyre and B. Crawley, "Camshaft and cam follower materials," *TRIBOLOGY international*, vol. 13, pp. 147-152, 1980.

- [95] C. M. Taylor, "Paper VI (i) Valve Train Lubrication Analysis," in Tribology Series. vol. Volume 18, C. M. T. D. Dowson and M. Godet, Eds., ed: Elsevier, 1991, pp. 119-131.
- [96] T. Haque, A. Morina, A. Neville, R. Kapadia, and S. Arrowsmith, "Non-ferrous coating/lubricant interactions in tribological contacts: assessment of tribofilms," Tribology International, vol. 40, pp. 1603-1612, 2007.
- [97] J. Burnell-Gray and P. K. Datta, Surface Engineering Casebook: Solutions to Corrosion and Wear-related Failures: Elsevier, 1996.
- [98] M. Nakada, "Special Issue Tribology for Automobiles in Japan Trends in engine technology and tribology," Tribology International, vol. 27, pp. 3-8, 1994/02/01 1994.
- [99] D. Sandoval and J. B. Heywood, "An improved friction model for spark-ignition engines," SAE Technical paper 0148-7191, 2003.
- [100] A. Dyson and H. Naylor, "Application of the flash temperature concept to cam and tappet wear problems," Proceedings of the Institution of Mechanical Engineers: Automobile Division, vol. 14, pp. 255-280, 1960.
- [101] M. Masuda, M. Ujino, K. Shimoda, K. Nishida, I. Marumoto, and Y. Moriyama, "Development of titanium nitride coated shim for a direct acting OHC engine," SAE Technical Paper 0148-7191, 1997.
- [102] J. Pieprzak, P. Willermet, and D. Dailey, "Experimental evaluation of tappet/bore and cam/tappet friction for a direct acting bucket tappet valvetrain," SAE Technical Paper1990.
- [103] J. Bell, "Reproducing the kinematic conditions for automotive valve train wear in a laboratory test machine," Proceedings of the Institution of Mechanical Engineers, Part J: Journal of Engineering Tribology, vol. 210, pp. 135-144, 1996.
- [104] A. Katoh and Y. Yasuda, "An analysis of friction reduction techniques for the direct-acting valve train system of a new-generation lightweight 3-Liter V6 Nissan engine," SAE Technical Paper1994.

- [105] M. Wakuda, Y. Yamauchi, S. Kanzaki, and Y. Yasuda, "Effect of surface texturing on friction reduction between ceramic and steel materials under lubricated sliding contact," *Wear*, vol. 254, pp. 356-363, 2// 2003.
- [106] A. Ronen, I. Etsion, and Y. Kligerman, "Friction-reducing surface-texturing in reciprocating automotive components," *Tribology Transactions*, vol. 44, pp. 359-366, 2001.
- [107] G. Ryk, Y. Kligerman, and I. Etsion, "Experimental investigation of laser surface texturing for reciprocating automotive components," *Tribology Transactions*, vol. 45, pp. 444-449, 2002.
- [108] F. Svahn, Å. Kassman-Rudolphi, and E. Wallén, "The influence of surface roughness on friction and wear of machine element coatings," *Wear*, vol. 254, pp. 1092-1098, 10// 2003.
- [109] H. Izumida, T. Nishioka, A. Yamakawa, and M. Yamagiwa, "A Study of the Effects of Ceramic Valve Train Parts on Reduction of Engine Friction," SAE Technical Paper1997.
- [110] M. Kano, "Super low friction of DLC applied to engine cam follower lubricated with ester-containing oil," *Tribology International*, vol. 39, pp. 1682-1685, 12// 2006.
- [111] A. Schamel, M. Grischke, and R. Bethke, "Amorphous carbon coatings for low friction and wear in bucket tappet valvetrains," SAE Technical Paper 0148-7191, 1997.
- [112] A. Morina, A. Neville, M. Priest, and J. H. Green, "ZDDP and MoDTC interactions and their effect on tribological performance – tribofilm characteristics and its evolution," *Tribology Letters*, vol. 24, pp. 243-256, 2006.
- [113] S. Kosarieh, A. Morina, E. Lainé, J. Flemming, and A. Neville, "Tribological performance and tribochemical processes in a DLC/steel system when lubricated in a fully formulated oil and base oil," *Surface and Coatings Technology*, vol. 217, pp. 1-12, 2013.

- [114] E. Ciulli, B. Piccigallo, and D. Vela, Experimental study of engine cam-followers, 2009.
- [115] M. A. Ofune, "Development of Single Cam Rig for Accurate Simulation of Valve Train Tribochemistry," University of Leeds, 2016.
- [116] M. T. Costello, "Effects of basestock and additive chemistry on traction testing," Tribology Letters, vol. 18, pp. 91-97, 2005.
- [117] P. Vergne, "Super low traction under EHD and mixed lubrication regimes," Superlubricity, pp. 429-445, 2007.
- [118] J. A. Brandao, M. Meheux, J. H. Seabra, F. Ville, and M. Castro, "Traction curves and rheological parameters of fully formulated gear oils," Proceedings of the Institution of Mechanical Engineers, Part J: Journal of Engineering Tribology, vol. 225, pp. 577-593, 2011.
- [119] D. N. Khaemba, F. Jarnias, B. Thiebaut, A. Neville, and A. Morina, "The role of surface roughness and slide-roll ratio on the decomposition of MoDTC in tribological contacts," Journal of Physics D: Applied Physics, vol. 50, p. 085302, 2017.
- [120] E. Ciulli, K. Stadler, and T. Draexl, "The influence of the slide-to-roll ratio on the friction coefficient and film thickness of EHD point contacts under steady state and transient conditions," Tribology International, vol. 42, pp. 526-534, 2009.
- [121] M. Meheux, C. Minfray, F. Ville, T. L. Mogne, A. Lubrecht, J.-M. Martin, et al., "Influence of slide-to-roll ratio on tribofilm generation," Proceedings of the Institution of Mechanical Engineers, Part J: Journal of Engineering Tribology, vol. 222, pp. 325-334, 2008.
- [122] Y. Shimizu and H. A. Spikes, "The influence of slide-roll ratio on ZDDP tribofilm formation," Tribology Letters, vol. 64, p. 19, 2016.
- [123] E. Lainé, A. Olver, M. Lekstrom, B. Shollock, T. Beveridge, and D. Hua, "The effect of a friction modifier additive on micropitting," Tribology Transactions, vol. 52, pp. 526-533, 2009.
- [124] B. Vengudusamy, A. Grafl, F. Novotny-Farkas, and W. Schöfmann, "Comparison of frictional properties of gear oils in boundary and mixed

lubricated rolling–sliding and pure sliding contacts," *Tribology International*, vol. 62, pp. 100-109, 2013.

- [125] J. Bell and P. Willemse, "Mid-life scuffing failure in automotive cam-follower contacts," *Proceedings of the Institution of Mechanical Engineers, Part J: Journal of Engineering Tribology*, vol. 212, pp. 259-269, 1998.
- [126] P. Purmer and W. Van den Berg, "Measurement of camshaft wear—Wear and kinematics of overhead camshafts," *SAE Technical Paper1985*.
- [127] E. W. Schneider and D. H. Blossfeld, "Real-Time Measurement of Camshaft Wear in an Automotive Engine—a Radiometric Method," *SAE Technical Paper 0148-7191*, 1990.
- [128] H. Shaub and L. Wong, "A real time radioactive marker technique for measuring valve train wear," *SAE Technical Paper1987*.
- [129] T. Kosako and K. Nishimura, "The thin layer activation technique applied to the on-line iron wear measurement of an engine cam nose," *Nuclear Instruments and Methods in Physics Research Section B: Beam Interactions with Materials and Atoms*, vol. 56, pp. 900-903, 1991/05/01 1991.
- [130] R. İpek and B. Selcuk, "The dry wear profile of cam shaft," *Journal of Materials Processing Technology*, vol. 168, pp. 373-376, 10/15/ 2005.
- [131] A. Gauthier and T. Delvigne, "Soot induced cam wear in diesel engines: An investigation using thin layer activation," *SAE Technical Paper 0148-7191*, 2000.
- [132] G. Roper and J. Bell, "Review and evaluation of lubricated wear in simulated valve train contact conditions," *SAE Technical Paper1995*.
- [133] A. Ito, L. Yang, and H. Negishi, "A study on cam wear mechanism with a newly developed friction measurement apparatus," *SAE Technical Paper1998*.

- [134] E. Liu and S. D. Kouame, "An XPS Study on the Composition of Zinc Dialkyl Dithiophosphate Tribofilms and Their Effect on Camshaft Lobe Wear," *Tribology Transactions*, vol. 57, pp. 18-27, 2014.
- [135] M. Kano and I. Tanimoto, "Wear resistance properties of ceramic rocker arm pads," *Wear*, vol. 145, pp. 153-165, 1991.
- [136] C. Alamsyah, S. Dillich, and A. Pettit, "Effects of initial surface finish on cam wear," *Wear*, vol. 134, pp. 29-47, 1989.
- [137] S. Kosarieh, A. Morina, E. Laine, J. Flemming, and A. Neville, "The effect of MoDTC-type friction modifier on the wear performance of a hydrogenated DLC coating," *Wear*, vol. 302, pp. 890-898, 2013.
- [138] D. Uy, S. J. Simko, R. Carter, R. K. Jensen, and A. K. Gangopadhyay, "Characterization of anti-wear films formed from fresh and aged engine oils," *Wear*, vol. 263, pp. 1165-1174, 2007.
- [139] D. D, C. M. Taylor, and Z. G, "An experimental study of the tribology of a cam and flat faced follower.," in: *proceedings of the second international conference on combustion engines IMechE*, pp. 97-108, 1989.
- [140] P. Ball, *Made to measure: New materials for the 21st century*: Princeton University Press, 1999.
- [141] S.-T. Lee, Z. Lin, and X. Jiang, "CVD diamond films: nucleation and growth," *Materials Science and Engineering: R: Reports*, vol. 25, pp. 123-154, 1999.
- [142] J. Robertson, "Diamond-like amorphous carbon," *Materials Science and Engineering: R: Reports*, vol. 37, pp. 129-281, 2002.
- [143] R. Hauert, "An overview on the tribological behavior of diamond-like carbon in technical and medical applications," *Tribology International*, vol. 37, pp. 991-1003, 11// 2004.
- [144] R. Narayan, *Diamond-based materials for biomedical applications*: Elsevier, 2013.

- [145] A. C. Ferrari and J. Robertson, "Interpretation of Raman spectra of disordered and amorphous carbon," *Physical review B*, vol. 61, p. 14095, 2000.
- [146] J. Robertson, "Properties of diamond-like carbon," *Surface and Coatings Technology*, vol. 50, pp. 185-203, 1992/02/06 1992.
- [147] A. Erdemir and C. Donnet, "Tribology of diamond-like carbon films: recent progress and future prospects," *Journal of Physics D: Applied Physics*, vol. 39, p. R311, 2006.
- [148] S. Aisenberg and R. Chabot, "Ion-beam deposition of thin films of diamondlike carbon," *Journal of applied physics*, vol. 42, pp. 2953-2958, 1971.
- [149] H. Ronkainen, "Tribological properties of hydrogenated and hydrogen-free diamond-like carbon coatings," 2001.
- [150] J. C. Angus, J. E. Stultz, P. J. Shiller, J. R. MacDonald, M. J. Mirtich, and S. Domitz, "Composition and properties of the so-called "Diamond-like" amorphous carbon films," *Thin Solid Films*, vol. 118, pp. 311-320, 1984.
- [151] C. Donnet, "Tribology of solid lubricant coatings," *Condensed Matter News*, vol. 4, pp. 9-24, 1995.
- [152] D. Tallant, J. Parmeter, M. Siegal, and R. Simpson, "The thermal stability of diamond-like carbon," *Diamond and related materials*, vol. 4, pp. 191-199, 1995.
- [153] C. Ong, X.-A. Zhao, J. Cheung, S. Lam, Y. Liu, C. Choy, et al., "Thermal stability of pulsed laser deposited diamond-like carbon films," *Thin Solid Films*, vol. 258, pp. 34-39, 1995.
- [154] Y. Liu, A. Erdemir, and E. I. Meletis, "A study of the wear mechanism of diamond-like carbon films," *Surface and Coatings Technology*, vol. 82, pp. 48-56, 1996/07/01 1996.
- [155] J. Sanchez-Lopez, A. Erdemir, C. Donnet, and T. Rojas, "Friction-induced structural transformations of diamondlike carbon coatings

under various atmospheres," *Surface and Coatings Technology*, vol. 163, pp. 444-450, 2003.

- [156] F. Bremond, P. Fournier, and F. Platon, "Test temperature effect on the tribological behavior of DLC-coated 100C6-steel couples in dry friction," *Wear*, vol. 254, pp. 774-783, 2003.
- [157] J. S. Sheasby, T. A. Caughlin, and J. J. Habeeb, "Observation of the antiwear activity of zinc dialkyldithiophosphate additives," *Wear*, vol. 150, pp. 247-257, 10/21/ 1991.
- [158] J. S. Sheasby, T. A. Caughlin, A. G. Blahey, and K. F. Laycock, "A reciprocating wear test for evaluating boundary lubrication," *Tribology International*, vol. 23, pp. 301-307, 1990/10/01/ 1990.
- [159] J. S. Sheasby, M. C. Jennings, and K. D. Cassells, "The effect of sample spin on boundary lubrication by several oil blends based upon zinc dialkyldithiophosphates," *Wear*, vol. 231, pp. 256-264, 7// 1999.
- [160] S. Jahanmir, "Wear reduction and surface layer formation by a ZDDP additive," *Journal of tribology*, vol. 109, pp. 577-586, 1987.
- [161] Y. Lin and H. So, "Limitations on use of ZDDP as an antiwear additive in boundary lubrication," *Tribology International*, vol. 37, pp. 25-33, 2004.
- [162] Y. Wu and B. Dacre, "Effects of lubricant-additives on the kinetics and mechanisms of ZDDP adsorption on steel surfaces," *Tribology International*, vol. 30, pp. 445-453, 1997.
- [163] H. So, Y. Lin, G. G. Huang, and T. S. Chang, "Antiwear mechanism of zinc dialkyl dithiophosphates added to a paraffinic oil in the boundary lubrication condition," *Wear*, vol. 166, pp. 17-26, 1993.
- [164] L. Taylor, A. Dratva, and H. Spikes, "Friction and wear behavior of zinc dialkyldithiophosphate additive," *Tribology transactions*, vol. 43, pp. 469-479, 2000.
- [165] S.-H. Choa, K. C. Ludema, G. E. Potter, B. M. Dekoven, T. A. Morgan, and K. K. Kar, "A model of the dynamics of boundary film formation," *Wear*, vol. 177, pp. 33-45, 1994.

- [166] P. Cann, G. Johnston, and H. Spikes, "The formation of thick films by phosphorus-based anti-wear additives," *Tribology-Friction, Lubrication and Wear. Fifty Years On.*, vol. 1, pp. 543-554, 1987.
- [167] P. Cann and A. Cameron, "Studies of thick boundary lubrication— influence of zddp and oxidized hexadecane," *Tribology international*, vol. 17, pp. 205-208, 1984.
- [168] R. Holinski, "The influence of boundary layers on friction," *Wear*, vol. 56, pp. 147-154, 1979.
- [169] S. Kennedy and L. Moore, "Additive effects on lubricant fuel economy," SAE Technical Paper 0148-7191, 1987.
- [170] K. Kubo, "The Effect on Friction of Lubricants Containing Zinc Dithiophosphate and Organo-molybdenum Compound," *IMEchE*, vol. 68, p. 121, 1985.
- [171] H. Spikes, "Film-Forming Properties of Zinc-Based and Ashless Antiwear Additives," 2000.
- [172] G. Tripaldi, A. Vettor, and H. Spikes, "Friction behaviour of ZDDP films in the mixed, boundary/EHD regime," SAE Technical Paper 0148-7191, 1996.
- [173] H. Spedding and R. Watkins, "The antiwear mechanism of zddp's. Part I," *Tribology international*, vol. 15, pp. 9-12, 1982.
- [174] R. Watkins, "The antiwear mechanism of zddp's. Part II," *Tribology international*, vol. 15, pp. 13-15, 1982.
- [175] R. Bird and G. Galvin, "The application of photoelectron spectroscopy to the study of EP films on lubricated surfaces," *Wear*, vol. 37, pp. 143-167, 1976.
- [176] G. Pereira, D. Munoz-Paniagua, A. Lachenwitzer, M. Kasrai, P. R. Norton, T. W. Capehart, et al., "A variable temperature mechanical analysis of ZDDP-derived antiwear films formed on 52100 steel," *Wear*, vol. 262, pp. 461-470, 2007.
- [177] Z. Yin, M. Kasrai, M. Fuller, G. M. Bancroft, K. Fyfe, and K. H. Tan, "Application of soft X-ray absorption spectroscopy in chemical

characterization of antiwear films generated by ZDDP Part I: the effects of physical parameters," *Wear*, vol. 202, pp. 172-191, 1997.

- [178] J. Bell, K. Delargy, and A. Seeney, "Paper IX (ii) The removal of substrate material through thick zinc dithiophosphate anti-wear films," in *Tribology series*. vol. 21, ed: Elsevier, 1992, pp. 387-396.
- [179] B. Dacre and C. Bovington, "The adsorption and desorption of zinc diisopropyldithiophosphate on steel," *Asle Transactions*, vol. 25, pp. 546-554, 1982.
- [180] C. Bovington and B. Dacre, "The adsorption and reaction of decomposition products of zinc diisopropyldiophosphate on steel," *ASLE transactions*, vol. 27, pp. 252-258, 1984.
- [181] R. Coy and R. Jones, "The thermal degradation and EP performance of zinc dialkyldithiophosphate additives in white oil," *ASLE transactions*, vol. 24, pp. 77-90, 1981.
- [182] R. Jones and R. Coy, "The chemistry of the thermal degradation of zinc dialkyldithiophosphate additives," *Asle Transactions*, vol. 24, pp. 91-97, 1981.
- [183] J. M. Martin, C. Grossiord, T. Le Mogne, S. Bec, and A. Tonck, "The two-layer structure of Zndtp tribofilms: Part I: AES, XPS and XANES analyses," *Tribology international*, vol. 34, pp. 523-530, 2001.
- [184] J. Habeeb and W. Stover, "The role of hydroperoxides in engine wear and the effect of zinc dialkyldithiophosphates," *ASLE transactions*, vol. 30, pp. 419-426, 1986.
- [185] J. Martin, "Lubricant additives and the chemistry of rubbing surfaces: metal dithiophosphates triboreaction films revisited," *Japanese Journal of Tribology*, vol. 42, p. 1095, 1997.
- [186] J. Williams, "The behaviour of sliding contacts between non-conformal rough surfaces protected by 'smart' films," *Tribology Letters*, vol. 17, pp. 765-778, 2004.
- [187] P. C. H. Mitchell, "Oil-soluble MO-S compounds as lubricant additives," *Wear*, vol. 100, pp. 281-300, 12// 1984.

- [188] C. Grossiord, K. Varlot, J.-M. Martin, T. Le Mogne, C. Esnouf, and K. Inoue, "MoS₂ single sheet lubrication by molybdenum dithiocarbamate," *Tribology international*, vol. 31, pp. 737-743, 1998.
- [189] J. Graham, H. Spikes, and S. Korcek, "The friction reducing properties of molybdenum dialkyldithiocarbamate additives: part I—factors influencing friction reduction," *Tribology transactions*, vol. 44, pp. 626-636, 2001.
- [190] J. Graham, H. Spikes, and R. Jensen, "The friction reducing properties of molybdenum dialkyldithiocarbamate additives: Part II-Durability of friction reducing capability," *Tribology transactions*, vol. 44, pp. 637-647, 2001.
- [191] K. T. Miklozic, J. Graham, and H. Spikes, "Chemical and physical analysis of reaction films formed by molybdenum dialkyldithiocarbamate friction modifier additive using Raman and atomic force microscopy," *Tribology Letters*, vol. 11, pp. 71-81, 2001.
- [192] Y. Yamamoto and S. Gondo, "Friction and wear characteristics of molybdenum dithiocarbamate and molybdenum dithiophosphate," *Tribology Transactions*, vol. 32, pp. 251-257, 1989.
- [193] A. R. Lansdown, *Molybdenum disulphide lubrication* vol. 35: Elsevier, 1999.
- [194] R. Unnikrishnan, M. Jain, A. Harinarayan, and A. Mehta, "Additive–additive interaction: an XPS study of the effect of ZDDP on the AW/EP characteristics of molybdenum based additives," *Wear*, vol. 252, pp. 240-249, 2002.
- [195] H. Spikes, "Film-forming additives-direct and indirect ways to reduce friction," *Lubrication Science*, vol. 14, pp. 147-167, 2002.
- [196] J. Sorab, S. Korcek, and C. Bovington, "Friction reduction in lubricated components through engine oil formulation," *SAE Technical Paper* 0148-7191, 1998.
- [197] M. Muraki, Y. Yanagi, and K. Sakaguchi, "Synergistic effect on frictional characteristics under rolling-sliding conditions due to a combination of

molybdenum dialkyldithiocarbamate and zinc dialkyldithiophosphate," *Tribology International*, vol. 30, pp. 69-75, 1997.

- [198] D. N. Khaemba, "Raman spectroscopic studies of friction modifier Molybdenum DialkyldiThioCarbamate (MoDTC)," University of Leeds, 2016.
- [199] Z. Zhang, W. Li, T.-W. Ng, W. Kang, C.-S. Lee, and W. Zhang, "Iron (ii) molybdate (FeMoO₄) nanorods as a high-performance anode for lithium ion batteries: structural and chemical evolution upon cycling," *Journal of Materials Chemistry A*, vol. 3, pp. 20527-20534, 2015.
- [200] Z. Zhang, C. Hu, M. Hashim, P. Chen, Y. Xiong, and C. Zhang, "Synthesis and magnetic property of FeMoO₄ nanorods," *Materials Science and Engineering: B*, vol. 176, pp. 756-761, 2011.
- [201] D. N. Khaemba, A. Neville, and A. Morina, "New insights on the decomposition mechanism of Molybdenum DialkyldiThioCarbamate (MoDTC): a Raman spectroscopic study," *RSC Advances*, vol. 6, pp. 38637-38646, 2016.
- [202] Y. Wang, P. He, W. Lei, F. Dong, and T. Zhang, Novel FeMoO₄/graphene composites based electrode materials for supercapacitors vol. 103, 2014.
- [203] B. C. Windom, W. Sawyer, and D. W. Hahn, "A Raman spectroscopic study of MoS₂ and MoO₃: applications to tribological systems," *Tribology Letters*, vol. 42, pp. 301-310, 2011.
- [204] M. Kasrai, J. Cutler, K. Gore, G. Canning, G. Bancroft, and K. Tan, "The chemistry of antiwear films generated by the combination of ZDDP and MoDTC examined by X-ray absorption spectroscopy," *Tribology transactions*, vol. 41, pp. 69-77, 1998.
- [205] R. Unnikrishnan, M. C. Jain, A. K. Harinarayan, and A. K. Mehta, "Additive-additive interaction: an XPS study of the effect of ZDDP on the AW/EP characteristics of molybdenum based additives," *Wear*, vol. 252, pp. 240-249, 2002.

- [206] J.-M. Martin, C. Grossiord, T. Le Mogne, and J. Igarashi, "Transfer films and friction under boundary lubrication," *Wear*, vol. 245, pp. 107-115, 10// 2000.
- [207] C. Grossiord, J. M. Martin, K. Varlot, B. Vacher, T. Le Mogne, and Y. Yamada, "Tribochemical interactions between ZnDTP, MoDTC and calcium borate," *Tribology Letters*, vol. 8, pp. 203-212, 2000.
- [208] Y. Sogawa, N. Yoshimura, and O.H. Iwasaki, "Sogawa, Y., N. Yoshimura, and O.H. Iwasaki," 2000.
- [209] D. G. Yablon, P. H. Kalamaras, D. E. Deckman, and M. N. Webster, "Atomic force microscopy and raman spectroscopy investigation of additive interactions responsible for anti-wear film formation in a lubricated contact," *Tribology transactions*, vol. 49, pp. 108-116, 2006.
- [210] J. Ye, M. Kano, and Y. Yasuda, "Evaluation of Local Mechanical Properties in Depth in MoDTC/ZDDP and ZDDP Tribochemical Reacted Films Using Nanoindentation," *Tribology Letters*, vol. 13, pp. 41-47, July 01 2002.
- [211] F. G. Rounds, "Additive interactions and their effect on the performance of a zinc dialkyl dithiophosphate," *ASLE Transactions*, vol. 21, pp. 91-101, 1978.
- [212] Y. Wan, M. S. Fuller, M. Kasrai, G. Bancroft, K. Fyfe, J. Torkelson, et al., "Effects of detergent on the chemistry of tribofilms from ZDDP: studied by X-ray absorption spectroscopy and XPS," in *Tribology series*. vol. 40, ed: Elsevier, 2002, pp. 155-166.
- [213] P. Willermet, "Some engine oil additives and their effects on antiwear film formation," *Tribology Letters*, vol. 5, pp. 41-47, 1998.
- [214] P. Kapsa, J. Martin, C. Blanc, and J. Georges, "Antiwear mechanism of ZDDP in the presence of calcium sulfonate detergent," *Journal of Lubrication Technology*, vol. 103, pp. 486-494, 1981.
- [215] M. Kasrai, M. S. Fuller, G. M. Bancroft, and P. R. Ryason, "X-ray absorption study of the effect of calcium sulfonate on antiwear film formation generated from neutral and basic ZDDPs: Part 1—

- phosphorus species," *Tribology Transactions*, vol. 46, pp. 534-542, 2003.
- [216] M. Shiomi, J. i. Mitsui, K. Akiyama, K. Tasaka, M. Nakada, and H. Ohira, "Formulation technology for low phosphorus gasoline engine oils," SAE Technical Paper 0148-7191, 1992.
- [217] S. Shirahama and M. Hirata, "The effects of engine oil additives on valve train wear," *Lubrication Science*, vol. 1, pp. 365-384, 1989.
- [218] N. Han, L. Shui, W. Liu, Q. Xue, and Y. Sun, "Study of the lubrication mechanism of overbased Ca sulfonate on additives containing S or P," *Tribology Letters*, vol. 14, pp. 269-274, 2003.
- [219] S. Ramakumar, A. M. Rao, and S. Srivastava, "Studies on additive-additive interactions: formulation of crankcase oils towards rationalization," *Wear*, vol. 156, pp. 101-120, 1992.
- [220] N. E. Gallopoulos and C. K. Murphy, "Interactions between a zinc dialkylphosphorodithioate and lubricating oil dispersants," *ASLE TRANSACTIONS*, vol. 14, pp. 1-7, 1971.
- [221] B. Vengudusamy, J. H. Green, G. D. Lamb, and H. A. Spikes, "Behaviour of MoDTC in DLC/DLC and DLC/steel contacts," *Tribology International*, vol. 54, pp. 68-76, 2012.
- [222] W. Yue, C. Liu, Z. Fu, C. Wang, H. Huang, and J. Liu, "Synergistic effects between sulfurized W-DLC coating and MoDTC lubricating additive for improvement of tribological performance," *Tribology International*, vol. 62, pp. 117-123, 2013.
- [223] K. Topolovec-Miklozic, F. Lockwood, and H. Spikes, "Behaviour of boundary lubricating additives on DLC coatings," *Wear*, vol. 265, pp. 1893-1901, 11/26/ 2008.
- [224] S. Miyake, T. Saito, Y. Yasuda, Y. Okamoto, and M. Kano, "Improvement of boundary lubrication properties of diamond-like carbon (DLC) films due to metal addition," *Tribology International*, vol. 37, pp. 751-761, 2004.

- [225] M. Kano, Y. Yasuda, and J. Ye, "The effect of ZDDP and MoDTC additives in engine oil on the friction properties of DLC-coated and steel cam followers," *Lubrication Science*, vol. 17, pp. 95-103, 2004.
- [226] T. Haque, A. Morina, and A. Neville, "Influence of friction modifier and antiwear additives on the tribological performance of a non-hydrogenated DLC coating," *Surface and Coatings Technology*, vol. 204, pp. 4001-4011, 9/15/ 2010.
- [227] T. Haque, A. Morina, and A. Neville, "Effect of friction modifiers and antiwear additives on the tribological performance of a hydrogenated DLC coating," *Journal of tribology*, vol. 132, p. 032101, 2010.
- [228] T. Haque, A. Morina, and A. Neville, "Tribological performance evaluation of a hydrogenated diamond-like carbon coating in sliding/rolling contact–effect of lubricant additives," *Proceedings of the Institution of Mechanical Engineers, Part J: Journal of Engineering Tribology*, vol. 225, pp. 393-405, 2011.
- [229] T. Shinyoshi, Y. Fuwa, and Y. Ozaki, "Wear analysis of DLC coating in oil containing Mo-DTC," *SAE Technical Paper*2007.
- [230] S. Kosarieh, A. Morina, E. Lainé, J. Flemming, and A. Neville, "The effect of MoDTC-type friction modifier on the wear performance of a hydrogenated DLC coating," *Wear*, vol. 302, pp. 890-898, 2013.
- [231] S. Kosarieh, A. Morina, J. Flemming, E. Lainé, and A. Neville, "Wear Mechanisms of Hydrogenated DLC in Oils Containing MoDTC," *Tribology Letters*, vol. 64, p. 4, 2016.
- [232] M. De Feo, M. D. B. Bouchet, C. Minfray, C. Esnouf, T. Le Mogne, F. Meunier, et al., "Formation of interfacial molybdenum carbide for DLC lubricated by MoDTC: Origin of wear mechanism," *Wear*, vol. 370, pp. 17-28, 2017.
- [233] M. De Feo, M. D. B. Bouchet, C. Minfray, T. Le Mogne, F. Meunier, L. Yang, et al., "MoDTC lubrication of DLC-involving contacts. Impact of MoDTC degradation," *Wear*, vol. 348, pp. 116-125, 2016.

- [234] R. A. Mufti, R. Zahid, F. Qureshi, J. Aslam, N. Afzal, and M. U. Bhutta, "Measuring the tribological performance of all the tappets in a production engine using magnetometer sensors and the effect of lubricant rheology," *Lubrication Science*, vol. 27, pp. 251-263, 2015.
- [235] R. A. Mufti and A. Jefferies, "Novel method of measuring tappet rotation and the effect of lubricant rheology," *Tribology International*, vol. 41, pp. 1039-1048, 2008.
- [236] L. Jelenschi, C. Cofaru, G. Sandu, and M. Aleonte, "State of The Art of Engine Valve and Tappet Rotation," *Engineering Sciences*, vol. 4 (53) No. 2, 2011.
- [237] K. J. Siczek, *Tribological Processes in the Valve Train Systems with Lightweight Valves: New Research and Modelling*, 1st ed.: Butterworth-Heinemann, 2016.
- [238] L. Jelenschi, C. Cofaru, and G. Sandu, "Investigating the hydraulic tappet rotation for a direct acting valve train," *Bulletin of the Transilvania University of Brasov, Series I: Engineering Sciences*, vol. 5 (54) No.1, 2012.
- [239] B. A. Gecim, "Tribological study for a low-friction cam/tappet system including tappet spin," *Tribology transactions*, vol. 35, pp. 225-234, 1992.
- [240] L. Jelenschi, C. Cofaru, G. Sandu, and I.-S. Radu, *THE NECESSITY FOR ROTATIONAL MOVEMENT OF VALVE AND TAPPET IN INTERNAL COMBUSTION ENGINES: SCIENTIFIC BULLETIN*, 2017.
- [241] G. Monteil, A. Gallmann, P. Sioshansi, and P. Loges, "Contribution of Nuclear Physics to Engine Design: Application of Surface Layer Activation to Tappet Rotation Measurements," *SAE Technical Paper*. 960711, 1996
- [242] J. Pieprzak, P. Willermet, and D. Klassen, "A tappet rotation monitor based on light reflectance-development and functional testing," *SAE Technical Paper*. 890722, 1989.

- [243] J. Pieprzak and D. Dailey, "Tappet rotation and friction reduction in a center pivot rocker arm contact," *Journal of Tribology*, vol. 112, p. 655, 1990.
- [244] M.-R. Cho, H.-J. Kim, T.-S. Moon, and D.-C. Han, "Theoretical and experimental evaluation of tappet rotation for a direct acting valve train system," *International journal of vehicle design*, vol. 34, pp. 35-51, 2004.
- [245] P. Willermet and J. Pieprzak, "Some effects of lubricant composition and tappet rotation on cam/tappet friction," *Journal of Tribology*, vol. 111, pp. 683-691, 1989.
- [246] C. Bona and F. Ghilardi, "Influence of tappet rotation on cam and tappet surface deterioration," *Proceedings of the Institution of Mechanical Engineers: Automobile Division*, vol. 180, pp. 269-278, 1965.
- [247] R. A. Mufti, R. Zahid, F. Qureshi, and J. Aslam, "Innovative technique of measuring follower rotation in real production engine using Gradiometer sensor and the effect of friction modifier," *Industrial Lubrication and Tribology*, vol. 67, pp. 285-291, 2015.
- [248] L.-H. Xu, Y.-B. Yuan, and L. Wang, "Selecting Principle and Equipment of Valve Tappets," *Applied Informatics and Communication*, pp. 619-630, 2011.
- [249] A. Neville, T. Haque, and A. Morina, "Friction and its importance in fuel economy—probing the nanoscale characteristics of surfaces in order to understand lubricant/surface interactions," *Journal of Physics: Condensed Matter*, vol. 20, p. 354019, 2008.
- [250] P. Instruments, "MTM2 (Mini Traction Machine)," Retrieved on 2nd of August, 2013.
- [251] R. Kapadia, R. Glyde, and Y. Wu, "In situ observation of phosphorous and non-phosphorous antiwear films using a mini traction machine with spacer layer image mapping," *Tribology international*, vol. 40, pp. 1667-1679, 2007.
- [252] Q. Xin, *Diesel engine system design*: Elsevier, 2011.

- [253] J. Jelita Rydel, R. H. Vegter, and P. E. J. Rivera-Díaz-del-Castillo, "Tribochemistry of bearing steels: A new AFM method to study the material-tribofilm correlation," *Tribology International*, vol. 98, pp. 74-81, 6// 2016.
- [254] A. Ghanbarzadeh, P. Parsaeian, A. Morina, M. C. T. Wilson, M. C. P. van Eijk, I. Nedelcu, et al., "A Semi-deterministic Wear Model Considering the Effect of Zinc Dialkyl Dithiophosphate Tribofilm," *Tribology Letters*, vol. 61, p. 12, 2015.
- [255] D. H. Buckley, "Surface Effects in Adhesion, Friction, Wear, and Lubrication.(Tribology Series, Vol. 5)," Elsevier Scientific Publishing Co., ix+ 630, 24 x 16 cm, illustrated(Dfl. 220. 00, 1981.
- [256] Brief Overview of Traditional, Microscopes http://www.eng.utah.edu/~lzang/images/Lecture_3_conventional-Microscope.pdf .
- [257] J. F. Moulder, W. F. Stickle, P. E. Sobol, and K. D. Bomben, "Standard Spectra for Identification and Interpretation of XPS data," Perkin Elmer, Eden Prairie, MN, 1992.
- [258] G. S. Bumbrah and R. M. Sharma, "Raman spectroscopy-Basic principle, instrumentation and selected applications for the characterization of drugs of abuse," *Egyptian Journal of Forensic Sciences*, 2015.
- [259] G. Gouadec and P. Colomban, "Raman Spectroscopy of nanomaterials: How spectra relate to disorder, particle size and mechanical properties," *Progress in crystal growth and characterization of materials*, vol. 53, pp. 1-56, 2007.
- [260] B. Vengudusamy, R. A. Mufti, G. D. Lamb, J. H. Green, and H. A. Spikes, "Friction properties of DLC/DLC contacts in base oil," *Tribology international*, vol. 44, pp. 922-932, 2011.
- [261] B. Vengudusamy, J. H. Green, G. D. Lamb, and H. A. Spikes, "Tribological properties of tribofilms formed from ZDDP in DLC/DLC

- and DLC/steel contacts," *Tribology International*, vol. 44, pp. 165-174, 2011.
- [262] D. N. Khaemba, A. Neville, and A. Morina, "A methodology for Raman characterisation of MoDTC tribofilms and its application in investigating the influence of surface chemistry on friction performance of MoDTC lubricants," *Tribology Letters*, vol. 59, p. 38, 2015.
- [263] P. De Aza, C. Santos, A. Pazo, S. De Aza, R. Cusco, and L. Artus, "Vibrational properties of calcium phosphate compounds. 1. Raman spectrum of β -tricalcium phosphate," *Chemistry of materials*, vol. 9, pp. 912-915, 1997.
- [264] G. Adamopoulos, K. Gilkes, J. Robertson, N. Conway, B. Kleinsorge, A. Buckley, et al., "Ultraviolet Raman characterisation of diamond-like carbon films," *Diamond and related materials*, vol. 8, pp. 541-544, 1999.
- [265] "Introduction A2 - Niinomi, Mitsuo," in *Metals for Biomedical Devices*, ed: Woodhead Publishing, 2010, pp. xv-xvii.
- [266] Y. Rai, A. Neville, and A. Morina, "Transient processes of MoS₂ tribofilm formation under boundary lubrication," *Lubrication Science*, vol. 28, pp. 449-471, 2016.
- [267] M. Ratoi, V. B. Niste, H. Alghawel, Y. F. Suen, and K. Nelson, "The impact of organic friction modifiers on engine oil tribofilms," *RSC Advances*, vol. 4, pp. 4278-4285, 2014.
- [268] T. Haque, A. Morina, A. Neville, R. Kapadia, and S. Arrowsmith, "Effect of oil additives on the durability of hydrogenated DLC coating under boundary lubrication conditions," *Wear*, vol. 266, pp. 147-157, 1/5/ 2009.
- [269] S. C. Tung and H. Gao, "Tribological characteristics and surface interaction between piston ring coatings and a blend of energy-conserving oils and ethanol fuels," *Wear*, vol. 255, pp. 1276-1285, 8// 2003.

- [270] D. Zhu and H. S. Cheng, "Paper VI (iv) Tribological Performance of Ceramic Roller Followers/Camshaft System in Automobile Valve Trains," Tribology Series, vol. 18, pp. 149-156, 1991/01/01 1991.
- [271] G. Zhu, "A Theoretical and Experimental Study of the Tribology of a Cam and Follower," The University of Leeds, 1988.
- [272] J. Erjavec and R. Thompson, Automotive technology: a systems approach: Cengage Learning, 2014.
- [273] M. Crobu, A. Rossi, F. Mangolini, and N. D. Spencer, "Chain-length-identification strategy in zinc polyphosphate glasses by means of XPS and ToF-SIMS," Analytical and bioanalytical chemistry, vol. 403, pp. 1415-1432, 2012.
- [274] J. Zhang, E. Yamaguchi, and H. Spikes, "The antagonism between succinimide dispersants and a secondary zinc dialkyl dithiophosphate," Tribology Transactions, vol. 57, pp. 57-65, 2014.
- [275] T. Weber, J. Muijsers, and J. Niemantsverdriet, "Structure of amorphous MoS₃," The Journal of Physical Chemistry, vol. 99, pp. 9194-9200, 1995.
- [276] M. Bowker, C. Brookes, A. Carley, M. House, M. Kosif, G. Sankar, et al., "Evolution of active catalysts for the selective oxidative dehydrogenation of methanol on Fe₂O₃ surface doped with Mo oxide," Physical Chemistry Chemical Physics, vol. 15, pp. 12056-12067, 2013.
- [277] L.-b. Wu, L.-h. Wu, W.-m. Yang, and A. I. Frenkel, "Study of the local structure and oxidation state of iron in complex oxide catalysts for propylene ammoxidation," Catalysis Science & Technology, vol. 4, pp. 2512-2519, 2014.
- [278] J. Temuujin, K. MacKenzie, G. Burmaa, D. Tsend-Ayush, T. Jadambaa, and A. Van Riessen, "Mechanical activation of MoS₂+ Na₂O₂ mixtures," Minerals Engineering, vol. 22, pp. 415-418, 2009.

- [279] A. Morina and A. Neville, "Understanding the composition and low friction tribofilm formation/removal in boundary lubrication," *Tribology International*, vol. 40, pp. 1696-1704, 2007.
- [280] M. Suzuki, "Comparison of tribological characteristics of sputtered MoS₂ films coated with different apparatus," *Wear*, vol. 218, pp. 110-118, 1998.
- [281] B. Podgornik and J. Vižintin, "Tribological reactions between oil additives and DLC coatings for automotive applications," *Surface and Coatings Technology*, vol. 200, pp. 1982-1989, 2005.
- [282] R. Mufti and M. Priest, "Effect of cylinder pressure on engine valve-train friction under motored and fired conditions," *Proceedings of the Institution of Mechanical Engineers, Part J: Journal of Engineering Tribology*, vol. 226, pp. 306-314, 2012.
- [283] K. Torii, H. Chida, K. Otsubo, and Y. Tsusaka, "Anti-wear Properties of Engine Oils-Effects of Oil Additives on Valve Train Wear," *SAE Technical Paper 0148-7191*, 1977.
- [284] M. Broda and R. Bethke, "Friction behavior of different DLC coatings by using various kinds of oil," *SAE International Journal of Materials and Manufacturing*, vol. 1, pp. 832-840, 2009.
- [285] S. Okuda, T. Dewa, and T. Sagawa, "Development of 5W-30 GF-4 fuel-saving engine oil for DLC-coated valve lifters," *SAE Technical Paper 0148-7191*, 2007.
- [286] A. Ghanbarzadeh, M. Wilson, A. Morina, D. Dowson, and A. Neville, "Development of a new mechano-chemical model in boundary lubrication," *Tribology International*, vol. 93, pp. 573-582, 2016.
- [287] R. Bosman and D. J. Schipper, "Running-in of systems protected by additive-rich oils," *Tribology letters*, vol. 41, pp. 263-282, 2011.